Université du Québec
Institut National de la Recherche Scientifique
Centre Eau Terre Environnement

Prévision thermique d'ensemble en rivière avec assimilation de données

Par

Sébastien Ouellet-Proulx

Thèse présentée pour l'obtention du grade de
Philosophiae doctor (Ph.D.)
en sciences de l'eau

Jury d'évaluation

Présidente du jury et
examinatrice interne

Sophie Duchesne
Institut national de la recherche
scientifique

Examinatrice externe

Pascale Biron
Département de géographie,
urbanisme et environnement
Université Concordia

Examinatrice externe

Florentina Moatar
Département Géosciences
environnement
Université François-Rabelais

Directeur de recherche

André St-Hilaire
Institut national de la recherche
scientifique

Codirectrice de recherche

Marie-Amélie Boucher
Université de Sherbrooke

REMERCIEMENTS

RÉSUMÉ

Les températures élevées de l'eau en rivière sont largement reconnues comme une source de stress pour certains organismes aquatiques, tels que les salmonidés. Dans plusieurs cours d'eau, des mesures d'atténuations doivent être mises en place pour réduire l'impact de ces températures sur la faune aquatique locale. Des travaux récents ont mis en évidence l'importance de la prévision de la température l'eau pour assurer la bonne implantation de ces mesures. On y insiste par ailleurs sur le besoin de mieux comprendre et quantifier l'incertitude associée à la prévision de température de l'eau.

Alors que plusieurs éléments de modélisation sont reconnus comme sources d'incertitude de la prévision de la température de l'eau, leur contribution spécifique demeure peu connue et faiblement documentée.

Les travaux qui composent ce document proposent une méthodologie qui s'insère dans un processus de modernisation du modèle hydrologique CEQUEAU. Ils ont été effectués dans le but de rendre possible la prévision de la température de l'eau à court terme. L'incertitude des intrants météorologiques a été investiguée à travers la production de prévisions d'ensemble. Pour assurer la bonne représentation des états initiaux au moment de la prévision, un algorithme d'assimilation de données hydrologiques et thermiques a été intégré au processus prévisionnel. Afin de contribuer à l'amélioration de la formulation du modèle, diverses méthodes d'estimation de l'évaporation et de l'évapotranspiration ont été testées. Cet exercice a notamment permis d'évaluer l'incertitude associée à la simulation de ces deux processus.

Pour la première fois, le modèle thermique a été utilisé afin de permettre la prévision à court terme. On observe une forte propagation de l'incertitude des intrants météorologiques sur l'incertitude de la prévision thermique (Article 1). Cette propagation est toutefois moindre sous un régime d'écoulement régulé par rapport à un écoulement naturel. Bien que la prise en considération de l'incertitude des intrants météorologiques permette d'assurer une bonne fiabilité (une bonne représentation statistique de l'incertitude) de la prévision thermique à moyen terme (cinq jours), un manque de fiabilité afflige la prévision à court terme (un jour). Le recours à l'assimilation de

données par filtres particulaires démontre un excellent potentiel pour assurer la correction des variables d'état du modèle avant l'émission d'une prévision thermique (Article 2). Lorsqu'un nombre adéquat de particules est utilisé, le filtre particulaire permet aussi de garantir une dispersion juste de la prévision d'ensemble, et en assure ainsi la fiabilité. Par ailleurs, les résultats ont permis de démontrer l'importance de distinguer l'estimation de l'évapotranspiration et l'évaporation à la surface des eaux libres lors d'une modélisation thermique (Article 3). Ils illustrent aussi la forte influence du choix de la méthode d'estimation sur les simulations hydrologiques et thermiques subséquentes. Cette influence est toutefois comparable à l'influence de la paramétrisation du modèle.

Enfin, cette thèse vise à mettre en évidence et documenter trois importantes sources d'incertitude associées à la modélisation de la température de l'eau : les états initiaux, la formulation du modèle ainsi que ses intrants. L'exercice est effectué dans un objectif de quantification et de représentation de cette incertitude pour l'émission de prévisions d'ensemble de la température de l'eau.

Mots clés : Modélisation; prévision d'ensemble; incertitude; évaporation; évapotranspiration; assimilation de données; filtre particulaire.

ABSTRACT

High water temperature is widely recognized as a cause of stress for aquatic organisms such as salmonids. In many river systems, mitigation measures must be put in place to reduce the impact of those temperatures on local aquatic fauna. Recent work has demonstrated the importance of using water temperature forecasts to ensure a proper implementation of such measures. The need to better understand and quantify uncertainties associated with water temperature forecasts is highlighted.

While various modelling elements are known to propagate uncertainty within a thermal forecast, their respective contribution to the overall model uncertainty remains little known and poorly documented.

Research work that is described in this document put forward a methodology that is an integral part of a modernisation process of the hydrological model CEQUEAU. It was conducted with the aim to enable the production of short-range water temperature forecasts. The uncertainty carried by meteorological inputs has been investigated through ensemble forecasts. To ensure a proper representation of the initial conditions of the model before launching the forecast, a data assimilation algorithm of both hydrological and thermal data was integrated into the forecasting process. In order to contribute to the improvement of the CEQUEAU model, various estimation methods of evaporation and evapotranspiration were tested. This work allowed to evaluate the uncertainty associated with simulating these two processes.

The thermal module of the CEQUEAU model was used for the first time to produce water temperature forecasts (Article 1). An important uncertainty was propagated to water temperature forecasts by meteorological inputs. This uncertainty propagation is however of lesser importance under regulated flow regime compared to a natural flow. Although the inclusion of meteorological uncertainty allows a good forecast reliability (adequate statistical representation of the uncertainty) for a mid-range forecast (five days), a lack of reliability is evident for short-range forecasts (one day). The use of particle filters showed an excellent potential to perform state variable correction before launching the model in forecasting mode (Article 2). When an adequate number of

particles is used, the particle filter allows to produce a properly spread forecast, and thus ensures reliability.

The results also showed the importance of separating the estimation of evapotranspiration and open water evaporation when modelling water temperature (Article 3). They also demonstrate the strong influence of the estimation of evaporative fluxes on subsequent hydrological and thermal modelling. However, this influence is similar to model parametrisation.

The following thesis aims at highlighting and documenting three important sources of uncertainty associated with water temperature modelling: initial conditions, model formulation and meteorological inputs. The research process was done with the objective of quantifying and representing this uncertainty within a water temperature forecasting framework.

Keywords: Modelling; ensemble forecast; uncertainty; evaporation; evapotranspiration; data assimilation; particle filter.

TABLE DES MATIÈRES

LISTE DES TABLEAUX

LISTE DES FIGURES

LISTE DES ABRÉVIATIONS

AIC *Critère d'information d'Akaike/Akaike information criterion*

CAT *Ruisseau Catamaran*

CMA-ES *Covariance matrix adaptation evolution strategy*

CMC *Centre météorologique Canadien*

CRPS *Continuous Ranked Probability Score*

ECMWF *Centre européen pour les prévisions météorologiques à moyen terme/European Centre for Medium-Range Weather Forecasts*

GR4J *Modèle du Génie Rural à 4 paramètres Journalier*

HBV *Hydrologiska Byråns Vattenbalansavdelning model*

KGE *Critère d'efficacité de Kling-Gupta*

LSWM *Little Southwest Miramichi*

MAE *Mean Absolute Error*

MIR *Bassin versant de la rivière Miramichi*

MPO *Ministère Pêches et Océans Canada*

NECH *Bassin versant de la rivière Nechako*

NFCP *Nechako Fisheries Conservation Program*

NSE *Critère d'efficacité de Nash-Sutcliffe*

NWM *Northwest Miramichi*

RMSE *Racine de l'erreur quadratique moyenne/Root mean squared error*

SLURP *Semi-distributed Land Use-based Runoff Processes*

SWAT *Soil and Water Assessment Tool*

SWM *Southwest Miramichi*

TIGGE *The Observing System Research and Predictability Experiment (THORPEX) Interactive Grand Global Ensemble portal*

PARTIE I : SYNTHÈSE

1   INTRODUCTION

L'incidence de la température de l'eau sur la qualité des écosystèmes aquatiques n'est plus à démontrer (Fry, 1971; Ward, 1982). Il a été établi que des périodes de hautes températures peuvent occasionner une dégradation de la capacité de nage des poissons (McCullough et al., 2001), limiter la croissance et ultimement entrainer la mort (Sullivan et al., 2000) de certains organismes aquatiques. Ces conséquences peuvent être exacerbées par la présence de facteurs de stress secondaires, tel que la pêche récréative (Dempson et al., 2002; Bartholomew et Bohnsack, 2005) ou la présence de pathogènes (Martins et al., 2012). Des mesures d'atténuation peuvent être mises en place par les organismes gestionnaires des rivières pour atténuer les effets des températures élevées. Ces mesures peuvent être de nature i) à prévenir le réchauffement de l'eau par le maintien de volumes d'eau suffisants dans le cours d'eau, (p. ex. augmenter les relâches d'eau stockée dans les réservoirs ou limiter les prélèvements) ou ii) à limiter la présence d'agents stressants (p.ex. fermeture de la pêche). Toutefois, en l'absence de connaissance des températures de l'eau à venir, ces décisions peuvent seulement être prises en réaction aux conditions observées plutôt qu'être prises de façon préventive (Hague et Patterson, 2014). Dans un tel contexte, la prévision à court terme en temps réel de la température de l'eau constitue un outil de gestion de premier ordre.

Selon Krzysztofowicz (2001), l'incertitude quant à la réalisation d'un évènement dans l'avenir est la raison principale qui motive la production d'une prévision. La prévision ne permet pas d'éliminer cette incertitude, mais tout au plus de la quantifier et possiblement de la réduire. Puisque l'on convient de l'existence de cette incertitude, il est primordial d'en connaitre l'importance. C'est cette connaissance du degré d'incertitude qui définira la confiance qu'on accorde à une prévision. Quelle que soit la variable prévue, l'incertitude associée à la prévision provient des intrants fournis au

modèle, des conditions initiales du système lors de l'émission de la prévision, du modèle lui-même, incluant sa formulation, sa structure et ses paramètres, et même des observations utilisées pour l'ajustement et la validation (Walker et al., 2003; Salamon et Feyen, 2010). Dans le domaine de la prévision de crue, et précédemment dans celui de la prévision météorologique, plusieurs outils ont été développés pour produire des prévisions d'ensemble (c'est-à-dire de multiples prévisions pour le même horizon temporel) qui représentent l'incertitude qui se propage à travers la prévision (Cloke et Pappenberger, 2009).

Dès le début des années 2000, Bartholow (2003) argumente en faveur de l'inclusion de l'incertitude dans la prévision de la température de l'eau. Quelques publications récentes proposent des méthodes, au degré de complexité variable, pour la prévision de température de l'eau (p. ex. Pike et al., 2013; Bal et al., 2014; Caissie et al., 2016). Toutefois, peu de ces travaux se sont affairés à quantifier et documenter l'incertitude. C'est pourquoi la présente thèse propose d'approfondir certains aspects de l'incertitude associée à la prévision de la température de l'eau en rivière. Sans prétendre s'y attaquer dans son ensemble, la thèse vise la mise en exergue de certains aspects de la prévision. Elle vise l'analyse de l'incertitude attribuable aux intrants météorologiques, aux conditions initiales du système hydrologique ainsi qu'à la structure du modèle, comme par exemple, le choix de la formulation du calcul d'estimation de l'évaporation dans un dessein prévisionnel sciemment dirigé vers des applications en gestion des ressources hydriques.

L'objectif global de cette thèse est de contribuer à l'acquisition d'une meilleure connaissance de l'incertitude qui se propage à la prévision de la température de l'eau en rivière effectuée à l'aide du modèle semi-distribué CEQUEAU. On vise à évaluer la performance du modèle dans un contexte de prévision hydrologique et thermique à court terme. Cet objectif se détaille en quatre objectifs spécifiques. Le premier objectif spécifique s'appuie sur l'hypothèse que l'utilisation de prévisions météorologiques d'ensemble comme intrants au modèle permettra de produire une prévision thermique fiable tout en quantifiant convenablement l'incertitude associée à ces intrants. On suppose que l'effet de cette incertitude sera davantage observable pour les prévisions à plus long terme. Le premier objectif vise donc la quantification de l'incertitude associée

aux intrants météorologiques qui se propage à la prévision à court terme de la température de l'eau.

Pour le second objectif spécifique, on pose l'hypothèse que l'utilisation d'un algorithme d'assimilation de données rendra possible la diminution de l'erreur des variables d'état hydrologiques et thermiques au moment de la prévision. On considère aussi que ce même algorithme permettra de bien quantifier l'incertitude associée à l'estimation de ces variables d'état. Cette incertitude serait ensuite majoritairement propagée à la prévision à court terme. Le second objectif spécifique vise la correction des états initiaux, hydrologiques et thermiques, d'un modèle semi-distribué préalablement à l'émission d'une prévision. Cet objectif est intimement lié au troisième objectif qui vise la quantification de l'incertitude des états initiaux corrigés sur la prévision à court terme de la température de l'eau.

Le quatrième et dernier objectif spécifique suppose que la séparation des processus d'évaporation à la surface de l'eau et d'évapotranspiration en milieu terrestre dans un modèle hydrologique et thermique permettrait de mieux modéliser chacun d'eux et réduirait l'erreur dans les simulations hydrologiques et thermiques subséquentes. Le quatrième objectif est d'évaluer l'incidence du choix de méthode d'estimation de l'évaporation en rivière sur la simulation de la température de l'eau. Cela inclut une évaluation de la pertinence d'une séparation des processus d'évaporation à la surface de l'eau et d'évapotranspiration en milieu terrestre dans un modèle hydrologique et thermique semi-distribué.

Cette thèse se divise en deux parties principales. La première partie offre une synthèse en français des travaux effectués pendant le parcours doctoral. Elle présente de façon succincte le contexte dans lequel ont été effectués les travaux, les objectifs de la thèse, la littérature qui s'y rattache, ainsi que les analyses et résultats inclus dans les trois articles de la partie II. Cette seconde partie de la thèse inclut les trois articles, publiés ou en processus de révision, qui ont été rédigés en anglais dans le cadre des travaux de recherche.

2 REVUE DE LITTÉRATURE

2.1 Prévision de la température de l'eau et incertitude

Les méthodes de modélisation de la température de l'eau en rivière sont abondantes et diffèrent par leur nature, leur structure et leur niveau de complexité (p. ex. Caissie et al., 2005; Morin et Couillard, 1990; Sinokrot et Stefan, 1993). On les divise généralement en deux catégories : les modèles à base physique (ou déterministes) et les modèles empiriques (ou statistiques; voir la revue de littérature de Benyahya et al., 2007). La première catégorie inclut typiquement les modèles qui utilisent les équations de transfert de chaleur et d'écoulement liquide, à partir d'une géométrie de chenal et des conditions météorologiques fournies par l'utilisateur, pour simuler la température de l'eau (Deas et Lowney, 2000). La seconde catégorie inclut les modèles qui se basent sur une relation statistique entre la température de l'eau et une ou plusieurs caractéristiques du système, comme la température et de l'air ou le débit, par exemple (Benyahya et al., 2007; Deas et Lowney, 2000). Malgré cette large classification, bien des modèles empruntent des concepts aux deux catégories. Dans certains cas, une troisième catégorie, nommée modèles mixtes, est ajoutée pour inclure ces modèles, comme par exemple, le modèle Air2Stream (Toffolon et Piccolroaz, 2015).

Chacune de ces catégories présente ses avantages et ses faiblesses. Les modèles à base physique prennent mieux en compte les processus inhérents au bilan thermique d'un cours d'eau (Cole et al, 2014). Cela permet de mieux représenter les impacts sur l'ensemble du bilan thermique d'un changement qui affecterait l'un de ces processus. Par ailleurs, cette bonne représentation des processus thermiques leur confère une meilleure transférabilité comparativement aux modèles empiriques. En revanche, ce type de modèle nécessite une grande quantité d'intrants (variables météorologiques, utilisation du sol et géométrie du chenal). Ces modèles sont donc plus difficiles à mettre en place sur un système donné que leurs homologues empiriques. Les modèles empiriques présentent quant à eux l'avantage de souvent nécessiter moins de données en intrants que les modèles déterministes. La température de l'air et le débit sont les variables les plus fréquemment mises en relation avec la température de l'eau. Cette

relation, spécifique au site, est difficilement transférable spatialement et temporellement.

Malgré sa pertinence pour la gestion des rivières, l'émission de prévisions à court terme de la température de l'eau en rivière demeure marginale. Depuis le début des années 2000, quelques publications, orientées vers une problématique de gestion, ont traité de la prévision thermique.

2.1.1 Prévision et incertitude

La projection dans l'avenir d'un système naturel est intrinsèquement incertaine (Toth et Kalnay, 1993). Le recours à un modèle prévisionnel permet de réduire l'importance de cette incertitude, mais ne permet en aucun cas de l'éliminer complètement (Krzysztofowicz, 2001). Dans un système météorologique, cette incertitude provient, de manière générale, du modèle utilisé (formulation, structure et paramètres), des intrants qui lui sont fournis et des conditions initiales du système modélisé (Orrell et al, 2001). L'une des thèses de plus en plus acceptée dans la communauté scientifique suggère qu'une quantification, suivie d'une bonne communication, de cette incertitude résiduelle induit un caractère scientifiquement plus honnête à la prévision (Cloke et Pappenberger, 2009; Krzysztofowicz, 2001; Schaake et al., 2007). Cela permet de chiffrer le degré de confiance, exprimé sous forme de probabilité, que l'on peut raisonnablement avoir envers une prévision. Une méthode éprouvée pour faire cela est la production de prévisions d'ensemble (p. ex. Molteni et al., 1996). Cette méthode peut être décrite comme étant la réalisation de multiples prévisions pour lesquelles les intrants, les conditions initiales ou encore les composantes du modèle ont été légèrement perturbées. À chaque pas de temps, pour chacune des variables prévues, une distribution de valeurs de la variable d'intérêt est produite (Roulin, 2007). Cette distribution permet de passer d'une prévision strictement déterministe (une seule valeur prédite) à une prévision probabiliste (une distribution de valeurs prédites) dont les valeurs individuelles sont appelées « membres ».

2.1.2 Prévision hydrologique

Depuis une vingtaine d'années, plusieurs travaux ont porté sur la représentation de l'incertitude dans la prévision hydrologique (Cloke et Pappenberger, 2009). Le cadre théorique de la prévision hydrologique probabiliste est d'ailleurs largement inspiré des travaux préalablement effectués en sciences de l'atmosphère (Gneiting et Raftery, 2007). L'une des façons les plus communes pour caractériser l'incertitude hydrologique est la production d'ensembles à partir de prévisions d'ensembles météorologiques. Pour y arriver, les ensembles météorologiques sont fournis à un ou plusieurs modèles hydrologiques pour produire des ensembles hydrologiques. Cette méthode s'est récemment méritée une grande attention de la part des prévisionnistes de crues (p. ex. Fleming et al., 2015; Matte et al., 2017; Stephens et Cloke, 2014; Thielen et al., 2009). Il en résulte une distribution de probabilité à partir de laquelle un risque d'occurrence peut être calculé (Roulin, 2007). Le recours à des méthodes multimodèles s'est montré efficace pour représenter l'incertitude structurale de la prévision hydrologique (p ex. Clark et al., 2015; Duan et al., 2007; Thiboult et al., 2016; Velázquez et al., 2011). Dans un tel cas, les intrants météorologiques provenant d'un ou de plusieurs modèles atmosphériques sont fournis à plusieurs modèles hydrologiques, ou au même modèle dont la structure a été modifiée.

Enfin, on compte les méthodes d'assimilation de données. L'assimilation de données peut être décrite comme étant une correction des variables d'état d'un modèle à partir de l'information disponible (p. ex. débit) sur le système. Cette méthode est couramment utilisée pour corriger les conditions initiales d'un système hydrologique avant d'émettre une prévision (Liu et al., 2012). Des méthode d'assimilation de données ont été développées et testées dans un cadre hydrologique afin de corriger les conditions initiales d'un système hydrologique. Certaines variantes peuvent être utilisées pour quantifier l'incertitude que les erreurs d'estimation de ces conditions initiales peuvent propager vers la prévision. Ce dernier thème sera abordé plus en détails à la section 2.2.

Le passage d'un cadre déterministe à un cadre probabiliste requiert un ajustement des indicateurs de performance pour tenir compte de distributions plutôt que de valeurs

ponctuelles. Pour ce faire, une panoplie d'outils existe pour évaluer certaines caractéristiques importantes de la prévision telles que l'exactitude, la fiabilité, le dépassement de seuil et la dispersion (p. ex. Gneiting et Raftery, 2007; Hersbach, 2000; Laio et Tamea, 2007). On distingue notamment les outils numériques, locaux et globaux, de même que les outils graphiques. Plusieurs publications récentes se sont intéressées à la question spécifique des outils de validation de la prévision (p. ex. Casati et al., 2008; Ebert et al., 2013; Wilks, 2011). Une liste des indicateurs les plus communément rencontrés dans la littérature associée aux prévisions d'ensemble est colligée au Tableau 2.1.

Tableau 2.1 Indicateurs de performance pour la prévision

Indicateur	Caractéristique vérifiée	Type	Prévision	Référence
Biais	Biais	Numérique	Ensemble et déterministe	---
CRPS	Exactitude et fiabilité	Numérique	Ensemble	Matheson et Winkler (1976)
Diagramme de fiabilité	Fiabilité et dispersion	Graphique	Ensemble	Stanski (1989)
Histogramme de rangs	Dispersion	Graphique	Ensemble	Hamill (1997) Talagrand (1997)
Erreur moyenne absolue (MAE)	Exactitude	Numérique	Déterministe	---
Score de Brier	Occurrence et non-occurrence	Numérique	Ensemble et déterministe	Brier (1950)
Score log	Exactitude	Numérique	Ensemble	Benedetti (2010)

Bien qu'une description exhaustive de ces scores dépasse le cadre de cette thèse, les plus couramment utilisés sont brièvement décrits ici. Le CRPS (*continuous ranked probability score*) a été utilisé pour évaluer la justesse de la prévision, c'est-à-dire la distance entre la prévision et l'observation. Le diagramme de fiabilité a été utilisé pour évaluer la fiabilité de la prévision, c'est-à-dire la qualité de la dispersion de l'ensemble

prévisionnel autour de l'observation. La statistique la plus répandue pour évaluer l'exactitude d'une prévision d'ensemble est le CRPS. Il représente la distance entre la fonction de répartition de la prévision (Figure 2.1 – ligne bleue) et celle de l'observation (Figure 2.1 – ligne noire). L'aire de la partie illustrée en gris sur la Figure 2.1 correspond donc à la valeur du CRPS de la prévision. Sa popularité tient notamment du fait qu'il est l'analogue probabiliste de l'erreur moyenne absolue (MAE) d'une prévision déterministe (p. ex. Boucher et al., 2011; Figure 2.1) et qu'il s'exprime dans l'unité de la variable d'intérêt. Il s'agit d'un score global et juste, qui tient compte de l'ensemble de la distribution (Gneiting et Raftery, 2007). Un score est dit « juste », ou « *proper* » en anglais, lorsqu'on peut démontrer mathématiquement que la seule façon pour un prévisionniste d'optimiser son score est d'émettre une prévision qui correspond vraiment à ce qu'il croit. La distribution de cette prévision se doit d'en maximiser la précision et représenter son incertitude réelle, donc d'être centrée sur l'observation (Gneiting & Raftery, 2007). Par exemple, une telle démonstration pour le score de Brier (Brier, 1950) est disponible dans Wilks (2010). Lorsqu'un score n'est pas juste, par exemple le score linéaire (Wilson et al., 1999), il existe une façon de le « déjouer ». Dans un tel cas, le risque existe qu'une prévision calibrée à partir de ce score ne soit pas la plus performante. Le prévisionniste a alors avantage à faire fi de ce qu'il croit être la vérité et émettre systématiquement certains types de prévisions.
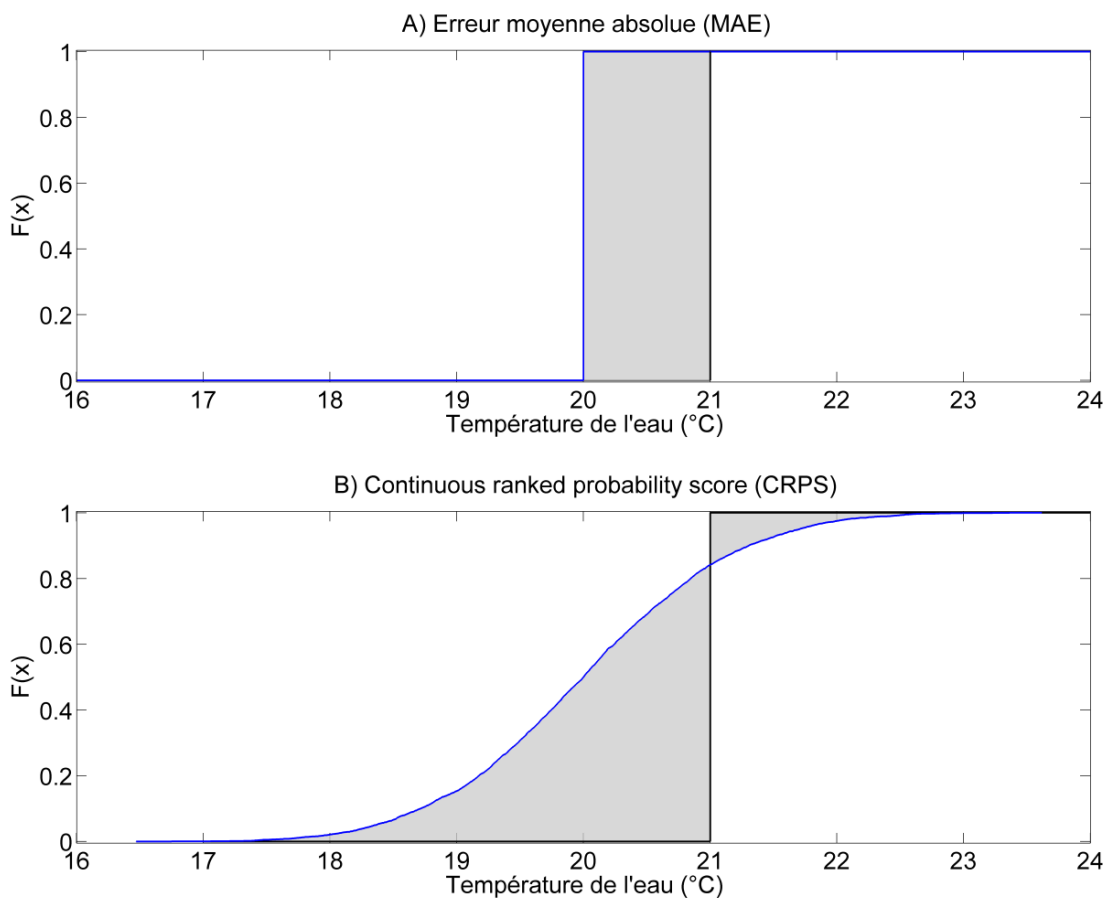
Figure 2.1 Exemple A) de MAE (erreur moyenne absolue) et B) de CRPS (*Continuous ranked probability score*)

L'une des caractéristiques importantes d'une prévision d'ensemble est sa fiabilité. Elle informe l'utilisateur quant à la qualité de la dispersion de l'ensemble ainsi que, comme son nom l'indique, sa fiabilité. La fiabilité peut être décrite comme la cohérence statistique entre les propriétés d'une prévision probabiliste et des observations correspondantes (Bröcker et Smith, 2007; Hersbach, 2000b). Le diagramme de fiabilité (Figure 2.2) est l'outil le plus communément utilisé pour représenter cette caractéristique (p. ex. Bröcker et Smith, 2007; Franz et al., 2003; Thiboult et al., 2016; Velázquez et al., 2011). Il met en relation la fréquence relative d'occurrence d'un évènement et la fréquence relative de sa prévision. Son fonctionnement se résume par le calcul d'intervalles de confiance pour divers niveaux de confiance (souvent par

incrément de 10 %). On calcule ensuite dans quelle proportion l'observation est comprise à l'intérieur de l'intervalle de confiance. Une prévision est considérée comme étant sur-confiante (et sous dispersée) lorsque la probabilité prévue est supérieure à la probabilité observée. Dans le cas contraire, lorsque la probabilité prévue est inférieure à la probabilité observée, on considère la prévision comme étant sous-confiante (et sur dispersée).
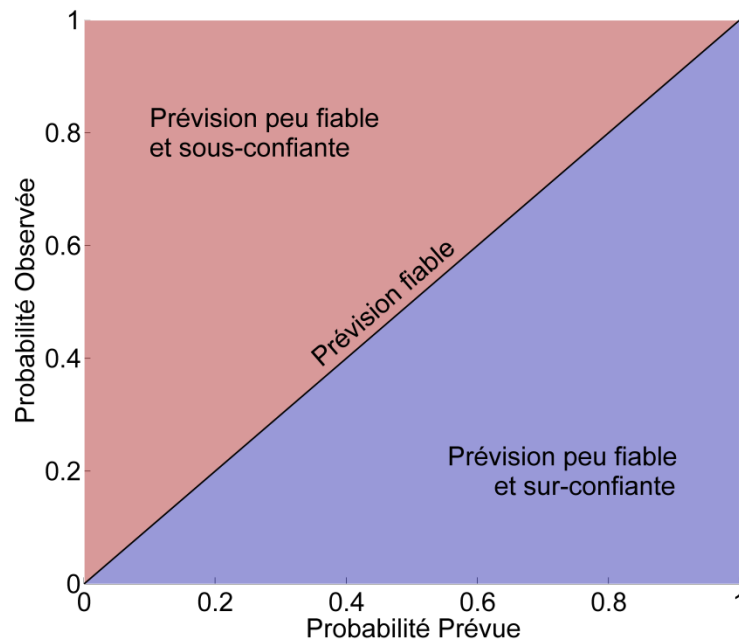
Figure 2.2 Exemple de diagramme de fiabilité.

2.1.3   Prévision thermique

Bien que la littérature qui traite de la prévision de la température de l'eau demeure relativement rare, certaines méthodologies ont été proposées. À titre d'exemple, Neumann et al. (2006) ont proposé un système d'aide à la décision pour la mise en place de mesures d'atténuation d'épisodes de températures de l'eau élevées sur la rivière Truckee au Nevada (États-Unis). Ce système se base sur une prévision à court terme émise à partir d'un modèle de régression linéaire. Par ailleurs, une prévision de

10 jours, basée sur un modèle à base physique, est aussi émise pour l'ensemble du bassin versant du fleuve Fraser pour la gestion des pêches (Morrison et Foreman, 2005). Plus récemment, d'autres méthodes basées sur des modèles statistiques (p.ex. Caissie et al., 2016; Hague et Patterson, 2014; Huang et al., 2011; Mestekemper et al., 2010; Sahoo et al., 2009) et des modèles à base physique (Pike et al., 2013) de prévision ont été proposés.

Le caractère intrinsèquement incertain de la prévision nécessite une quantification de l'incertitude pour une prise en compte dans les processus décisionnels (Krzysztofowicz, 2001). Le cas de l'incertitude dans la prévision de la température de l'eau a été discuté depuis un bon moment dans la littérature scientifique (p. ex. Bartholow, 2003; Danner et al., 2012; Neumann et al., 2006). Pourtant, très peu de publications s'y sont attardées. Les travaux exhaustifs de Pike et al. (2013) proposent un cadre de prévision hydrologique et thermique en temps réel qui tient compte de l'incertitude associée aux intrants météorologiques et aux conditions initiales du bassin versant dans un modèle dynamique stochastique. Hague et Patterson (2014) se sont servis de données historiques de température de l'air, de débits observés et d'une combinaison de prévisions de températures de l'air et de débits décalés (*lagged discharge*) comme intrants à quatre modèles statistiques. Les résultats ont permis de représenter l'incertitude attribuable au choix de modèle statistique et à leurs intrants. Bal et al. (2014) ont quant à eux tenu compte de l'incertitude dans des projections de température de l'eau sur un horizon de 50 ans à l'aide d'une approche bayésienne hiérarchique. Malgré la grande pertinence de ces publications, aucune d'entre elles ne décrit une quantification explicite de la contribution des diverses sources d'incertitude.

2.2 Assimilation de données hydrologiques et thermiques

L'assimilation de données vise à corriger les variables d'état d'un système modélisé grâce aux observations disponibles (Liu et al., 2012). Au moment d'émettre une prévision, l'état actuel du système (p. ex. hydrologique, météorologique, etc.) doit être simulé, définissant ainsi les états initiaux du modèle prévisionnel. L'incertitude des intrants du modèle, et le modèle lui-même (Aronica et al., 1998; Beven et Freer, 2001;

Kelleher et al., 2016), entrainent inévitablement une incertitude quant à ces états simulés. Cette incertitude est ensuite propagée à la prévision (p. ex. Li et al., 2009; Rodriguez-Rincon et al., 2015). Les observations rendues disponibles permettent une correction de ces états afin d'initier la prévision à partir d'une représentation plus réaliste du système d'intérêt, et ainsi de limiter l'incertitude transmise à la prévision subséquente. Les variables d'état et la nature des données assimilées dépendent naturellement de la, ou des, variable(s) d'intérêt et du modèle utilisé. Dans le cas d'une modélisation hydrologique, l'observation la plus fréquemment utilisée dans l'assimilation est le débit, alors que les variables d'état corrigées sont, par exemple, l'humidité du sol, le niveau des réservoirs, la hauteur de neige, etc. Certaines variables, telles que la hauteur de neige, peuvent à la fois être considérées comme une observation à partir de laquelle la correction sera effectuée et de variable d'état qui subira une correction. Cette opposition peut être aussi rencontrée lors de l'assimilation de la température de l'eau. Cette dernière est utilisée pour calculer la quantité d'énergie contenue dans le cours d'eau tout en étant l'observation à partir de laquelle l'assimilation est effectuée. Ce problème peut être contourné à travers la perturbation des intrants météorologiques plutôt que des variables d'état elles-mêmes (p. ex. Clark et al., 2008; Weerts et El Serafy, 2006). Il a été démontré que, dans une prévision hydrologique à court terme (1-2 jours), l'incertitude des conditions initiales est dominante par rapport aux autres sources d'incertitude (Thiboult et al., 2016). Au-delà d'un horizon de 2 jours, l'incertitude associée aux intrants météorologiques doit être prise en compte afin d'assurer une bonne dispersion de l'ensemble (et, par le fait même, des prévisions fiables).

La première tentative, malheureusement ratée, de prévision météorologique numérique a été effectuée à la main par Richardson, en 1917. L'échec de cette prévision a plus tard été attribué à la mauvaise qualité de son estimation des conditions initiales de l'atmosphère. Selon Lynch (2003), si un simple lissage des conditions initiales avait été effectué, la prévision de Richardson aurait été de bien meilleure qualité. Il s'agit du premier exemple documenté de la nécessité de corriger les conditions initiales d'un système avant d'émettre une prévision. Les travaux précurseurs de Lorenz (1963) ont ensuite démontré qu'une petite perturbation des conditions initiales d'un modèle météorologique se propage et s'accentue en fonction de l'horizon de la prévision. Ne

pouvant éliminer toute incertitude de modélisation, sa quantification explicite revêt une importance primordiale. Depuis, plusieurs méthodes systématiques ont été proposées pour réaliser ces corrections dans divers domaines de la prévision (p. ex. Chen et al., 2013; Liu et al., 2012; Reichle, 2008; Thirel et al., 2010; Tsuyuki et Miyoshi, 2007; van Leeuwen, 2009). Parmi les méthodes systématiques les plus courantes pour l'assimilation du débit, on compte le filtre de Kalman d'ensemble (Komma et al., 2008; Papadakis et al., 2010; Pathiraja et al., 2016; Shen et Tang, 2014) et le filtre particulaire (Moradkhani et al., 2012; Noh et al., 2011; Plaza et al., 2012; Seo et al, 2003; van Leeuwen, 2009) ou même la combinaison de ces méthodes (Fan et al., 2017). Les travaux de Weerts et El Serafy (2006) suggèrent une meilleure performance du filtre de Kalman par rapport au filtre particulaire, dans un contexte hydrologique. Toutefois, les travaux de Leisenring et Moradkhani (2011) démontrent plutôt le contraire.

Malgré l'accessibilité de ces méthodes, en hydrologie, plusieurs agences prévisionnelles ont toujours recours à l'altération manuelle des intrants météorologiques (ou insertion manuelle) pour la correction des conditions initiales (Mamono, 2010). L'insertion manuelle présente le désavantage de dépendre largement de l'intuition et du niveau d'expertise du prévisionniste, peut demander beaucoup de temps et rend la procédure plus difficile à documenter et à retracer (Liu et al., 2012).

La prévision de la température de l'eau en temps réel est un champ d'expertise en développement. Jusqu'à présent, peu de travaux se sont intéressés directement à cette problématique. Il en va de même pour l'assimilation de la température de l'eau, sujet pour lequel seulement quelques publications ont pu être recensées. Morrison et Foreman (2005) ont proposé une méthode itérative pour l'assimilation des débits et des températures de l'eau observés sur le fleuve Fraser en Colombie-Britannique. Un facteur de correction est appliqué aux variables d'état du modèle en fonction de l'erreur par rapport aux valeurs observées jusqu'à ce qu'à ce qu'un seuil de tolérance de l'erreur soit atteint. La procédure a permis de réduire l'erreur des conditions initiales de l'ordre de 20-30 % dans le cas de la température de l'eau et de 50-60 % dans le cas du débit. Les travaux de Pike et al. (2013) ont démontré la bonne performance d'un filtre de Kalman d'ensemble pour la correction des conditions initiales, hydrologiques et thermiques, et la prise en compte de l'incertitude dans une prévision horaire d'horizon

72 h sur un tronçon de la rivière Sacramento. On y rapporte une diminution de l'erreur de la prévision de la température de l'eau de 0.5°C à 0.25°C lorsque l'assimilation de données est effectuée. Kim et al. (2014) se sont intéressés à l'assimilation de données de qualité de l'eau, incluant la température, sur le bassin versant de la rivière Kumho (Corée) à l'aide d'un filtre d'ensemble par maximum de vraisemblance et d'un filtre de Kalman d'ensemble. Il en résulte une réduction de l'erreur des conditions initiales de 29 % pour la température de l'eau et de 41 % pour le débit par le biais d'un ensemble de neuf membres. Ces trois études constituent les seuls travaux où l'assimilation de données de température de l'eau est clairement traitée. Il existe donc un fossé considérable entre l'état de la connaissance en assimilation de données et son application en prévision de la température de l'eau.

2.3 Évapotranspiration, évaporation, et modélisation hydrologique et thermique

L'évapotranspiration et l'évaporation constituent deux processus apparentés, mais qui se doivent d'être traités séparément. Dans certains écrits (p. ex. McMahon et al., 2013), le terme évaporation est utilisé pour désigner les processus qui mènent au transfert de molécules d'eau de la surface de la terre (liquide) à l'atmosphère (vapeur d'eau). Toutefois, en hydrologie, cette même définition inclusive est davantage associée au terme évapotranspiration (p. ex. Katerji et Rana, 2011). Ce terme combine la perte d'eau par vaporisation à partir des eaux de surface (évaporation) et des sols non végétalisés (évaporation), aux pertes par transpiration des plantes à travers le flux de vapeur d'eau par leurs stomates. Dans la présente thèse, le terme évapotranspiration sera retenu pour définir l'ensemble des pertes par vaporisation alors que le terme évaporation sera utilisé pour définir la perte d'eau par vaporisation à partir des eaux de surface et des sols non végétalisés.

L'évaporation est principalement guidée par le déficit en pression de vapeur entre l'eau et l'air subjacent, alors que la transpiration végétale dépend à la fois des conditions hydrométéorologiques et des caractéristiques de l'espèce végétale (Ahrens, 2015). Pourtant, des méthodes d'estimation développées pour l'un de ces processus sont

souvent employées pour en estimer l'autre (Xu et Singh, 2000). Par exemple, Winter et al. (1995) ont comparé 11 équations pour déterminer l'évaporation mensuelle du lac Williams au Minnesota. Parmi celles-ci, 10 étaient des équations originalement élaborées pour l'estimation de l'évapotranspiration et une seule était destinée à estimer l'évaporation. Quelle qu'en soit la méthode d'estimation, l'évapotranspiration influence les systèmes hydrologiques de deux façons : i) elle réduit le volume d'eau disponible pour le ruissellement (Jobson, 1980) et ii) elle agit comme un mécanisme de refroidissement par la perte de chaleur latente lors du passage de la phase liquide à la phase gazeuse (Caissie et al., 2007).

Les méthodes d'estimation de l'évapotranspiration sont souvent classées en fonction de leurs intrants (p. ex. Oudin et al., 2005). On compte les équations basées sur la température de l'air (p. ex. Thornthwaite, 1948; Blaney et Criddle, 1950; Linacre, 1977), la radiation solaire (p. ex. Jensen et Haise, 1963; McGuinness et Bordne, 1972), le bilan hydrique (p. ex. Guitjens, 1982), le transfert de masse (p. ex. Harbeck, 1962) et les méthodes mixtes qui combinent des éléments des catégories précédemment nommées (p. ex. Penman, 1948; Monteith, 1965; Priestley et Taylor, 1972).

Quelques études se sont intéressées à la comparaison de méthodes d'estimation de l'évapotranspiration. Pour ce faire, la méthode privilégiée vise à comparer les flux évaporatifs estimés à des mesures de terrain (p. ex. Sumner et Jacobs, 2005; Isabelle et Giroux, 2014). Parmi ces études, quelques-unes se démarquent par leur exhaustivité. Par exemple, Jensen et al. (1990) ont comparé 19 méthodes d'estimation de l'évapotranspiration à 11 sites situés aux États-Unis, au Danemark, au Zaïre et en Australie. Au pas de temps mensuel et journalier, les méthodes mixtes, soit Penman (1948), Kimberly-Penman (Wright, 1982) et Peman-Monteith (Monteith, 1965) ont offert les meilleures performances. En l'absence de mesures sur le terrain, d'autres études (p. ex. Mohan, 1991; Amatya et al., 1995) ont comparé diverses méthodes d'estimation de l'évapotranspiration à une méthode de référence, souvent celle de Penman ou de Penman-Monteith.

Or, ces travaux se limitent à la l'évaluation de la qualité de l'estimation de l'évapotranspiration sans placer celle-ci dans un contexte hydrologique. Malgré la

pertinence de leurs résultats, ils ne peuvent être directement applicables à la modélisation hydrologique Par ailleurs, en raison de contraintes logistiques ou financières, certaines études hydrologiques ne peuvent baser leurs résultats sur des mesures d'évapotranspiration relevées sur le terrain et se fient uniquement à la qualité de simulations hydrologiques subséquentes évaluée grâce aux mesures de débits (p. ex. Parmele, 1972; Andersson, 1992).

Barr et al. (1997) ont comparé les méthodes de Morton (1983), de Granger (1989) et l de Spittlehouse (1989) dans le modèle hydrologique semi-distribué SLURP (*Semi-distributed Land Use-based Runoff Processes*). Ils en arrivent à la conclusion que la méthode de Spittlehouse permet une meilleure reproduction des débits et tient compte plus adéquatement des processus physiques de l'évapotranspiration, dont la fluctuation de l'eau disponible dans le sol. Toutefois, cette méthode demande une connaissance de l'humidité du sol extractible par le système racinaire et du point de flétrissement du couvert végétal, ce qui peut rendre son application difficile puisque des mesures *in situ* de ces variables sont rarement disponibles. Par ailleurs, les travaux de Parmele (1972) ont démontré qu'une précision de ± 20 % dans l'estimation de l'évapotranspiration est suffisante dans un processus de modélisation hydrologique. Un travail du même acabit effectué par Andersson (1992) suggère que l'utilisation de l'équation de Penman (1948), celle de Thornthwaite (1948) ou l'utilisation d'une valeur mensuelle moyenne d'évapotranspiration qui découle de l'équation de Penman entraîne une différence marginale quant à la modélisation hydrologique effectuée avec le modèle HBV (*Hydrologiska Byråns Vattenbalansavdelning*). Toutefois, ce type de conclusion peut suggérer que les bons résultats de simulation sont obtenus grâce à des éléments compensatoires tels que l'ajustement de paramètres, et non grâce à une bonne modélisation du processus auquel on s'intéresse (e.g. Kirchner, 2006; Savenije, 2009). Dans un esprit similaire, Oudin et al. (2005) ont dressé une liste de 27 équations fréquemment rencontrées dans la littérature. Celles-ci ont été comparées sur la base des performances de quatre modèles hydrologiques calés sur 308 bassins versants français, australiens et états-uniens. Cette étude a permis de mettre de l'avant l'efficacité équivalente de certaines méthodes qui nécessitent peu de données météorologiques, dont la méthode de McGuinness et Bordne (1972), comparativement

à des méthodes qui demandent davantage de données comme celle de Penman-Monteith (Monteith, 1965).

De la même façon que pour l'évapotranspiration, les méthodes d'estimation de l'évaporation sont nombreuses (p. ex. Singh et Xu, 1997; Xu et Singh, 2000; Rosenberry et al., 2007) et peuvent être classifiées. Par exemple, Xu et Singh (2000) classent ces méthodes en sept catégories : empiriques, bilan hydrologique, bilan d'énergie, transfert de masse, combinatoires, radiation et par mesures directes.

L'évaporation dépend principalement de la température de l'eau, qui influence la pression de vapeur à sa surface, de la pression de vapeur de l'air, dictée par son humidité relative et sa température, et de la vitesse du vent au-dessus de la surface de l'eau. Plusieurs équations d'évaporation ont été développées pour reproduire l'évaporation à la surface de lacs (Rosenberry et al., 2007). Toutefois, elles présentent certaines lacunes pour leur utilisation en rivière (Maheu et al., 2014). L'une des méthodes d'estimation de l'évaporation les plus fréquemment rencontrées dans la littérature est la méthode par transfert de masse (p. ex. Jobson, 1980; Singh et Xu, 1997; Guenther et al., 2012). Dans sa forme générale, proposée par Harbeck (1962) pour de grands lacs, l'équation de transfert de masse multiplie le déficit en pression de vapeur de l'air par une fonction de vent, souvent linéaire. Singh et Xu (1997) dressent une liste des variantes de cette équation et en comparent la performance. Bien que ce type d'équation soit utilisé pour l'estimation de l'évaporation en rivière, sa performance dépend d'un ajustement des paramètres propre au site d'étude.

Toutefois, Jobson (1980) relève une sous-estimation de l'évaporation lors de l'implémentation de ce type d'équation en milieu fluvial. Les processus d'évaporation en lac et en milieu fluvial diffèrent, notamment par le *fetch* (distance de parcours du vent en surface libre d'obstacle) moins grand en rivière (Guenther et al., 2012). Par ailleurs, sous certaines conditions météorologiques, l'eau fluviale turbulente s'évapore à un taux plus élevé que l'eau calme (Benner, 1999). Certains auteurs ont utilisé des équations issues de la littérature sans ajustement spécifique de la fonction de vent au site d'étude (p. ex. Hannah et al., 2004; Leach et Moore, 2010). Ce type de calibration nécessite la prise de mesures directes en rivière, ce qui peut être difficile dans certains contextes.

Jobson (1980) ainsi que Guenther et al. (2012) ont ajusté une telle fonction à partir de mesures d'évaporation effectuées à l'aide d'un évaporimètre. Maheu et al. (2014) ont aussi ajusté une fonction de vent similaire à partir de valeurs d'évaporation mesurées à l'aide d'un petit bac flottant. D'autres ont calibré la fonction de vent de l'équation de transfert de masse par un bilan d'énergie (Fulford et Sturm, 1984; Jobson, 1980).

Malgré la reconnaissance de la différence entre les deux processus, les méthodes d'estimation en hydrologie amalgament toujours les termes évapotranspiration et évaporation (p. ex. Savenije, 2004). De nombreux modèles hydrologiques (p. ex. SWAT, CEQUEAU, HYDROTEL, GR4J, TOPMODEL) omettent donc de discriminer la perte d'eau par évapotranspiration et celle par évaporation. Le choix d'une méthode d'estimation de l'évapotranspiration est une source d'incertitude en modélisation hydrologique (p. ex. Thompson et al., 2014). L'évaporation en rivière est, quant à elle, connue pour constituer l'une des deux principales pertes de chaleur en période estivale avec la réémission de rayonnement de grandes longueurs d'ondes (Evans et al., 1998; Webb et Zhang, 1997). On recense dans la littérature des contributions qui dépassent les 30 % (Maheu et al., 2014; Webb et Zhang, 1997) et qui approchent les 100 % (Hannah et al., 2008) des pertes de chaleur totales. Pourtant, il existe un manque de connaissance quant à l'incertitude associée à l'estimation de l'évaporation en rivière, et du flux thermique correspondant, dans le cadre d'une modélisation de la température de l'eau.

3   SYNTHÈSE DES TRAVAUX DE RECHERCHE

L'élément intégrateur de cette thèse est le thème de l'incertitude propagée dans un processus de modélisation et de prévision de la température de l'eau en rivière. La Figure 3.1 présente les différentes parties du travail de recherche effectué et indique comment chacune de ces parties sont interreliées. Les trois sources majeures d'incertitude y sont abordées, soit les intrants météorologiques du modèle (objectif 1), ses conditions initiales (objectif 2) ainsi que la formulation du modèle lui-même

(objectif 3). Le présent chapitre fait la synthèse des travaux de recherche qui ont mené aux publications présentées à la partie II de la thèse.
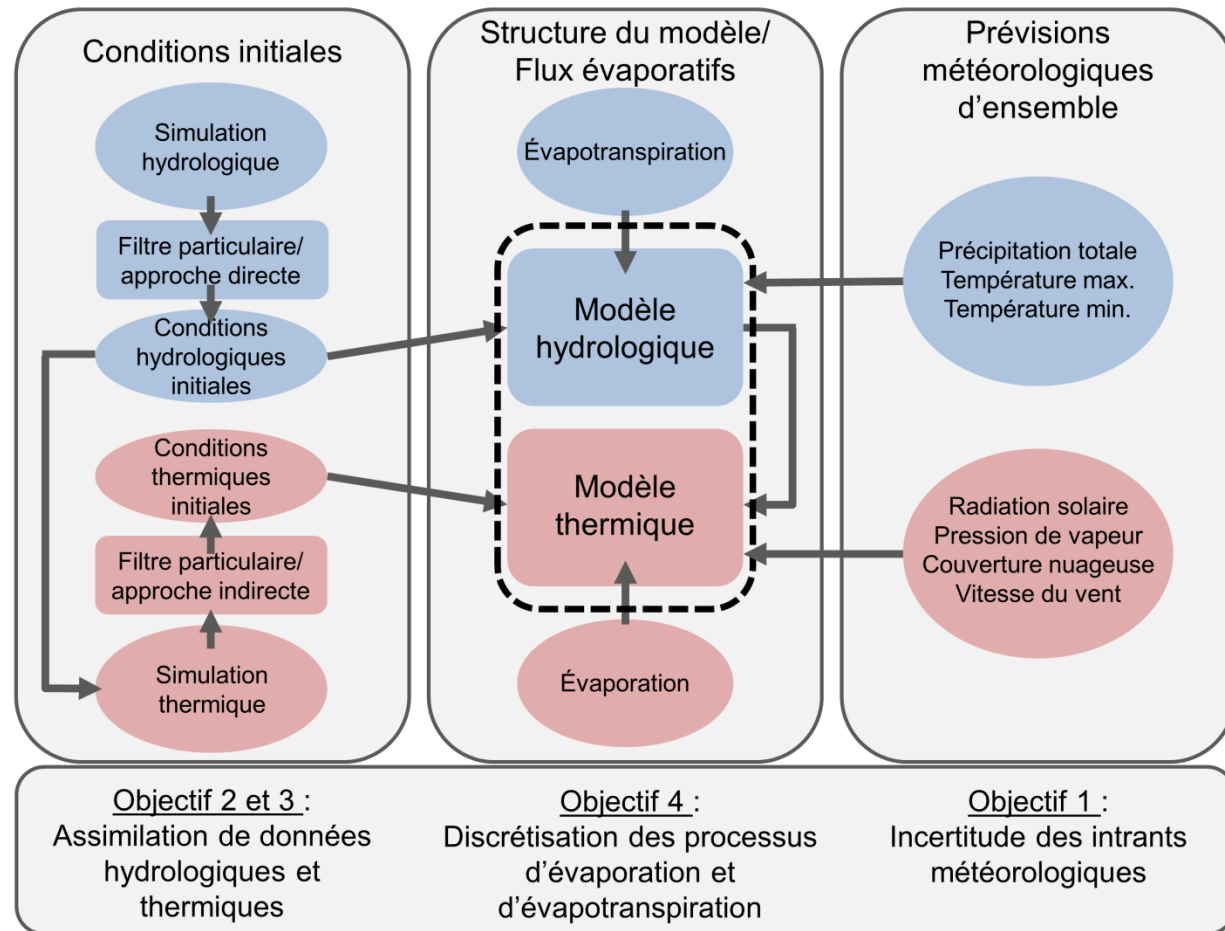
Figure 3.1 Schéma des éléments qui relient les objectifs de la thèse

3.1 Cadre de modélisation hydrologique et thermique

3.1.1 Modèle CEQUEAU

Le modèle hydrologique utilisé tout au long de cette thèse est le modèle hydrologique CEQUEAU (Morin et Paquet, 1995). Il s'agit d'un modèle semi-distribué à réservoirs (Figure 3.2). Il se divise en deux composantes : un module hydrologique est utilisé pour simuler le cheminement de l'eau précipitée à l'intérieur d'un bassin versant, et un module thermique simule la température de l'eau en rivière grâce à un bilan d'énergie.

Lors de sa mise place, le bassin versant d'intérêt est divisé en unités hydrologiques de même taille nommées carreaux entiers. Ces unités sont par la suite subdivisées en carreaux partiels selon la ligne de partage des eaux (Figure 3.3). Lors d'une simulation, l'hydrologie est d'abord simulée sur l'ensemble des carreaux entiers à l'aide d'une fonction de production. Cette fonction de production distribue la précipitation dans les divers réservoirs : (i) sol, (ii) nappe, (iii) lac et marais, et (iv) couvert de neige en milieu non végétalisé et sous couvert forestier sur chacun des carreaux entiers. Ensuite, le volume d'eau produit est partagé entre les carreaux partiels, proportionnellement à leur superficie, et acheminé vers l'aval par une fonction de transfert. La précipitation totale (mm), et la température maximale (°C) et minimale (°C) sont fournies en intrant au modèle hydrologique à chaque pas de temps de simulation (Tableau 3.1). À ceux-ci s'ajoutent la radiation solaire nette (MJ m^{-2}), la pression de vapeur de l'air (mm Hg), la couverture nuageuse (0-1) et la vitesse du vent (km h^{-1}) pour effectuer une simulation thermique.
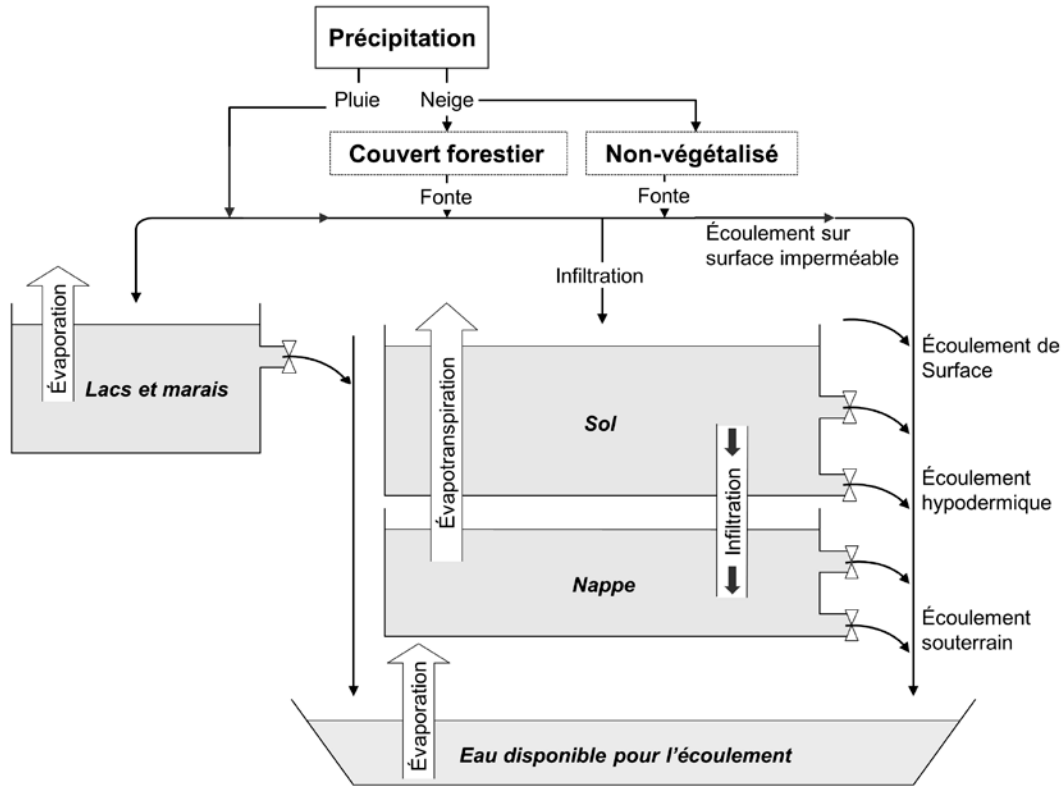
Figure 3.2 Schéma de production du modèle CEQUEAU (tiré de Morin et Paquet, 1995)

Tableau 3.1 Intrants et donnée de validation du modèle CEQUEAU

Intrant	Unités
Hydrométriques	
Débit	$m^3 s^{-1}$
Température de l'eau*	°C
Physiographiques	
Modèle numérique d'altitude	m
Occupation du sol	Lac et rivière, forêts, et marais
Barrage (facultatif)	Type, et règle de gestion ou débit relâché
Météorologiques	
Température de l'air maximale	°C
Température de l'air minimale	°C
Précipitation totale	mm
Radiation solaire nette*	$MJ\ m^{-2}$
Pression de vapeur*	mm Hg
Vitesse du vent*	$m\ s^{-1}$
Nébulosité*	0-1

* Variable propre au modèle thermique

L'hydrologie simulée à chaque pas de temps est ensuite fournie comme intrant au modèle thermique à partir duquel le ratio d'enthalpie (H_{tot} en MJ) sur le produit du volume d'eau (V en m^3) et de la capacité calorifique ($C = 4.187$ MJ m^{-3} $°C^{-1}$) est calculé pour obtenir la température de l'eau (T_w en °C), tel que décrit par l'Equation 3.1 :

$$T_w = \frac{H_{tot}}{VC} \qquad \text{Equation 3.1}$$

L'enthalpie totale (H_{tot} en MJ; Equation 3.2) est calculée par la somme de l'enthalpie initiale (H_{ini}), des flux advectifs (H_{adv}; transfert amont-aval) et des échanges d'énergie à l'interface entre l'air et le cours d'eau.

$$H_{tot} = H_{ini} + H_s + H_{IR} + H_e + H_c + H_{adv} \qquad \text{Equation 3.2}$$

où H_s représente la radiation solaire nette, H_{IR} est la réémission du rayonnement de grandes longueurs d'ondes par le cours d'eau et l'atmosphère, H_e est le flux de chaleur latente dû à l'évaporation et H_c est le flux de chaleur sensible.
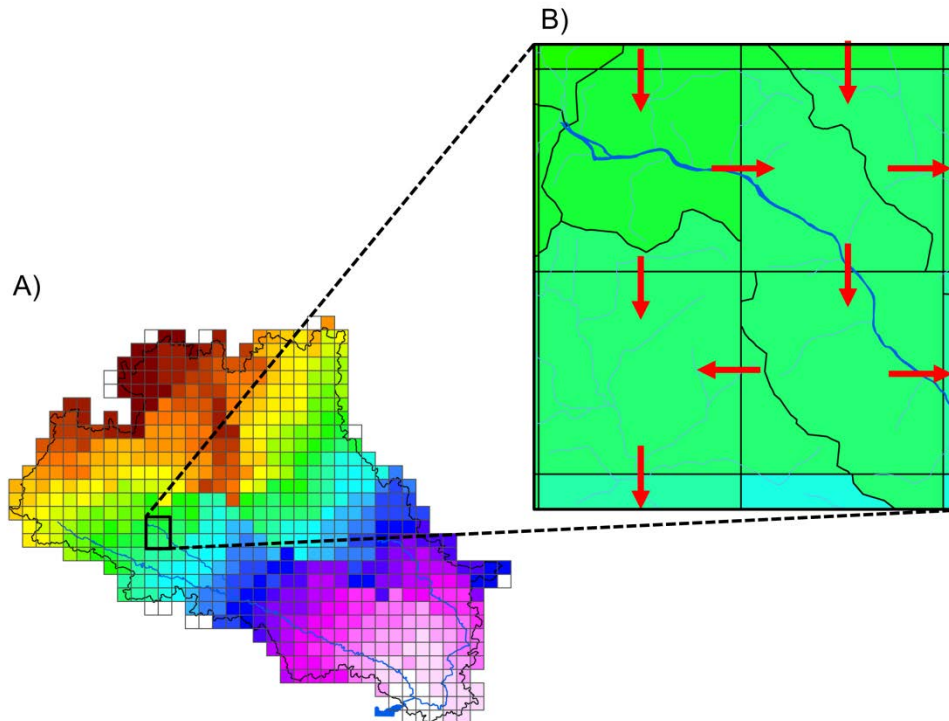
Figure 3.3 Exemple de division d'un bassin versant en A) carreaux entiers et B) carreaux partiels. Les flèches indiquent le sens de l'écoulement, les lignes noires sont les limites de carreaux partiels et la ligne bleue est la rivière.

La composante hydrologique comprend 28 paramètres dont 16 ont un sens physique (modèle de neige, évapotranspiration, transfert amont-aval, etc.) et 12 sont des coefficients qui sont ajustés en fonction de la minimisation de l'erreur du débit simulé (Tableau 3.2). La composante thermique nécessite quant à elle l'ajustement de 12 paramètres. Les modèles distribués ou semi-distribués tel que CEQUEAU sont en général fortement paramétrés (e.g Khakbaz et al., 2012). Cette caractéristique fait en sort qu'une stratégie de calibration doit être mise en place afin d'estimer les paramètres du modèle. Tout au long des travaux de la thèse, l'ajustement des paramètres du

modèle a été optimisé à l'aide de l'algorithme CMA-ES (*covariance matrix adaptation evolution strategy;* Hansen et Ostermeier, 1996).

Le projet dans lequel s'insère la présente thèse a été l'occasion d'apporter des modifications au modèle CEQUEAU. Celles effectuées dans le cadre de cette thèse sont documentées ici. Les autres modifications sont décrites dans St-Hilaire et al. (2015).

Dans sa version originale, seulement la moyenne mensuelle des intrants du module thermique était fournie à CEQUEAU. À partir de celles-ci un cycle annuel était dérivé, permettant une modélisation journalière. Cette caractéristique a été modifiée au cours du présent projet afin de permettre l'utilisation d'intrants météorologiques journaliers. Cela a permis de mieux représenter les échanges thermiques associés aux conditions météorologiques à ce pas de temps.

Par ailleurs, différentes méthodes d'estimation de l'évapotranspiration et de l'évaporation ont été ajoutées en option au modèle afin de remplir le quatrième objectif de la thèse. Ces méthodes sont décrites à la section 3.5.1 de ce document.

Tableau 3.2 Paramètre des composantes hydrologique et thermique du modèle CEQUEAU (adapté de Morin et Paquet, 1995)

Paramètres	Description du paramètre
Paramètres des réservoirs SOL-NAPPE-MARAIS	
CIN	Coefficient d'infiltration du réservoir SOL au réservoir NAPPE
CMAR	Coefficient de vidange du réservoir LACS et MARÉCAGES
CVNB	Coefficient de vidange du réservoir NAPPE (vidange basse)
CVNH	Coefficient de vidange du réservoir NAPPE (vidange haute)
CVSB	Coefficient de vidange du réservoir SOL (vidange basse)
CVSI	Coefficient de vidange du réservoir SOL (vidange intermédiaire)
HINF	Seuil d'infiltration vers le réservoir NAPPE
HINT	Seuil de vidange intermédiaire du réservoir SOL
HMAR	Seuil de vidange du réservoir LACS et MARÉCAGES
HNAP	Seuil de vidange du réservoir NAPPE
HRIMP	Seuil de vidange du réservoir NAPPE
HSOL	Hauteur du réservoir SOL
Paramètres du modèle de fonte	
STRNE	Seuil de transformation pluie-neige
TFC	Taux de fonte en forêt
TFD	Taux de fonte en clairière
TSC	Seuil de température de fonte en forêt
TSD	Seuil de température de fonte en clairière
TTD	Coefficient de déficit calorifique de la neige
TTS	Seuil de mûrissement du stock de neige
Paramètres d'évapotranspiration	
EVNAP	Pourcentage d'évapotranspiration pris dans le réservoir NAPPE
HPOT	Seuil de prélèvement de l'eau à taux potentiel
XAA	Exposant de la formule de Thornthwaite
XIT	Valeur de l'index thermique de Thornthwaite
Paramètre et constante du transfert	
EXXKT	Paramètre d'ajustement du coefficient de transfert
ZN	Temps de concentration du bassin
Paramètres et constates divers	
JOEVA	Date d'insolation potentielle maximale respectivement pour l'évapotranspiration
JONEI	Date d'insolation potentielle maximale respectivement pour la neige
XINFMA	Infiltration maximale par jour
XLA	Latitude moyenne du bassin versant
TRI	Pourcentage de surface imperméable
Modèle thermique	
COPRO	Coefficient permettant de modifier la profondeur minimale du tronçon de rivière pour tous les carreaux partiels.
COLARG	Coefficient permettant de modifier la largeur du tronçon de rivière pour tous les carreaux partiels.
C_s	Coefficient permettant d'augmenter ou de diminuer l'importance du rayonnement solaire dans le bilan d'énergie.
C_i	Coefficient permettant d'augmenter ou de diminuer l'importance du rayonnement infrarouge dans le bilan d'énergie.
C_e	Coefficient permettant d'augmenter ou de diminuer l'importance de l'évaporation dans le bilan d'énergie.
C_c	Coefficient permettant d'augmenter ou de diminuer l'importance de la convection dans le bilan d'énergie.
CRIGEL	Critère de gel vérifié à chaque carreau partiel: si le stock de neige au sol est supérieur à CRIGEL, la température des eaux de ruissellement est fixée à 0°C; si le stock de neige est inférieur à CRIGEL, la température des eaux de ruissellement est linéairement fixée entre 0oC et la température de l'air en fonction du stock; si le stock de neige est nul, les eaux de ruissellement sont supposées être à la température de l'air (CRIGEL est exprimé en mm d'eau).
TNAP	Température moyenne annuelle des eaux souterraines sur le bassin versant (°C).
PANAP	Paramètre permettant d'ajuster la température de l'écoulement souterrain arrivant en rivière. Lorsque PANAP = 0,0, cette température vaut TNAP; lorsque PANAP = 1,0, cette température vaut la température de l'air si positive. PANAP peut être fixé entre 0,0 et 1,0 et son influence est linéaire entre ces deux limites.
TINIT	Température moyenne de l'eau sur l'ensemble du bassin versant estimée au premier jour des simulations (°C).
BASSOL	Lame de précipitation totale permettant de détecter les jours de faible rayonnement solaire (mm d'eau).
CORSOL	Correction du rayonnement solaire moyen (RSM) pour les jours sans pluie et les jours de fortes pluies (varie entre 0,0 et 1,0).

3.2 Sites d'étude

Pour remplir les objectifs énumérés à la section 1, le modèle CEQUEAU a été ajusté sur le bassin versant de la rivière Nechako, en Colombie-Britannique, et celui de la rivière Miramichi, au Nouveau-Brunswick (Figure 3.4). Le bassin de la rivière Nechako couvre une superficie de 47000 km^2 alors que celui de la Miramichi s'étend sur une superficie de 13000 km^2. Les deux bassins sont majoritairement forestiers avec un pourcentage de respectivement 85 % et 75 % de couvert forestier pour Nechako et Miramichi. Ils diffèrent par leur altitude moyenne alors que la rivière Nechako coule à travers le plateau britanno-colombien à une altitude moyenne de 950 m et la rivière Miramichi coule dans les plaines côtières de l'Atlantique à 210 m d'altitude en moyenne. Les principales caractéristiques physiques des bassins versants sont résumées dans le Tableau 3.3. Il s'agit de deux bassins versants largement différents, dont l'un est hautement régulé (Nechako) et l'autre a un régime d'écoulement naturel (Miramichi). Ces rivières ont été sélectionnées comme sites expérimentaux puisqu'elles font toutes deux face à une problématique de température de l'eau estivale élevée. Ces températures engendrent un stress thermique pour les populations de saumons locales. Des mesures d'atténuation sont mises en place afin de limiter le réchauffement ou encore en réduire les effets négatifs sur les organismes aquatiques. Du côté de la rivière Nechako, un seuil supérieur de 20°C guide la gestion des volumes d'eau déversés du réservoir Nechako en période estivale afin d'assurer la conservation du saumon rouge ou Sockeye (*Oncorhynchus nerka*) en période de fraie (Nechako Fisheries Conservation Program [NFCP], 2005). Le bassin versant de la rivière Miramichi abrite quant à lui une population de saumon atlantique (*Salmo salar*). La stratégie de gestion des pêches sur les rivières de ce bassin versant prévoit un seuil de 20°C en ce qui a trait à la température journalière minimale et un seuil de 23°C pour ce qui est de la température journalière maximale (Ministère Pêches et océans Canada [MPO], 2012). Un dépassement de ces conditions a entraîné la fermeture de la pêche dans le passé.

Sur le bassin de la rivière Nechako, les données de débit et de température de l'eau des stations Vanderhoof, Cheslatta Falls et Nautley (Figure 3.4) ont été extraites de la

base de données du Relevé hydrologique du Canada (http://www.ec.gc.ca/rhc-wsc/).
Les données de température de l'eau sur le bassin versant de la rivière Miramichi ont
été extraites de la base de données collaborative RivTemp (http://rivtemp.ca) pour les
stations suivantes (Figure 3.4) : Southwest Miramichi (SWM) à Wades Lodges, Little
Southwest Miramichi (LSWM) à Oxbow, Northwest Miramichi (NWM) à Call Pool et
Catamaran Brook (CAT). Les données de débits ont quant à elles été récupérées de la
base de données de Relevé hydrologique du Canada aux stations suivantes (Figure
3.4) : Southwest Miramichi à Blackville, Little Southwest Miramichi à Lyttleton,
Northwest Miramichi à Trout Brook et Catamaran Brook à Repap Road Bridge.
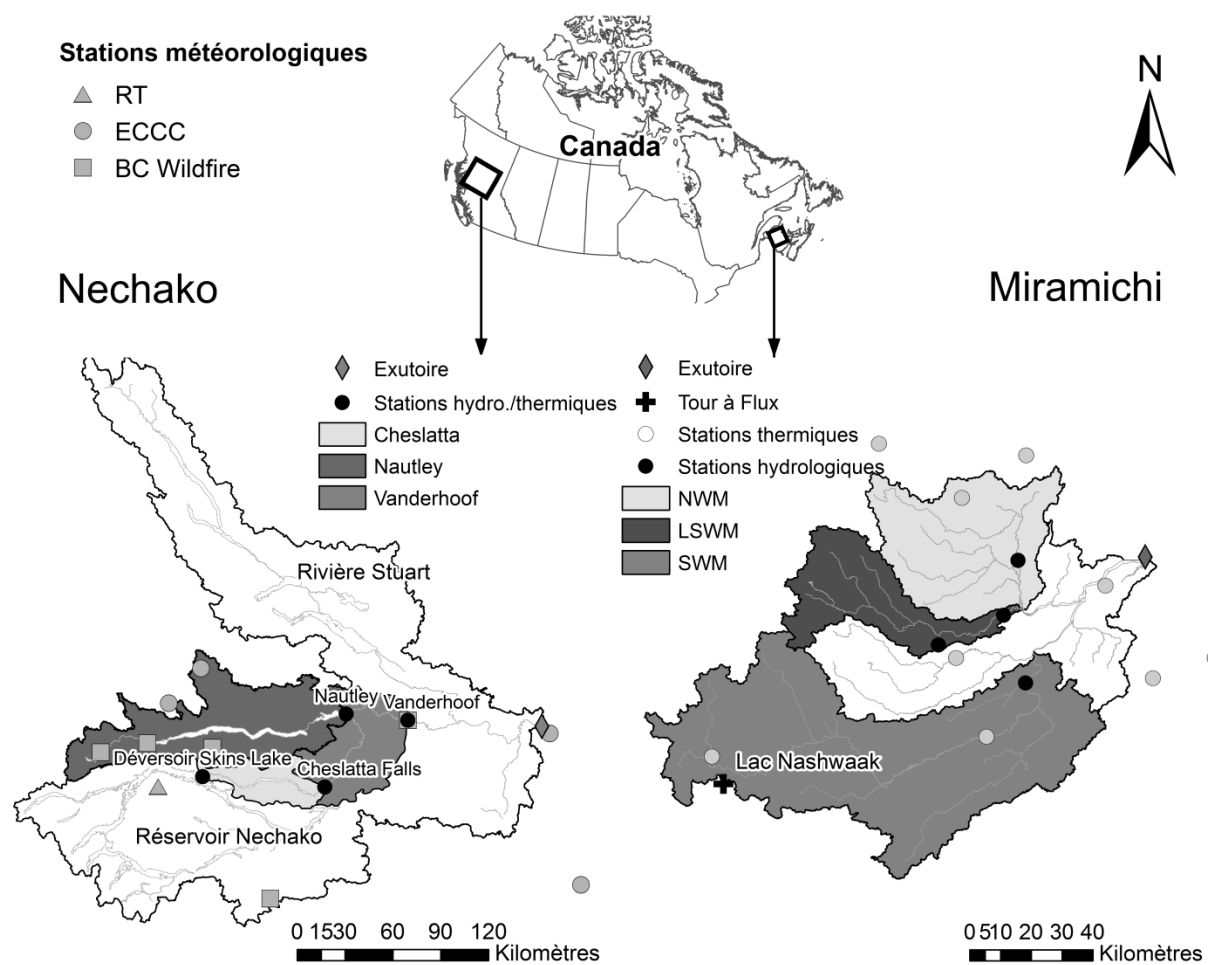
Figure 3.4 Carte des bassins versants de la rivière Nechako et de la rivière Miramichi.

28

Tableau 3.3 Caractéristiques physiques des deux bassins versants analysés dans la thèse. Les débits sont ceux mesurés à Vanderhoof (Nechako) et Southwest Miramichi à Blackville (Miramichi) par le relevé hydrologique du Canada. Les données climatiques proviennent des stations météorologiques de Ootsa Lake (Nechako) et Miramichi A (Miramichi) d'Environnement Canada.

Caractéristique	Nechako	Miramichi
Taille du bassin versant (km^2)	47000	13000
Altitude moyenne (m)	950	210
Température de l'air annuelle moyenne (°C)	3.2	4.9
Précipitations annuelle (mm)	417	1072
Type d'écoulement	Régulé	Non-régulé
Débit moyen (m^3/s)	121	120
Débit minimal (m^3/s)	30	11
Débit maximal (m^3/s)	786	2190
Pourcentage de forêt (%)	85	75

3.3 Prévision de la température de l'eau et incertitude des intrants

Le premier objectif de la thèse est la quantification de l'incertitude associée aux intrants météorologiques qui se propage à la prévision à court terme de la température de l'eau. Dans cette partie, (1) on présente un cadre de modélisation qui sera utilisé pour produire des prévisions à court terme (5 jours) de la température de l'eau dans deux contextes hydrologiques différents soit (a) un système hydrologique hautement régulé et (b) un système naturel; (2) on quantifie l'incertitude associée à huit intrants météorologiques qui se propagent à une prévision de la température de l'eau; et (3) on compare la propagation de cette incertitude dans un système régulé et un système non régulé. Dans la cadre de la thèse, l'ensemble des simulations et des prévisions qui ont été réalisées, l'ont été fait à un pas de temps journalier. Les débits et les températures de l'eau sont donc des moyennes journalières.

3.3.1 Méthodologie

Les bassins versants de la rivière Nechako et de la rivière Southwest Miramichi, présentés à la section 5.1.2.5, ont été utilisés pour répondre aux objectifs de la présente section.

Des prévisions d'ensemble de débit et de température de l'eau, d'horizons allant de un (hz1) à cinq (hz5) jours, ont été produites sur ces deux bassins versants pour la période du 15 juin au 15 septembre des années 2009 à 2014 inclusivement. Afin de représenter l'incertitude transmise par les intrants météorologiques à la prévision de la température de l'eau, des prévisions météorologiques d'ensemble ont été fournies en intrants au modèle CEQUEAU. En raison de la structure du modèle CEQUEAU, la prévision est effectuée dans une cascade où, à chacun des pas de temps, l'hydrologie est d'abord simulée et fournie en intrant au module thermique. Les prévisions d'ensemble produites par le Centre météorologique canadien (CMC) ont été utilisées pour tous les intrants des modules hydrologique et thermique mis à part la radiation solaire, qui n'était pas disponible. Pour pallier ce manque, les prévisions de radiation produite par le Centre européen pour les prévisions météorologiques à moyen terme (ECMWF en anglais) ont été utilisées. Les prévisions du CMC sont formées de 20 membres alors que celles de l'ECMWF en comptent 50. Un jeu de 20 membres a donc été échantillonné de façon aléatoire afin d'assurer la correspondance entre les deux sources de prévisions. Toutes les prévisions météorologiques ont été extraites du portail TIGGE (*The Observing System Research and Predictability Experiment (THORPEX) Interactive Grand Global Ensemble portal*). Le CRPS (Matheson et Winkler, 1976) a été utilisé pour évaluer la performance des prévisions météorologiques fournies au modèle CEQUEAU ainsi que les prévisions hydrologiques et thermiques résultantes. En plus de ce score, l'indice de Brier (Brier, 1950) a permis de vérifier la capacité du système de prévision à prévoir le dépassement ou le non-dépassement du seuil d'intérêt. Dans ce cas-ci, un score de 0 indique une capacité parfaite à prédire le seuil alors qu'un score de 1 démontre le contraire. Des seuils de 18°C (température élevée) et 20°C (température critique; tolérance du saumon rouge) ont été évalués pour la rivière Nechako (Martins et al., 2012) et de 20°C (température élevée) et 23°C (température critique; tolérance du

saumon atlantique) pour la rivière Miramichi (MPO, 2012). Des diagrammes de fiabilité ont aussi été produits afin de rendre compte de la dispersion des ensembles et de leur fiabilité statistique.

3.3.2 Résultats

Les paramètres du modèle CEQUEAU ont été ajustés avec succès (Tableau 3.3). L'ajustement du modèle hydrologique a permis d'obtenir des valeurs du critère d'efficacité de Nash-Sutcliffe (NSE; Nash et Sutcliffe, 1970) au-dessus de 0,7 sur les deux bassins versants sur les périodes de calibration et de validation. Sur le bassin de la Miramichi, les débits moyens sont respectivement de 110 m^3/s et de 139 m^3/s en calibration et en validation. Dans le cas de la Nechako, les débits moyens sont respectivement de 111 m^3/s et de 129 m^3/s en calibration et en validation. On remarque des performances légèrement meilleures sur le bassin versant de la rivière Nechako (régulé) que sur celui de la rivière Miramichi (non régulé). Dans le cas du modèle thermique, on obtient des valeurs de la racine carrée de l'erreur quadratique moyenne (RMSE) en dessous de 1,6°C sur les deux bassins versants, en calibration et en validation, que ce soit pour l'ensemble de l'année ou uniquement pour la période estivale.

Tableau 3.4 Résultats de la calibration des modèles hydrologique et thermique sur les bassins versants des rivières Nechako (NECH) et Miramichi (MIR)

	Débit						Température de l'eau							
	Année						Année				Été			
	NSE		Biais (m^3/s)		Biais Relatif		RMSE (°C)		Biais (°C)		RMSE (°C)		Biais (°C)	
Période	NECH	MIR	NECH	MIR	NECH	MIR	NECH	MIR	NECH	MIR	NECH	MIR	NECH	MIR
Calibration MIR : 2000-2005 Nech : 2002-2006	0,96	0,84	8,87	-3,03	0,08	0,03	1,38	1,37	0,24	-0,54	0,78	1,23	0,43	-0,76
Validation MIR : 2006-2010 Nech : 2007-2010	0,86	0,72	-10,4	-18,6	0,08	0,13	1,54	1,51	0,2	0,09	0,95	1,46	0,37	0,18

Tel qu'illustré au Tableau 3.4, le CRPS calculé sur la prévision de la précipitation totale journalière est relativement faible sur les deux bassins versants pour les cinq horizons, allant de 0,7 mm (hz1 - Nechako) à 3,0 mm (hz5 – Miramichi). Dans le cas du

rayonnement solaire, le CRPS varie entre 2,32 MJ/m^2 (hz1- Miramichi) et 3,75 MJ/m^2 (hz5 - Miramichi). Pour ce qui est de la température de l'air, impliquée dans la modélisation hydrologique et thermique, on obtient un CRPS qui varie entre 1,97 et 3,80°C pour la température minimale journalière comparativement à 1,35 à 1,81°C pour la température maximale.

Tableau 3.5 CRPS calculé entre les prévisions météorologiques d'ensemble et les observations sur le bassin versant de la rivière Nechako (NECH) et celui de la rivière Southwest Miramichi (MIR).

	Hz1		Hz2		Hz3		Hz4		Hz5	
	NECH	MIR	NECH	MIR	NECH	MIR	NECH	MIR	NECH	MIR
t_{min} (°C)	3,30	1,97	3,50	2,14	3,70	2,25	3,70	2,26	3,80	2,47
t_{max} (°C)	1,60	1,35	1,50	1,42	1,60	1,53	1,60	1,66	1,80	1,81
$pTot$ (mm)	0,70	2,03	1,00	2,18	1,60	2,04	2,00	2,87	2,80	3,00
R_S (MJ/m^2)	2,50	2,32	2,50	2,40	2,50	2,76	2,70	3,75	3,10	3,25
CC (0-1)	0,15	0,16	0,14	0,16	0,14	0,17	0,14	0,18	0,15	0,19
U (km/h)	1,35	2,13	1,36	2,05	1,34	2,07	1,29	2,18	1,55	2,16
e_a (mm Hg)	3,17	1,24	3,10	1,19	3,04	1,19	2,96	1,22	3,06	1,28

La première étape de la cascade prévisionnelle (hydrologique et thermique) est la prévision du débit. On remarque (Section 5.1; Figure 5.4) que très peu d'incertitude (< 1 m^3/s [hz1]; 6 m^3/s [hz5]) est transmise de la prévision météorologique à la prévision du débit dans le système régulé (Nechako). Il en résulte un CRPS qui varie entre 17,1 m^3/s (hz1) et 21,4 m^3/s (hz5), pour un débit moyen estival de 214 m^3/s (2009-2014). Ces valeurs de CRPS sont très près de la valeur de la MAE en simulation (17,7 m^3/s). Sur le système naturel (Miramichi), la dispersion de l'ensemble est beaucoup plus grande (4 m^3/s [hz1]; 125 m^3/s [hz5]). Cela se traduit par des valeurs de CRPS plus élevées qui varient entre 31,7 m^3/s et 34,4 m^3/s avec un débit moyen estival de 89 m^3/s (2009-2014).

L'incertitude de la prévision hydrologique en écoulement naturel (Miramichi) se propage à la prévision thermique. La dispersion de l'ensemble prévisionnel de la température de l'eau varie de 0,73°C (hz1) à 2,29°C (hz5) dans le système régulé (Nechako) et de

0,92°C (hz1) à 3,14°C (hz5) dans le système naturel (Miramichi). La propagation de cette incertitude fait passer le CRPS de 0,77°C (0,92°C) pour hz1 à 0,82°C (1,00°C) pour hz5 sur la rivière Nechako (Miramichi). La capacité du système prévisionnel à prévoir un dépassement de seuil est évaluée grâce à l'indice de Brier (1950). Sur la rivière Nechako, pour un seuil de 18°C, on obtient des valeurs qui passent de 0,15 pour hz1 à 0,13 pour hz5. Ces valeurs passent à 0,01 et 0,02, respectivement pour hz1 et hz5, pour un seuil critique de 20°C. Sur la Miramichi, l'indice de Brier atteint 0,15 pour hz1 et hz5. Il s'abaisse à respectivement 0,05 et 0,06 pour une température critique de 23°C.

Les diagrammes de fiabilité de la Figure 3.5 démontrent l'amélioration de la fiabilité en fonction de l'horizon de prévision sur les deux bassins versants. Malgré cette amélioration, l'emplacement des courbes de fiabilité (en dessous de la bissectrice) suggère une sous-dispersion des ensembles, et donc une faible fiabilité. Une partie de l'incertitude de la prévision n'y est donc pas représentée.
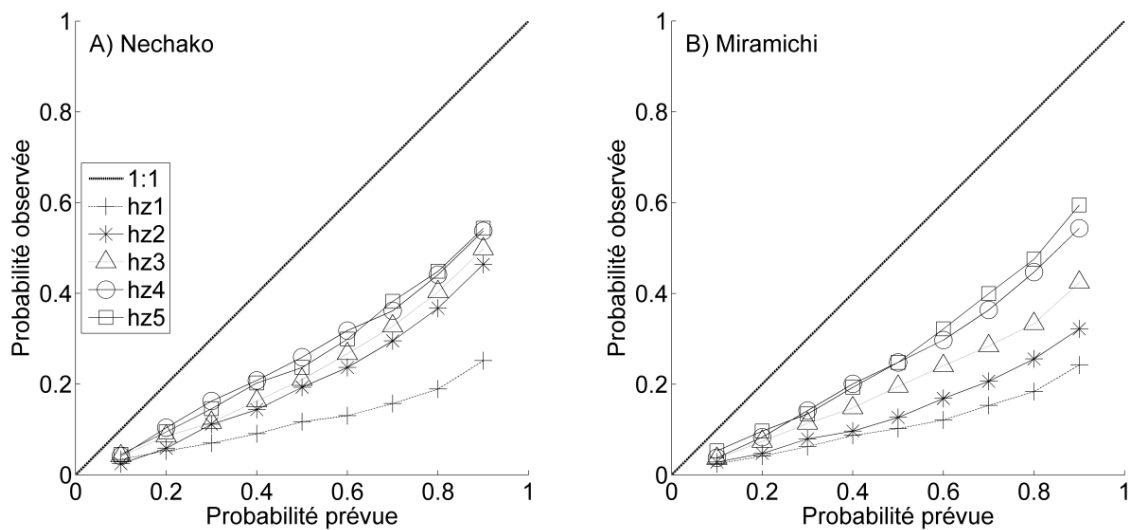
Figure 3.5 Diagramme de fiabilité pour les prévisions de température de l'eau sur A) la rivière Nechako et B) la rivière Miramichi.

3.4 Assimilation de données hydrologiques et thermiques

Le deuxième et le troisième objectifs de la thèse visent à utiliser une méthode d'assimilation des données, c'est-à-dire la correction des états initiaux, hydrologiques et thermiques, d'un modèle semi-distribué avant l'émission d'une prévision. Cela comprend les objectifs implicites suivant : 1) effectuer l'assimilation de données de débits et de températures de l'eau à l'aide d'un filtre particulaire; 2) produire une prévision de débit et de température de l'eau qui tient de compte de l'incertitude des conditions initiales; et 3) quantifier l'incertitude associée à cette prévision. Une approche jamais utilisée au préalable en prévision thermique, les filtres particulaires, a été privilégiée dans ce volet de la thèse. Les filtres particulaires constituent une méthode spécialement intéressante pour les problèmes hydrologiques puisqu'ils n'exigent pas la linéarité du système (p. ex. Doucet et al., 2000) et ne présument pas que les états du modèle et l'erreur des observations suivent une distribution de densité de probabilité spécifique (p. ex. Moradkhani et al., 2005; Weerts et El Serafy, 2006).

3.4.1   Méthodologie

Le bassin versant de la rivière Nechako a été utilisé pour répondre aux objectifs de cette section. Seulement un bassin versant a été utilisé pour réaliser cet objectif en raison du travail plus conséquent y étant associé. Le lecteur peut se référer à la section 5.1.2.5 pour une description complète des caractéristiques du bassin versant.

On propose l'utilisation de filtres particulaires pour effectuer l'assimilation des données de débit et de température de l'eau. Dans ce contexte, ils permettront de 1) corriger les conditions initiales avant une prévision hydrologique et thermique, et 2) représenter l'incertitude de ces conditions initiales qui se propagent à la prévision. Le cadre théorique du filtre particulaire s'appuie sur l'hypothèse qu'une distribution de probabilité *a priori* peut être estimée à partir d'un grand nombre d'échantillons aléatoires de vecteurs d'état, appelés particules (van Leeuwen, 2009; Weerts et El Serafy, 2006). Il s'ancre dans le théorème de Bayes pour l'estimation d'une probabilité conditionnelle *a*

posteriori $p\left(X_t \middle| y_{1:t}\right)$ d'obtenir un état modélisé X_t selon l'observation y_t aux pas de temps $1:t$. Cet état modélisé peut ensuite être mis à jour en combinant l'information préalable (p. ex. débit modélisé à partir des états X_t) à la nouvelle information (p. ex. nouvelle mesure de débits).
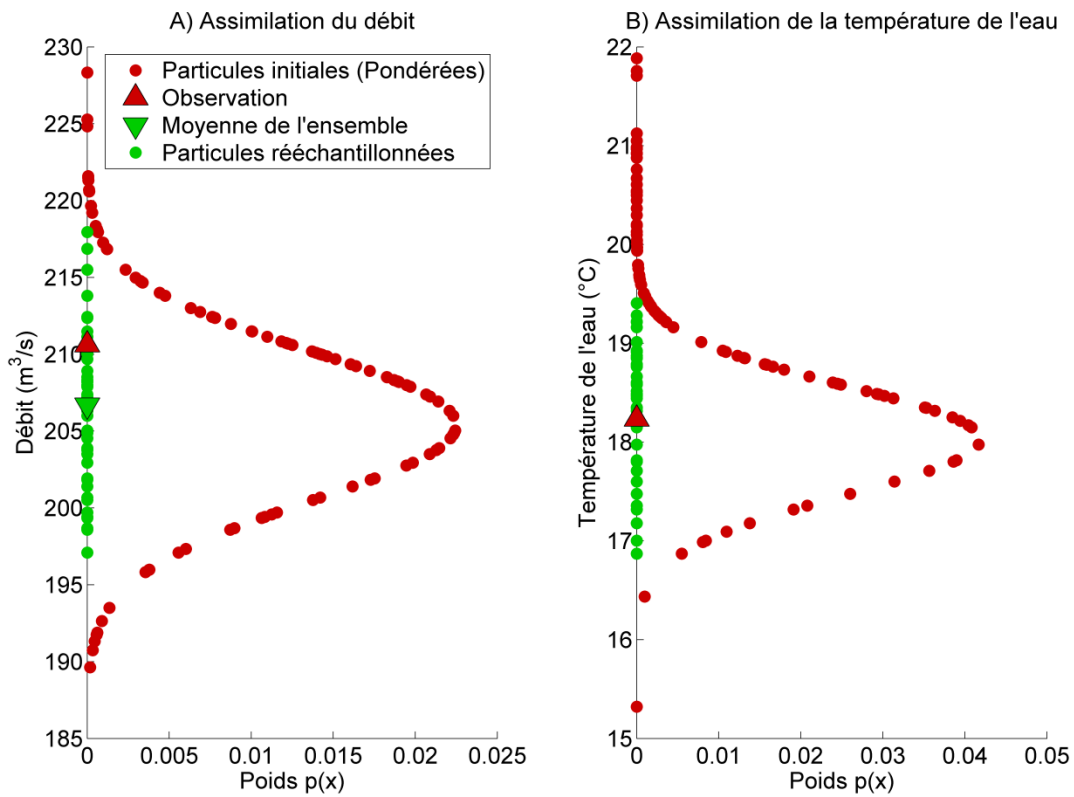
Figure 3.6 Exemple de la cascade d'assimilation de données de A) débits et B) de température de l'eau.

Un échantillonnage aléatoire des variables d'état est d'abord effectué pour créer les états initiaux de base du pas de temps d'intérêt (Figure 3.6). Ces particules sont utilisées pour effectuer les simulations initiales. Quand de nouvelles observations sont disponibles, des poids sont accordés à chaque particule en fonction de leur proximité à l'observation. À chaque pas de temps, cette séquence est d'abord exécutée pour l'assimilation du débit (Figure 3.6 – A) et ensuite pour l'assimilation de la température de l'eau (Figure 3.6 – B). Cette succession est nécessaire puisque le volume d'eau

simulé influence le calcul de sa température tel que démontré à l'Equation 3.1. Les poids sont mis à jour de manière séquentielle par l'Equation 3.3.

$$w_t^i = w_{t-1}^i \frac{p\left(y_t \middle| X_t^i\right)}{\sum_{i=1}^{N_p} p\left(y_t \middle| X_t^i\right)}$$
Equation 3.3

où $p\left(y_t \middle| X_t^i\right)$ est la probabilité conditionnelle de l'observation y_t selon l'état modélisé X_t^i, N_p est le nombre de particules, w_t^i est le poids de la particule i au temps t.

Le nombre de particules doit être préalablement fixé par l'utilisateur. Dans le cadre de cette étude, l'algorithme a été testé avec un nombre de particules allant de 5 à 200. L'algorithme de Douglas et Peucker (2011) a été utilisé pour localiser les points de rupture entre les performances et le nombre de particules utilisées. Sur le bassin versant Nechako, des observations de débits et de températures de l'eau étaient disponibles pour deux stations hydrométriques sur le tronçon principal de la rivière Nechako, soit Vanderhoof et Cheslatta Falls (Figure 3.4). L'erreur des conditions initiales a donc été minimisée à ces deux sites simultanément. Pour ce faire, la probabilité conditionnelle $p\left(y_t \middle| X_t^i\right)$ est remplacée par la probabilité conjointe des probabilités conditionnelles à chaque site. Pour l'observation y_1 à Cheslatta Falls et y_2 à Vanderhoof, la probabilité conjointe est donc $p\left(y_t^1 \middle| X_t^i\right) p\left(y_t^2 \middle| X_t^i\right)$.

Afin de quantifier simultanément l'incertitude associée aux conditions hydrologiques et thermiques initiales ainsi que celle associée aux intrants météorologiques, différents scénarios ont été construits. Ces scénarios représentent diverses combinaisons de ces composantes afin d'en discrétiser leur apport à l'incertitude totale de la prévision de température de l'eau. Le Tableau 3.5 présente les scénarios ainsi que le nombre de membres qu'ils incluent. L'inclusion des prévisions d'ensemble météorologiques au système de prévision a été effectuée tel que décrit à la section 3.3.1.

Tableau 3.6 Scénarios utilisés dans cette section et nombre total de membres qu'ils comprennent.

Composante	S1	S2	S3	S4	S5*	S6**	S7*
Source d'incertitude évaluée	Aucune	Conditions hydrologiques initiales	Conditions thermiques initiales	Intrants météorologiques	Conditions initiales	Conditions initiales et intrants météorologiques	Conditions initiales et intrants météorologiques
Nombre de conditions hydrologiques initiales	1	40	1	1	40*	40*	40
Nombre d conditions thermiques initiales	1	1	40	1	40*	40*	40
Nombre d'intrants météorologiques	1	1	1	20	1	20**	20
Nombre total de membres	**1**	**40**	**40**	**20**	**40**	**40**	**800**

* Un jeu de conditions thermiques initiales, assigné de manière aléatoire, est combiné à chaque jeu de conditions hydrologiques initiales.

** Un membre de la prévision météorologique, assigné de manière aléatoire, est combiné à un jeu de conditions thermiques initiales et un jeu de conditions hydrologiques initiales.

3.4.2 Résultats

Il a été identifié qu'au-delà de 40 particules le gain de performance était marginal aux deux stations de mesure, et ce, pour les deux variables d'intérêt (débit et température de l'eau). Les analyses suivantes ont donc été effectuées en utilisant 40 particules. Cela permet de maximiser les performances tout en minimisant le temps de calcul.

Les résultats du Tableau 3.6 présentent l'amélioration des conditions initiales hydrologiques et thermiques grâce à l'assimilation par filtre particulaire, relativement à la diminution de l'erreur exprimée en MAE/CRPS. En ce qui a trait au débit, une amélioration de 78,6 %, à Cheslatta Falls et de 75,5 % à Vanderhoof est obtenue. Ces valeurs sont respectivement de 71,1 % et 65,2 % dans le cas de la température de l'eau. L'utilisation du filtre particulaire permet donc d'obtenir une erreur résiduelle (CRPS) inférieure à 5 m^3/s pour le débit simulé et inférieure à 0,45°C pour la température de l'eau simulée.

Tableau 3.7 Amélioration relative apportée aux conditions initiales par l'assimilation de données. Les performances sont exprimées en MAE pour les simulations déterministes et en CRPS pour les simulations avec assimilation.

	Débit - MAE/CRPS (m³/s)		Température de l'eau - MAE/CRPS (°C)	
	Cheslatta Falls	Vanderhoof	Cheslatta Falls	Vanderhoof
Conditions initiales originales (sans assimilation)	10,91	17,78	1,52	0,69
Conditions initiales après assimilation	2,33	4,35	0,44	0,24
Amélioration relative	78,6 %	75,5%	71,1%	65,2%
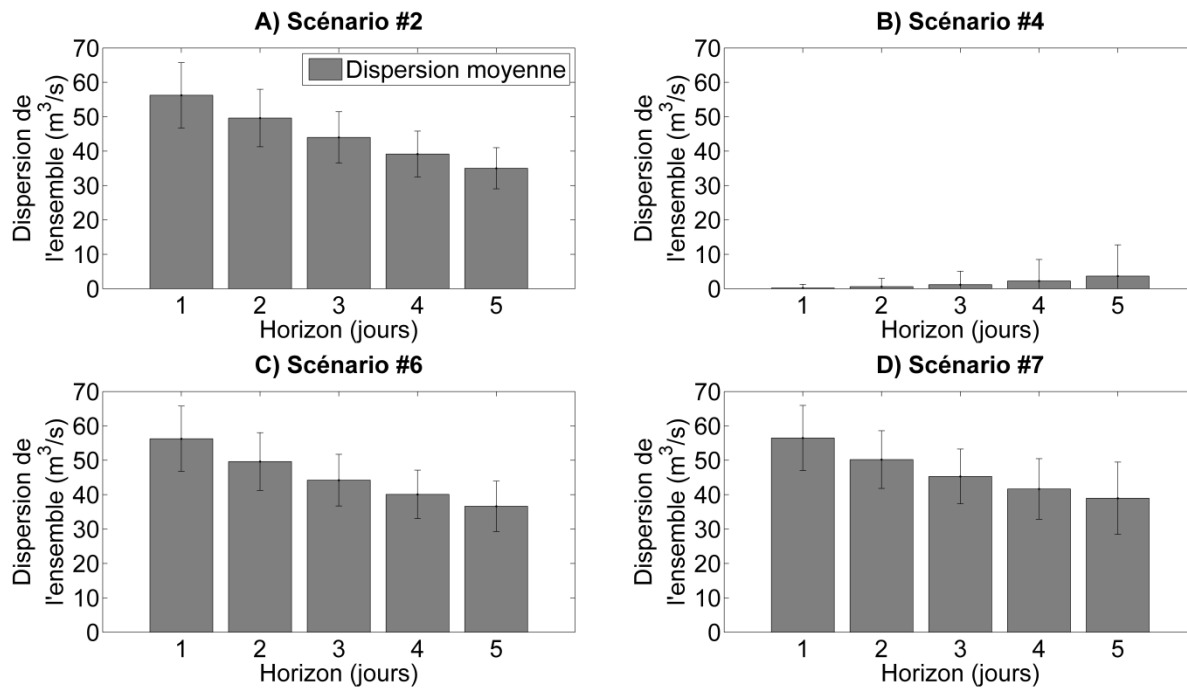
Figure 3.7 Dispersion de l'ensemble des prévisions de débits pour les scénarios 2, 4, 6 et 7.

Les débits prévus grâce à chacun des scénarios ne diffèrent que très peu. Les valeurs de CRPS varient entre 7,3 m^3/s et 9,4 m^3/s pour hz1 et entre 13,7 m^3/s et 15,4 m^3/s pour hz5. La Figure 3.7 montre l'incertitude transmise à la prévision du débit par les conditions initiales (Figure 3.7 – A), par les intrants météo (Figure 3.7 – B), et par la combinaison de ces deux sources (Figure 3.7 – C et D). On constate que la majeure partie de l'incertitude transmise à la prévision du débit provient des conditions initiales, et très peu des intrants météorologiques. Cela fait en sorte que l'incertitude diminue avec l'horizon de prévision pour les scénarios qui incluent les deux sources d'incertitude (Figure 3.7 – C et D), passant de 56 m^3/s (hz1) à 35 m^3/s (hz5). Normalement, on s'attend à une augmentation de l'incertitude en fonction de l'horizon de prévision. Ce résultat contre-intuitif peut s'expliquer par la forte régulation du débit de la rivière Nechako par le contrôle du débit relâché au déversoir de Skins Lake. Cela fait en sorte que les intrants météo n'influencent que marginalement la prévision du débit.

La performance de la prévision thermique est faiblement influencée par l'incertitude de la prévision météorologique fournie en intrant. On observe (voir article 2, section 5.2.4.2) une différence moyenne de seulement 0,07°C (CRPS) lorsque les prévisions météorologiques d'ensemble sont fournies au modèle (S4) comparativement au cas où des observations météorologiques sont utilisées (S1-S3). Cette différence croît avec l'horizon pour atteindre 0,12°C.

On remarque par ailleurs une meilleure capacité à prédire un dépassement de seuil, évaluée par l'indice de Brier (1950) pour des seuils de 16°C, 18°C et 20°C, quand l'ensemble des conditions thermiques initiales (S2, S6) est utilisé plutôt qu'une valeur moyenne (S1).

La dispersion absolue de la prévision du S2 à hz1, équivalent à l'incertitude transmise à hz1 lorsque seulement l'incertitude des conditions thermiques initiales est considérée, est de 1,11°C. Pour le même horizon, la dispersion moyenne de l'ensemble de S4, où seulement l'incertitude des intrants météorologiques est considérée, est inférieure, soit 0,67°C. L'importance de ces valeurs s'inverse dès le second horizon. Elles deviennent alors 0,98°C (S2) et 1,09°C (S4), et atteignent respectivement 0,54°C et 1,89°C à hz5.

Lorsque les trois sources d'incertitude sont incluses, la dispersion de l'ensemble varie entre 1,81°C (hz1) et 2,67°C (hz5).

En termes de dispersion et de fiabilité, on remarque une très bonne fiabilité des scénarios bénéficiant des ensembles de conditions initiales thermiques à l'horizon 0 (S3, S5, S6 et S7; Figure 3.8). Cela indique que, pour ces scénarios, la prévision est initiée à partir d'ensembles convenablement dispersés. Le scénario qui tient uniquement compte de l'incertitude des conditions initiales thermiques (S3) voit sa fiabilité diminuer en fonction de l'horizon. L'effet contraire est observable lorsqu'uniquement l'incertitude des intrants météorologiques est tenue en compte (S4). Dans un tel cas, la fiabilité augmente en fonction de l'horizon. Dans le cas de S2, où seulement l'incertitude des conditions hydrologiques initiales est considérée, on remarque un manque de fiabilité flagrant à tous les horizons. La fiabilité s'accroit tout de même en fonction de l'horizon, par la propagation de l'incertitude de l'hydrologie prévue. De tous les horizons de prévision, les scénarios qui tiennent compte des trois sources d'incertitude (S6 et S7) conservent une meilleure fiabilité statistique et des ensembles mieux dispersés. Toutefois, ceux-ci demeurent toujours en dessous de la bissectrice, indiquant une sous-dispersion des ensembles.
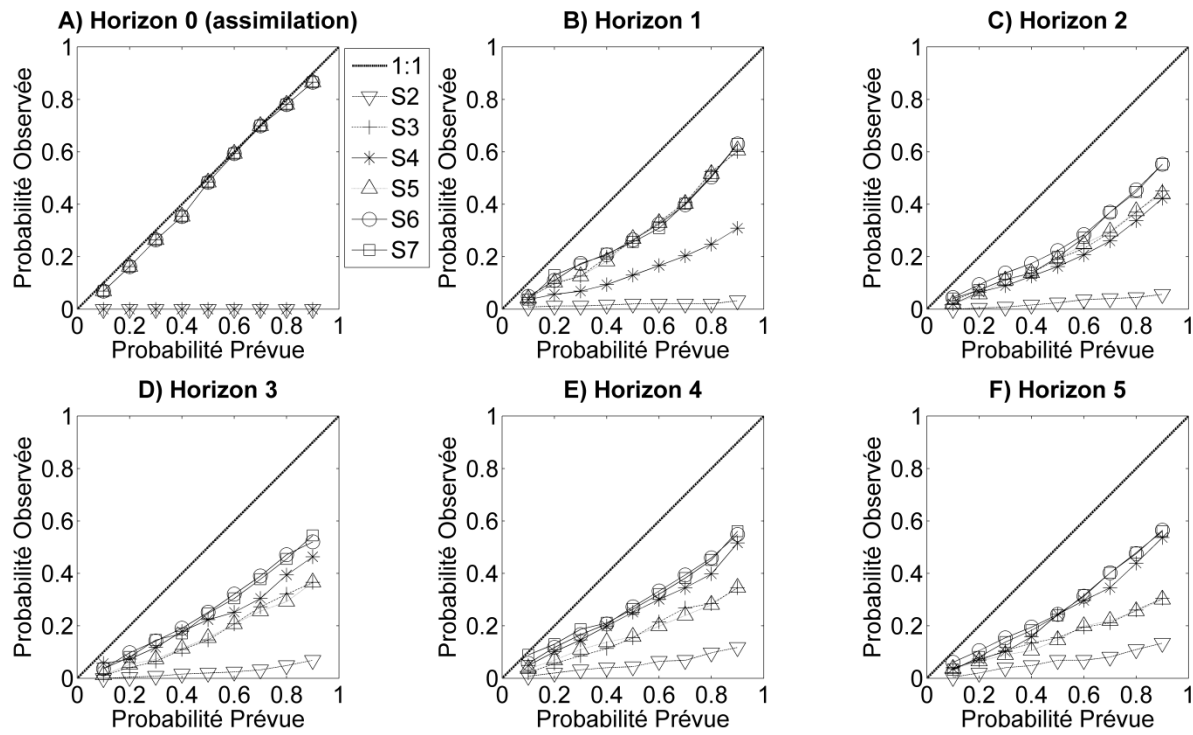
Figure 3.8 Diagramme de fiabilité des prévisions de température de l'eau à Vanderhoof pour les scénarios S2 à S7 aux horizons 0 (conditions initiales) à 5 (A-F).

3.5 Évapotranspiration, évaporation, et modélisation hydrologique et thermique

Le premier objectif de la thèse est la quantification de l'impact du choix d'une méthode d'estimation de l'évaporation et de l'évapotranspiration sur la modélisation hydrologique et thermique. Les objectifs spécifiques de cette section sont : 1) d'évaluer l'impact de la sélection d'une méthode d'estimation de l'évapotranspiration sur une simulation hydrologique, dans un modèle semi-distribué; 2) d'évaluer l'impact de la sélection d'une méthode d'estimation de l'évaporation sur une modélisation de la température de l'eau dans ce même modèle; et 3) de vérifier les limites possibles de l'utilisation d'une même méthode pour l'estimation de l'évapotranspiration et l'évaporation.

3.5.1 Méthodologie

Sous sa configuration originale, le modèle CEQUEAU utilise une équation de Thornthwaite (1948) modifiée pour estimer la perte d'eau par évapotranspiration journalière. Elle prend la forme suivante :

$$ETP_{TW} = \frac{10}{30.4}1.62\left(10\frac{T_a}{XIT}\right)^{XAA} \qquad\qquad \text{Equation 3.4}$$

Les paramètres *XIT* et *XAA* peuvent être assignés par l'utilisateur ou estimés à partir des températures moyennes mensuelles de l'air (Morin et Paquet, 1995), alors que T_a représente la température moyenne journalière de l'air.

Afin de remplir le premier objectif de la thèse, portant sur l'évapotranspiration et l'évaporation, cinq équations alternatives d'évapotranspiration et cinq équations alternatives d'évaporation ont été intégrées au modèle. Ces équations ont été sélectionnées en fonction de leur complexité (nombre d'intrants), de l'accessibilité des intrants et de leur performance démontrée dans la littérature (p. ex. Allen et al., 2005; Oudin et al., 2005; Rosenberry et al., 2007; Singh et Xu, 1997; Winter et al., 1995; Xu et Singh, 2000). Dans le cas de l'évapotranspiration, il s'agit des équations de Kimberly-Penman (Wright, 1982), de Priestley-Taylor (1972), de McGuinness-Bordne (1972), de Penman-Monteith (Monteith, 1965) et de Morton (1983). Dans le cas de l'évaporation, il s'agit de cinq équations de transfert de masse, basées sur celle de Harbeck (1962), dont la fonction de vent diffère. Les fonctions de vent intégrées sont celles de Benner (1999), de Webb et Zhang (1997), de Maheu et al. (2014), de Guenther et al. (2012) et de Jobson (1980). Ces équations sont rendues disponibles en options dans la présente version du modèle. Les équations ont été testées sur les bassins versants des rivières Nechako et Miramichi, décrits à la section 3.2 (Figure 3.4).

Ces équations ont été testées selon deux approches. D'abord, les équations d'évapotranspiration ont été utilisées pour estimer l'évapotranspiration ainsi que pour estimer la perte de chaleur latente par évaporation. Bien qu'elle ne représente pas adéquatement la physique de ces deux processus (l'évaporation et l'évapotranspiration sont des processus distincts; section 2.3), cette méthode réplique la structure actuelle

du modèle CEQUEAU. Cela permet aussi de vérifier l'efficacité de l'utilisation d'une seule et même méthode dans un processus de modélisation hydrologique et thermique. Ensuite, la méthode originale du modèle, soit celle de Thornthwaite (1948) a été conservée, alors que les diverses fonctions de vent ont été utilisées pour estimer la perte de chaleur par évaporation. Dans ce cas-ci, les deux processus (évapotranspiration et évaporation en eau libre) sont entièrement dissociés. Un test de Kruskall-Wallis (Kruskal et Wallis, 1952) a été effectué pour évaluer si les distributions d'évapotranspiration calculées par les différentes méthodes ont une médiane significativement différente. Un test non paramétrique a été utilisé plutôt qu'une analyse de variance ANOVA puisque les distributions n'étaient pas normalement distribuées La normalité a été vérifiée par un test de Kolmogorov-Smirnov (Massey, 1951). L'hypothèse alternative du test est que la médiane d'au moins une des méthodes d'évapotranspiration est significativement différente des autres. Le test *a posteriori* de Tukey-Kramer (Tukey, 1949) a permis de connaitre quelles méthodes différaient entre elles et lesquelles appartenaient au même groupe.

La performance de chacune des méthodes testées a été évaluée à partir de la modélisation subséquente du débit et de la température de l'eau. Pour la portion hydrologique, la maximisation du critère d'efficacité de Kling-Gupta (KGE; Gupta et al., 2009) a été priorisée. Il s'agit d'un indice de performance qui tient compte de l'exactitude de la simulation du débit moyen, de sa variance et de la corrélation entre le débit simulé et observé. Il est reconnu pour accorder moins d'importance aux débits élevés comparativement au, très utilisé, critère de Nash-Sutcliffe (NSE). Dans le cas de la température de l'eau, l'erreur moyenne quadratique (RMSE) a été minimisée.

À l'été 2015, un lysimètre à pesée expérimental a été installé sur le bassin versant de la rivière Nechako à environ 400 m de la station météorologique Ootsa Lake/Skins Lake (station # 1085836 d'Environnement et changements climatiques Canada; Figure 3.4). Le lysimètre inclut un tuyau de PVC de 60 cm de hauteur par 30 cm de diamètre. Ce tuyau est d'abord enfoncé dans le sol pour isoler une colonne tout en minimisant sa perturbation. La base est ensuite scellée pour empêcher les échanges d'eau entre la colonne de sol et le milieu ambiant. La colonne est déposée sur une balance (PL-100 - UMS) connectée à un enregistreur de données (CR1000 – Campbell Scientific). La

balance a une précision de 14 g, ce qui équivaut à 0,2 mm d'eau. Des mesures ont été récoltées du 4 juin 2015 au 1er octobre 2015. Les différences négatives traduisent une perte par évapotranspiration alors qu'une différence positive indique un apport par précipitation.

La précipitation journalière totale observée à la station météorologique Ootsa Lake/Skins Lake a été tracée au-dessus de la précipitation mesurée par le lysimètre (Figure 3.9). Une bonne adéquation a été observée entre la précipitation dérivée du lysimètre et celle mesurée à la station météorologique. Cela confirme le bon fonctionnement dudit lysimètre.
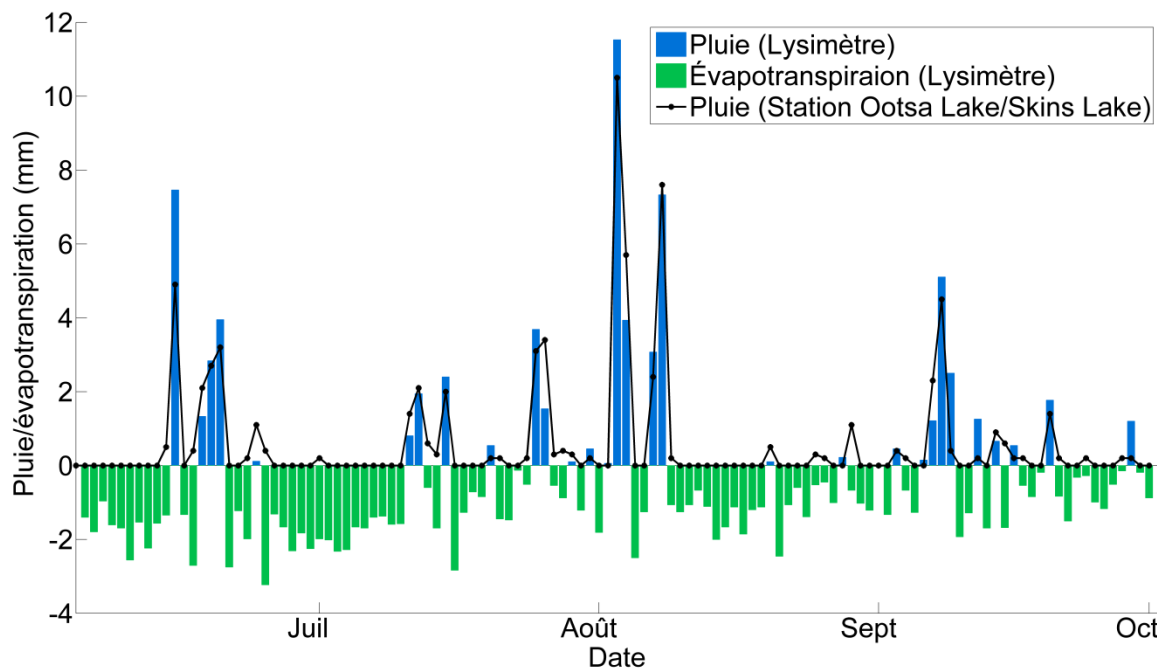
Figure 3.9 Pluie et évapotranspiration mesurées à l'aide du lysimètre à l'été 2015.

Sur le bassin versant de la rivière Miramichi, des données d'évapotranspiration récoltées à partir d'une tour à flux (Nashwaak Lake; 2003-2005; Figure 3.4) extraites de la base de données FluxNet (http://fluxnet.ornl.gov) ont aussi été utilisées pour évaluer la performance des méthodes d'estimation de l'évapotranspiration testées.

3.5.2 Résultats

Le Tableau 3.7 présente les performances de chacune des méthodes en terme de RMSE (mm), de biais relatif, de coefficient de corrélation de Pearson, d'AIC (critère d'information d'Akaike; p. ex. Ahmadi-Nedushan et al., 2007) et de biais annuel moyen (mm) en comparaison aux mesures d'évapotranspiration obtenues par la tour à flux du Lac Nashwaak. On remarque une bonne corrélation entre les valeurs mesurées et celles observées lorsque les méthodes de Kimberly-Penman (r = 0,70), Priestley-Taylor (r = 0,72), Penman-Monteith (r = 0,71) et Morton (r = 0,73) sont utilisées alors toutes les autres méthodes présentent un coefficient de corrélation inférieur à 0,2. Malgré son coefficient de corrélation élevé, la méthode de Penman-Monteith présente un biais important (biais relatif = 0,46). De l'autre côté du spectre, les méthodes de Morton et de Priestley-Taylor ne sont que faiblement biaisées, avec des biais relatifs de respectivement 0,01 et 0,06. De manière générale, les indicateurs de performance suggèrent une meilleure performance de la méthode de Morton. Toutefois, lorsque la complexité (nombre d'intrants) de la méthode est prise en compte (AIC), la méthode de Priestley-Taylor est favorisée.

Tableau 3.8 : Indicateur de performance pour les méthodes d'estimation de l'évapotranspiration en rapport aux mesures par tour à flux au Lac Nashwaak (bassin versant de la rivière Miramichi)

	RMSE (mm)	Biais	r	AIC	Biais annuel moyen (mm)
Thornthwaite	1,51	0,25	0,19	341	98,81
Kimberly-P.	1,11	0,12	0,70	87	-7,81
Priest.-Taylor (alpha = 0,82)	<u>0,98</u>	0,06	0,72	<u>3</u>	-37,74
McGuinness	1,58	0,29	0,18	370	108,97
Penman-Mont.	1,73	0,46	0,71	356	207,15
Morton (alpha = 0,43)	1,01	<u>0,01</u>	<u>0,73</u>	15	<u>0,89</u>
Benner	1,51	0,25	0,19	341	98,81
Webb et Zhang	1,46	0,21	0,17	325	77,16
Maheu et al.	1,51	0,25	0,19	341	98,81
Guenther et al.	1,33	0,04	0,13	252	-45,65
Jobson	1,51	0,25	0,19	341	98,81

Les résultats de modélisation démontrent que le choix de la méthode d'estimation de l'évaporation n'influence que marginalement le volume d'eau total perdu par vaporisation. Toutefois, sur le bassin de la rivière Nechako on remarque une différence significative entre l'évapotranspiration estimée par la méthode de Thornthwaite couplée à une équation de transfert de masse et celle estimée par la méthode de Thornthwaite telle qu'utilisée dans CEQUEAU (Figure 3.10 - A). Cette différence n'est toutefois pas significative sur le bassin de la rivière Miramichi (Figure 3.10 - B). Lorsque comparé aux données disponibles dans la littérature (Brown et al., 2014 pour la Nechako; Malloy et Price, 2014, et Xing et al., 2008 pour la Miramichi) ainsi qu'aux données de lysimètre, on remarque une surestimation de la valeur journalière médiane de l'évapotranspiration par les méthodes de Kimberly-Penman (Wright, 1982) et de Penman-Monteith (Monteith, 1965; Figure 3.10). Notons que ces méthodes utilisent toutes deux la vitesse du vent et la pression de vapeur de l'air en intrants. La vitesse du vent a une grande

variabilité spatiale et est donc plus difficile à interpoler sur l'étendue d'un bassin versant (Luo, Taylor, & Parker, 2008). Elle peut être une source d'erreur importante. D'après les données de la littérature (Brown et al., 2014) et celles du lysimètre, l'ensemble des méthodes surestiment l'évapotranspiration sur le bassin Nechako. La méthode de Priestley-Taylor (Priestley et Taylor, 1972) présente toutefois la surestimation la moins importante. Sur le bassin de la Miramichi, la méthode qui performe le mieux est celle de Morton tel que démontré au Tableau 3.7.
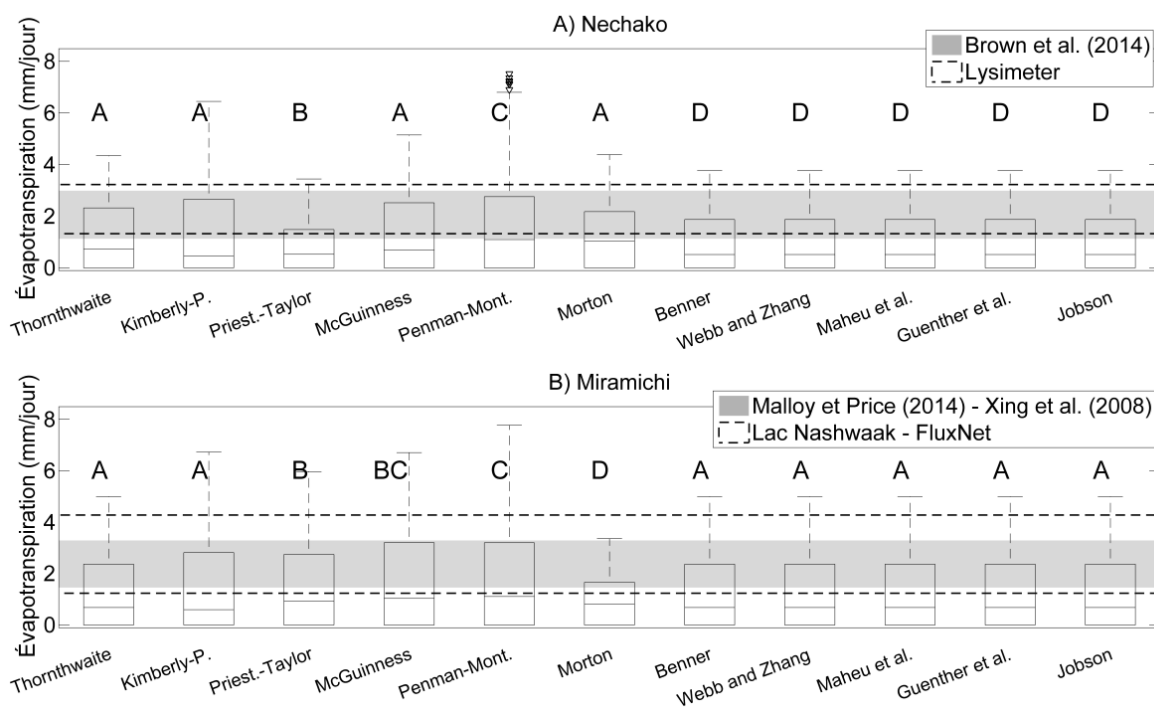
Figure 3.10 Diagramme à boîtes de l'évapotranspiration journalière moyenne estimée sur A) le bassin versant de la rivière Nechako et B) le bassin versant de la rivière Miramichi pendant la période estivale (juin à septembre). Les méthodes qui ont la même lettre n'ont pas une médiane significativement différente.

Dans le cas de l'évaporation, on observe davantage de variabilité entre les méthodes (Figure 3.11) comparativement à l'évapotranspiration. Sur le bassin de la rivière Nechako, les méthodes de Thornthwaite, Kimberly-Penman, McGuinness, Morton, Maheu et al. et Jobson appartiennent toutes au même groupe (A). Les méthodes de

McGuinness, Morton et Benner ne présentent pas, elles non plus, de différence significative (groupe D). Sur le bassin de la Miramichi, les méthodes de Thornthwaite, Kimberly-Penman et Morton ne sont pas significativement différentes (groupe A), Priestley-Taylor, McGuinness et Penman-Monteith appartiennent au même groupe (B), Morton, Benner et Jobson forment le groupe (D) et Maheu et al. et Jobson forment le dernier groupe (F). La méthode de Guenther et al. est quant à elle significativement différentes des autres. Lorsque mises en relation avec les données de la littérature, on remarque que les équations proposées par Maheu et al. et Kimberly-Penman semblent les plus appropriées.
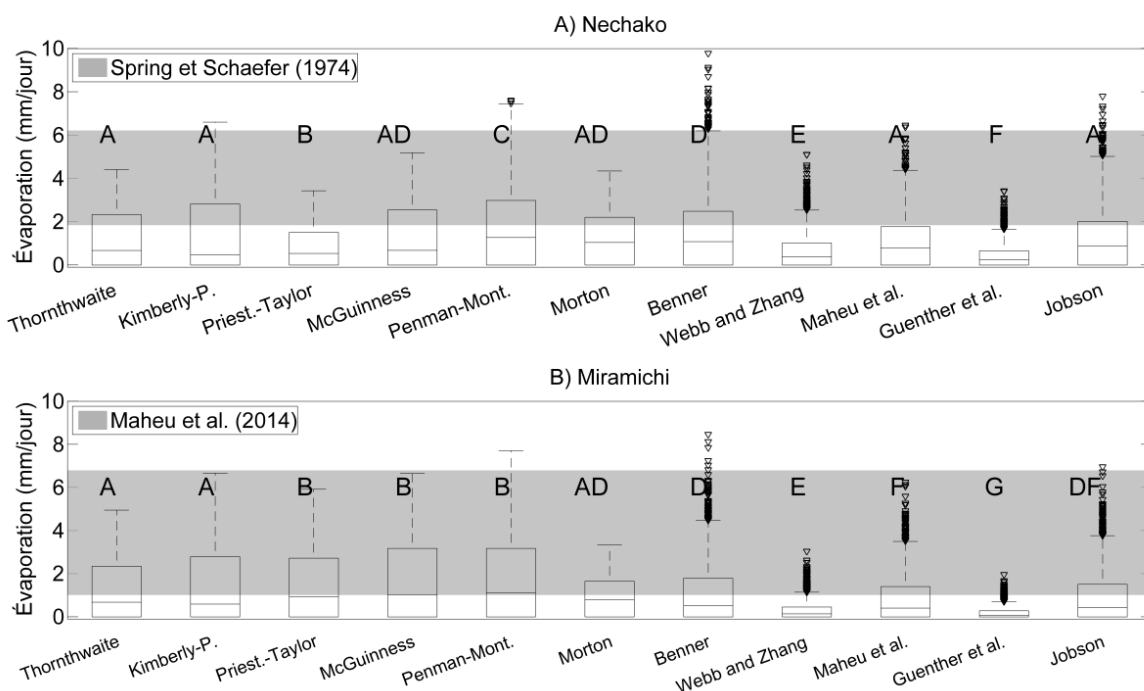
Figure 3.11 Diagramme à boîte de l'évaporation journalière moyenne estimée sur A) le bassin versant de la rivière Nechako et B) le bassin versant de la rivière Miramichi pendant la période estivale (juin à septembre). Les méthodes qui ont la même lettre n'ont pas une médiane significativement différente.

Les pourcentages de la perte de chaleur totale attribuable à l'évaporation obtenue à partir de chacune des méthodes ont été représentés graphiquement (Figure 3.12). On remarque que lorsque la même méthode est utilisée pour estimer l'évapotranspiration et l'évaporation en rivière, trois des cinq méthodes estiment des pourcentages supérieurs

à 50 %. Lorsqu'une fonction de vent est utilisée, cette contribution varie entre 30 % et 45 % à l'exception des équations de Webb et Zhang (1997) et Guenther et al. (2012) pour lesquelles cette proportion chute en dessous de 25 %.
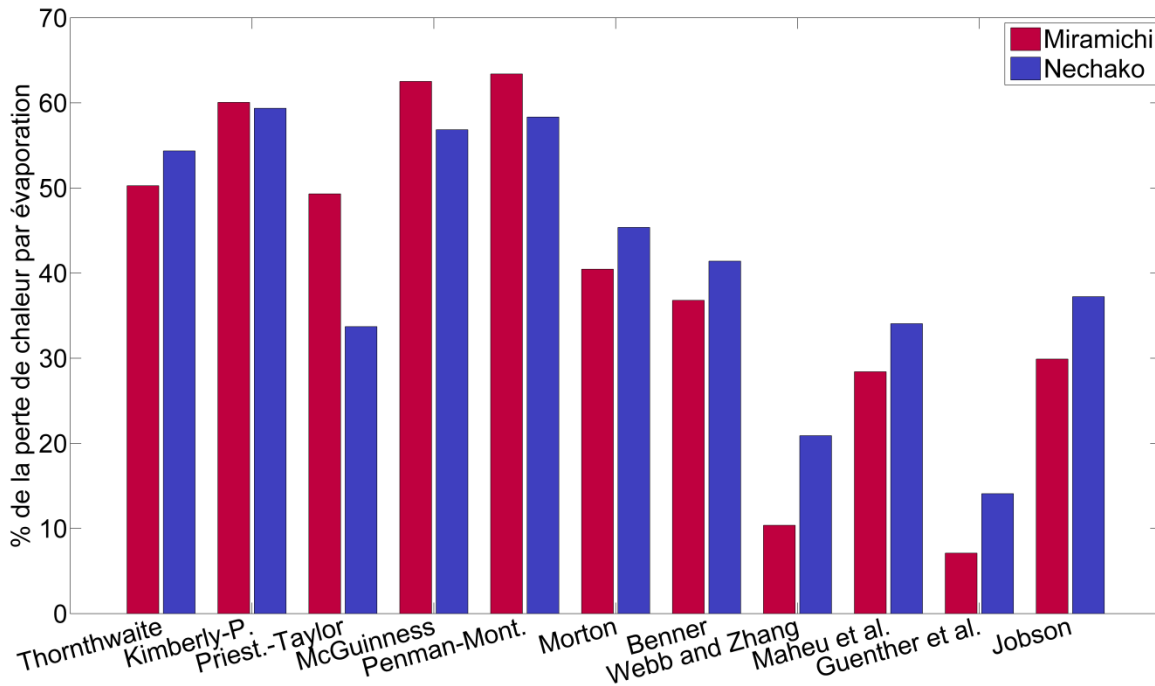
Figure 3.12 Proportion de la perte de chaleur totale attribuable à l'évaporation sur la rivière Nechako et la rivière Miramichi.

4 CONCLUSION ET PERSPECTIVES

La quantification de l'incertitude dans la modélisation (p. ex. Beven, 1993; Clark et al., 2015; Montanari et Di Baldassarre, 2013), la prévision à court terme (p. ex. Cloke et Pappenberger, 2009; Roulin et Vannitsem, 2015; Thiboult et al., 2016) ou les projections climatiques (p. ex. Chen et al., 2011; Clark et al., 2016; Van Vliet et al., 2013) en hydrologie sont désormais bien documentées dans la littérature scientifique. Les résultats présentés dans la présente thèse démontrent clairement le besoin d'inclure une prise en compte de l'incertitude lors de l'émission d'une prévision de la

température de l'eau en rivière. Sans en faire l'analyse exhaustive, on y expose l'incertitude inhérente à un processus hydrologique d'importance (section 3.5), aux intrants météorologiques (section 3.3) ainsi qu'aux conditions initiales, hydrologiques et thermiques, du modèle utilisé (section 3.4).

L'incertitude des intrants météorologiques est fréquemment considérée dans une prévision hydrologique (p.ex. Kavetski et al., 2006; McMillan et al., 2011). À la section 3.3 de cette thèse, une quantification explicite de l'incertitude des intrants météorologiques dans la prévision thermique a été réalisée. Cela constitue une première dans la littérature qui porte sur la thermie en rivière, et représente donc un apport notable à la recherche sur la modélisation et la prévision de la température de l'eau en rivière.

Les résultats démontrent la nécessité de considérer l'incertitude des intrants météorologiques fournis à un modèle thermique dans un contexte prévisionnel. Une fiabilité croissante avec l'horizon de prévision, entre un et cinq jours, a été observée à la fois pour la prévision hydrologique et la prévision thermique. Toutefois, l'inclusion exclusive de cette source d'incertitude ne permet pas de maintenir une dispersion et une fiabilité adéquates pour une prévision thermique, et ce particulièrement pour une prévision à court terme (p. ex. un jour). Cette conclusion démontre par ailleurs le besoin de considérer davantage de sources d'incertitude dans le système de prévision. Ces résultats supportent d'ailleurs ceux disponibles dans la littérature traitant de la prévision hydrologique (p. ex. Hopson et Webster, 2010; Thiboult et al., 2016). Dans ce cas-ci, le manque de fiabilité est particulièrement visible pour l'horizon un jour (Figure 3.5). Par ailleurs, ces résultats mettent en évidence la nécessité d'inclure une méthode d'assimilation lors de l'émission de prévisions de la température de l'eau. La méthode choisie doit permettre de quantifier et de représenter l'incertitude des conditions initiales (hydrologiques et thermiques) du bassin versant.

L'ajout d'une méthode d'assimilation de données par filtres particulaires a permis, en partie, de pallier ce problème. Il s'agit d'une première application d'une méthode d'assimilation de données probabiliste en thermie. Les filtres particulaires demandent habituellement un grand nombre de particules pour assurer de bonnes performances

(p. ex. Moradkhani et al., 2012; van Leeuwen, 2009). D'autres études ont toutefois démontré l'efficacité de cette méthode avec un nombre plus faible de particules (Weerts et El Serafy, 2006). Les bonnes performances démontrées des filtres particulaires avec un nombre relativement faible de particules a permis, dans ce cas-ci, de limiter le temps de calcul de la prévision tout en assurant une prise en compte adéquate de l'incertitude des conditions hydrologiques et thermiques initiales du modèle. Tout en assurant une correction des variables du modèle avant la prévision, les filtres particulaires ont permis de quantifier la contribution de l'incertitude des états initiaux à celle de la prévision à court terme. L'objectif deux de la thèse a donc mené à la proposition d'un cadre méthodologique pour l'assimilation en cascade de données hydrologiques et thermiques en plus d'expliciter la propagation de l'incertitude des états initiaux à la prévision.

Enfin, l'objectif 3 de la thèse constitue un pas en avant vers l'élaboration de prévisions multimodèles thermiques où diverses formulations sont utilisées pour estimer les divers flux de chaleur. Dans ce cas-ci, on s'intéresse plus particulièrement à l'évaporation, considérée comme une perte de chaleur dominante dans le bilan d'énergie d'une rivière (Hannah et al., 2004; Maheu et al., 2014). Dans cette section, on évalue la performance de différentes méthodes d'estimation de l'évapotranspiration et de l'évaporation tout en exposant l'influence du choix de méthode sur la modélisation hydrologique et thermique subséquente. Grâce à cette méthodologie, on démontre la nécessité de distinguer les méthodes d'estimation de l'évapotranspiration et d'évaporation. On souligne, dans un même temps, l'incertitude conjointe associée au choix de la méthode d'estimation, mais aussi à la sélection des paramètres du modèle. Ces conclusions devraient être intégrées à l'élaboration d'un cadre de prévision multimodèle. Ce type de méthode gagne effectivement en popularité pour la prise en compte de l'incertitude structurale, intrinsèque aux modèles (p. ex. Seiller et al., 2012; Velázquez et al., 2011). Une étape préalable à l'utilisation de méthodes multimodèles est l'évaluation individuelle de ces modèles, ou des structures de modèle, incluse dans l'approche (Ye, Meyer, & Neuman, 2008). Les conclusions de la section 3.5 représentent des bases préalables à l'élaboration d'une prévision multimodèle, ou plutôt « multimodule » puisqu'elle touche uniquement une composante du modèle, soit celle de la température de l'eau.

Malgré l'ajout de l'incertitude associée aux conditions hydrologiques et thermiques initiales par l'assimilation de données au système de prévision, un manque de fiabilité est toujours visible (Figure 3.8). Cela suggère que la totalité de l'incertitude du système n'est pas prise en compte. Les principales composantes contributrices à l'incertitude totale d'une prévision sont les conditions initiales, les intrants et le modèle (p. ex. Thiboult et al., 2016). L'incorporation des résultats obtenus reliés à l'objectif 3 (section 3.5) constitue une avenue intéressante pour intégrer l'incertitude associée à l'estimation des flux évaporatifs à la prévision thermique d'ensemble. L'efficacité des techniques « multimodules » a notamment été démontrée par Clark et al. (2015) dans une étude exhaustive de l'incertitude structurelle en modélisation hydrologique. Bien que cette étape n'ait pu être intégrée à la thèse, elle en représente néanmoins une avenue à privilégier. Une progression logique aux travaux de cette thèse inclurait l'intégration de différentes méthodes de calcul de l'évaporation en rivière, pour l'estimation du flux de chaleur latente en eau libre, à la méthodologie de prévision d'ensemble de température de l'eau proposée ci-haut. Cela permettrait une quantification de l'incertitude associée à l'estimation de l'évaporation, mise en relief à la section 3.5. de la présente thèse, à l'incertitude combinée attribuable aux intrants météorologiques et aux conditions initiales du système.

PARTIE II : ARTICLES

5 ARTICLES

Les travaux réalisés dans ce chapitre sont présentés sous la forme d'articles scientifiques rédigés en anglais.

5.1 Article 1 : Water Temperature Ensemble Forecasts: Implementation Using the CEQUEAU Model on Two Contrasted River Systems

Prévision d'ensemble de la température de l'eau à l'aide du modèle CEQUEAU sur des systèmes hydrologiques contrastés

Sébastien Ouellet-Proulx[1], André St-Hilaire[1] et Marie-Amélie Boucher[2]

[1]Canadian Rivers Institute and INRS-ETE, 490, rue de la Couronne, Québec, Canada

[2]Université de Sherbrooke, département de génie civil, 2500 Boulevard de l'Université, Sherbrooke, Qc, J1K 2R1

Contribution des auteurs :

L'idée qui a mené à l'article a été élaborée par les Pr. André St-Hilaire et Marie-Amélie Boucher avec la collaboration de l'étudiant (Sébastien Ouellet-Proulx). Les codes pour

l'extraction des prévisions météorologiques d'ensemble ont été rédigés par la Pr. Marie-Amélie Boucher. Le calage des modèles, les analyses et la rédaction ont été effectués par l'étudiant (Sébastien Ouellet-Proulx) sous la supervision des Pr. André St-Hilaire et Marie-Amélie Boucher. Le processus de correction et de réponse aux commentaires des réviseurs a été effectué par l'étudiant sous la supervision des Pr. André St-Hilaire et Marie-Amélie Boucher.

Résumé

Dans certains systèmes hydrologiques, des stratégies d'atténuation sont mises en place en fonction de prévisions de température à court terme pour réduire le stress thermique causé aux organismes aquatiques. Alors que les diverses sources d'incertitudes qui affectent la modélisation de la température de l'eau sont connues, leur impact sur sa prévision demeure mal compris. L'objectif de cet article est de caractériser l'incertitude induite à la prévision de la température de l'eau par ses intrants météorologiques dans deux contextes hydrologiques différents. Des prévisions journalières de température de l'eau ont été produites à l'aide du modèle CEQUEAU pour les rivières Nechako (régulée) et Miramichi Sud-Ouest (naturelle) pour des horizons de 1 à 5 jours. Les résultats démontrent qu'une plus grande incertitude est propagée à la prévision effectuée sur la rivière non régulée (0,92-3,14°C) que sur la rivière régulée (0,73-2,29°C). De meilleures performances sont observées sur la rivière Nechako avec des indices continus de probabilité ordonnée moyens (MCRPS < 0,85°C) pour le tous les horizons comparativement à ceux de obtenus pour la Miramichi Sud-Ouest (MCRPS ≈ 1°C). Tout en informant l'utilisateur sur les conditions thermiques à venir, la prévision d'ensemble de la température de l'eau fournit une évaluation de l'incertitude associée à celle-ci et constitue un outil additionnel pour la prise de décision pour la gestion de rivières.

Abstract

In some hydrological systems, mitigation strategies are applied based on short-range water temperature forecasts to reduce stress caused to aquatic organisms. While various uncertainty sources are known to affect thermal modelling, their impact on water temperature forecasts remain poorly understood. The objective of this paper is to characterize uncertainty induced to water temperature forecasts by meteorological inputs in two hydrological contexts. Daily ensemble water temperature forecasts were produced using the CEQUEAU model for the Nechako (regulated) and the Southwest Miramichi (natural) rivers for 1-5 day horizons. The results demonstrate that a larger uncertainty is propagated to the thermal forecast in the unregulated river (0.92- 3.14°C) than on the regulated river (0.73-2.29°C). Better performances were observed on the Nechako with a mean continuous ranked probability score (MCRPS) < 0.85°C for all horizons compared to the Southwest Miramichi (MCRPS ≈ 1°C). While informing the end-user on future thermal conditions, the ensemble forecasts provide an assessment of the associated uncertainty and offer an additional tool to river managers for decision-making.

5.1.1   Introduction

The inherent links between fish biological processes and water temperature have been well documented over the last fifty years (Fry, 1971; D. McCullough, 2010; Ward & Stanford, 1982). It has been shown that sustained periods of high water temperature can result in impaired fish swimming capacity (McCullough et al., 2001), weight loss, disease proliferation (Ouellet et al., 2013) and death (Sullivan et al., 2000).

In unregulated rivers, the thermal regime is governed by environmental characteristics such as meteorological forcings, topography, hydrology and geology (Caissie, 2006; Maheu, Poff, & St-Hilaire, 2016). The impoundment of a watercourse can alter this thermal regime in different ways depending on the type of dam, the timing and magnitude of the water releases, reservoir stratification (Crisp, 1987; Poff and Hart, 2002; Ward, 1982) and the depth in the upstream reservoir from which water is released (Cole et al., 2014; Gu, Montgomery, & Austin, 1998). In some hydrological systems

where dams have altered natural flows and thermal patterns (e.g. Klamath River, US; Delaware River, US) management strategies have been implemented to protect aquatic communities while maintaining socio-economic benefits delivered by freshwater resources. Research on water temperature has provided the water management community with a plethora of modelling tools (see Benyahya et al., 2007 for a partial review). Many of these models are key elements for dam operators because they help to meet environmental flow requirements and water quality criteria, while at the same time assisting in the optimization of operations (Cole et al., 2014; Pike et al., 2013).

One criterion that is often used as a guideline for river management is minimizing exposure of aquatic organisms to high water temperature (Breau, 2012; McCullough, 2010; Olden and Naiman, 2010). Such guidelines are often established using a threshold for maximum allowable temperature in order to ensure the protection of endangered species, to maintain economic benefits provided by recreational fishing or for public health issues (Pike et al., 2013). When such guidelines are promulgated, water temperature forecasts can be used, along with other operational tools, to keep temperatures below the maximum threshold while optimizing the operations.

The last few years have seen a growth of interest for water temperatures forecasting or predictions at various time scales (Webb et al., 2008) from industrial and governmental organizations involved in water management and hydro-power production. Short and medium term thermal forecasting are often used. Such forecasts have proven useful, from both an environmental (Danner et al., 2012; Huang et al., 2011) and an economical (Huang, Langpap, & Adams, 2012) point of view. Notably, they can help improving management strategies by allowing operators to reduce their response time based on a priori information.

Hydrological forecasting methods have received much attention in the last 20 years. Particular emphasis has been put on quantifying the uncertainty that propagates within the forecasting framework and on communicating it properly (Boucher et al., 2011; Casati et al., 2008; Thiboult et al., 2016). More specifically, the use of ensemble prediction systems (EPS) initiated in the field of weather forecasting has gained much

interest in hydrological forecasting before expanding to other disciplines such as climate change research (Cloke and Pappenberger, 2009).

However, the quantification of uncertainty in water temperature forecasts has received much less attention, although it is widely recognized that water temperature forecasts are inherently uncertain (Bartholow, 2003; Hague and Patterson, 2014; Yearsley, 2009). Bartholow (2003) advocates for a quantitative assessment of uncertainty in water temperature modelling as a tool to improve the decision making process. To the best of our knowledge, only a few recent studies used various methods to account for uncertainty in water temperature forecasting (Bal et al., 2014; Hague & Patterson, 2014; Pike et al., 2013). Although instructive findings were provided by these studies, none of them explicitly took interest in quantifying the uncertainty induced by meteorological inputs involved in their respective forecasting framework. Such work has been carried out extensively for flood forecasting (Cloke and Pappenberger, 2009) by forcing hydrological models with meteorological ensemble forecasts. Hence, the water temperature forecasting community could learn from the experience gained in the context of flood forecasting and account for uncertainty in decision-making. Interestingly, while precipitation and air temperature forecasts are sufficient for most stream flow forecasting frameworks, issuing water temperature forecasts requires many more atmospheric variables as inputs to the model. Therefore, ensemble water temperature forecasting provides an interesting context to assess the quality and usefulness of ensemble meteorological forecasts for variables such as solar radiation, which are seldom exploited for operational purposes.

This paper proposes a first attempt to produce ensemble water temperature forecasts from ensemble meteorological forecasts. The use of ensemble meteorological forecasts as model inputs allows for a shift from a deterministic to a probabilistic paradigm in water temperature forecasting. The objective of this paper is to produce ensemble water temperature forecasts and to compare them with deterministic water temperature forecasts, in the particular context of decision-making related to water temperature regulation constraints. In this paper, (1) we present a modelling framework used to produce ensemble water temperature forecasts in two different hydrological contexts: (a) a strongly regulated system and (b) a natural system; (2) we quantify the uncertainty

associated with forecasts of eight input variables from an atmospheric model that propagates to water temperature forecasts; and (3) we compare the propagation of the uncertainty in the regulated and the natural systems mentioned above.

5.1.2 Materials and Methods

5.1.2.1 Model and Modeling Framework

The hydrological model used in this study is CEQUEAU (Morin & Couillard, 1990). It is a semi-distributed model divided in two components. A rainfall-runoff conceptual "tank type" module first simulates the hydrological states of the watershed from total precipitation (*pTot*), minimum and maximum air temperature (*tMin* and *tMax*), and physiographic inputs through a production function. The production function essentially distributes water vertically to update the state of various reservoirs that conceptualize lake and soil water storage. These states are composed of the snowpack in open and forested areas, evapotranspiration, water in the unsaturated zone, water in the saturated zone and storage in lakes and marshes (St-Hilaire et al., 2000). Water is then routed downstream on a predetermined grid with cells of equal area by a transfer function to simulate discharge at each time step. At the same time step, the simulated hydrological states on each grid cell are subsequently fed to the thermal module along with additional meteorological input data (i.e. solar radiation, wind speed, air vapour pressure and cloud cover) to estimate water temperature (T_w, Equation 5.1) using the ratio of enthalpy (H_{tot} in MJ) over the product of the volume of water (V in m^3) by the heat capacity of water (C; 4.187 MJ m^{-3} °C^{-1}):

$$T_w = \frac{H_{tot}}{VC}$$

Equation 5.1

The total enthalpy is estimated by summing the initial enthalpy, the advective fluxes and the various energy fluxes at the air-water interface, according to Equation 5.2:

$$H_{tot} = H_{ini} + H_s + H_{IR} + H_e + H_C + H_{adv}$$

Equation 5.2

where all terms are computed in MJ. H_{ini} is the initial enthalpy, H_s is the net solar radiation, H_{IR} is the net longwave radiation, H_e is the evaporative heat flux, H_c is the sensible heat flux and H_{adv} represents the advective fluxes. These advective fluxes include the energy transferred by surface runoff, interflow, groundwater, and overflow from lakes and marshes (St-Hilaire et al., 2000). The terms of the energy budget are estimated using Equation 5.3 to Equation 5.7:

$$H_s = C_s A R_s$$

Equation 5.3

$$H_{IR} = C_i A \sigma \left(\beta T_a^4 - T_w^4 \right)$$

Equation 5.4

where β is described as:

$$\beta = \left(0.74 + 0.0065 e_a \right) \left(1 + 0.17 CC \right)$$

Equation 5.5

$$H_e = C_e L_e A H$$

Equation 5.6

$$H_c = C_c A \left(0.2 U \left(T_a - T_w \right) \right)$$

Equation 5.7

where A is the heat-exchange surface (m^2), corresponding to the air-water interface, R_s is net solar radiation (MJ m^2), T_a is air temperature (°K), σ is the Stefan–Boltzmann constant (4.9 x 10-9 MJ m^{-2} °K^{-4}), β is the sky emissivity (0-1), L_e is the height of evaporated water as calculated by the hydrological model (m), H is the latent heat of vaporization (2480 MJ m^{-3}), CC is the cloud cover fraction (0-1), U is wind speed (km/h), e_a is air vapour pressure (mm Hg) and C_s, C_i, C_e and C_c are empirical coefficients to be adjusted during model calibration. In both the hydrological and the thermal model, H is estimated using a modified Thornthwaite equation (Morin & Couillard, 1990):

$$H = \frac{10}{30.4} 1.62 \left(10 \frac{T_a}{XIT} \right)^{XAA}$$

Equation 5.8

where *XIT* and *XAA* are empirical coefficients calculated from mean monthly air temperatures.

Both the water budget and the water temperature calculations are performed on each square area of a predefined grid. A complete description of the original model is available in Morin and Couillard (1990). A thorough description of recent model modifications is available in (St-Hilaire et al., 2015).

5.1.2.2   *Ensemble Forecasting System*

In order to provide an estimation of the uncertainty associated with water temperature forecasts, an ensemble method is proposed. The core of this system is the CEQUEAU model described in section 5.1.2.1, fed with meteorological ensemble forecasts as inputs.

In a typical operational setting, the hydrological and thermal forecasting process begins by estimating the best possible values for the initial state of the watershed. This initial state is described by state variables, for instance current soil humidity, which are typically difficult to monitor. Thus, this estimation is most often performed by running the hydrological model in simulation mode for at least a year prior to the initial time of the forecast (spin up period). In the context of this study, instead of repeating this process of 'state estimation then forecast', the initial states were estimated for each time step in a single run and preserved for future use. Then, for each time step (*t*), the hydrological and thermal initial states of the watershed are retrieved at time *t* and provided to the model. The ensemble meteorological forecasts for time *t+1* to *t+5* are used as model inputs to produce a one to five day forecasts. Those meteorological ensemble forecasts are described in greater details in section 5.1.2.5. Each set of meteorological forecasts, called members (*k*), that composes the ensemble is fed to the model individually. To produce a 5 day forecast of 20 members, the CEQUEAU model is thus run 20 times.

The output is a distribution of 20 hydrological and thermal forecasts for each forecasted time step. Those outputs for each forecasting horizons are then stored individually to build complete time series of each of the five lead-time forecasts. The temperature ensemble forecasts for these five days are henceforth analysed separately and referenced as forecasting horizons one to five (hz1 to hz5). The forecasting framework is summarized in Figure 5.1.

The model was run from 2009 to 2014 during the summer period (i.e. between June 15th and September 15th) for both the regulated and natural systems. The length of this period is limited by the availability of the archived ensemble meteorological forecasts and the water temperature data.
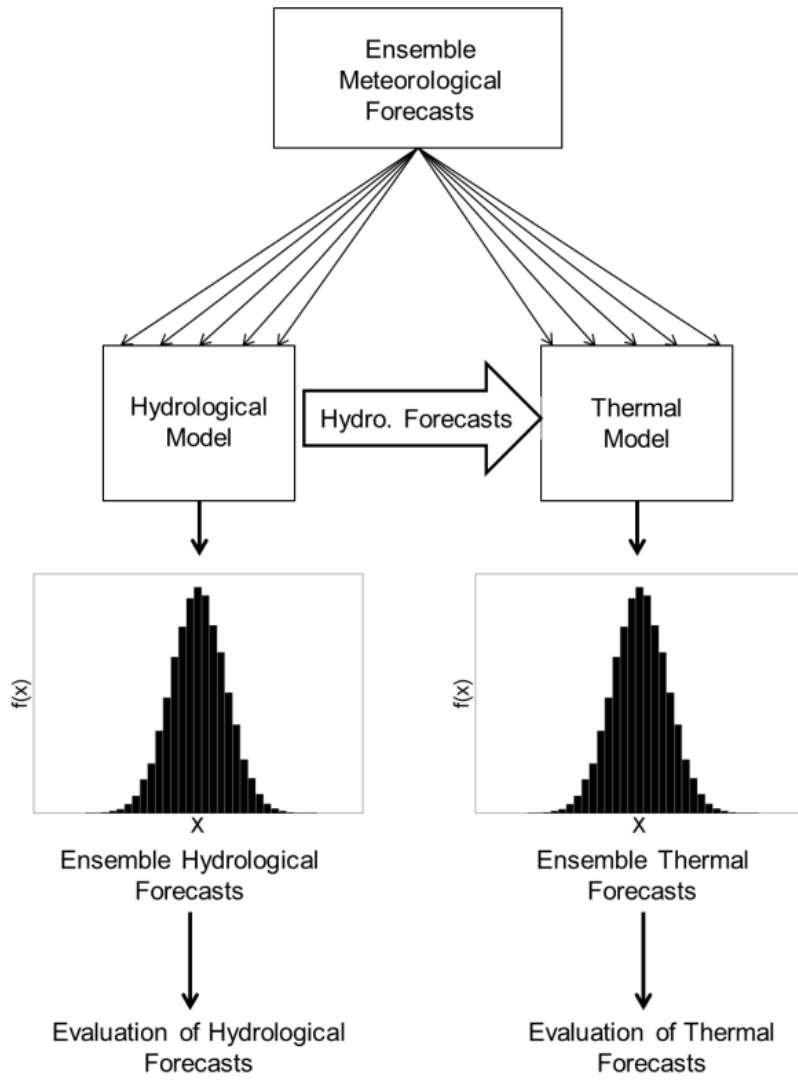
Figure 5.1: Forecasting framework of discharge and water temperature

5.1.2.3   *Model Calibration*

Both the thermal and the hydrological models contain parameters that must be calibrated based on a comparison of streamflow simulations with observations. They were calibrated using a split sample method. Because of the cascade structure of the model, the hydrological parameters were adjusted prior to those of the thermal model. The parameters of both models were optimized using a covariance matrix adaptation evolution strategy (CMA-ES; Hansen & Ostermeier, 1996). The hydrological model includes 28 parameters from which 16 have physical meaning and 12 are adjusted

based on goodness of fit only. The reader is referred to St-Hilaire et al. (2000) for a complete list and description of the parameters. The hydrological model was optimized based on Nash-Sutcliffe efficiency criterion (NS; Equation 5.9) and bias (Equation 5.10), while the calibration of the thermal model relied on minimizing the root mean squared error (RMSE; Equation 5.11) between observed and simulated water temperatures. In all cases, the parameters were obtained from 1500 iterations of the CMA-ES optimization algorithm.

$$NS = 1 - \frac{\sum_{t=1}^{n}(y_t - \hat{y}_t)^2}{\sum_{t=1}^{n}(y_t - \bar{y})^2} \qquad\qquad \text{Equation 5.9}$$

$$Bias = \frac{1}{n}\sum_{t=1}^{n}(\hat{y}_t - y_t) \qquad\qquad \text{Equation 5.10}$$

$$RMSE = \sqrt{\frac{1}{n}\left(\sum_{t=1}^{n}(\hat{y}_t - y_t)^2\right)} \qquad\qquad \text{Equation 5.11}$$

In Equation 5.9 to Equation 5.11, n is sample size, y_t is the observed value (flow or temperature) at time t, and $\hat{y}_t$ is the simulated value (flow or temperature) at time t.

5.1.2.4 *Forecasts Verification and Explicit Consideration of Uncertainty*

An extensive toolbox of evaluation criteria was developed to rightfully assess the quality of an ensemble forecast (Gneiting and Raftery, 2007; Hamill and Colucci, 1997; Hersbach, 2000; Laio and Tamea, 2007). One of the most frequently encountered scores in the hydrological ensemble forecasting literature is the Continuous Ranked Probability Score (CRPS). Basically, the CRPS compares the cumulative distribution function (CDF) of the forecast members with the CDF of the observation. If the observation is represented by a single value, its CDF is a Heaviside function. As

demonstrated by Gneiting and Raftery (2007), the mean CRPS (Equation 5.12; MCRPS) is the probabilistic analog of the mean absolute error (MAE). The MCRPS is defined as:

$$MCRPS(F, y) = \frac{1}{n} \sum_{t=1}^{n} \left(\int_{0}^{\infty} \left(F(x_t) - H(x_t \geq y_t) \right)^2 dx \right) \qquad \text{Equation 5.12}$$

where *F(x)* is the cumulative density function (CDF) of the forecasted variable at time step *t (xt)* for all ensemble members, $H(x_t \geq y_t)$ is the Heaviside (step) function of the tth observed value (*yt*) and *n* is the number of time steps. A normal distribution is typically accepted for temperature (Gneiting et al., 2005) and was thus used in the present analysis. A Monte-Carlo approximation proposed by Gneiting and Raftery (2007) was used to solve the integral in Equation 5.12, which is therefore estimated using Equation 5.13:

$$MCRPS(F, y) = \frac{1}{n} \sum_{t=1}^{n} \left(E|X - y_t| - \frac{1}{2} E|X - X'| \right) \qquad \text{Equation 5.13}$$

for which *X* and *X'* are vectors containing many random draws (*N* = 1000) from the predictive distribution function (*F*) in Equation 5.12.

Standard model evaluation strategies are based on the quality of the fit between the measurements and the simulations (or forecasts). However, Hague and Patterson (2014) suggest that this type of evaluation might not "aptly evaluate" a model's performance when it comes to water temperature modelling for fisheries management. They suggest looking at the capacity of a model to predict a threshold exceedance instead of solely focusing on the traditional best fit. Given the fact that in many systems, thermal forecasts are issued in order to keep water temperature below a target threshold (Cole et al., 2014; Macdonald, Morrison, & Patterson, 2012; Pike et al., 2013) the evaluation of threshold prediction capacity of the forecasting system is essential to assess its usefulness. Hence, in addition to the MCRPS, the Brier Score (BS; Equation 5.14; Brier, 1950) was calculated as:

$$BS = \frac{1}{n}\sum_{t=1}^{n}\left(p(x_t) - p(y_t)\right)^2 \qquad\qquad \text{Equation 5.14}$$

where $p(x_t)$ is the probability of exceeding the threshold according to the forecast on day t and $p(y)$ is the outcome according to the observation (y). In the case of a deterministic forecast, the value of $p(x_t)$ can only be 1, if the temperature x_i exceeds the threshold or 0 if it is predicted not to happen. The same logic applies to $p(y)$. On the other hand, if the forecast is a distribution of values (i.e. an ensemble forecast), $p(x_t)$ can take any value between 0 and 1.

The overall uncertainty of the ensembles was tracked for all forecasting horizons by calculating the spread of the daily distribution (maximum – minimum). Reliability plots (Stanski et al., 1989) were also produced to assess the reliability of the water temperature forecasts. Confidence intervals, named forecast nominal probability, for confidence levels of 10% increments were first calculated for the ensemble forecast only (hz1-hz5). Then, the observed probability of each confidence interval was computed by calculating the frequency at which the observation was included in a given interval. The results were then displayed as a scatter plot with the forecast nominal probabilities on the x-axis and the observed probability on the y-axis. For a perfectly reliable forecasting system, nominal probabilities should be equal to the observed probabilities. For instance, the computed 90% interval should include the observed temperature 9 days out of 10 on average.

5.1.2.5   Study Sites and Data

The CEQUEAU model described above was implemented on the Nechako watershed (125°59' W and 53°46' N) in the province of British Columbia, Canada and on the Southwest Miramichi River (65°82' W and 46°74' N) in the province of New Brunswick, Canada (Figure 5.2).
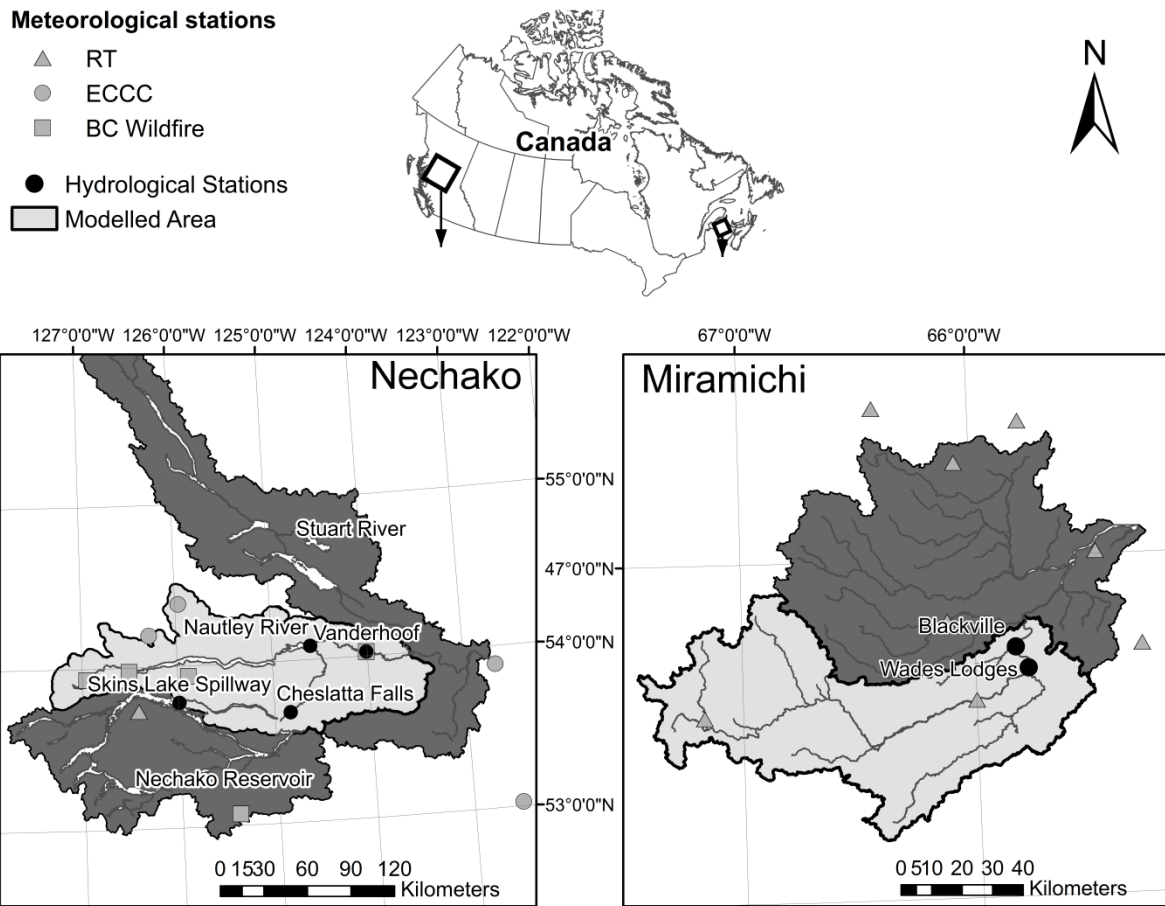
Figure 5.2: Maps of the Nechako and the Miramichi watersheds

Nechako

The Nechako River flows from the Skins Lake Spillway eastward for about 245 km before it reaches its junction with the Stuart River. It begins its course in the coastal range, and then it drains the Nechako Plateau and flows into the Fraser River at Prince George, British Columbia. The watershed covers about 47 000 km^2. The Stuart and Nautley Rivers are its major tributaries (Figure 5.2). A major dam in the Nechako Canyon and nine saddle dams were built in the early 1950's to create the Nechako reservoir, which is about 181 kilometers long (Boudreau, 2005). The Skins Lake spillway (Figure 5.2) typically discharges between 170 and 283 m^3/s from July 11th to August 20th and between 14.2 and 49 m^3/s throughout the rest of the year.

An average total annual precipitation of 417 mm was monitored at the Ootsa Lake meteorological station between 1981 and 2010, 37% of which fell as snow. The average air temperature is 3.2°C with an average maximum of 19.8°C occurring in August and an average minimum of -11.8°C in January.

A protocol called the Summer Temperature Management Program (STMP) was implemented in the Nechako River to monitor water temperature downstream from the dam and to ensure that water temperature remains below 20°C at a control section near the city of Finmoore (i.e. upstream of the confluence of the Nechako and Stuart Rivers). This protocol is in effect between July 20th and August 20th (Nechako Fisheries Conservation Program [NFCP], 2005). The measure was introduced to benefit sockeye salmon (*Oncorhynchus nerka*) during its spawning period. During that period, water releases at Skins Lake are increased in order to reach a minimum discharge of 170 m^3/s at Cheslatta Falls. To assess the capacity of the model to predict the exceedance of the 20°C threshold, a Brier Score (Equation 5.14) was calculated for a value of 20°C identified as critical temperature. A Brier Score for a threshold value of 18°C was also calculated and labelled as early warning.

The model was set up for the management of summer water releases at the Skins Lake Spillway. Therefore, only the portion of the watershed located between the Skins Lake Spillway and the confluence of the Nechako and Stuart Rivers (Figure 5.2) was modelled. At its upstream boundary, the model was fed with the discharge released at the Skins Lake Spillway. Water temperature was also necessary at the model upstream boundary. Data were available for 2013 and 2014 but modelling was required to provide input reservoir temperatures for previous years (2009-2012). An autoregressive model with exogenous variables (ARX) that uses air temperature residuals as predictors (Ahmadi-Nedushan et al., 2007) was calibrated using data from moored thermographs. The calibrated model was subsequently used to generate water temperature at the surface of the reservoir. Model performances are presented in the results section.

The travel time between the Spillway and the site that is subject to the thermal constrain is estimated to be 5 days (Envirocon Ltd., 1984). Discharge and water temperature at the outlet of the Nautley River were kept constant for all forecasting horizons (hz1 to

hz5) in forecasting mode. The last observation of both discharge and water temperature recorded at the Nautley station (Figure 5.2) were thus fed to the model. This was done in order to replicate the actual forecasting framework used for operations.

Southwest Miramichi

The Southwest Miramichi flows in the main stem of Miramichi River before it empties in the Atlantic Oceans. It occupies about 60% (7800 km^2) of the total drainage area (13,000 km^2) of the Miramichi watershed. Measurement sites are located at Blackville (discharge) and Wades Lodges (water temperature) which drains about 5600 km^2. The two measurement sites are separated by 10 km of river. Mean discharge at the Blackville hydrological station (Figure 5.2) is 120 m^3/s with peaks reaching more than 2000 m^3/s and low flows around 20 m^3/s. Its hydraulic regime is considered as naturel by the Water Survey of Canada (http://wateroffice.ec.gc.ca). It receives an average annual total precipitation of 1175 mm (Doaktown – Environment and Climate Change Canada) of which 25% falls as snow.

Water temperatures in the Miramichi system are known to exceed the optimal range of 16-20°C for Atlantic salmon (*Salmo Salar*; Caissie and Breau, 2013). Between 1997 and 2016, mean daily summer water temperature recorded in the Southwest Miramichi was 19.33°C with a maximum of 25.87°C (July 9th, 2010) and a minimum of 11.36°C (September 21st, 2014). Thresholds of 20°C for minimum daily water temperature and 23°C for maximum daily water temperature were identified for management strategies in the system (Department of Fisheries and Oceans Canada [DFO], 2012). Brier Scores were therefore calculated for thresholds values of 20°C (early warning) and 23°C (critical temperature).

Since the Miramichi is unregulated, no input discharge or water temperatures had to be provided to the model as a boundary condition. The period between June 15th and July 5th, 2011 on the Miramichi were removed from the analysis because the radiation forecasts were not available. For ease of reading, the Southwest Miramichi will be referred to as the Miramichi.

Meteorological and Hydrological Data

On the Nechako, meteorological data used to adjust the hydrological model parameters (*pTot*, *tMin* and *tMax*) were provided by British Columbia Wildfire (BC Wildfire) management branch, Environment and Climate Change Canada (ECCC) and Rio Tinto (RT), an aluminium producer who manages the watershed for hydro-power production (Figure 5.2). BC Wildfire data were preferred over most of the data from RT's meteorological stations because of their better representation of the meteorological conditions on the watershed. Cloud cover (*CC*) was retrieved from ECCC stations Bella Coola, Quesnel, Prince George and Terrace. Net solar radiation (R_s), relative humidity (R_H) and wind speed (*U*) were extracted from the NASA Prediction of Worldwide Energy Resource (POWER) on a grid with 1° horizontal resolution.

A string of 13 temperature loggers (Onset HOBO Pendant temperature loggers; ±0.53 °C accuracy) placed at a 0.91 m (3 feet) vertical distance from each other was attached to a buoy, located at about 150 m upstream of the Skins Lake Spillway from May to October 2013 and 2014 and for July to October during the summer of 2015. These data confirmed that the water column was well mixed during the period of the year where the STMP applies. Data from the first two sensors from the surface were used to calibrate the ARX surface water temperature model in the reservoir, which is subsequently used as the upstream thermal boundary condition. Water temperature time series for Vanderhoof (station #08JC001) and Cheslatta Falls (station #08JA017) were provided by the Water Survey of Canada. On the Nechako River, the calibration dataset for the model includes time series from 2002 to 2006 while the validation period includes years 2007 to 2010. The forecasting period is 2009-2014.

On the Miramichi, *pTot*, *tMin* and *tMax* were provided by Environment and Climate Change Canada (ECCC) and net solar radiation, relative humidity and wind speed were also extracted from the POWER database. CC was derived from the proportion of extra-terrestrial solar radiation reaching the earth surface. All of the aforementioned data were downscaled to the grid used by CEQUEAU using a three nearest neighbours' method.

Discharge data at Blackville (station #01BO001) were retrieved from the Water Survey of Canada database. Water temperature data from Department of Fisheries and Oceans Canada at the Wades Lodges station (46.6716 N and 65.7738 W) retrieved from the rivTemp database (http://rivtemp.ca) were used. Gaps in the data were filled using corrected data from Millerton station (46.8779 N and 65.6639 W). The calibration dataset for the model spanned from 2000 to 2005 and the validation dataset spanned from 2006 to 2010. The forecasting period was also 2009-2014 on the Miramichi watershed. These periods were limited by the availability of the water temperature time series and the availability of the observed meteorological inputs.

On both watersheds, RH and mean daily air temperature (T_a; °C) were used to estimate air vapour pressure (e_a; kPa) with Tetens (1930) formula as given by Equation 5.15 and Equation 5.16.

$$e_s = 6.11 \cdot 10^{\left(\frac{7.5 \cdot T_a}{237.3 + T_a}\right)}$$

Equation 5.15

$$e_a = RH \cdot e_s / 100$$

Equation 5.16

where e_s is the saturated vapour pressure.

The ensemble meteorological forecasts were extracted in grib2 format through The Observing System Research and Predictability Experiment (THORPEX) Interactive Grand Global Ensemble (TIGGE) portal. They include variables that are typically used for the purpose of hydrological forecasting, namely, total precipitation, and minimum and maximum air temperature. In this study the net solar radiation, dew point temperature, wind speed, and cloud cover are also required. These additional variables are used by the thermal model that follows the hydrological model in the modelling/forecasting cascade. Forecasts for the relative humidity are not available on the TIGGE portal. Therefore, the dew point (T_d; °C) was used to estimate air vapour pressure (e_a; kPa) using equation 15 with T_d replacing T_a. The two orthogonal vectors for wind speed, 10_u (east-west axis) and 10_v (north-south axis), were transformed in a single wind component.

Forecasts emitted by the Canadian Meteorological Center (CMC) were preferred, as they are the most susceptible of being used operationally in Canada. However, CMC's net solar radiation forecasts are not available on the TIGGE portal. Consequently, net solar radiation forecasts from the European Centre for Medium Range Weather Forecasts (ECMWF) were used. Forecasts for all other variables are from the CMC. The Canadian ensemble forecasts are composed of 20 members generated from different initial conditions of the atmosphere, physical parameters and perturbed observations (Gagnon et al., 2014). ECMWF forecasts are composed of 50 members also generated from different initial conditions and model's physics perturbations. In order to use the ECMWF and CMC forecasts in the same forecasting framework, only 20 members out of the 50 emitted by the ECMWF were retained for each forecast (hz1 to hz5). At each time step, a sub-sample of 20 members was drawn randomly and kept for the five forecasting horizons. Another random sub-sample was then drawn for the subsequent time step. All forecasts were extracted at a 0.6° horizontal resolution and downscaled on the CEQUEAU grid using a bilinear interpolation. A CEQUEAU grid resolution of 5 km was used for Nechako watershed and 12 km for the Miramichi watershed. The difference between the grid resolutions is due to the use of pre-existing structures. Previous work by Dugdale et al. (2017) showed minor differences in model performance between grids resolutions of 2.5 km and 20 km.

A MCRPS (Equation 5.12) was calculated between observations at the meteorological stations and the corresponding grid cell of the meteorological forecasts for *tMin*, *tMax*, *pTot* and R_s. Note that MCRPS for R_s was only calculated for 2014 (Jul 25th to Aug. 20th) on the Nechako watershed. With regards to the remaining R_s forecast and the other input variables (*CC*, *U* and e_a), MCRPS was calculated by comparing data interpolated on the CEQUEAU grid including data extracted from the POWER database with the forecasts interpolated on the same grid. This was done in order to assess the quality of ensemble meteorological forecasts used as inputs for the hydrological and thermal models. A particular attention was paid to solar radiation because of its importance in the estimation of the surface thermal budget of a river.

5.1.3   Results

5.1.3.1   Model Calibration and Evaluation

Hydrological and water temperature model calibration performance metrics are summarized in Table 5.1. Both models show satisfactory performances, with relatively low RMSE values for simulated water temperatures during the critical summer period. The parameters of the thermal model were optimized to best reproduce water temperature at Vanderhoof (Nechako) and Wades Lodges (Miramichi) during the summer period (June 15th to September 15th). This was successfully achieved, with a RMSE under 1.6°C during both calibration and validation periods (Table 5.1). The ARX model (temperature of the water release; see section 5.1.2.3) yielded a RMSE of 1.18°C and 1.28°C in calibration and validation, respectively.

Table 5.1. Calibration results for the hydrological and the thermal model on the Nechako (NECH) and Miramichi (MIR) watersheds

	Discharge						Water Temperature							
							Year-Round				Summer			
	NS		Bias (m³/s)		Relative Bias		RMSE (°C)		Bias (°C)		RMSE (°C)		Bias (°C)	
Period	NECH	MIR	NECH	MIR	NECH	MIR	NECH	MIR	NECH	MIR	NECH	MIR	NECH	MIR
Calibration	0.96	0.84	8.87	-3.03	0.08	0.03	1.38	1.37	0.24	-0.54	0.78	1.23	0.43	-0.76
Validation	0.86	0.72	-10.4	-18.6	0.08	0.13	1.54	1.51	0.2	0.09	0.95	1.46	0.37	0.18

Meteorological Forecasts Evaluation

The MCRPS calculated for the meteorological forecasts are summarized in Table 5.2. Total precipitation showed relatively low MCRPS for all lead-times on both watersheds, ranging between 0.7 mm (hz1 - Nechako) to 3.0 mm (hz5 - Miramichi). With regards to air temperature, a higher MCRPS was found for *tMin* (1.97-3.80°C) compared to *tMax* (1.35-1.81°C). Between Jul. 25th and Aug. 20th, MCRPS for R_s ranges between 2.5 MJ/m^2 (hz1) and 3.1 MJ/m^2 (hz5) at Skins Lake on the Nechako watershed. In relative terms, it represents 13% and 21% of the observed values respectively. Troccoli and Morcrette (2014) calculated relative MAE's between 18% and 45% for direct solar radiation forecasted by the ECMWF's Global Atmospheric Model in Australia. These values are of the same order of magnitude than those obtained in the present study.

Table 5.2: MCRPS between ensemble forecasts and observations for all meteorological variables on the A) Nechako and B) Miramichi

	Hz1		Hz2		Hz3		Hz4		Hz5	
	NECH	MIR	NECH	MIR	NECH	MIR	NECH	MIR	NECH	MIR
t_{min} (°C)	3.30	1.97	3.50	2.14	3.70	2.25	3.70	2.26	3.80	2.47
t_{max} (°C)	1.60	1.35	1.50	1.42	1.60	1.53	1.60	1.66	1.80	1.81
$pTot$ (mm)	0.70	2.03	1.00	2.18	1.60	2.04	2.00	2.87	2.80	3.00
R_S (MJ/m²)	2.50	2.32	2.50	2.40	2.50	2.76	2.70	3.75	3.10	3.25
CC (0-1)	0.15	0.16	0.14	0.16	0.14	0.17	0.14	0.18	0.15	0.19
U (km/h)	1.35	2.13	1.36	2.05	1.34	2.07	1.29	2.18	1.55	2.16
e_a (mm Hg)	3.17	1.24	3.10	1.19	3.04	1.19	2.96	1.22	3.06	1.28

Figure 5.3 shows MCRPS's calculated between the forecasted radiation interpolated (hz5) on the CEQUEAU grid and the corresponding observations interpolated on the same grid. For ease of reading, only radiation is presented because of its major importance for thermal modelling. Figure 5.3-A highlights an east-west gradient of the adequacy between the grid of observed and forecasted solar radiation on the Nechako watershed. Lower MCRPS values were found in the western section of the watershed while higher values were observed in the middle section before it diminishes again towards the eastern part. In the eastern section, where sits the main stem of the Nechako, MCRPS's remained fairly high with values above 3 MJ/m². Although not shown here, such an east-west gradient was observed for all forecasted variables.
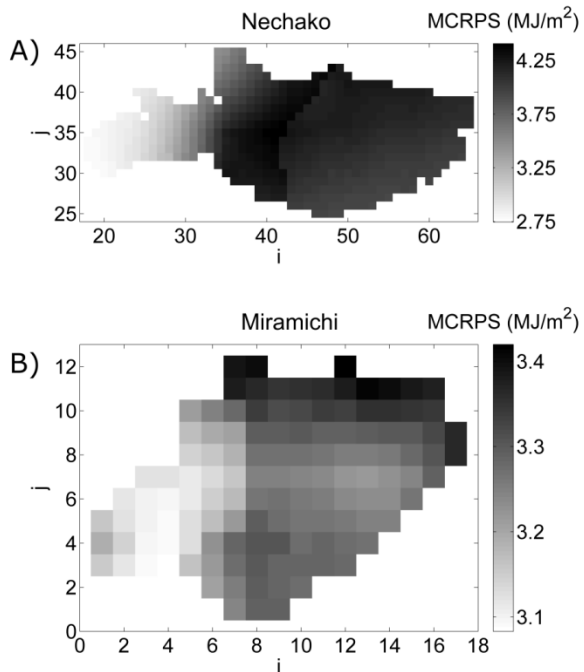
Figure 5.3: MCRPS of interpolated solar radiation compared to interpolated observations on A) the Nechako watershed and B) the Miramichi watershed.

On the Miramichi watershed, the MCRPS values are slightly higher in the north-eastern part of the watershed but no clear spatial pattern was observed with respect to the accuracy of the solar radiation forecast (Figure 5.3-B) or other forecasted meteorological variables. As observed for the Nechako watershed, the MCRPS for solar radiation is quite high across the watershed and remained above 3 MJ/m^2.

On the Nechako watershed, the total precipitation showed large relative bias (>100%). In absolute terms, this bias remained fairly low (< 2 mm) while the same metrics were much lower on the Miramichi watershed with relative biases under 25% (< 1 mm). With regards to air temperature, both *tMax* and *tMin* had a relative bias under 20% on both watersheds, which translates into a larger bias for *tMax* in absolute terms (> 3°C) compared to *tMin* (< 1°C). On the Nechako watershed, maximum air temperature was strongly biased in the upper part the watershed while bias diminishes towards its eastern border. Air temperature is used in the estimation of longwave radiation (Equation 5.4), convection (Equation 5.7) and evaporation (Equation 5.8). Cloud Cover (*CC*) on the Nechako watershed showed a positive bias of 32% which was higher in the eastern part of the watershed than in the western part. On the Miramichi maximum

biases of 20% were calculated and were constant across the watershed. Forecasted e_a had a maximum relative bias of 30% on the Nechako watershed while it reached 12% on the Miramichi. The highest bias values were found in the lower eastern part of the Nechako watershed and were spatially constant on the Miramichi. *CC* and e_a are both used in the calculation of sky emissivity (Equation 5.4), involved in the estimation of energy fluxes associated with longwave radiation (equation Equation 5.5). Wind speed, which is used along with air temperature in the calculation of convective heat fluxes (Equation 5.7), was biased by 35% (2.5 km/h) on average with a stronger bias in the upper part of the Nechako watershed. On the Miramichi watershed, biases were constant around 15% (1.2 km/h). Solar radiation, used directly as heat input in thermal modelling, was positively biased by 17% (3.14 MJ/m^2) on the Nechako watershed and negatively biased by 6% (-1.07 MJ/m^2) on the Miramichi watershed.

5.1.3.2   *Hydrological and Thermal Forecasts Evaluation*

The first step of the forecasting cascade is the hydrological forecast. Since discharge was imposed at the Skins Lake Spillway and at the outlet of the Nautley River in forecasting mode, very low uncertainty (< 1 m^3/s) was induced to the hydrological forecast by the ensemble precipitation forecast on the Nechako watershed (Figure 5.4). Therefore, MCRPS's calculated from resulting discharge ensembles (Figure 5.6-A), which range from 17.1 m^3/s (hz1) to 21.4 m^3/s (hz5), are very similar to MAE calculated from simulations using observed meteorological inputs (17.7 m^3/s). On the Miramichi, MCRPS's ranging between 31.7 m^3/s (hz1) and 34.4 m^3/s (hz3; Figure 5.6-B) were in the same order of magnitude than the MAE calculated for simulated discharge (34.9 m^3/s).
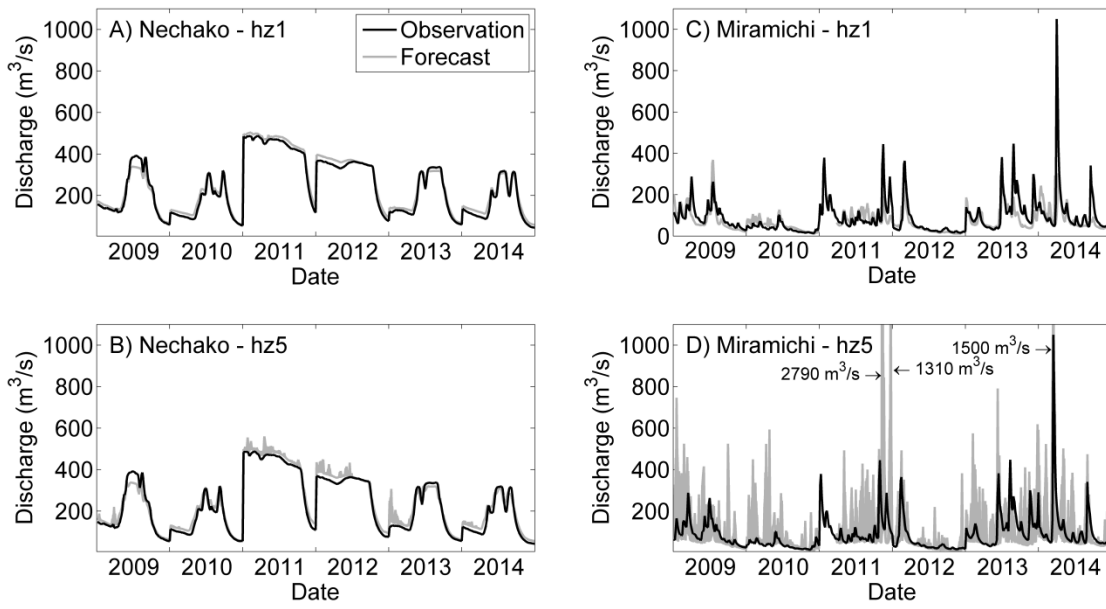
Figure 5.4: Ensemble discharge forecasts for a A) one day lead-time on the Nechako, B) five day lead-time on the Nechako, C) one day lead-time on the Miramichi and D) five day lead-time on the Miramichi.

Figure 5.5 presents the ensemble forecasts produced for water temperature on both watersheds for 1 day-ahead and 5 day-ahead lead-times. One day-ahead forecast showed good performances on both rivers with a MCRPS somewhat higher on the Miramichi (0.92°C) than on the Nechako (0.77°C) but both under 1°C (Figure 5.6-B). The spread of the ensemble was also larger on the Miramichi (0.92°C) than on the Nechako (0.73°C). On the Nechako, the MCRPS increased with lead-time to reach 0.82°C on hz5. On the Miramichi, MCRPS reaches 1.08°C on hz2 and decreases to 1.00°C on hz5. Figure 5-B shows that some 5 day lead-time forecasts are strongly biased at the beginning of 2011 and 2012 on the Nechako.
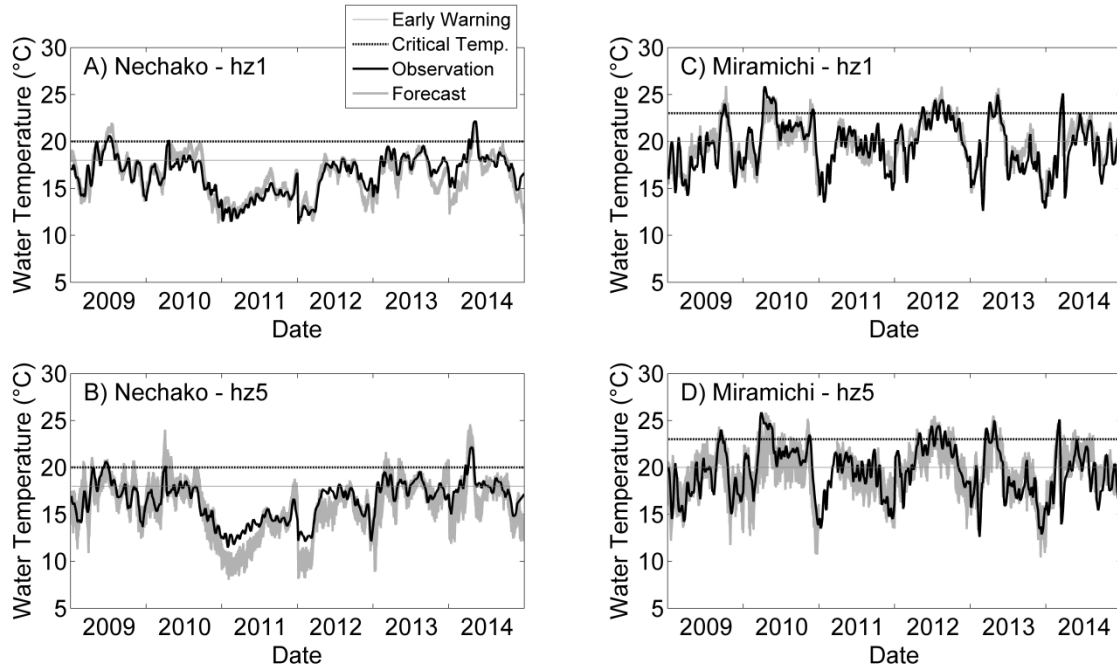
Figure 5.5: Ensemble water temperature forecasts for a A) one day lead-time on the Nechako, B) five day lead-time on the Nechako, C) one day lead-time on the Miramichi and D) five day lead-time on the Miramichi.

In terms of threshold exceedance predictions indicated by the BS, similar values for the early warning were obtained for both rivers with BS = 0.15 for hz1 (Nechako and Miramichi) and respectively 0.13 and 0.15 for the Nechako and the Miramichi at hz5 (Figure 5.6-C). When the BS is calculated for higher temperature thresholds (critical temperature), both rivers performed well with lower scores obtained on the Nechako (BS = 0.01-0.02) compared to Miramichi (BS = 0.05-0.06). Both thresholds were represented on Figure 5.5. Over the forecasting period, the early warning temperature was exceeded 46% of the time on the Miramichi and 24% on the Nechako and the critical temperature was exceeded 10% of the time on the Miramichi and 3% on the Nechako.
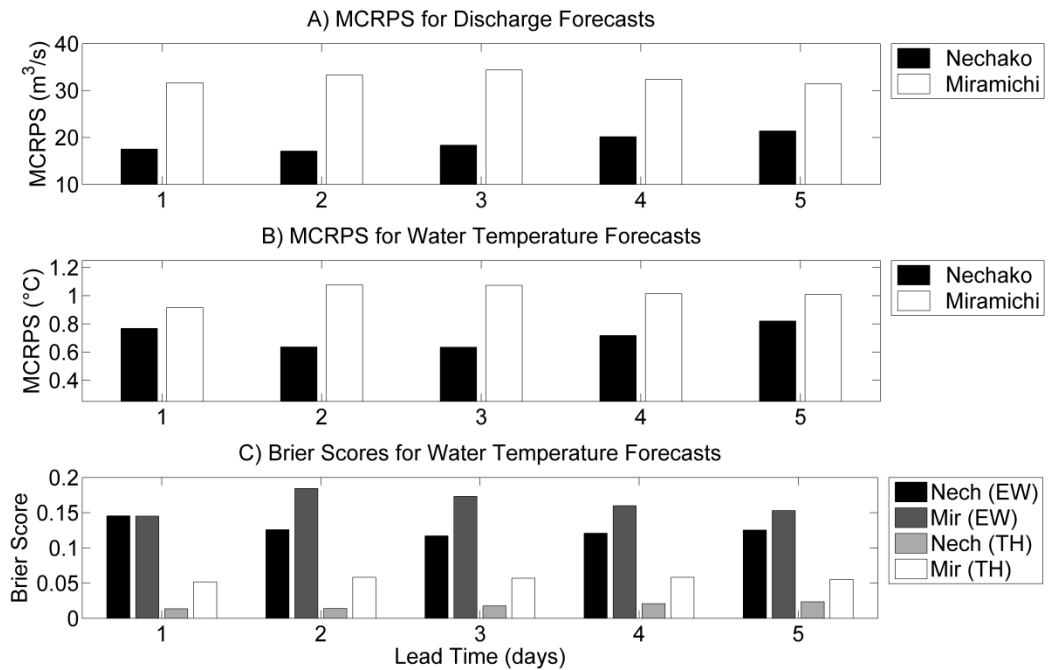
Figure 5.6: A) MCRPS for discharge forecasts, B) MCRPS for water temperature forecasts and C) Brier Scores for both sets of forecasts. Brier Scores are represented for early warnings (EW) and threshold exceedance (TH).

5.1.3.3   Uncertainty and Reliability of the Forecasts

One of the main objectives of this work is to assess and represent the uncertainty that is propagated to a water temperature forecast by the meteorological inputs. Figure 5.4 shows that the spread of the discharge ensemble forecast is much larger on the Miramichi than on the Nechako at hz5 with values between 3.74 m^3/s and 125.9 m^3/s. Important variability was observed during the forecasting period, especially for longer lead-times with a standard deviation of 194 m^3/s for hz5 (Figure 5.4).

Figure 5.7 shows the spread of the water temperature ensemble forecasts. The central line displays the mean spread of the ensemble for a given lead-time and the vertical bars represent one standard deviation of the same spread. We observed a larger ensemble spread on the Miramichi compared to the Nechako for both forecasting horizons. On both rivers, the spread of the ensemble increased with lead-time to reach 2.29°C on the Nechako and 3.14°C on the Miramichi. However, the spread of the

79

ensemble as well as the variability of the spread increased more rapidly on the Miramichi than on the Nechako (Figure 5.7). Therefore, more uncertainty was propagated in the Miramichi water temperature forecasting system. These observations are also visible on the time series plot on Figure 5.4. It should be noted that the water temperature forecasts spread on the Miramichi is exacerbated by the propagation of the uncertainty of the discharge forecast to the water temperature forecast.
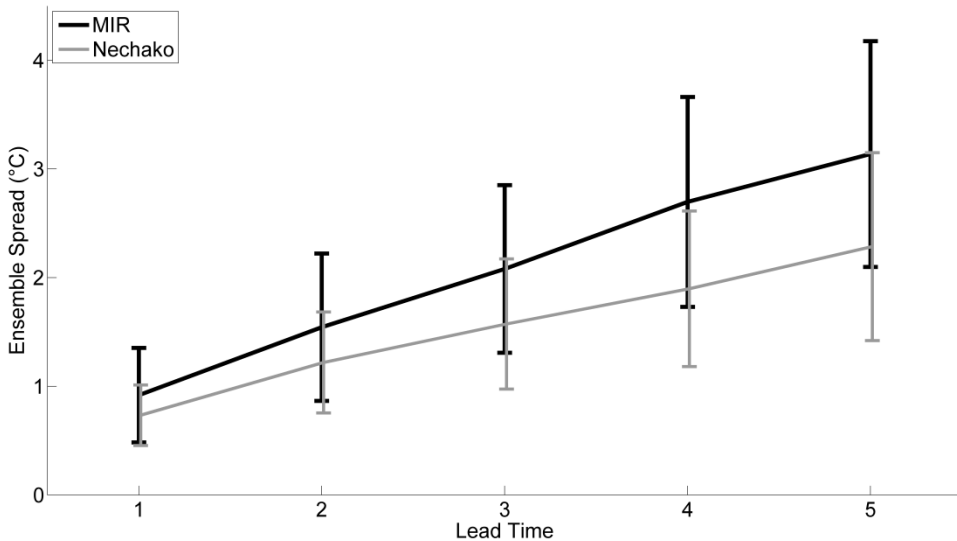
Figure 5.7: Ensemble spreads *of water temperature forecasts* **for lead-times of one to five days on the Nechako (grey line) and the Miramichi (black line).**

Figure 5.8 shows the reliability plots of discharge forecasts for all lead-times. The reliability plot for the Nechako (Figure 5.8- A) clearly demonstrates the lack of spread of the discharge forecast. For all forecasting horizons, the observed probabilities stay close to zero for all forecast nominal probabilities. This indicates that observed discharge almost never falls into the ensemble and that the forecasting framework does not include enough uncertainty to be reliable. On the Miramichi (Figure 5.8- B), the reliability increases constantly with lead-time. Although the reliability of the discharge forecast is better on the Miramichi than it is on the Nechako, the lines being under the bisector indicates an under-dispersion of the ensemble. For a forecasted probability of 0.9, the observed probability goes from 0.02 (hz1) to 0.5 (hz5). Although a clear surge in reliability was visible between the first and the fifth horizon, the observed probability remained lower than the forecasted probability for all levels of confidence.
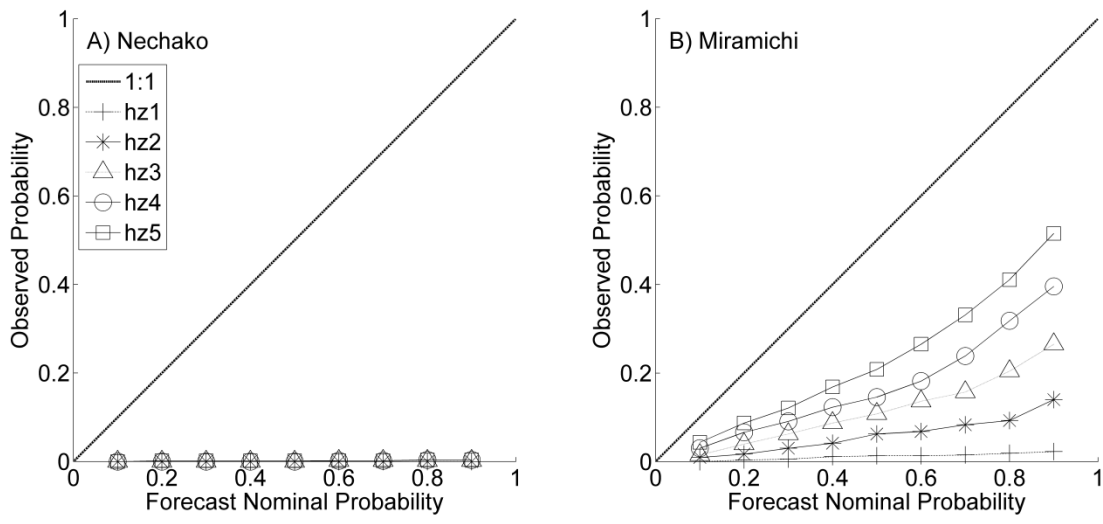
Figure 5.8: Reliability plots for discharge ensemble forecasts on A) the Nechako and B) the Miramichi.

Figure 5.9 displays the reliability plots for water temperature forecasts for all forecasting horizons. It can be seen that on both rivers reliability increases with lead-time. However, more disparity is visible between hz1 and hz5 on the Miramichi. For a nominal probability of 0.9 the observed probability goes from 0.24 to 0.59 while it goes from 0.25 to 0.54 on the Nechako. In both cases, this suggests an over-confidence of the forecasts, meaning that the spread of the ensemble is narrower than it should be in order to convey the total uncertainty related to the forecasting situation. The ensembles of all five lead-time forecasts are thus found to be under dispersed.
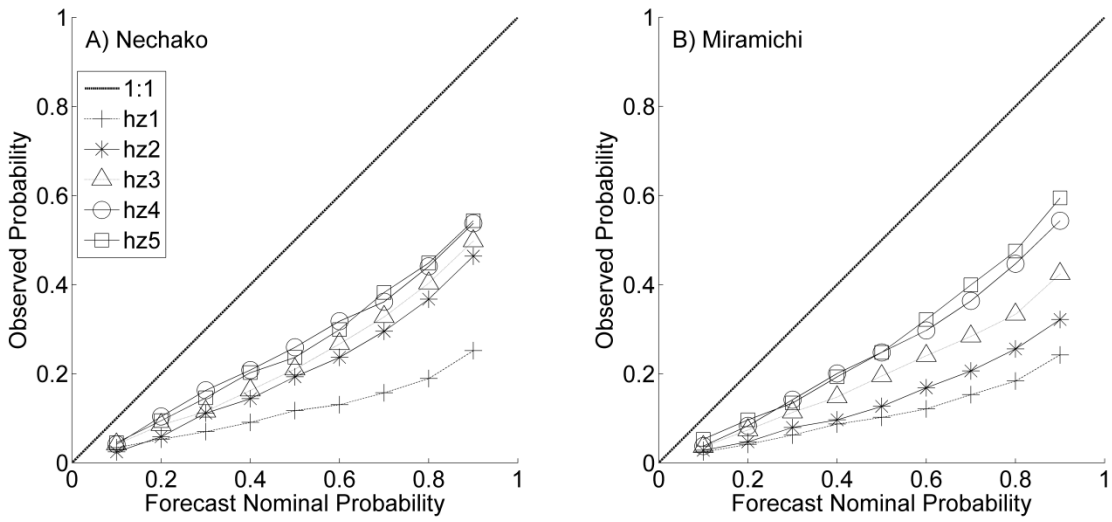
Figure 5.9: Reliability plots for water temperature ensemble forecasts on A) the Nechako and B) the Miramichi.

5.1.4   Discussion

In this paper we produced 5 day ahead forecasts on two Canadian watersheds with special emphasis directed towards uncertainty of meteorological inputs. As expected, the spread of the water temperature ensemble, representative of the meteorological and hydrological uncertainty propagated within the forecast, grows larger with the forecasting horizon. This translated into an improvement in reliability with lead-time. This improvement of reliability is somewhat artificial, as it results from an increase in uncertainty rather than from a better accuracy of individual forecast members. As demonstrated in section 5.1.3.2, meteorological forecasts for all variables were diagnosed as biased. Obviously, the best way to improve the reliability of forecasts is to correct those biases. However, this operation was left out of the present study for two reasons: first, there is a certain disagreement among the hydrologic ensemble forecasting community as to whether it is better to pre-process meteorological inputs, or post-process the hydrological forecasts to remove bias. For instance, Kang et al. (2010)

showed that post-processing was much more efficient than pre-processing to improve the quality of their final streamflow forecasts. Verkade et al. (2013) found that pre-processing meteorological forecasts to remove bias and correct dispersion resulted in very little gain, if any at all, for the final streamflow forecasts. To the best of our knowledge, a comparative study between pre and post processing was never undertaken in the context of water temperature forecasting, since ensemble forecast and quantification of uncertainty is a very new topic to this field. Second, many different pre and post processing methods exist, spanning from very simple (Gudmundsson et al., 2012) to more elaborate (e.g. BMA; Raftery et al., 2005). An adequate comparison of methods is outside of the scope of the present study, which is a first attempt at assessing the potential of ensemble forecasts in the context of water temperature. An in-depth comparative study on the merits of various methods for pre and post processing to improve the reliability of water temperature forecasts is a potential subsequent research avenue.

On the Nechako watershed, despite the large MCRPS for the ensemble precipitation forecasts (2.8 mm at hz5), the effects of this uncertainty on the forecasted discharge are very small. This is due to the fact that discharge is imposed at the model upstream boundaries, namely the Skins Lake Spillway and the outlet of the Nautley River. The large spread observed in forecasted water temperatures for the unregulated Miramichi, even for the first forecasting horizon, suggests an influence of the precipitation uncertainty that propagates into the discharge and ultimately to the water temperature forecasts. This indicates the apparent consequences of the quality of the precipitation forecasts on the subsequent hydrological and thermal forecasting in a natural river. Naturally, the uncertainty propagated within the discharge forecast is transferred to the water temperature forecast. Further analysis would be required to quantify in details this propagation of precipitation uncertainty across the model cascade.

Surprisingly, the ensemble forecast's accuracy (MCRPS) and its capacity to predict a threshold exceedance (BS) remained fairly constant with lead-time. Both metrics (MCRPS and BS) were expected to increase with increasing lead-times indicating a lower accuracy and threshold exceedance prediction capacity. This can be explained by the fact that the initial conditions of the watershed at the beginning of the forecast are

estimations dependent on the spin up period and are necessarily uncertain themselves. The ensemble forecasts were produced from initial states generated from simulations with observed meteorological conditions as inputs without the assimilation of the observed hydrological and thermal conditions. Therefore, the thermal inertia of the system limits the deviation of the short term forecasts from the initial conditions. Thiboult et al. (2016) showed the important influence of the initial conditions of the watershed on hydrological forecast accuracy and reliability through data assimilation. They also suggested that these initial conditions mostly influence the quality of the forecasts for shorter lead-times. In the present study, results indicate that the lower reliability for shorter lead-times can be attributable to the absence of data assimilation. This is especially visible for the discharge forecast on the Nechako River where a relatively narrow ensemble spread translates into low reliability forecasts. Although the proposed model shows satisfactory performances in both calibration and validation modes, initial states still carry a modelling error. In this case, the thermal inertia of the system will carry this modelling error through the forecast horizons but will dissipate with lead-time. Although the proposed forecasting framework performed well both in a regulated and an unregulated river system, the problem related with initial states uncertainty should also be addressed in future work.

The MAE obtained from archived deterministic operational forecasts using a one-dimensional unsteady state water temperature model on the Nechako (personal communication Triton Environmental Consulting; Table 5.3) for a one day ahead forecasts was lower (MAE = 0.49°C) than those obtained in the present study but only spanned from July 20th to August 20th and did not include 2011 and 2012. For the same forecasting period and the same years, the proposed framework yields a MCRPS of 0.85°C. However, for a five day ahead forecast, performance is very similar to the archived forecasts having a MAE of 0.68°C while the proposed framework yielded a MCRPS of 0.69°C. Forecasts were also produced on a tributary of the Southwest Miramichi, the Little Southwest Miramichi (LSWM), by Caissie et al. (2016). An autoregressive models with air temperature as an exogenous variables (ARX) was used for one to three day lead-times from 1992 to 2011 during the summer (June-September). Results show RMSE of 0.87°C for one day ahead forecast and 1.48°C for

a 3 day ahead forecast (Table 5.3). For the same lead-times, the proposed method returned MCRPS of respectively 0.92°C and 1.07°C. Although both metrics cannot be directly compared, these results suggest a slightly better performance of the ARX model for a one day ahead forecast but a better performance of our proposed method for a three day ahead forecast. Although the main objective of this paper is to highlight the uncertainty associated with meteorological inputs in a hydrological and thermal forecast, these comparisons suggest a good potential of CEQUEAU to produce 5 day lead-time forecasts with reasonable accuracy. A thorough model comparison would be of interest for future work.

Table 5.3: Forecasts previously produced on the Nechako and on the Little Southwest Miramichi River (LSWM) on the Miramichi watershed.

	Nechako*				
	Hz1	**Hz2**	**Hz3**	**Hz4**	**Hz5**
MAE (°C)	0.49	0.58	0.55	0.54	0.68
	Miramichi (LSWM)**				
	Hz1	**Hz2**	**Hz3**	**Hz4**	**Hz5**
RMSE (°C)	0.87	1.24	1.48	-	-
Bias	-0.01	-0.03	-0.03	-	-

*Rio Tinto, personal communication; *Caissie et al. (2016)

All forecasts carry uncertainty from various sources. In the absence of knowledge on this uncertainty, the level of confidence into a forecast can hardly be estimated. One of the aims of this study was to provide information on the uncertainty from eight input variables from an atmospheric model that propagates to water temperature forecast in both a regulated and a natural river. We showed the satisfactory accuracy of the ensemble forecast and its capacity to accurately predict threshold exceedance for management purpose for a one to five day lead-time. From a management point of view, these good performances on longer lead-times are valuable, given the fact that decisions and management strategies can be better adapted with longer lead-times.

Knowledge of the uncertainty associated with a water temperature forecast is also valuable and should be integrated in decision making processes. This can be done by basing decisions (at least in part) on probabilistic forecasts like those proposed in the present study. Such framework helps to explicitly communicate the risk associated with a decision. In this case, the probability of exceedance of the water temperature threshold can be calculated from the ensembles. For instance, when 5 out of 20 members predict the exceedance of 20°C water temperature for a given water release, then the risk of having a threshold exceedance is 25%. A decision therefore can be made based on knowledge of the risk associated with this decision. In fact, it was recently shown that the level of risk aversion of a decision-maker is a key factor in assessing the comparative benefits of forecasting systems for decision-making (Matte et al., 2017). In the case of a fully deterministic forecast, that notion of risk is much more difficult to assess and to communicate to the decision-makers, although they are usually aware of its existence (Weijs et al., 2010). From this point of view, ensemble forecasts are clearly advantageous over deterministic forecasts and can even be seen as more « complete ».

While understanding of the uncertainty associated with meteorological inputs was improved with this study, further work is required to fully and accurately capture the uncertainty in water temperature ensemble forecasts, especially for short lead-times (one to three days). The lack of reliability associated with these forecasts also suggests that uncertainty sources that dominate for short lead-times have yet to be fully understood and incorporated in the forecasting framework. Among other sources, the choice of particular hydrological and thermal models, initial conditions, and the level of model parameterization are known to induce uncertainty to the hydrological modelling/forecasting (Beven, 1993). The combination of ensemble forecasting approaches (data assimilation, multi-model and ensemble meteorological forecasts) was shown complementary to represent uncertainty over short (one day) to long-term (10 days) hydrological forecasts (Thiboult et al., 2016). River temperature forecasting would likely benefit from a similar, more complete approach.

5.1.5 Conclusion

The study presented in this paper proposes a modelling framework used to produce ensemble water temperature forecasts in a regulated and a natural river systems. Uncertainty associated with meteorological forecast inputs was quantified throughout the forecasting process. The resulting water temperature forecasts showed good performances on both watersheds for a five day lead-time with a better accuracy on the regulated river system (Nechako) and a better reliability on the natural river system (Miramichi). The present study improved our knowledge of the risk associated with water temperature forecast. As far as the authors know, this paper represents the first published attempt to produce ensemble water temperature forecasts by feeding ensemble meteorological forecasts to a hydrological and thermal model cascade. Further work is required to address accuracy and reliability of short term ensemble forecasts (one to three days). Structural uncertainty and initial state error should thus be investigated in combination with ensemble meteorological forecasts in future work in water temperature forecasting.

5.1.6 Acknowledgements

5.2 Article 2 : Assimilation of Water Temperature and Discharge Data for Ensemble Water Temperature Forecasting

Assimilation de données de température de l'eau et de débit pour la prévision thermique d'ensemble

Sébastien Ouellet-Proulx[1], Olivier Chimi Chiadjeu[1], Marie-Amélie Boucher[2] et André St-Hilaire[1]

[1]Canadian Rivers Institute and INRS-ETE, 490, rue de la Couronne, Québec, Canada

[2]Université de Sherbrooke, département de génie civil, 2500 Boulevard de l'Université, Sherbrooke, Qc, J1K 2R1

Contribution des auteurs :

L'idée qui a mené à l'article a été élaborée par les Pr. André St-Hilaire et Marie-Amélie Boucher avec la collaboration de M. Olivier Chimi Chiadjeu et de l'étudiant (Sébastien Ouellet-Proulx). La programmation de l'algorithme des filtres particulaires a été réalisée par l'étudiant (Sébastien Ouellet-Proulx) et par M. Chimi Chiadjeu. L'ensemble des analyses, et de la rédaction de l'article a été fait par l'étudiant (Sébastien Ouellet-Proulx) sous la supervision des Pr. André St-Hilaire et Marie-Amélie Boucher.

Résumé

Les travaux récents ont démontré la valeur de la prévision de la température de l'eau pour la bonne allocation des ressources en eaux en plus de mettre en évidence l'importance de quantifier son incertitude adéquatement. Dans cette étude, nous effectuons une assimilation multisite en cascade de débits et de températures de l'eau sur la rivière Nechako (Canada) à l'aide de filtres particulaires. Des conditions initiales hydrologiques et thermiques ont été fournies à un modèle de ruissellement des précipitations couplé à un module thermique, avec comme intrants des prévisions météorologiques d'ensemble. Il en résulte une prévision d'ensemble de la température de l'eau d'horizon de 1 à 5 jours. Les résultats illustrent la bonne performance des filtres particulaires qui mènent à une amélioration des conditions initiales de plus de 65 % comparativement aux simulations sans assimilation de données, et ce, pour les composantes hydrologique et thermique. Un indice continu de probabilité ordonnée (CRPS) inférieur à 0,8°C a été calculé pout toutes les prévisions obtenues lorsqu'un ensemble de 40 conditions initiales et de prévisions météorologiques d'ensemble de 20 membres était utilisé. Une plus grande contribution des conditions initiales à l'ensemble de l'incertitude du système pour une prévision d'horizons d'une journée est observée (dispersion moyenne = 1,1°C) comparativement aux forçages météorologiques (dispersion moyenne = 0,6°C). L'inclusion de l'incertitude des intrants météorologiques est essentielle pour maintenir la fiabilité de la prévision et conserver une dispersion appropriée de l'ensemble pour une prévision de 2 jours ou plus. Ces travaux démontrent la capacité des filtres particulaires à actualiser correctement les conditions initiales d'un modèle hydrologique couplé à un modèle thermique. Ils offrent également une réflexion quant à la contribution de deux sources majeures d'incertitude à l'ensemble de l'incertitude propagée à l'intérieur d'une prévision de la température de l'eau.

Abstract

Recent work demonstrated the value of water temperature forecasts to improve water resources allocation and highlighted the importance of quantifying their uncertainty adequately. In this study, we perform a multisite cascading ensemble assimilation of discharge and water temperature on the Nechako River (Canada) using particle filters. Hydrological and thermal initial conditions were provided to a rainfall-runoff model, coupled to a thermal module, using ensemble meteorological forecasts as inputs to produce 5 day ensemble thermal forecasts. Results show good performances of the particle filters with improvements of the accuracy of initial conditions by more than 65% compared to simulations without data assimilation for both the hydrological and the thermal component. All thermal forecasts returned continuous ranked probability scores under 0.8°C when using a set of 40 initial conditions and meteorological forecasts comprising 20 members. A greater contribution of the initial conditions to the total uncertainty of the system for 1-day forecasts is observed (mean ensemble spread = 1.1°C) compared to meteorological forcings (mean ensemble spread = 0.6°C). The inclusion of meteorological uncertainty is critical to maintain reliable forecasts and proper ensemble spread for lead-times of 2 days and more. This work demonstrates the ability of the particle filters to properly update the initial conditions of a coupled hydrological and thermal model and offers insights regarding the contribution of two major sources of uncertainty to the overall uncertainty in thermal forecasts.

5.2.1 Introduction

Water temperature is an important variable for aquatic ecosystems (Fry, 1967; Steel et al., 2012; Ward and Stanford, 1982; Webb et al., 2008). For ectotherm organisms such as fish species, extended exposure to elevated water temperature can induce acute stress (e.g. Olden and Naiman, 2010; Poole and Berman, 2001). In the event of elevated water temperatures on impounded rivers, mitigation approaches can be initiated, such as cold water releases from reservoirs. To ensure the optimal implementation of these mitigation actions, reliable water temperature forecasts have to be issued for various lead-times. The appropriate lead-time depends on the size of the system and on the mitigation measures to be applied. For instance, Huang et al. (2011) demonstrated the benefits on fish populations of using 7 days thermal forecasts to apply mitigation actions (reservoir water release and leasing water from agriculture) on the Klamath River (California, USA) and the John Day River (Oregon, USA).

Various water temperature models were proposed over the last 20 years. These models are often broadly divided in two categories: (i) statistical/empirical models (e.g Ahmadi-Nedushan et al., 2007; Ducharne, 2008; Mohseni et al., 1998); and (ii) deterministic/physics-based models (Cole et al., 2014; Sinokrot and Stefan, 1993; Yearsley, 2009). Physics-based models are often preferred to assess alterations in the thermal budget (Benyahya et al., 2007) or to predict water temperature at various locations within a drainage basin (Cole et al., 2014). The major drawback of such models is their extensive data requirements, which typically include physiographic, hydrological and meteorological variables. As an alternative, statistical models can be adjusted using a reduced number of input variables, but lack in transferability and physical representativeness (Jackson et al, 2017).

Only a few models are commonly used to produce short (i.e. typically < 3 days) and medium range (i.e. typically < 10 days) water temperature forecasts, either for research purposes or operationally. Among them, Morrison and Foreman (2005) performed discharge and water temperature forecasts using a physics-based model for the entire

Fraser River (B.C., Canada). Neumann et al. (2006) developed a regression method to forecast water temperature in a decision support system for the Truckee River (Nevada and California). Other applications of modelling tools for water temperature forecasting can be found in the literature (Bal et al., 2014; Hague & Patterson, 2014; Huang et al., 2011; Pike et al., 2013).

The uncertainty that is associated with water temperature modelling and forecasting has long been discussed and recognized (e.g. Bartholow, 2003; Danner et al., 2012; Neumann et al., 2006). However, the quantification of this uncertainty and subsequent correction of errors are still not systematically performed and demand greater research efforts. Recent studies by Pike et al. (2013), Bal et al. (2014) and Hague and Patterson (2014) have addressed this issue through various methods. For instance, Pike et al. (2013) produced 72 h water temperature forecasts that account for initial conditions uncertainty by performing data assimilation using an ensemble Kalman filter. Hague and Patterson (2014) combined historical air temperature observations, river discharge observations, a combination of air temperatures forecasts and lagged river discharge as inputs to four statistical models. This allowed them to account for the uncertainty attributable to model selection and inputs. Bal et al. (2014) addressed the uncertainty in water temperature modelling using a hierarchical Bayesian approach on 50 years climate change scenarios. Despite the growing body of knowledge, a gap remains in the full understanding of sources of uncertainty and the magnitude of their relative contribution in water temperature forecasting. This gap is especially apparent considering the significant progress achieved over the last 10 years regarding ensemble forecasting for the assessment of uncertainty in discharge forecasting (e.g. Lohani et al., 2014; Nester et al., 2016; Schaake et al., 2007). In fact, most of the aforementioned studies related to water temperature forecasting deal with uncertainty in a fully deterministic framework. Experiences in meteorology and hydrology show that ensemble and probabilistic approaches can provide greater insight than deterministic approaches and can better account for the different sources of errors in the modelling framework (Boucher et al., 2011; Richardson, 2000; Viney et al., 2009).

In the last decades, extensive work has been carried out to quantify and understand uncertainty in hydrological forecasts (e.g. Beven, 1993; Cloke and Pappenberger, 2009;

Thiboult et al., 2016) and more specifically to properly quantify the uncertainty that propagates along the successive components of a hydrological/meteorological forecasting systems (e.g. Cloke and Pappenberger, 2009). The sources of uncertainty that are most commonly considered are the initial conditions of the system, the inputs to the model and the structures of the models (both atmospheric and hydrologic; Liu and Gupta, 2007). A recent study by Thiboult et al. (2016) highlighted the added value of including these sources of uncertainty to improve the accuracy and spread of short to medium range hydrological forecasts. Their results demonstrate the importance of correcting model initial conditions through data assimilation to produce reliable forecasts. It is also stated that, for longer lead-times (> 2 days), an important portion of the total uncertainty is attributable to meteorological inputs. Hence, the use of ensemble (rather than deterministic) meteorological forecasts as inputs to hydrological models is essential to maintain reliability at lead-times greater than 3-4 days.

In discharge forecasting, feeding ensemble meteorological forecasts to a hydrological model, to produce ensemble hydrological forecasts, is one of the most common approaches to assess uncertainty (e.g. Boucher et al., 2012; Renner et al., 2009; Roulin and Vannitsem, 2015). In such cases, the uncertainty of the meteorological inputs propagates through the hydrological model.

When a model is created, decisions are made about how the physical processes are to be represented. These decisions induce uncertainty to the whole modelling/forecasting process. Multimodel approaches have been successfully applied to assess the uncertainty attributable to the structure of the models (e.g. Velázquez et al., 2011). For instance, Clark et al. (2015) recently proposed an exhaustive modelling framework that addresses structural uncertainty through a modular platform.

Data assimilation can be described as a correction of the state variables of a model using observed data (Liu et al., 2012). Prior to producing a forecast, model parameters have to be adjusted based on available historical data. These data are imperfect, which leads to parameterization uncertainties. When a forecast is produced, initial conditions are fed to the model as the best available representation of the actual state of the river/watershed. The uncertainty of these inevitably imperfect initial conditions

contributes to the overall uncertainty of the resulting forecasts. The nature of the state variables (characteristics of the watershed such as soil water content, snow cover, reservoir levels, etc.) depends on the formulation of the model. As observations become available (e.g. discharge measurements, snow cover, etc.), their informative content can be used to "update" the state variables of the model prior to a forecast. Data assimilation also allows for an assessment of the uncertainty associated to initial conditions, which cannot be known perfectly. Despite the increase in available approaches, many operational forecasters still use manual data assimilation (manual alteration of meteorological inputs) to reproduce accurate initial conditions before forecasting (e.g. Mamono, 2010). In that case, recent meteorological inputs are perturbed (through additive or multiplicative coefficients) according to expert judgement. This forces the model to recompute new state variables that allows for a better simulation of the observed discharge of the day. Manual data assimilation has numerous drawbacks. It is time consuming, very dependent on the intuition and level of skill of the forecaster and makes traceability very difficult (Liu et al., 2012). More systematic probabilistic ensemble data assimilation methods allow to evaluate the effect of residual uncertainty associated with these initial conditions on the subsequent forecasts. The ensemble Kalman filter and the particle filter are the most commonly used methods in hydrology (e.g. Liu et al., 2012).

In water temperature forecasting, only a few studies clearly addressed the use of data assimilation. Pike et al. (2013) used the ensemble Kalman filter for a reach of the Sacramento River downstream from a dam and evaluated 72-hour water temperature forecast results with and without data assimilation. Morrison and Foreman (2005) successfully assimilated discharge and water temperature for the Fraser River using an iterative procedure. They applied a correction factor to the model's state variables based on the magnitude of errors, until a predefined tolerance was reached. While useful data assimilation methods were made available for water temperature forecasting by the aforementioned authors, further work is needed to better understand the propagation of initial conditions uncertainty in a thermal forecast. In addition, to the authors' knowledge, no systematic data assimilation method other than the ensemble Kalman filter has ever been applied in the context of water temperature forecasting.

Hence, this study presents a first attempt at using a particle filter for data assimilation in water temperature forecasting. The aims of this study are to: (i) perform cascading data assimilation of discharge and of water temperature, using particle filters; (ii) produce 5 day ensemble water temperature forecasts that account for uncertainties related to hydrological and thermal initial conditions, as well as to meteorological inputs; and (iii) quantify the respective contribution of those two sources of uncertainty to the quality of water temperature forecasts for up to 5 days. These aims primarily provide the structural sub-headings.

5.2.2   Study site and Materials

5.2.2.1   Nechako watershed

The present study was conducted on the Nechako River watershed in British Columbia, Canada (125°59' W and 53°46' N; Figure 5.10). The Nechako River flows from the Pacific Coast Ranges towards the Fraser River. It is impounded in its upstream portion. The Nechako Reservoir covers an area of 890 km^2 with a volume of 23840 hm^3 when full (Boudreau, 2005). Water is released into the Nechako River from the Skins Lake Spillway. Prior to reaching the Nechako River, water is routed through the Cheslatta River, Cheslatta Lake (length ≈ 40 km) and Murray Lake (length ≈ 8 km). To protect local sockeye salmon from thermal stress during their spawning season, water temperature must be kept under 20°C. Hence, the operator must release enough water between July 20th and August 20th of each year in order to comply with a thermal constraint located about 245 km downstream of Skins Lake Spillway. The travel time between the spillway and the location of the thermal constraint is estimated at 5 days (Envirocon Ltd., 1984). The operations are therefore based on 5 day hydrological and thermal forecasts.

About half of the distance between Skins Lake Spillway and the main stem of the Nechako River is occupied by two lakes (Cheslatta and Murray Lake). Cheslatta Lake covers a 43 km^2 area at a mean depth of 30 m (max. depth is 114 m) for a mean volume of 1266 hm^3. Murray Lake, located between Cheslatta Lake and Cheslatta Falls, covers 5.7 km^2, at a mean depth of 12 m for a mean volume of 68 hm^3. Based on

temperature data recorded during the summer of 2014 (available in supplementary material), thermal stratification occurs under normal regime (before July 20th) but gradually diminishes during cooling operations to attain a vertical difference of 1.17°C from surface to bottom in Cheslatta Lake and 0.19°C in Murray Lake. Lake water outflows are controlled by natural weirs, which create the Cheslatta Falls. Water routed downstream thus comes from the top layer. Its temperature depends mostly on atmospheric conditions. Consequently, the discharge flowing out into the Nechako River is a function of the storage in Murray Lake, located immediately above Cheslatta Falls.
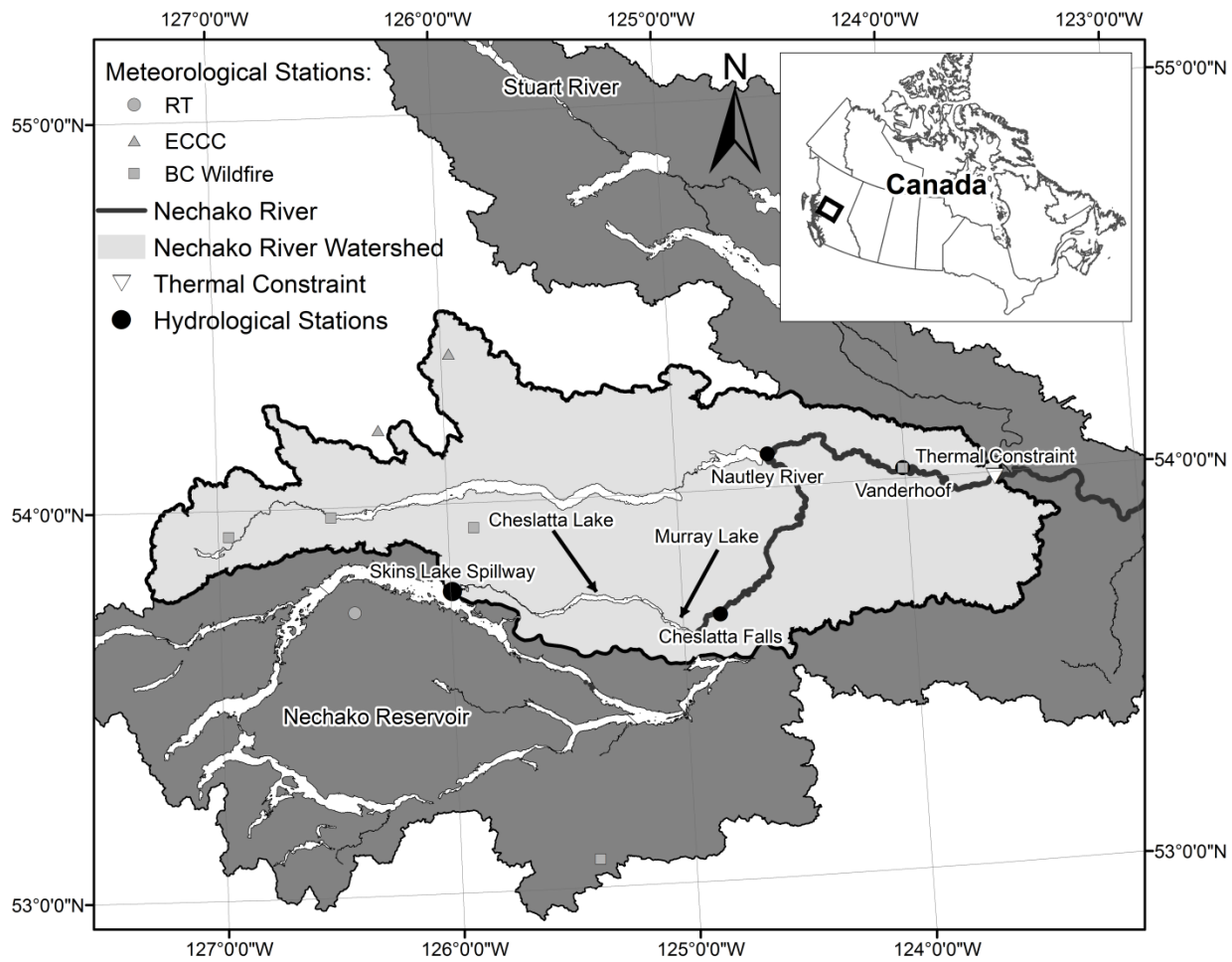
Figure 5.10: Map of the Nechako Watershed with meteorological stations from Rio Tinto (RT), Environment and Climate Change Canada (ECCC) and British Columbia Wildfire (BC Wildfire) and hydrological stations from the Water Survey of Canada

5.2.2.2   Hydrological and meteorological data

Both discharge and water temperature was measured at the Skins Lake Spillway (station #08JA023; discharge only), Cheslatta Falls (station #08JA017) and Vanderhoof (station #08JC001). The largest tributary of the Nechako River is the Nautley River. Its contribution to the total annual discharge recorded at Vanderhoof is estimated to be 25%. In periods of cooling water releases, this proportion diminishes to less than 15%. Please refer to Macdonald et al. (2012) and Ouellet-Proulx et al. (2017) for a complete description of the river and watershed. During calibration, the observed discharge and temperatures of the Nautley River (station #08JB003) were provided to the model. For forecasting, they were kept constant (equal to the last measured discharge and water temperature) for all lead-times.

Meteorological data from Rio Tinto (RT), Environment and Climate Change Canada (ECCC) and British Columbia Wildfire (BC Wildfire) stations were used (Figure 1) for all meteorological variables except solar radiation. Solar radiation data were retrieved from the NASA Prediction of Worldwide Energy Resource (POWER) on a grid with 1° horizontal resolution.
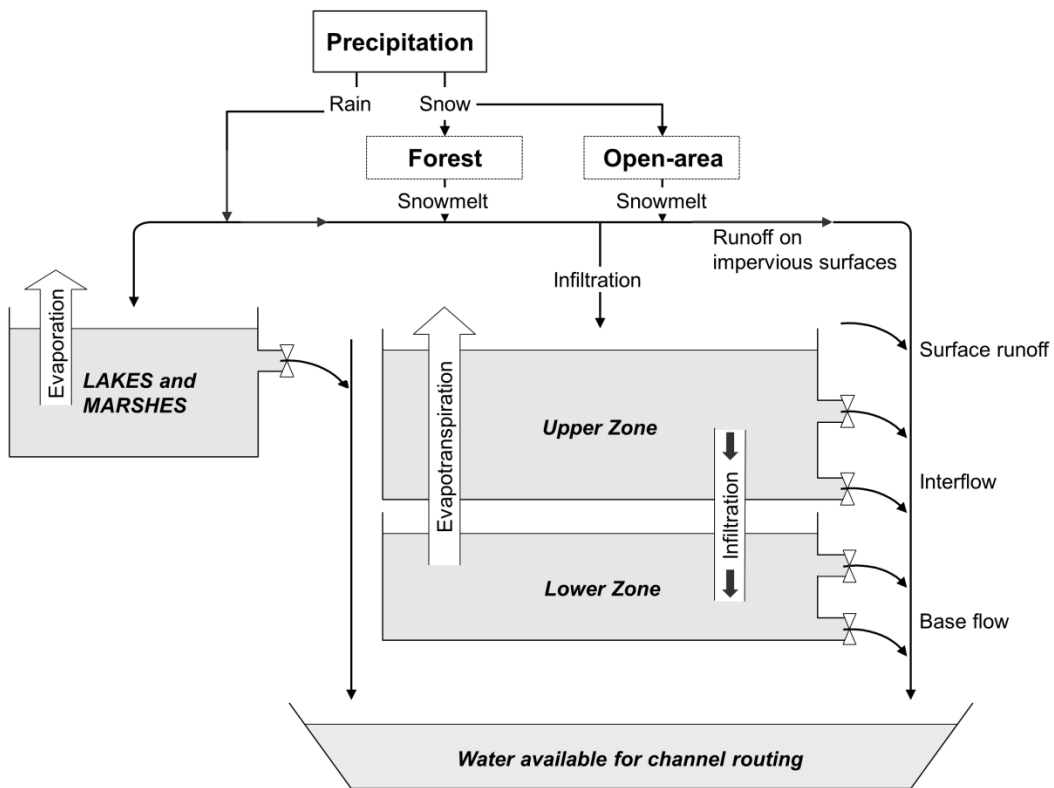
Figure 5.11: Schematic representation of the CEQUEAU model (adapted from Morin and Paquet, 1995)

5.2.2.3   *Hydrological and thermal model*

The model used in this study is CEQUEAU. It is a semi-distributed "tank-type" model that uses a production function (vertical routing of water) and a transfer function (upstream-downstream) to simulate discharge over an entire watershed (Figure 5.11). The model structure is based on calculating both the hydrological and heat budget at a daily time step at each node of a grid. The grid consists in physiographic units of equal size, each with its own land use, physiographic data and meteorological inputs. The required model input variables are minimum and maximum air temperature (°C), and total precipitation (mm). Net solar radiation (MJ), cloud cover (0-1), wind speed (km/h) and air vapour pressure (kPa) must be added to run the thermal component. Both the

hydrological and the thermal components of the model have been thoroughly described in previous publications (e.g. St-Hilaire et al., 2015). CEQUEAU has six state variables including: (i) water level in the upper reservoir; (ii) water level in the lower reservoir; (iii) water level in lakes and marshes; (iv) snow pack in unforested areas; (v) snow pack in forested areas; and (vi) actual evapotranspiration. From now on, the state variables associated with the hydrological component of the model will be referred to as hydrological state variables while the state variables related with the thermal component will be referred to as thermal state variables.

The CEQUEAU model allows the user to indicate the presence of a dam at any location along with the relation between outflow and water storage. To estimate inflow and outflow in reservoirs, it uses the Goodrich method (Goodrich, 1931). Its implementation in CEQUEAU is described in Morin and Paquet (1995).

In the Goodrich method, as implemented in CEQUEAU, the outflow of the reservoir is calculated by Equation 5.17:

$$\bar{O} = f\left(V_t\right)$$ Equation 5.17

where $\bar{O}$ is the outflow (m³/s) of the reservoir (Murray Lake) at time t, V_t (hm³) is the volume of the reservoir at time t and f is the relationship between $\bar{O}$ and V_t in the form of a polynomial function. Using discharge measurement at Cheslatta Falls (Water Survey of Canada; 2002-2007) and water levels (manual readings; 2002-2007) translated into volumes, the following linear (1st order polynomial) function was established:

$$\bar{O} = 1.5022V_t - 954.84$$ Equation 5.18

5.2.3 Methods

5.2.3.1 Assimilation of discharge and water temperature data using particle filters

Discharge is the most commonly used variable for data assimilation in hydrological modelling. In this study, discharge observations are used for the data assimilation of the hydrological component of the model while water temperature is used for the data assimilation of the thermal component, both using particle filters.

The particle filter relies on the hypothesis that the prior probability distribution can be estimated using a large number of random samples of state vectors called "particles". The filter uses Bayes' theorem to estimate a conditional posterior probability $p\left(X_t \middle| y_{1:t}\right)$ of obtaining the modelled state variable X_t given the observation y_t at time *1:t*. The theorem supposes that the modelled state can be updated (improved) by combining prior information (the simulated streamflow corresponding to an initial estimation of X_t by the model) and new information (e.g. discharge observation). Previous studies offer complete descriptions of the Bayes' theorem in the context of the particle filter (van Leeuwen, 2009; Weerts & El Serafy, 2006).

Random samples of state variables are first drawn to create the initial particles at a given time step (Figure 5.12). These particles are used as a starting point for model simulations. When new observations become available, a weight is given to each particle according to their proximity to the observation by:

$$p\left(X_t \middle| y_{1:t}\right) \approx \sum_{i=1}^{N_p} w_t^i \delta\left(y_t - x_t^i\right)$$

Equation 5.19

where x_t^i is the simulated value of the ith particle at time *t*, y_t is the observation at time *t*, N_p is the number of particles, w_t^i is the weight of the ith particle at time *t* and δ is the Dirac delta function. The sum of weights is equal to one. A resampling of the same state variables is then performed according to their weights. This creates the final ensemble of state variables for this time step, to be used to initiate the forecast. These particles

are then propagated forward in time to estimate the state variables at the next time step. While constituting a more accurate representation of the hydrological and thermal conditions of the watershed, the particles also account for the initial condition uncertainty.

The weights are updated sequentially as:

$$w_t^i = w_{t-1}^i \frac{p\left(y_t \middle| X_t^i\right)}{\sum_{i=1}^{N_p} p\left(y_t \middle| X_t^i\right)}$$

Equation 5.20

The conditional probability ($p\left(y_t \middle| X_t^i\right)$) of the observation ($y_t$) given the modelled state (X_t^i) is considered Gaussian.

One potential problem in the implementation of the particle filter is degeneracy. This term refers to a situation where number of particles might decrease to a point where only a very few particles (or even just one) will be given a non-zero weight and persist. To avoid this, an algorithm involving auxiliary sampling importance resampling (e.g. Vrugt et al., 2013) and close monitoring involving a numerical degeneracy criterion was used. For more details on particle filtering, readers are referred to Weerts and El Serafy (2006) and van Leeuwen (2009).

Data assimilation can be performed using either a direct or an indirect approach. The main distinction between these approaches depends on how the state variables are updated. When using the direct approach, modifications are made directly on the state variables (e.g. soil water content modified from 30 mm to 50 mm). For the indirect approach, the state variables of the model are updated by perturbing the meteorological inputs which influence the state variables (e.g. increased rainfall to raise the soil water content). Previous studies (Sakov & Oke, 2008; Yilmaz, DelSole, & Houser, 2012) have shown that a direct approach (without perturbing the forcing observations) reduces the water budget residual without significant error increases. The direct approach was thus

chosen for the hydrological component of the model in this study. In this case, X_t (Equation 5.20) are the state variables of the hydrological component at time t and y_t is the discharge measurement at the same time step.

With regards to water temperature assimilation, the direct approach could not be applied because water temperature is the only "updatable" state variable of the model while also being the observation. An indirect approach was therefore used for the thermal component of the model. In this case, X_t (Equation 5.20) are the meteorological inputs at time t and y_t is the water temperature measurement at the same time step. Although in this case water temperatures is the only data available for assimilation, other variables such as net solar radiation, evaporation or longwave reemission could be updated if they were measured above the watercourse.

Given the sequential nature of the hydrological-thermal model (i.e. simulated discharge is an input of the thermal component), data assimilation of discharge and water temperature have to be carried out in a cascade. Therefore, at each time step, the assimilation of discharge was first executed to create a set of perturbed hydrological states (Figure 5.12- A). This ensemble of hydrological initial conditions was saved for further use in forecasting. However, only the ensemble mean was fed to the thermal component as the initial hydrological condition to avoid the multiplication of the hydrological members by the thermal members and reduce computation time. The assimilation of water temperature was then performed for the same time step (Figure 5.12- B). As for the hydrological states, the thermal states were saved for future use in forecasting. The new sets of initial conditions were propagated forward in time and provided to the model as initial conditions for the assimilation of the next time step.
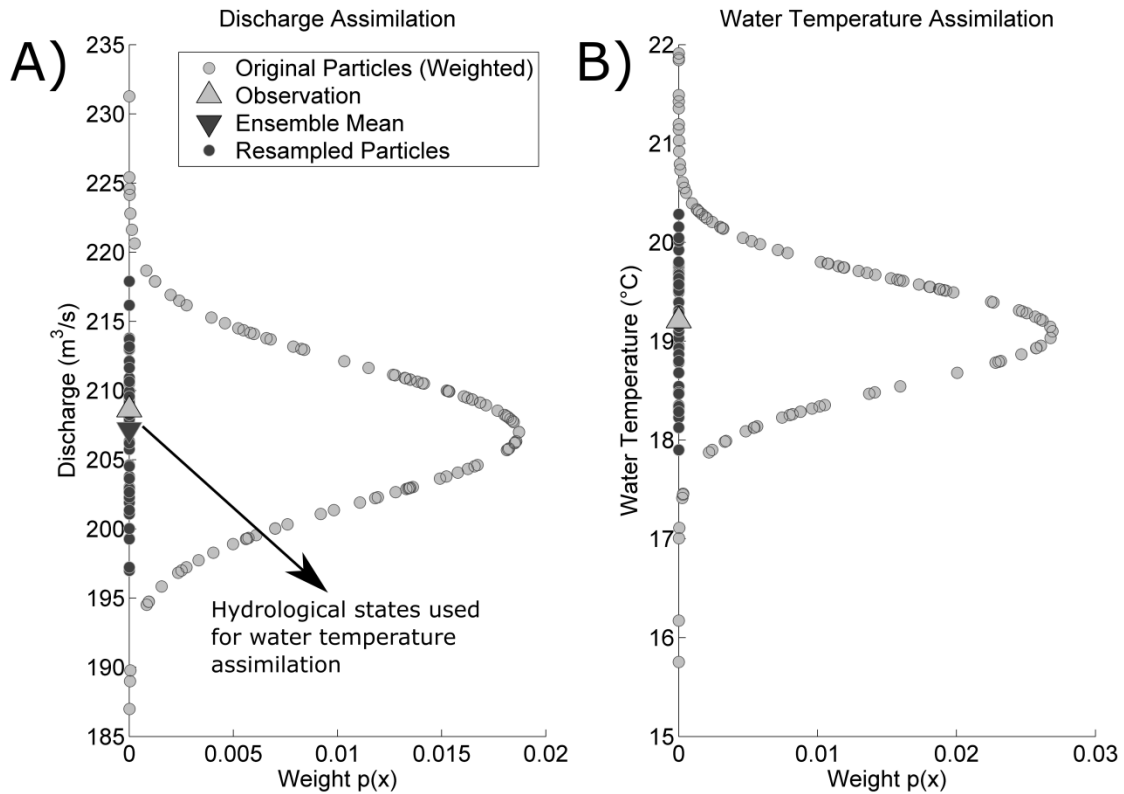
Figure 5.12: Example of the assimilation cascade of A) discharge and B) water temperature using particle filters

Discharge and water temperature data were available at two sites on the watershed, Cheslatta Falls and Vanderhoof (Figure 5.10). Errors were minimized at each of those sites simultaneously. The conditional probability therefore becomes the joint probability of both conditional probabilities. If y_1 is the observation at Cheslatta Falls and y_2 is the observation at Vanderhoof, the joint conditional probability is $p\left(y1_t \middle| X_t^i\right) p\left(y2_t \middle| X_t^i\right)$. The number of particles to be produced by the algorithm has to be set a priori by the user. This number was established by a trial and error process, during which the algorithm was tested on 5 to 200 particles.

In this study, the conditional probability $p\left(y_t \middle| X_t^i\right)$ is considered as a Gaussian function centered on the simulated value y_t with a standard deviation of σ. In the case of

103

discharge assimilation, Salamon and Feyen (2010) suggested error-dependent values of σ in the form of:

$$\sigma_t = \alpha\, y_t + \beta$$

to ensure homoscedasticity. In Equation 5.21, α represents the percentage of measurement error, while β is added to reduce the influence of low discharge values on the posterior distributions (Noh et al., 2011; Salamon & Feyen, 2009, 2010). With regards water temperature assimilation, a constant σ was used. Salamon and Feyen (2010) used $\alpha = 0.125$ and $\beta = 5$ m^3/s and Noh et al. (2011) used $\alpha = 0.1$ and $\beta = 5$ m^3/s. Several values of α, β and σ (Equation 5.21) as well as various numbers of perturbations were tested to ensure the best performances of the particle filter. The final values were chosen based on CRPS calculated from the results of the assimilation. A line simplification algorithm (Douglas & Peucker, 2011) was used to locate the break points in CRPS values as a function of the number of particles. The algorithm recursively removes nodes from a line based on the distance between the nodes and a distance tolerance. This was done to highlight the number of particles for which the performances improve significantly. Results are presented in section 5.2.4.1.

The particle filter was set-up to perturb the water level in the upper reservoir (soil water content), in the lower reservoir (groundwater), and in lakes and marshes (Figure 5.11). In addition to these three reservoirs levels, the volume of water in Murray Lake (Equation 5.17; Figure 5.10), represented as a reservoir, was perturbed to account for the uncertainty associated with its estimation. Perturbations limits ranging between 1 and 100 mm for the soil variables and ranging between 1 and 100 hm^3 for the volumes of water in Murray Lake were tested.

With regards to water temperature assimilation, all meteorological inputs were perturbed, except for total precipitation, which negligibly contributes to the heat budget calculations. A maximum perturbation of 20% was allowed for all meteorological

variables. This limit was chosen based on Tait and Liley (2009) who obtained interpolation errors ranging between 20% and 30% for solar radiation and Xia et al. (2000) who found interpolation errors ranging between 14% and 30% also for solar radiation during the summer. Lower values were found for wind interpolation (i.e. between 6% and 14%) and relative humidity in Yuan et al. (2014). The temperature of the water release was perturbed by ±2.5°C to account for the uncertainty associated with its estimation. The absolute perturbation limits of the thermal component are presented in Table 5.4.

Table 5.4: Perturbation limits of the thermal component

Meteorological Input	Perturbation	Units
Air Temperature (min. and max.)	2.3	°C
Net Solar Radiation	6.7	$MJ\,m^{-2}$
Air Vapour Pressure	2.9	mm Hg
Wind Speed	6.7	km/h
Cloud Cover	0.2	0-1
Temperature of the water released	2.5	°C

5.2.3.2   Ensemble water temperature forecasting

The same procedure was executed to compute all water temperature forecasts. The model was run in simulation mode (i.e. meteorological observations as inputs) during 365 days prior to the forecasted period (Figure 5.13 – model spin-up). Then, the observed discharges and water temperatures were assimilated on the day prior to the forecast (Figure 5.13 – data assimilation). These initial conditions were then provided to the model along with 1 to 5 days meteorological forecasts to obtain hydrological and thermal forecasts (Figure 5.13 – forecast). Then, instead of imposing a model spin-up time of 365 days, before every forecasting time step, the assimilated initial conditions were provided to the model and the forecasting process was continued forward. To account for input uncertainty, ensemble meteorological forecasts were fed to the model

as performed in Ouellet-Proulx et al. (2017). Meteorological forecasts produced by the Canadian Meteorological Center (CMC) were used for all variables but solar radiation, for which forecasts from the European Centre for Medium-Range Weather Forecasts (ECMWF) were used. The CMC ensemble forecasts are composed of 20 members. Twenty members out of the 50 members available at ECMWF were randomly sampled to complete the CMC forecasts. The systematic inclusion of the lower and the upper bounds would artificially yield more dispersed distributions of the resulting forecasts with an overrepresentation of extreme values. The same members were retained for each 5 day forecast while 20 new members were sample for the next forecast. All meteorological forecasts were retrieved from the TIGGE (THORPEX Interactive Grand Global Ensemble; Park et al. 2008) data portal. The hydrological and thermal forecasts were produced for 2009-2014 according to the availability of the archived meteorological forecasts and validation data. Although forecasts made a posteriori are called hindcasts, the word forecast will be used in this paper for ease of reading.

Throughout model calibration, data assimilation and forecasting, the measured discharge at the Skins Lake Spillway was imposed in CEQUEAU. The temperature of the water released was not available for the whole period (only for 2013-2014). The temperature of the water released was thus estimated using an autoregressive model with exogenous variables (ARX; Ahmadi-Nedushan et al., 2007). This model uses air temperature residuals as predictors. It was validated using the available measurements with root mean squared errors of 1.18°C (calibration) and 1.28°C (validation).

The quality of the assimilation process as well as the subsequent forecasts was evaluated using the mean continuous ranked probability score (CRPS, Matheson and Winkler, 1976) for both the hydrological and the thermal model and using the Brier Score (Brier, 1950) for the thermal model only. The CRPS is a commonly used metric to evaluate ensemble forecasts. It is the ensemble analog of the mean absolute error (MAE) as demonstrated by Gneiting and Raftery (2007) and it evaluates the accuracy and reliability of the forecast. Therefore, the performance of deterministic simulation and forecasts can be compared to ensemble ones using respectively the MAE and the CRPS. The Brier Score is used to evaluate the capacity of a forecast to predict the exceedance or non-exceedance of particular threshold by comparing the probability of

exceedance of the model prediction to the outcome. In the present work, the Brier Score was calculated for three temperature thresholds of 16, 18, and 20°C, respectively representing low, medium and high warning levels of elevated water temperatures for salmonids (based on Martins et al., 2011).
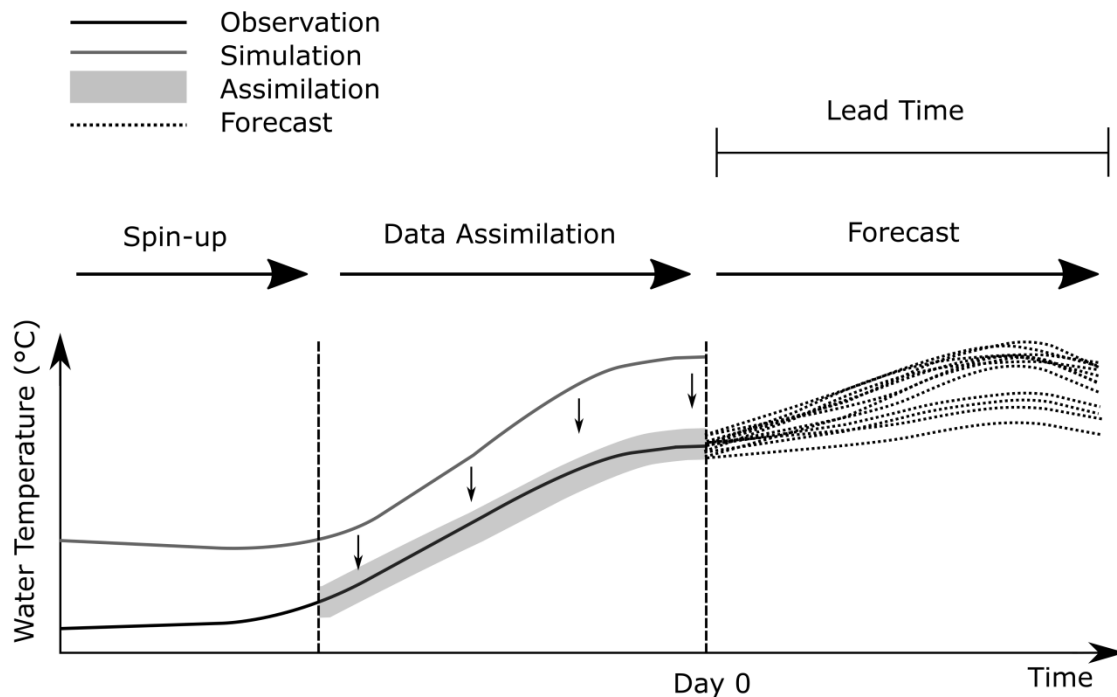
Figure 5.13: Forecasting framework including model spin-up time, data assimilation and forecast.

5.2.3.3   *Quantification of uncertainty in water temperature forecasts*

In uncertainty analysis, computation time can be an issue. When many sources of uncertainty are accounted for, the model has to be launched several times to try all possible combinations. To alleviate this problem, we built various scenarios (inspired by Thiboult et al., 2016) of initial conditions and meteorological inputs as presented in Table 2. The seven scenarios are named S1 to S7. S1 is composed of the mean hydrological and thermal initial conditions, and observed meteorology. The use of meteorological observations as inputs does not represent a real forecasting context but

rather the reference simulation in terms of performances. S2 and S3 include all 40 members of hydrological and thermal initial conditions, respectively. They were included to assess the uncertainty related to the initial conditions of these two components of the model. S4 was obtained when 20-member meteorological forecasts are used as CEQUEAU's input variables. For scenario S4, only the mean hydrological and thermal initial conditions at each time step are used. S4 was included to characterize the uncertainty strictly associated with atmospheric conditions. The three remaining scenarios are combinations of S1 to S4. S5 includes a random combination of the 40 initial hydrological and thermal conditions members and observed meteorology for a total of 40 members. The combined uncertainty from the hydrological and thermal initial conditions is thus accounted for by S5. S6 is similar to S5, to which a randomly selected meteorological forecast member is added. It keeps the total number of members to 40 while considering meteorological input uncertainty. S7 combines all 40 members of the hydrological initial conditions and thermal initial conditions, with all 20 meteorological forecasts members totaling 800 members.

Table 5.5: Forecasts scenarios used in this study with the number of members for each one.

Source of uncertainty	S1	S2	S3	S4	S5*	S6**	S7*
Source of Uncertainty evaluated	None	Hydrological initial conditions	Thermal initial conditions	Meteorological inputs	Initial conditions	Initial conditions and meteorological inputs	Initial conditions and meteorological inputs
Initial conditions Q	1	40	1	1	40	40	40
Initial conditions Tw	1	1	40	1	40	40	40
Meteorological Inputs	1	1	1	20	1	20	20
Total nb of members	**1**	**40**	**40**	**20**	**40**	**40**	**800**

One set of thermal initial conditions randomly assigned for each set of hydrological initial conditions
*** One meteorological member randomly assigned to each set of thermal initial conditions and each set of hydrological initial conditions*

The total spread of the ensemble was also calculated to summarize the level of uncertainty that each source propagates into a forecast. Reliability plots (Stanski et al., 1989) were also produced for water temperature forecasts to allow for further comparison of the different scenarios. These diagrams represent the observed probability of an event as a function of the theoretical probability of the forecast, based on the distribution of the ensemble. Reliable forecasts should be close to the bisector on this graph, while over (under) dispersion is identified as being above (below) this bisector line.

A Kruskal-Wallis test (Kruskal & Wallis, 1952) was performed to evaluate if the CRPS of the different scenarios come from the same underlying population, given that data were non-normal (Kolmogorov-Smirnov normality test; Massey, 1951). The alternative hypothesis of the Kruskal-Wallis test is that at least one of the CRPS methods yields values that are significantly different than the others. The Tukey-Kramer method (Tukey, 1949) was used a posteriori to verify which scenarios have CRPS values significantly different from other scenarios. Results are presented as letters where scenarios associated with the same letter do not return significantly different CRPS values.

5.2.4   Results

5.2.4.1   *Assimilation of discharge and water temperature data using particle filters*

Perturbations limits of ±30 mm (CRPS = 7.6 m^3/s at Vanderhoof) were selected for soil variables and ±10 hm^3 (CRPS = 2.2 m^3/s at Cheslatta Falls) for Murray Lake based on best model performances (Table 5.6). Perturbations of 30 mm and 40 mm returned similar CRPS (7.6 m^3/s). To ensure minimal perturbation, a ±30 mm value was retained.

Table 5.6: Perturbation limits for the hydrological component

Reservoirs Perturbation (mm)	CRPS at Vanderhoof (m^3/s)	CRPS at Cheslatta Falls (m^3/s)	Murray Lake Perturbation (hm^3)	CRPS at Vanderhoof (m^3/s)	CRPS at Cheslatta Falls (m^3/s)
2	15.7	10.8	2	12.9	5.7
10	10.1	10.5	10	11.6	2.2
20	8.3	10.4	20	11.6	3.6
30	7.6	10.3	30	11.5	5.4
40	7.6	10.4	40	11.4	7.2
50	8.0	10.4	50	11.4	9.0
70	8.1	10.4	70	11.4	12.4
100	8.5	10.5	100	11.1	17.9

Results showed that lower (better) CRPS values were obtained when using smaller values for parameters α and β (Equation 5.21) compared to previous studies. In Figure 5.14-A, CRPS for the Cheslatta Falls station varied very slightly for β between 1 m^3/s and 10 m^3/s ($\Delta = 0.41$ m^3/s) with lowest value observed for $\beta = 3$ m^3/s (CRPS = 3.06 m^3/s). As for the Vanderhoof station, CRPS increased constantly as a function of β with an optimal value of $\beta = 1$ m^3/s (CRPS = 4.26 m^3/s). Similar results were obtained for α at Cheslatta Falls (Figure 5.14-B) with slight variations in the CRPS between 0 m^3/s and 0.05 m^3/s ($\Delta = 0.34$ m^3/s). The lowest CRPS value was found using $\alpha = 0.02$ (CRPS = 3.14 m^3/s). At the Vanderhoof station, similar CRPS values were obtained using α values between 0 and 0.01 ($\Delta = 0.46$ m^3/s) with a lowest CRPS of 4.31 m^3/s at $\alpha = 0.005$. Parameters $\alpha = 0.005$ and $\beta = 1$ m^3/s were retained for the remaining analysis based on the lowest CRPS obtained at Vanderhoof, which also showed satisfactory results for the Cheslatta Falls station. Since sampling in the particle filter is a random process, slight variations are expected between each use of the algorithm with the same parameters.
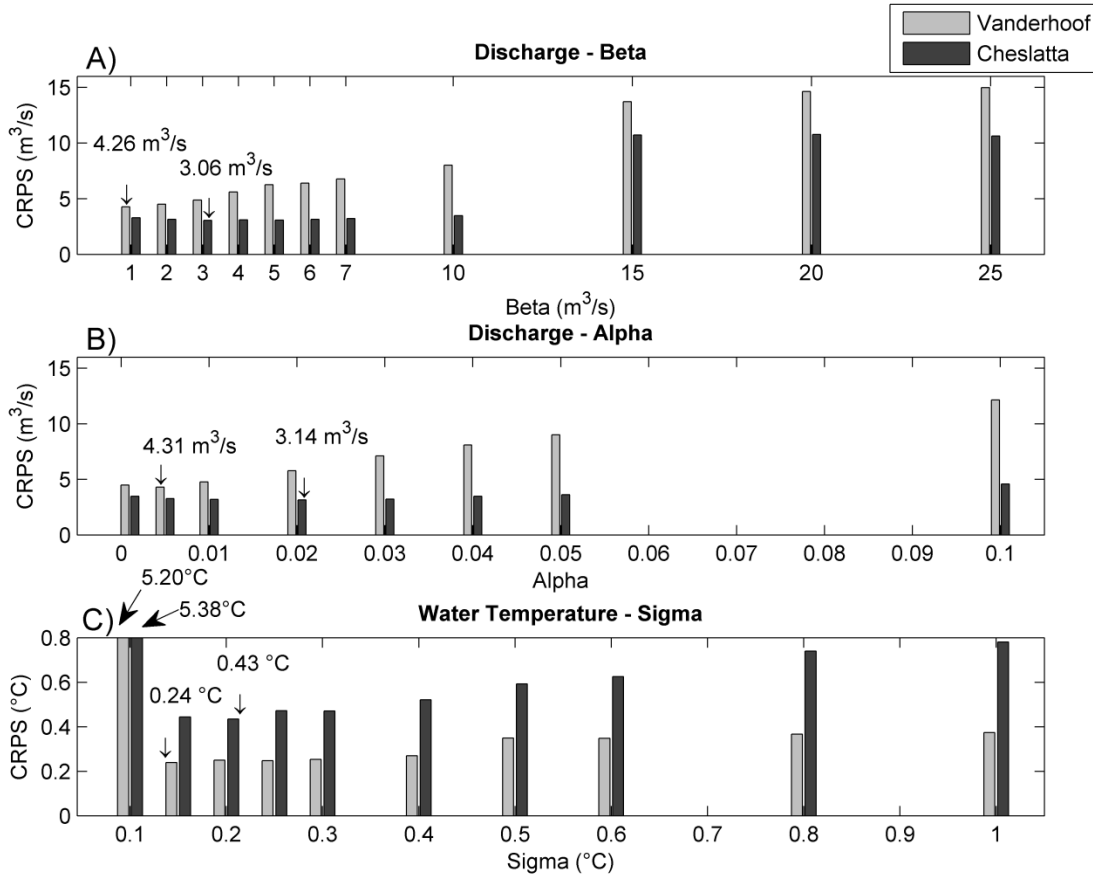
Figure 5.14: Mean CRPS values (2009-2014) as a function of A) β (α = 0.01), B) α, (β = 1 m³/s) and C) σ (α = 0) of Equation 5.21.

In the case of water temperature (Figure 5.14-C), best results were obtained using σ = 0.2°C for Cheslatta Falls (CRPS = 0.43°C) and σ = 0.15°C (CRPS = 0.24°C) at Vanderhoof. At both sites results varied slightly between σ = 0.15°C and σ = 0.4°C with differences in CRPS of 0.09°C and 0.03°C for Cheslatta Falls and Vanderhoof, respectively. In light of those results, the parameter σ was assigned a value of 0.15°C.

According to Figure 5.15 (A and B), CRPS reductions are observed from 5 to 40 particles. The selection of 40 particles minimizes computation time while maximizing initial conditions accuracy. To satisfy both variables at both sites, sets of 40 particles were used for the assimilation process and consistently for the hydrological and thermal forecasts. Table 5.7 presents the final results of the assimilation process using the

optimized parameters. Discharge simulations were improved by over 75% at both sites, compared to simulation without data assimilation. As for water temperature, improvements of 71% and 65% were calculated for Cheslatta falls and Vanderhoof stations respectively, lowering the error values below 0.5°C in both cases. More uncertainty was observed for the water temperature assimilation compared to discharge assimilation (Figure 5.16).

Table 5.7: Relative improvement provided by data assimilation in terms of MAE (deterministic simulation) and CRPS (after data assimilation)

	Discharge MAE/CRPS (m^3/s)		Water Temperature MAE/CRPS (°C)	
	Cheslatta	Vanderhoof	Cheslatta	Vanderhoof
Original initial conditions	10.91	17.78	1.52	0.69
Initial conditions after assimilation	2.33	4.35	0.44	0.24
Relative improvement	78.6%	75.5%	71.1%	65.2%
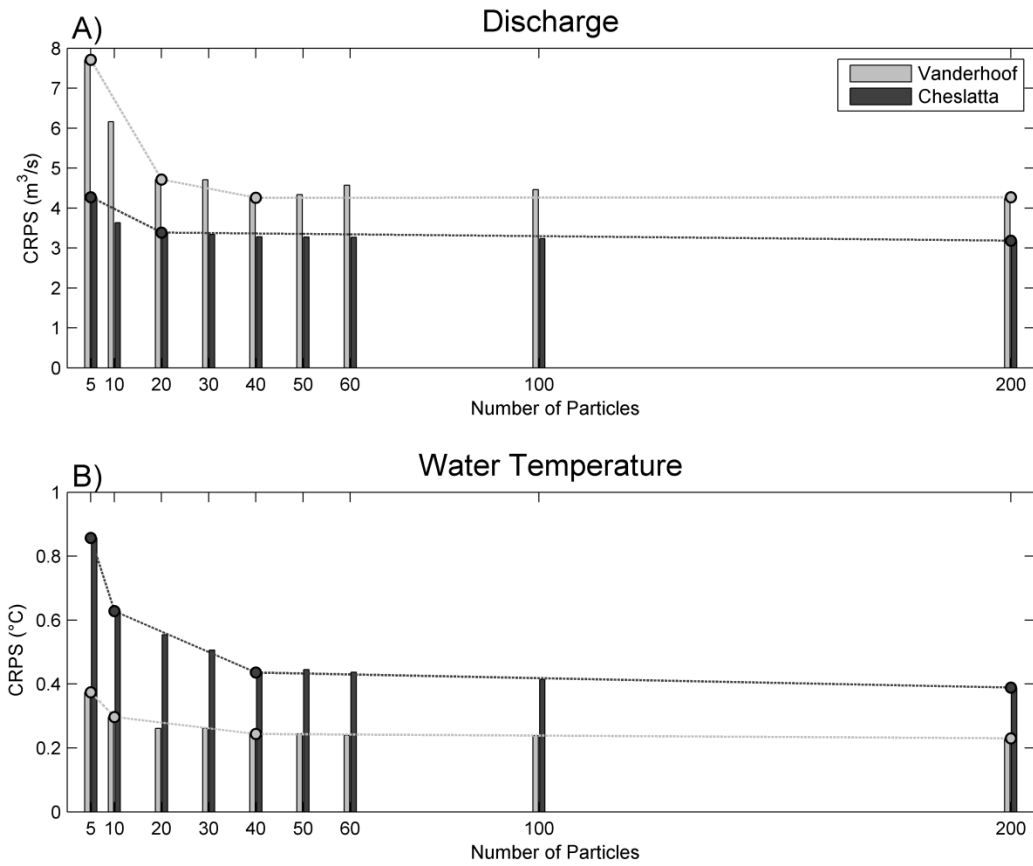
Figure 5.15: Mean CRPS values (2009-2014) as a function of the number of particles created by the particle filter for A) discharge and B) water temperature. Dotted lines represent breakpoints locations estimated using Douglas-Peucker (2011) line simplification algorithm.
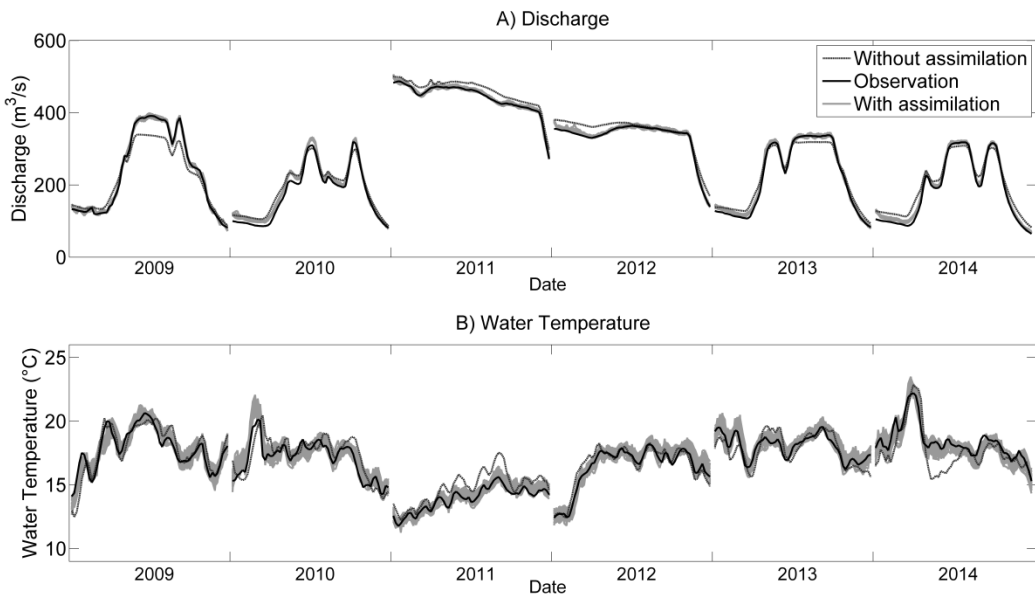
Figure 5.16: Ensembles of initial conditions of A) discharge and B) water temperature at Vanderhoof with and without data assimilation.

5.2.4.2 *Ensemble water temperature forecasting*

Discharge forecasts performances were very similar among the scenarios. CRPS values ranged between 7.3 m^3/s (S2, S5 and S6) and 9.4 m^3/s (S1, S3 and S4) for a 1-day forecast and between 13.7 m^3/s (S4) and 15.4 m^3/s (S6) for a 5 day forecast (Table 5.8). Most of the uncertainty propagated within the discharge forecasts originates from hydrological initial conditions with mean spread of 56 m^3/s for the first day of the forecast and 35 m^3/s for the fifth day. Very small uncertainty was induced by meteorological inputs, with mean spread values ranging between 0.2 m^3/s (1 day) and 3.68 m^3/s (5 days). S1 (no uncertainty) and S6 (uncertainty from initial conditions and meteorological inputs) for 1 and 5 day lead-times are represented on Figure 5.17. It can be seen that most of the time the observed discharge is included inside the uncertainty range represented by S6 for a 1 day lead-time, but most often not for Day 5. However, the observation still remained fairly close to the observed discharge.

114

Table 5.8. CRPS for forecasting scenarios S1 to S7 for lead-times of 1 and 5 day at Vanderhoof[1].

MCRPS (m³/s)	1	2	3	4	5
S1	9.4	9.3	10.7	12.5	13.8
S2	7.3	9.5	12.7	14.5	15.1
S3	9.4	9.3	10.7	12.5	13.8
S4	9.4	9.3	10.6	12.4	13.7
S5	7.3	9.5	12.7	14.5	15.1
S6	7.3	9.5	12.7	14.6	15.4
S7	7.5	9.6	12.7	14.5	15.4
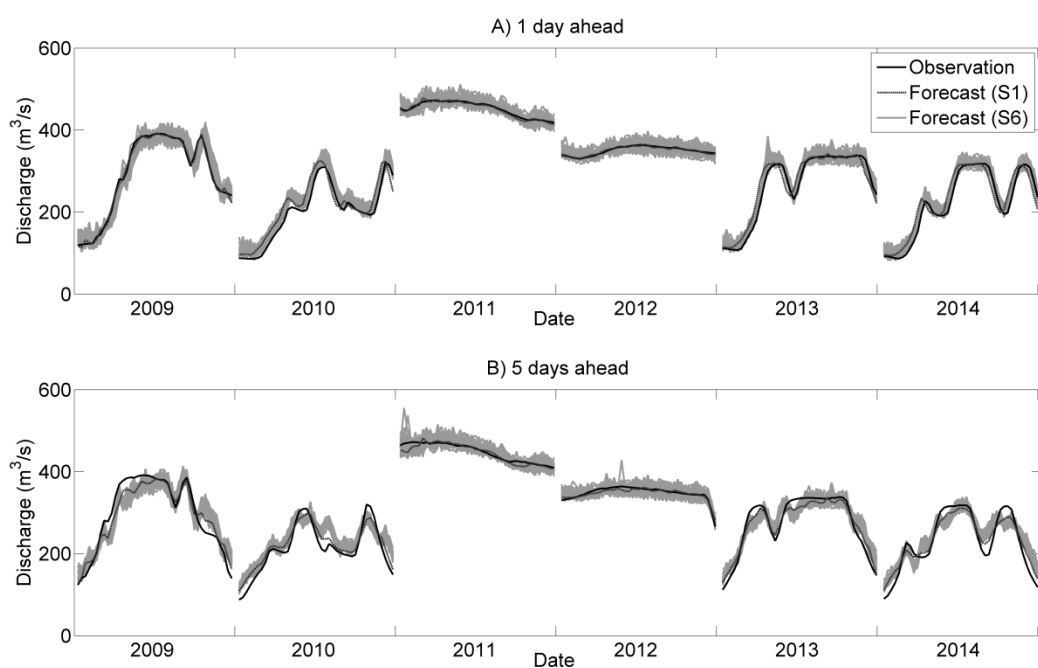
Figure 5.17: A) 1 day and B) 5 days discharge forecast at Vanderhoof for S1 and S6.

---

[1] Ce tableau n'apparait dans la version de l'article publiée dans Journal of Hydrology.

Figure 5.18 shows water temperature forecasts for two selected scenarios: S1 (no uncertainty) and S6 (uncertainty from initial conditions and meteorological inputs). It can be seen that for a 1-day lead-time (Figure 5.18-A) both S1 and S6 were positively biased (e.g. 2010 and 2013) but all forecasts are close to the observations. For a 5 day lead-time (Figure 5.18-B), more variability in the performances can be observed. For instance, forecasts for 2011 and the beginning of 2012 had a strong negative bias while the performance for other periods, such as 2009 and 2010 was better.

All CRPS values calculated for the thermal forecasts are shown in Figure 5.19. Letters (A and B) on Figure 5.19 show results of the Kruskal-Wallis test. Similar performance was observed for 1 day forecast using all 40 thermal initial conditions (S3) and the mean thermal initial conditions (S1) with CRPS = 0.41°C in both cases. The accuracy of the water temperature forecasts was marginally impacted by meteorological conditions for the 1 day lead-time. A very small increase in CRPS of 0.07°C was observed when ensemble meteorological forecasts are provided as inputs (S4) instead of observed meteorological conditions (S1). Both scenarios did not return significantly different CRPS values. When both ensemble meteorological inputs and ensemble hydrological and thermal initial conditions were used (S6 and S7), the CRPS marginally increased to reach 0.49°C for the first day of the forecast. These scenarios returned CRPS values significantly different from S1 to S3.
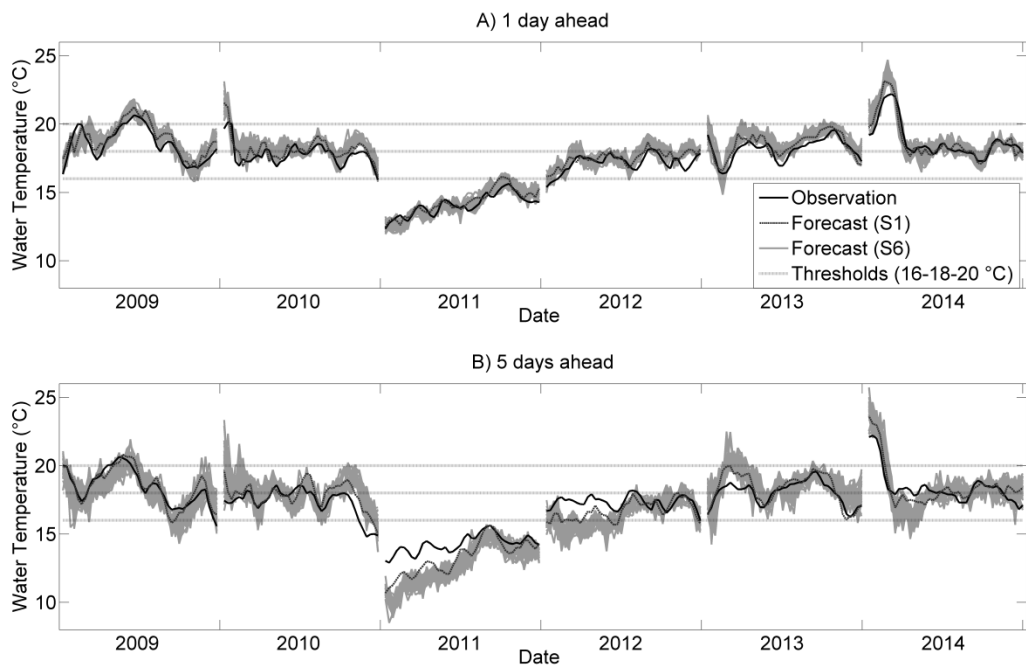
Figure 5.18: A) 1 day and B) 5 days water temperature forecast at Vanderhoof for S1 and S6.
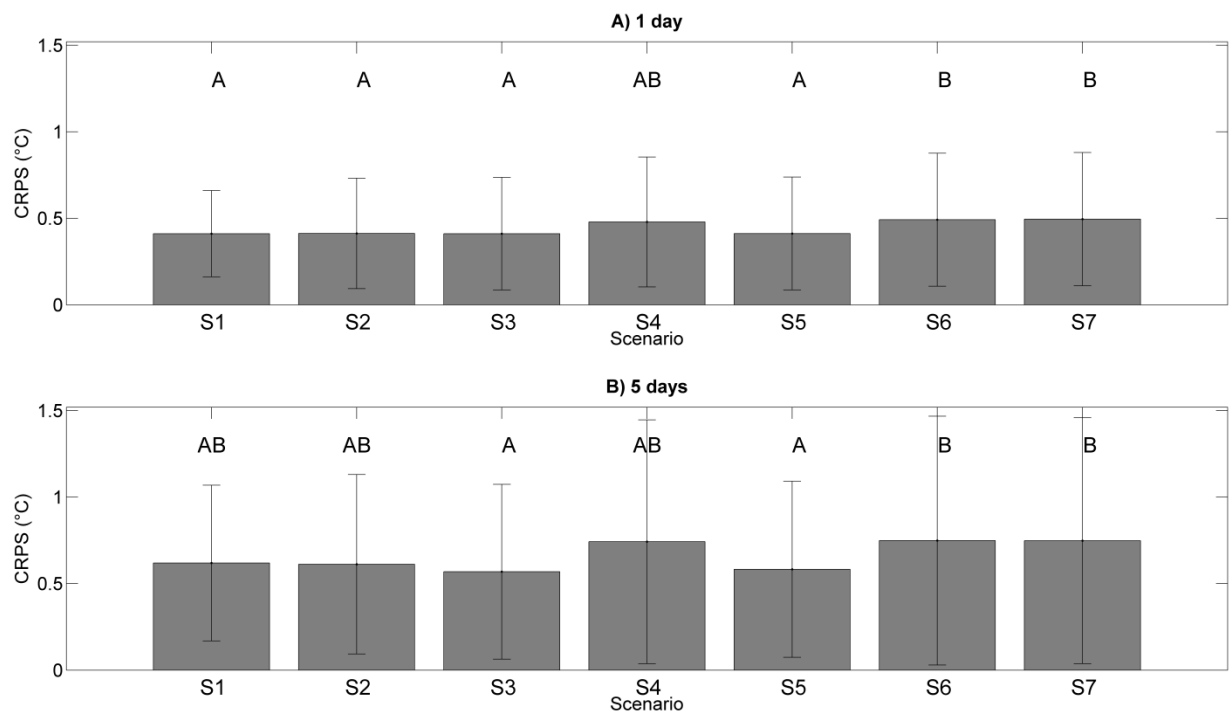
Figure 5.19: CRPS for forecasting scenarios S1 to S7 for lead-times of 1 and 5 days (A-B) at Vanderhoof. Error bars represent ± one standard deviation.

For the fifth day of the forecast, ensemble thermal initial conditions induced a minor decrease in CRPS of 0.05°C (S3 compared to S1; not statistically significant). The most important components for the fifth day of the thermal forecast were the meteorological forecasts inputs making the CRPS shift from 0.57°C (S3) to 0.75°C (S6) (statistically significant, p-value <0.05). The variability of the CRPS values for a single scenario also increases with lead-time. The mean standard deviation of the CRPS's for all scenarios goes from 0.35°C (1 day) to 0.61°C (5 days). For short lead-times (1 day), the variability of the CRPS values is similar for all scenarios. A difference in standard deviation of 0.07°C was observed between S7 (0.32°C) and S2 (0.39°C). This difference in variability among the scenarios grows with lead-time to reach 0.21°C (5 days) between S6 (0.72°C) and S3/S5 (0.52°C).

According to the Brier Score, all three temperature thresholds were better predicted when ensemble thermal initial conditions were used rather than a mean value (Figure 5.20). Higher Brier Scores also were obtained when ensemble meteorological forecasts were used, for any temperature thresholds (S4, S6 and S7). All scenarios showed lower capacity to predict a threshold exceedance of 18°C compared to threshold of 16°C or 20°C. Brier Scores ranged between 0.12 (S5; 1 day) and 0.22 (S4; 2 days) for the 18°C threshold, while it fluctuated between 0.02 (all scenarios; 1 day) and 0.07 (S4 and S6; 5 day) for 16°C. For the 20°C threshold, Brier Scores were very similar (between 0.01 and 0.03) for all scenarios and all lead-times. The higher Brier Score obtained for the 18°C threshold can be partly explained by the fact that water temperature mostly fluctuates between 16°C and 20°C. Only 5% of the observed water temperatures at Vanderhoof were equal or above 20°C and only 15% were below 16°C. However, the percentages of observed temperatures above and below 18°C were respectively 58% and 42%. The same level of uncertainty could therefore translate into a poor threshold exceedance projection for temperatures close to 18°C as opposed to warmer or colder temperatures. Nonetheless, a Brier Score of 0.17 (S6 and S7), which is the poorest result for a 5 day forecast indicates that on average 60% of the members correctly predicted the exceedance or non-exceedance of the 18°C threshold.
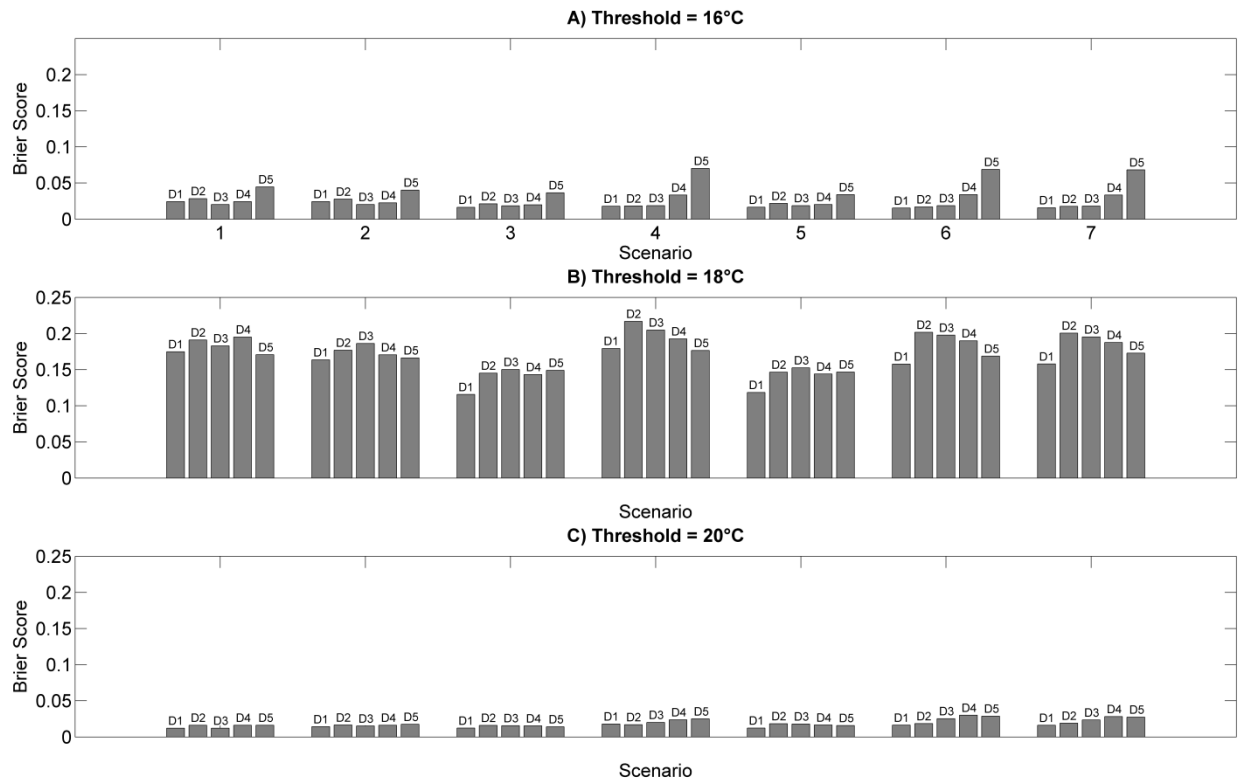
Figure 5.20: Brier Score for a A) the 16°C threshold, B) the 18°C threshold and C) the 20°C threshold as a function of lead-time for scenarios S1 to S7 at Vanderhoof.

5.2.4.3   Quantification of uncertainty in water temperature forecasts

Figure 5.21 displays the spread of thermal forecasts at Vanderhoof from S2 to S7. When comparing S2 to S4 (i.e. one type of uncertainty represented in each scenario), it can be seen that uncertainty from thermal initial condition (S3) contributed the most to the uncertainty of 1 day forecasts (mean spread = 1.11°C) followed by meteorological inputs (0.67°C). Uncertainty from hydrological initial condition was much lower with a mean spread of 0.09°C. Overall, meteorological inputs were the primary contributors to total forecast uncertainty for lead-times longer than 1 day. This is easily seen when comparing the mean spread of S4 (1.09°C) to S3 (0.98°C), for instance. Error bars on Figure 5.21 also show that the variation among spread values was greater for S4 than

for scenarios S2, S3 and S5. In addition, the contribution of meteorological inputs uncertainty increases with lead-time (Figure 5.21 - C) while thermal initial conditions uncertainty decreases (Figure 5.21- B). For a 5 day forecast, uncertainty induced by thermal initial conditions and meteorological inputs was respectively 0.54°C (S3; Figure 5.21- B) and 1.89°C (S4; Figure 5.21- C). The simultaneous inclusion of thermal and hydrological initial conditions uncertainty (S5) yielded ensemble spreads similar to those obtained for thermal initial conditions alone (S3). The same mean spread value was obtained for a 1-day forecast (1.11°C) for both scenarios (S3 and S5; Figure 5.21– B and D) but the mean spread was 0.13°C higher for S5 (0.67°C) than for S3 (0.54°C). The quality of an ensemble forecast cannot be appraised solely on the magnitude of the spread of its ensemble but more on its distribution around the observation. Reliability plots allow further assessment of and eventual under or overdispersion of the ensemble.
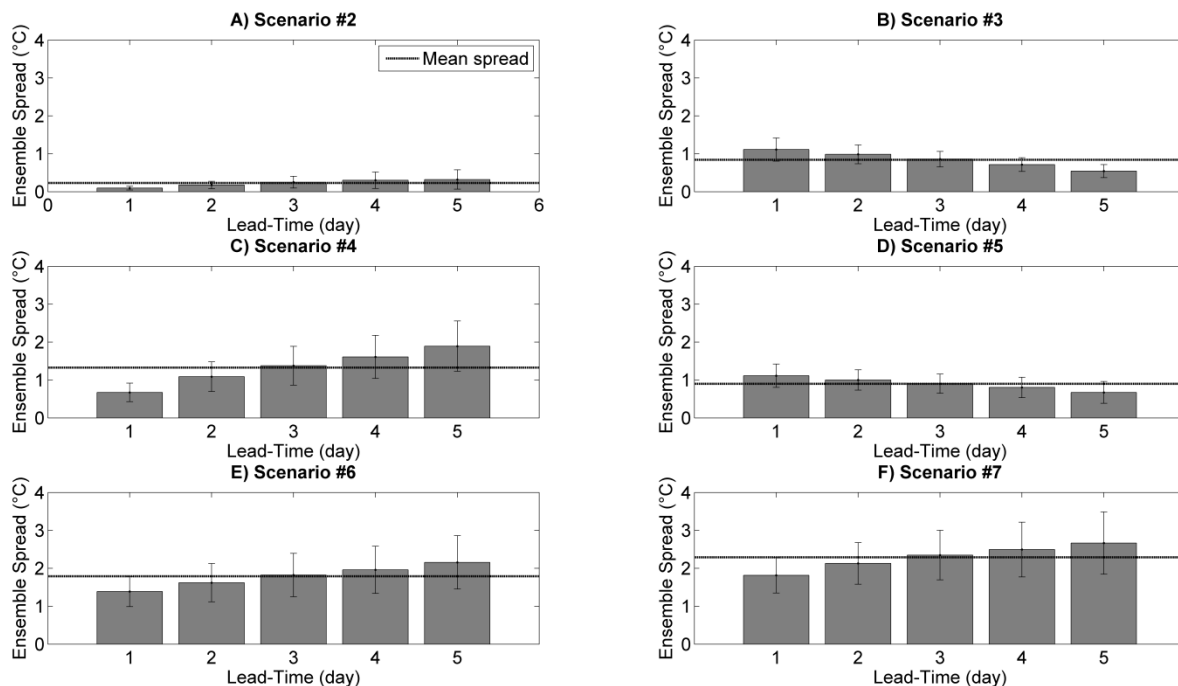
Figure 5.21: Ensemble spread as a function of lead-time for scenarios S2 to S7 (A-F) at Vanderhoof. Scenario 1 is not displayed because it has no spread. Error bars represent ± one standard deviation.

The reliability plot at day 0 (Figure 5.22 - A) shows the adequate spread of the thermal initial conditions (S3, S6 and S7) created by the particle filter. These scenarios also presented the best spread and reliability for a 1-day forecast (Figure 5.22 - B) followed by S4. On Figure 5.22 C-E, it can be seen that scenarios that were not supported by meteorological ensemble forecasts had a decreasing reliability caused by the diminishing spread of their ensemble. This enforces the conclusion about the importance of considering meteorological inputs uncertainty when forecasting lead-times longer than 1 day. For the 5 day forecasts (Figure 5.22 - F), S4, S6 and S7 were very similar, once again indicating the strong influence of meteorological inputs on the reliability of the 5 day water temperature forecasts. Finally, although S2 presented a strong underdispersion and lacks reliability, it still improved with lead-time showing a contribution of the hydrological assimilation process to the overall reliability of the forecasts.
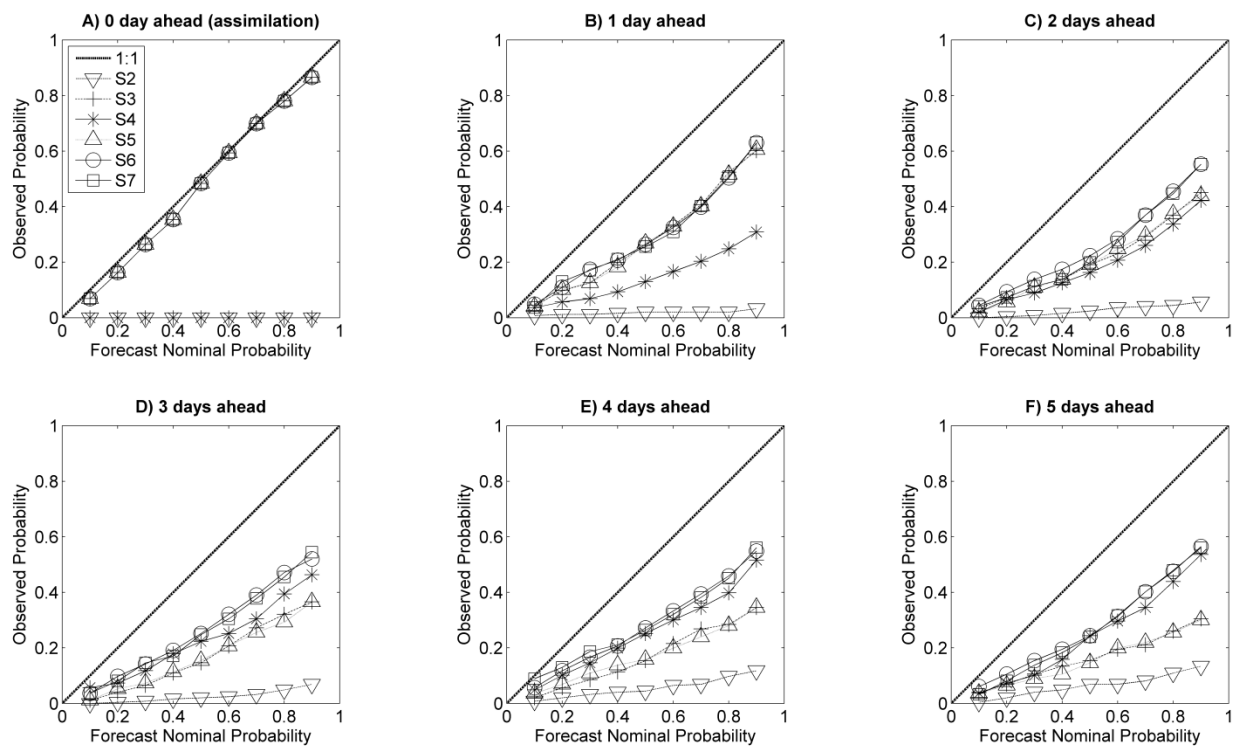
Figure 5.22: Reliability plots of scenarios S1-S7 for water temperature forecasts from 0 to 5 days (A-F) at Vanderhoof.

5.2.5 Discussion

5.2.5.1 *Assimilation of discharge and water temperature data using particle filters*

The need for proper quantification of uncertainty of initial conditions in the field of hydrology has led to several publications directed towards discharge data assimilation (e.g. Chen et al., 2013; Clark et al., 2008; Liu et al., 2012; Moradkhani et al., 2012; Seo et al., 2009; Weerts and El Serafy, 2006). Water temperature forecasting being a relatively recent topic, the case of water temperature assimilation was only addressed in a few publications (Table 5.8; Kim et al., 2014; Morrison and Foreman, 2005; Pike et al., 2013). This study highlights the need for developing and adapting suitable algorithms for data assimilation of water temperature for short and medium range forecasting. For this purpose, particle filters were adapted and tested for the successive assimilation of discharge and water temperature using data from two measurement stations. Error reductions (quantified using CRPS) of 70-74% and 65-71% were obtained respectively for discharge and water temperature data assimilation. These results compare favorably to previous studies. For instance, Morrison and Foreman (2005) obtained error reductions (RMSE) of 56-66% for discharge assimilation and error reductions of 20-30% for water temperatures both using an iterative data assimilation procedure. Pike et al. (2013) were able to reduce water temperature forecasting error by 50% (0.5° to 0.25°C) using an ensemble Kalman filter in a stochastic dynamic modelling approach. As in water quality forecasting, Kim et al. (2014) obtained error reductions of 41% for discharge and 29% for water temperature using a maximum likelihood ensemble filter in the HSPF (Hydrologic Simulation Program – Fortran) model. These studies were conducted in different hydrological contexts using different hydrological models. Therefore no conclusion can be drawn as to whether particle filters as implemented here outperforms these other methods. The most common method in discharge assimilation are ensemble Kalman filtering (e.g. Komma et al., 2008; Papadakis et al., 2010; Pathiraja et al., 2016; Shen and Tang, 2014; Thiboult et al., 2016) and the particle filtering (Moradkhani et al., 2012; Noh et al., 2011; Plaza et al., 2012; D.-J. Seo et al., 2003; van Leeuwen, 2009). A combination of both approaches is also possible, as in

Fan et al. (2017). Weerts and El Serafy (2006) found that better performances were obtained using the ensemble Kalman filter than particle filter. However, Leisenring and Moradkhani (2011) concluded the opposite for snow water equivalent data assimilation. A throughout comparison of the two methods in various hydrological contexts would be required to draw further conclusions pertaining water temperature.

Table 5.9: Summary of relevant literature associated with the three objectives of this study: (1) the assimilation of discharge and water temperature data; (2) ensemble water temperature forecasting; (3) quantification of uncertainty in water temperature forecasts.

Reference	Variable/Model	Assimilation Method	River, Country	Key Results
1. Morrison and Foreman (2005)	Discharge and water temperature/UBC flow model and IOSRTM water temperature model	Iterative procedure	Fraser River, Canada	1. Error reductions of 20-30% for water temperature and error reductions of 56-60% for discharge; 2. 10-day forecasts during salmon migration season; RMSE of 0.86-1.18°C; 3. Acknowledge the need for uncertainty consideration in the data assimilation process.
2. Neumann et al. (2006)	Water temperature/Multiple regression	N/A	Truckee River, USA	1- N/A 2- Decision support system implemented using statistical temperature model, 6-10 hours forecasts; 3- Risk assessment improves water allocation during warm season; No uncertainty quantification explicitly reported.
3. Sahoo et al. (2009)	Water temperature/Regression, artificial neural network, and chaotic non-linear dynamic models	N/A	Lake Tahoe tributaries, USA	1- N/A 2. RMSE ranges from 0.79-1.54°C for a 3-day forecasts; 3. N/A
4. Mestekemper et al. (2010)	Water temperature/Lag varying autoregressive model	N/A	Wupper, Germany	1. N/A 2. 1-3 day hourly forecasts with RMSE < 1°C; 3. No explicit uncertainty quantification. Confidence intervals are calculated.
5. Huang et al. (2011)	Water temperature/regression model	N/A	Klamath River, USA John Day River, USA	1. N/A 2. The use of 7-10 forecasts allows for better water allocation and results in increased fish production; 3. Uncertainty included in decision making model using Bayesian statistical analysis. No specific uncertainty analysis for water temperature forecasts.
6. Pike et al. (2013)	Discharge and water temperature/River Assessment for Forecasting Temperature	Ensemble Kalman filter	Sacramento River, USA	1. Error reduced from 0.5°C to 0.25°C with data assimilation; 2. 72 hours discharge and water temperature forecasts, 100 km reach downstream of dam; 3. Use of ensemble Kalman filter to quantify uncertainty.
7. van Vliet et al.	Discharge and water	N/A	Global analysis;	1. N/A

(2013)	temperature/Variable Infiltration Capacity (VIC) macro- scale hydrological model and stream temperature model (RBM)		Many rivers across the globe on a 0.5° x 0.5° spatial resolution	2. Climate forecasts. Global increase of 0.8-1.6°C for United States, Europe, eastern China, and parts of southern Africa and Australia; 3. N/A
8. Hague and Patterson (2014)	Water temperature/four statistical models based on time series decomposition	N/A	Fraser River, Canada	1.N/A 2. 10 day forecasts; Inclusion of air temperature and discharge is essential for accurate forecasts; 3 Need to incorporate model uncertainty and site-specific thresholds in forecasting model evaluation.
9. Kim et al. (2014)	Water quality variables including water temperature/Hydrologic Simulation Program – Fortran	Maximum likelihood ensemble filter and ensemble Kalman filter	Kumho River, Korea	1. Error reductions of 29% for water temperature and error reductions of 41% for discharge. 9 ensemble members; 2. 3 day forecasts with RMSE > 1.5°C; 3. Data assimilation used to reduce initial conditions uncertainty. Additional research needed to assess the accuracy of the uncertainty modelling as stated by the authors.
10. Bal et al. (2014)	Water Temperature/Linear regression, and time series decomposition with hierarchical Bayesian model	N/A	3 rivers, France	1. N/A 2. 50 year climate forecasts; RMSE > 2°C; 3. Model parameter uncertainty is considered. Larger uncertainty calculated using the Bayesian model compared to the confidence intervals of the regression.
11. Kamarianakis et al. (2016)	Water temperature/nonlinear mixed models	N/A	43 rivers, Spain	1. N/A 2. 1 day forecasts; Accuracy around 1°C; 3. N/A
12. Caissie et al. (2016)	Water temperature/Autoregressive models	N/A	Little Southwest Miramichi River, Canada	1. N/A 2. 3 day forecasts; RMSE from 0.87°C to 1.48°C; 3. N/A
13. Ouellet-Proulx et al. (2017)	Discharge and water temperature/CEQUEAU	N/A	Nechako River and Southwest Miramichi River, Canada	1. N/A 2. 5 day forecasts with accuracy (CRPS) from 0.77°C to 1.08°C. Probabilistic evaluation of forecasts; 3. Propagation of uncertainty from meteorological inputs. Biased meteorological forecasts. Need for quantification of initial conditions uncertainty.
14. This Study	Discharge and water temperature/CEQUEAU	Particle filters	Nechako River, Canada	1. Error reductions of 65-71% for water temperature and error reductions of 76-79% for discharge; 2. 5 day forecasts with accuracy (CRPS) from 0.49°C-0.75°C. Probabilistic evaluation of forecasts; 3. Initial conditions are key contributors to uncertainty for 1 day forecasts; Meteorological inputs are key contributors to uncertainty for 2-5 day forecasts.

Particle filters are known to require large ensemble size (Moradkhani et al., 2012; van Leeuwen, 2009). However, this study showed good performances of the particle filter for both the hydrological and the thermal components using only 40 particles (Figure 5.15). Other studies (e.g. Weerts and El Serafy, 2006) successfully used similar number of particles for the assimilation of discharge data.

5.2.5.2   Ensemble water temperature forecasting

The second part of the methodology proposed herein is the ensemble forecasting of discharge and water temperature with an emphasis on the latter. We produced 5 day ensemble forecasts and quantified the effect of uncertainty of different components of the system (inputs and initial conditions). A few other studies have focused on water temperature forecasts (Caissie et al., 2016; Huang et al., 2011; Kamarianakis et al., 2016; Mestekemper et al., 2010; Morrison and Foreman, 2005; Neumann et al., 2006; Ouellet-Proulx et al., 2017; Pike et al., 2013; Sahoo et al., 2009). The reported accuracy of these studies ranges from 0.57°C (72 h; stochastic dynamic approach; Pike et al., 2013) to 1.48°C (3 days; autoregressive model; Caissie et al., 2016). However, a direct comparison of performances between those studies and ours can hardly be performed as ensemble forecasts call for a probabilistic assessment (for instance using the CRPS and BS). The RMSE is the most commonly used metric for quality assessment of deterministic (single value) forecasts. A previous study (Ouellet-Proulx et al., 2017) on the Nechako River presented CRPS's of 0.77°C (1 day) to 0.82°C (5 days) without data assimilation. In this study, the inclusion of data assimilation returned lower CRPS's of 0.49°C (1 day; S6) to 0.75°C (5 days; S6).

We showed improvements in the quality of water temperature forecasts both in accuracy and reliability, as indicated by CRPS values, when ensemble thermal initial conditions were used. This supports results from earlier studies (Morrison & Foreman, 2005; Pike et al., 2013) where data assimilation improved initial conditions as well as forecasting accuracy. On the other hand, the accuracy of the forecast decreases when ensemble meteorological forecasts are provided as inputs. This lower accuracy can be accountable to the uncertainty carried by the ensemble meteorological forecasts provided as inputs. The higher variability of CRPS's (Figure 5.19) suggests that accuracy, as well as reliability, are more variable for longer lead-times. It also shows that the inclusion of meteorological inputs uncertainty (S4, S6 and S7) induces more variability in accuracy within the time series (error bars on Figure 5.19) than the

ensemble created from hydrological and thermal initial conditions alone (S2, S3, and S5).

5.2.5.3 *Quantification of uncertainty in water temperature forecasts*

Uncertainty in water temperature forecasts was discussed in previous studies including initial conditions (Pike et al., 2013), model input uncertainty (Hague & Patterson, 2014; Ouellet-Proulx et al., 2017), uncertainty in climate change projections (Bal et al., 2014) and risk assessment in decision making (Neumann et al., 2006). However, to the best of the authors' knowledge, this study is the first to explicitly document the respective contribution of hydrological and thermal initial conditions as well as meteorological inputs to total forecasts uncertainty. We proposed quantification through scenarios that target either specific or combined source of uncertainty (Table 5.5).

For the shorter lead-time (1 day), we found that water temperature uncertainty is dominated by thermal initial conditions (Figure 5.21- B). Its influence decreases quickly as a function of the forecasting horizon. Meteorological input uncertainty becomes most influential for longer lead-times. For a 2-day forecast, similar contributions were observed from those two sources of uncertainty. When short lead-time (1 day) water temperature forecasts are produced, priority should hence be on reducing the uncertainty related to the knowledge of the thermal conditions of the watershed. However, our results also suggest that the quality of the meteorological inputs have a strong influence on the overall quality of water temperature forecasts, at all lead-times. The consideration of meteorological uncertainty in water temperature forecasting is thus of paramount importance to properly quantify the total forecast uncertainty. These findings are coherent with previous studies in discharge forecasting, where ensemble meteorological inputs are required to maintain properly dispersed forecasts (Hopson & Webster, 2010; Thiboult et al., 2016). In this study, scenarios S3 and S5 were used to demonstrate how initial conditions uncertainty is propagated with lead-time. However, such framework in which uncertainty decreases with lead-time cannot be used operationally. In a real life setting, ensemble spread increases with lead-time as more uncertainty is induced in the forecast by meteorological forecasts that becomes

increasingly uncertain. These findings are central elements of this study which constitutes the first quantification of distinct sources of uncertainty in water temperature forecasting using a semi-distributed model.

These observations are supported by the reliability plots presented on Figure 5.22. It can clearly be observed that reliability is ensured by properly dispersed thermal initial conditions and maintained by ensemble meteorological inputs. Although a good spread of the ensemble was obtained throughout all forecasting lead-times, a deficiency in reliability is still present in all tested scenarios (reliability line below the bisector). This could be attributed to structural uncertainty which was not considered and is known to impact the spread at all lead-times in hydrological forecasting (Thiboult et al., 2016). Choices regarding the representation of hydrological and atmospheric processes, as well as their respective parametrization, are known to induce forecasting uncertainty. Clark et al. (2015) showed the equivalent and sometimes stronger influence of model parameters compared to processes representation on modelling uncertainty. The effect of structural uncertainty on water temperature forecasts should hence be further investigated.

In water temperature forecasting, the exceedance of specific temperature thresholds is crucial for the conservation of certain species such as Salmonids (Breau & Caissie, 2013). Our research showed the capacity of the proposed framework to predict threshold exceedances according to various threshold values. Expressing threshold exceedance in probabilistic terms (Brier Score) facilitates the inclusion and assessment of uncertainty through ensemble forecasts for operational river management.

5.2.5.4   Future directions for uncertainty assessment in water temperature forecasts

This paper contributes to uncertainty quantification in water temperature forecasts. However, further work is needed to fully understand the whole uncertainty propagation within a water temperature forecasting framework. Additional research is required to compare the particle filter to other ensemble data assimilation methods, such as the widely used ensemble Kalman filter. In this study, all forecasting scenarios showed a lack of reliability which can be detected by the underdispersion of the forecasts in

reliability diagrams. This suggests that the proposed framework does not include all the uncertainty of the system. For one thing, no structural uncertainty was included in the present work. The addition of structural uncertainty to this analysis should be carefully investigated. A similar study using different models or different parameterizations of the same model would inform on the contribution of the structural uncertainty in comparison to the sources of uncertainty considered in the present work. The study was performed in a single strongly regulated river system. Therefore, its transferability to other hydrological contexts is limited. Additional work on other regulated as well as unregulated river systems would help broaden the scope on the present study.

5.2.6 Conclusion

This paper contributes to uncertainty quantification in water temperature forecasts. However, further work is needed to fully understand the whole uncertainty propagation within a water temperature forecasting framework. Additional research is required to compare the particle filter to other ensemble data assimilation methods, such as the widely used ensemble Kalman filter. In this study, all forecasting scenarios showed a lack of reliability which can be detected by the underdispersion of the forecasts in reliability diagrams. This suggests that the proposed framework does not include all the uncertainty of the system. For one thing, no structural uncertainty was included in the present work. The addition of structural uncertainty to this analysis should be carefully investigated. A similar study using different models or different parameterizations of the same model would inform on the contribution of the structural uncertainty in comparison to the sources of uncertainty considered in the present work.

5.2.7 Acknowledgements

5.3 Article 3 : Implication of evaporative losses estimation methods in discharge and water temperature modelling

Le rôle des méthodes d'estimation des pertes par évaporation dans la modélisation hydrologique et thermique

Sébastien Ouellet-Proulx[1], André St-Hilaire[1] et Marie-Amélie Boucher[2]

[1]Canadian Rivers Institute and INRS-ETE, 490, rue de la Couronne, Québec, Canada

[2]Université de Sherbrooke, département de génie civil, 2500 Boulevard de l'Université, Sherbrooke, Qc, J1K 2R1

L'article a été soumis pour publication à la revue Hydrological Processes. La version de l'article présentée dans la thèse correspond à la version soumise.

Contribution des auteurs :

L'idée qui a mené à l'article a été élaborée par les Pr. André St-Hilaire et Marie-Amélie Boucher avec la collaboration de l'étudiant (Sébastien Ouellet-Proulx). La programmation des équations d'évapotranspiration et d'évaporation a été effectuée par l'étudiant (Sébastien Ouellet-Proulx) avec le support de M. Richard Loubier (Rio Tinto). Le calage du modèle, les analyses et la rédaction de l'article ont été réalisés par l'étudiant (Sébastien Ouellet-Proulx) sous la supervision des Pr. André St-Hilaire et Marie-Amélie Boucher.

Résumé

L'évaporation est une composante importante du bilan hydrologique. Les pertes en eau dues à l'évapotranspiration réduisent le volume disponible pour le ruissellement. La transition de l'état liquide à l'état gazeux à la surface de l'eau demande de la chaleur. Conséquemment, l'évaporation agit comme un mécanisme de refroidissement pendant l'été. Le débit et la température de l'eau simulés à l'aide de modèles sont donc tous deux influencés par la façon d'estimer ces flux évaporatifs. Dans cet article, l'impact du choix de méthode d'estimation de l'évapotranspiration sur les simulations de débit est évalué à l'aide d'un modèle semi-distribué sur deux bassins versants canadiens. L'impact du choix de méthode d'estimation de l'évaporation sur la simulation de la température de l'eau est aussi évalué. Enfin, la pertinence d'utiliser la même formulation pour simuler ces deux processus (évaporation et évapotranspiration) est investiguée. Cinq modèles d'évapotranspiration connus et cinq modèles d'évaporation avec différentes fonctions de vent ont été testés. Les résultats exposent une grande disparité parmi les modèles d'évapotranspiration, qui ont mené à d'importantes différences dans les simulations de débits. Les résultats suggèrent aussi que la méthode d'estimation de l'évaporation n'a qu'une influence marginale sur l'évapotranspiration totale estimée et donc sur le débit estimé à l'échelle du bassin versant. Une part plus importante des pertes de chaleur totales dues à l'évaporation est observée quand des méthodes d'évapotranspiration sont utilisées pour estimer l'évaporation plutôt que des modèles d'évaporation en eau libre. De manière générale, cette étude suggère que l'évapotranspiration et l'évaporation en eau libre devraient être représentées séparément dans un cadre de modélisation hydrologique, et ce particulièrement lorsqu'une modélisation de la température de l'eau est nécessaire.

Abstract

Evaporative flux is a key component of hydrological budgets. Water loss through evapotranspiration reduces volumes available for runoff. The transition from liquid to water vapour on open water surfaces requires heat. Consequently, evaporation acts as a cooling mechanism during summer. Both river discharge and water temperature simulations are thus influenced by the methods used to model evaporation. In this paper, the impact of evapotranspiration estimation methods on simulated discharge is assessed using a semi-distributed model on two Canadian watersheds. The impact of evaporation estimation methods on water temperature simulations is also evaluated. Finally, the validity of using the same formulation to simulate both of these processes is verified. Five well known evapotranspiration models and five evaporation models with different wind functions were tested. Results show a large disparity among the evapotranspiration methods, leading to important differences in simulated discharge. Results also suggest that the method used for the estimation of river evaporation only has a marginal influence on total evapotranspiration and discharge at the watershed scale. Larger portions of evaporative heat losses are observed when evapotranspiration models are used to estimate river evaporation compared to open water evaporation models. Overall, the results of this study suggest that evapotranspiration and open water evaporation should be represented separately in a hydrological modelling framework, especially when water temperature simulations are required.

5.3.1 Introduction

One crucial component of hydrological and water temperature modelling is the mathematical representation of evapotranspiration fluxes. They occur through plant transpiration on vegetated ground and evaporation from open water and bare soil. Open water evaporation is essentially related to vapour pressure deficit between the air above the watercourse and air saturation vapour pressure. Plant transpiration depends on hydrometeorological conditions and on the characteristics of plant species (Ahrens, 2015). When the variable of interest is the total amount of water loss from the earth surface in the form of vapour, including both of the aforementioned definitions, the term evapotranspiration is used. Regardless of the surface of interest, the evaporative processes affect the hydrological system through two keys elements: (i) it reduces the volume of water available for runoff (Jobson, 1980) and (ii) it acts as a cooling mechanism in the summer through latent heat exchange (Caissie et *al.*, 2007).

Estimation models for evapotranspiration are often classified based on the input data they require (e.g. Oudin et al., 2005). The spectrum of available models includes empirical approaches, those that are temperature-based (e.g. Blaney and Criddle, 1950; Linacre, 1977; Thornthwaite, 1948), radiation-based models (e.g. Jensen and Haise, 1963; McGuinness and Bordne, 1972), water budget (e.g. Guitjens, 1982), mass transfer (e.g. Harbeck, 1962) and hybrid methods (Penman, 1948; Monteith, 1965; Priestley and Taylor, 1972).

The comparison of models to estimate evapotranspiration for hydrological modelling is usually performed by comparing evaporative loss rates to field measurements (Sumner and Jacobs, 2005; Isabelle et al., 2015). Because of technical considerations and economic constraints, only a minority of studies include a comparison with field measurements. Many studies rely exclusively on the subsequent hydrological simulations for indirectly assessing the quality of evapotranspiration modelling (e.g. Andersson, 1992; Oudin et al., 2005; Parmele, 1972). For instance, Parmele (1972) showed that the cumulative effect of a 20% bias in the estimation of evapotranspiration

induces a significant error in the hydrological simulations. Similarly, Oudin et al. (2005) performed an exhaustive comparison of 27 potential evapotranspiration equations on 308 watersheds using four lumped hydrological models. This work highlighted the equivalent efficiency of methods requiring few input data, such as the method of McGuinness and Bordne (1972), compared to methods with high input data requirements such as the Penman-Monteith method (Monteith, 1965). In Canada, Barr et al. (1997) compared the Morton method (1983), a modified version of the Penman method (Granger and Gray, 1989) and the Spittlehouse method (Spittlehouse, 1989) in the SLURP hydrological model. The Spittlehouse method accounts for the physical processes involved in evapotranspiration, including the soil water availability, and it was shown to improve hydrological simulations. However, to be properly implemented, the Spittlehouse method requires data that are not widely available, such as the soil moisture extractable by the root system as well as the wilting point of the local vegetation.

During the summer, the main heat loss mechanisms of a river are evaporative (latent) and convective (sensible) heat fluxes as well as longwave radiation reemission (Webb and Zhang, 1997; Maheu *et al.*, 2014). In some systems, evaporative fluxes can dominate and account for up to near 100% of river heat loss during the summer (Hannah *et al.*, 2008). In water temperature modelling, most studies estimate the latent heat loss (Chikita et al., 2012) using formulations generally based on a mass transfer equation (Harbeck, 1962). The mass transfer model for evaporation calculates the difference between the actual and saturation water vapour pressure of the air above the river, factored by a wind function. When precise evaporation measurements are available, a site specific wind function can be adjusted. However, *in situ* river evaporation data are often difficult to acquire, and modellers commonly have to rely on readily available wind functions to estimate river evaporative fluxes (e.g. Hannah *et al.*, 2004; Leach and Moore, 2010).

Rosenberry *et al.*, (2007) compared 14 evaporation estimation methods to the Bowen-ratio energy-budget method for a small lake (0.15 km^2) in a mountainous area in northeastern USA. They found the best performances using combination methods: Priestley and Taylor (1972), deBruin and Keijman (1979), and Penman (1948). They

reported mean daily evaporation values (averaged for a specific month) ranging between 0.69-3.43 mm (May to November). Spring and Schaefer (1974) measured maximum daily evaporation of 6.22 mm on Babine Lake (British Columbia, Canada) with a mean value of 1.83 mm during the open water season of 1973.

To the best of our knowledge, very few publications about river evaporation estimation rely on direct measurements to validate estimation methods. Among them, Benner (1999) measured hourly evaporation above 1.0 mm/h on the John Day River (Oregon, USA). Guenther et al. (2012) measured hourly evaporation before and after wood harvest on Griffin Creek (British Columbia, Canada) with an hourly average of 0.03 mm/h. No daily value was reported. Maheu et al. (2014) measured a maximum daily evaporation of 6.8 mm in the Little-Southwest Miramichi River (forested watershed in New Brunswick, Canada) and a maximum daily evaporation of 2.8 mm in the Catamaran Brook (third order tributary), with mean values of 3.0 mm and 1.0 mm, respectively.

In practice, despite the differences between the two processes (evapotranspiration and evaporation), many models combine the two processes and use one equation to estimate all evaporative fluxes (Xu and Singh, 2000). For instance, Winter et al. (1995) compared 11 equations to estimate monthly evaporation on Williams Lake in Minnesota (USA). Among the 11 formulations they tested, only one was originally developed to model open water evaporation. Similarly, many hydrological models (e.g. SWAT, CEQUEAU, HYDROTEL, GR4J, and TOPMODEL) do not distinguish water loss through open water or bare soil evaporation and evapotranspiration. Since these formulations are sometimes employed without prior investigation, it is reasonable to wonder whether or not a unique equation is suitable to estimate both evapotranspiration and open water evaporation. This question becomes even more relevant when the same formulation is further used for the estimation of latent heat loss at the water surface in a water temperature modelling framework. The following study is based on the underlying hypothesis that the two processes should be modelled separately using different formulations.

Most studies focusing on evaporative processes and water temperature provide crucial insights on the best adapted formulation to estimate evaporation in a specific region (e.g. Guenther et al., 2012; Maheu et al., 2014). These formulations can subsequently be used in a water temperature-discharge modelling framework. In the present study, the goal is not to find the best model to estimate evaporative fluxes. The goal is rather to quantify the impact of choosing a particular evaporation or evapotranspiration estimation method on subsequent hydrological and thermal simulations.

More specifically, the objectives of this study are to 1) evaluate the impact of different evapotranspiration estimation methods on discharge simulations in a semi-distributed model; 2) assess the impact of the implementation of selected evaporation estimation methods on water temperature simulations; and 3) finally evaluate the possible limitations of using the same method to evaluate both evapotranspiration and open water evaporation for discharge and water temperature modelling.

5.3.2   Methodology

5.3.2.1   *CEQUEAU model*

Throughout this study, the CEQUEAU hydrological and water temperature model provides a general modelling framework to implement and compare different equations to model evapotranspiration. Different mass transfer equations for open water evaporation are also compared. The model was successfully used to simulate discharge and water temperature in previous studies (e.g. St-Hilaire et al., 2000; Kwak et al., 2017; Larabi et al., 2018)

The hydrological component of CEQUEAU is a semi-distributed rainfall runoff model that uses total precipitation and air temperature as inputs to simulate discharge. This rainfall-runoff model is composed of a production function that distributes water vertically and a transfer function that routes it downstream. This routing is performed on a predefined grid with cells of equal area. The production function considers the total precipitation that falls on the watershed and distributes it into different reservoirs, with proportions deduced based on information about land use. Possible reservoirs are: lakes and marshes, upper soil, lower soil and rivers. The two soil reservoirs can store

136

and release volumes of water for runoff, depending on the meteorological conditions and on the values of soil-related parameters. Water is also depleted from the soil reservoirs by evapotranspiration. In open water reservoirs (lakes, marshes and rivers), water is lost through evaporation only. Both evapotranspiration and evaporation are estimated using Thornthwaite (1948) equation.

Once discharge is simulated, the thermal module of CEQUEAU evaluates the heat budget on each grid cell by summing the advective heat fluxes with the various thermal energy fluxes at the air-water interface, according to Equation 5.22:

$$H_{tot} = H_s + H_{IR} + H_e + H_c + H_{adv}$$ Equation 5.22

where H_{adv} represents the energy exchanged by advective fluxes, H_s is the net solar radiation, H_{IR} is the net longwave radiation re-emitted by the atmosphere above the water course, H_c is the sensible (convective) heat flux and H_e is the evaporative flux. Water temperature, T_w, is then estimated using the ratio of enthalpy (H_{tot} in MJ) over the volume of water (V in m^3) times the heat capacity of water (C; 4.187 MJ m^{-3} °C^{-1}):

$$T_w = \frac{H_{tot}}{VC}$$ Equation 5.23

In CEQUEAU, the Thornthwaite (1948) equation is implemented to calculate potential evapotranspiration (PET_{TW}) as follows:

$$PET_{TW} = \frac{10}{30.4} 1.62 \left(10 \frac{T_a}{XIT} \right)^{XAA}$$ Equation 5.24

The parameters *XIT* and *XAA* can be estimated using Equation 5.25 and Equation 5.26.

$$XIT = \sum_{i=1}^{12} \left(\frac{TM_i}{5} \right)^{1.51}$$

Equation 5.25

$$XAA = 67.5 \times 10^{-8} \, XIT^3 - 77.1 \times 10^{-6} \, XIT^2 + 0.0179 \, XIT + 0.492$$

Equation 5.26

where TM_i is the mean monthly air temperature (°C) during month i. In the CEQUEAU formulation, PET_{TW} is adjusted according to the weighting parameter $Hrad$, which takes into account the day of the year with maximum solar radiation approximated using Equation 5.27:

$$Hrad = \frac{2}{\pi} \cos^{-1} \left(-\tan \left(\sin^{-1} \left(\frac{23.45\pi}{180} \sin \left(\frac{2\pi}{365} (J_D - JOEVA) \right) \right) \right) \tan(XLA) \right)$$

Equation 5.27

where J_D is the day of the year, $JOEVA$ is the day of the year with maximum insolation and XLA is the mean latitude of the watershed. $JOEVA$ can be estimated to 80 (June 21st) in the northern hemisphere and can be verified if radiation data are available. Equation 5.24 becomes:

$$PET_{TW} = HRad \frac{10}{30.4} 1.62 \left(10 \frac{T_a}{XIT} \right)^{XAA}$$

Equation 5.28

The actual evapotranspiration is then estimated according to PET_{TW} and the fraction of the grid cell occupied by forested area, using Equation 5.29 below. In its actual form, the model estimates river evaporation to be a fixed fraction (80%) of the PET estimated by the hydrological component (Thornthwaite method; Equation 5.24). The latent heat

loss is obtained by multiplying the height of water evaporated (m) with the latent heat of vaporization of water considered constant at 2480 MJ m^{-3}. Land use is crudely taken into account using Equation 5.29:

$$ET_{TW} = PET_{TW} \times ARF$$

<div align="right">Equation 5.29</div>

A totally forested grid cell would have an *ARF* value of 1 and a grid cell completely deforested would have a value of 0.8.

Overall, the hydrological component of CEQUEAU has 28 parameters, from which 16 have a physical meaning (snowmelt model, evapotranspiration, water routing, etc.). The other 12 parameters are coefficients to be adjusted to achieve the best possible goodness of fit between observed and simulated discharge. The water temperature model has 12 parameters. Those parameters adjust channel geometry, the importance of each energy fluxes and the timing of freezing/thawing. While the parameters *XIT* and *XAA* can be estimated according to the meteorology of the watershed, they can also be manually adjusted to better replicate the observed discharge. In case of thermal modelling, such adjustments impact the subsequent estimation of latent heat losses. For the present study, parameters calculated from monthly temperatures (Equation 5.25 and Equation 5.26) are used. Readers can find more detailed information in St-Hilaire et al. (2000) and (2015), including a complete list of parameters and a full description of the model.

5.3.2.2 *Evapotranspiration and evaporation formulations*

Two approaches were prioritized in the assessment of the evaporation estimation methods. First, we used alternative methods to estimate evapotranspiration in the hydrological model without changing the structure of the model (i.e. use evapotranspiration to estimate latent heat loss). Although such formulations are not physically accurate (open water evaporation and evapotranspiration processes are not

the same), they replicate the current structure of the model. This step allows for the evaluation of the impact of using different evapotranspiration formulations on discharge simulations, and associated effects on the subsequent thermal modelling. An ideally adapted method would return realistic evaporation estimates and the best discharge and water temperature estimations when compared to other methods. Second, we kept the original Thornthwaite evapotranspiration method but implemented a mass transfer method for estimating open water evaporation. Alternate wind functions were tested to evaluate the latent heat loss. A set of five equations for estimating evapotranspiration (Table 5.9) and the same number of wind functions for open water evaporation (Table 5.10) were selected. Those equations and associated assumptions are described further in section 5.3.2.2.

The evapotranspiration estimation models were selected based on their different levels of complexity (i.e. number of input data), the availability of those input data and their performance according to the recent hydrological literature.

Table 5.10. Description of the five evapotranspiration methods selected for comparison

Method	Type	Number of inputs
Thornthwaite (1948)	Empirical (temperature)	1
McGuinness et Bordne (1972)	Empirical (temperature); extra-terrestrial radiation)	1
Priestley-Taylor (1972)	Radiation	2
Penman-Monteith (Allen et al., 1998)	Radiation; mass transfer	5
Kimberley-Penman (Wright, 1982)	Radiation; mass transfer	5
Morton (1983)	Radiation; mass transfer; longwave radiation; extra-terrestrial radiation	6

Evapotranspiration

The method of McGuinness and Bordne ($ET_{M\text{-}B}$; McGuinness and Bordne, 1972) was selected for its good performance compared to more complex methods in a hydrological modelling study (Oudin et al., 2005) while only requiring air temperature and extra-terrestrial radiation as inputs.

$$ET_{M-B} = \frac{R_e}{\lambda \rho} \cdot \frac{T_a + 5}{68}$$

Equation 5.30

This equation relies on extra-terrestrial Radiation (R_e; MJ m^{-2}), air temperature (T_a; °C), the latent heat of vaporization (λ; 2.45 MJ kg^{-1}) and water density (ρ 1000 kg L^{-1}). This method was first implemented for humid regions (Coshocton, Ohio, U.S.) while most evapotranspiration methods were developed for arid regions.

The Priestley-Taylor equation ($ET_{P\text{-}T}$; Priestley and Taylor, 1972) is a simplified version of Penman (1948) equation for which the evaporation capacity is replaced by the Priestley-Taylor coefficient (α). This equation showed good performances to estimate both evapotranspiration (Oudin et al., 2005) and open water evaporation (Rosenberry et al., 2007). It requires three input variables, namely air temperature, solar radiation, and atmospheric pressure to calculate the psychometric constant. $ET_{P\text{-}T}$ is written:

$$ET_{P-T} = \frac{1}{\lambda} \cdot \frac{\Delta R_n}{\Delta + \gamma} \cdot \alpha$$

Equation 5.31

where R_n is net solar radiation (MJ m^{-2}), Δ is the slope of vapour pressure (kPa °C^{-1}) and γ is the psychrometric constant (kPa °C^{-1}). The α coefficient corresponds to the slope of the regression between equilibrium evaporation and actual evapotranspiration. Although the initial α was first estimated to be 1.26 (Priestley and Taylor, 1972), a wide

range of coefficient values have been applied since. Cristea et al. (2013) compiled a list of 52 different α values from the literature, ranging from 0.6 (Oklahoma; Kustas et al., 1996) to 2.47 (southeast Iran; Daneshkar Arasteh and Tajrishy, 2008).

With a level of complexity somewhat superior to Priestley-Taylor, the Kimberly-Penman equation ($ET_{K\text{-}P}$; Wright, 1982) was also retained for comparison in this study:

$$ET_{K-P} = \frac{\Delta R_n + \gamma \left(e_s - e_a\right)\psi}{\lambda \rho \left(\Delta + \gamma\right)} \qquad \text{Equation 5.32}$$

where e_s is saturation vapour pressure (kPa), e_a is actual vapour pressure (kPa) and ψ is a wind function. This is another modification of the Penman (1948) equation, where the wind function is modulated according to the day of the year (J_D):

$$\psi = \left[0.4 + 0.14\exp\left(\left(\frac{J_D - 173}{58}\right)^2\right)\right] + \left[0.605 + 0.345\exp\left(-\left(\frac{J_D - 243}{80}\right)^2\right)\right]u_2 \qquad \text{Equation 5.33}$$

where u_2 is the wind speed (m s^{-1}) at 2 m height.

This equation is considered as a standard equation by the American Society of Civil Engineers (ASCE; Allen et al., 2005) and showed better performances than the original Penman formulation in the context of lumped conceptual hydrological simulation (Oudin et al., 2005). It was developed for 30-50 cm vegetation with constant sufficient water supply.

The Penman-Monteith equation ($ET_{P\text{-}M}$; Monteith, 1965) is the reference method recommended by the Food and Agriculture Organization of the United Nations (FAO) for evapotranspiration estimation. Among all the methods selected for this study, it has the highest number of input variables (six). Herein, we used a simplified version (Allen et

al., 1998) which excludes stomatal and aerodynamic resistances. It is computed using Equation 5.34:

$$ET_{P-M} = \frac{0.408\Delta(R_n) + \gamma\dfrac{900}{T_a + 273}u_2(e_s - e_a)}{\Delta + \gamma(1 + 0.34u_2)}$$

Equation 5.34

Lastly, Morton complementary relationship areal evaporation model (1983) was retained as a higher complexity method. It connects potential evapotranspiration (*ETP*) with a wet environment evapotranspiration rate (*ETW*) to estimate actual evapotranspiration (*ET$_M$*).

$$ET_M = 2ETW - ETP$$

Equation 5.35

Potential evapotranspiration is estimated using a modified Penman equation:

$$ETP = \frac{\Delta R_n}{\lambda(\Delta + \gamma)} + \frac{\gamma\psi(e_s - e_a)}{\lambda(\Delta + \gamma)}$$

Equation 5.36

where wet environment evapotranspiration rate is estimated as:

$$ETW = \frac{\alpha\Delta(R_n - M)}{\lambda(\Delta + \gamma)}$$

Equation 5.37

where:

$$M = 1.37R_{IR} - 0.394R_s$$

Equation 5.38

With incoming solar radiation (MJ m^{-2}) represented by R_s and longwave radiation (MJ m^{-2}) represented by R_{IR}.

Various formulations derived from Morton's method were proposed in past research (Xu and Singh, 2005). However, only the formulation described in Barr et al. (1997) was retained in this study because it showed good performances under similar climate (British Columbia, Canada).

Evaporation

In the case of river evaporation, aside from the evapotranspiration methods, the mass transfer equation was used in the form of Equation 5.39:

$$E = \psi \left(e_s - e_a \right)$$
Equation 5.39

where *E* is evaporation. The wind function is given by:

$$\psi = \alpha_\psi + \beta u_x$$
Equation 5.40

This wind function (ψ) includes two coefficients (Equation 5.40): the intercept (α_ψ) controls the importance of the evaporation resulting from vapour pressure deficit, referred to as free convection, while the slope (β) controls the importance of forced convection or wind induced convection. Table 5.9 presents the five wind functions that are compared in this study. All wind functions have the same linear form but differ in terms of α_ψ and β coefficient. To ease the reading and save space, the above-mentioned methods are henceforth referred to without their year of publication.

Table 5.11: Description of the five wind functions selected for comparison

Reference	α Free Convection	β Forced Convection	Height of wind measurements (m)	Region
Benner (1999)	3.46	2.04	0.5	Oregon, USA
Webb and Zhang (1997)	0.12	1.43	2	Devon, UK
Maheu et al. (2014)	3.09	0.84	2	New Brunswick, CAN
Guenther et al. (2012)	0	1.02	1.5	British Columbia, CAN
Jobson (1980)	3.01	1.13	4	California, USA

5.3.3   Study sites and data

The methodology was applied to two Canadian watersheds: the Nechako River drainage basin, located in British Columbia and the Miramichi River basin, located in New Brunswick. The two watersheds are spawning ground for Pacific (Nechako) and Atlantic (Miramichi) salmon and face overheating during the summer. The accurate modelling of their discharge and water temperature is therefore an essential component of the fisheries management efforts.

5.3.3.1   Nechako

The Nechako River is a 47 000 km^2 watershed impounded in its upper reaches to create the Nechako reservoir (Figure 5.23). Its discharge is strongly regulated by the Skins Lake Spillway and flows eastward to the Fraser River. The main tributary of the upper Nechako is the Nautley River. Discharge is recorded at four hydrometric stations on the watershed, namely Skins Lake Spillway, Cheslatta Falls, the outlet of the Nautley River and Vanderhoof (Figure 5.23). Water temperatures are recorded at the same locations apart from the Skins Lake Spillway. The Skins Lake Spillway is operated by

Rio Tinto, the owner of an aluminum smelter located in Kitimat. During the spawning season of the Sockeye salmon, Rio Tinto is required to release sufficient volumes of water to maintain water temperature below 20°C at the confluence of the Nechako and the Stuart Rivers (Figure 5.23). The present paper focuses on the reach of the Nechako River located between the Skins Lake Spillway and the Vanderhoof hydrological station (about 50 km upstream of the confluence with the Stuart River; Figure 5.23). This totalises 12 400 km^2 of drainage area. Simulated discharge and water temperature were validated at the Cheslatta Falls (1 460 km^2), Nautley (6 030 km^2) and Vanderhoof (12 400 km^2) hydrometric stations. The model was calibrated to best replicate discharge during the summer period (day 152 to 273) at Vanderhoof but results for all hydrometric stations are shown to allow full appreciation of the model's capabilities.
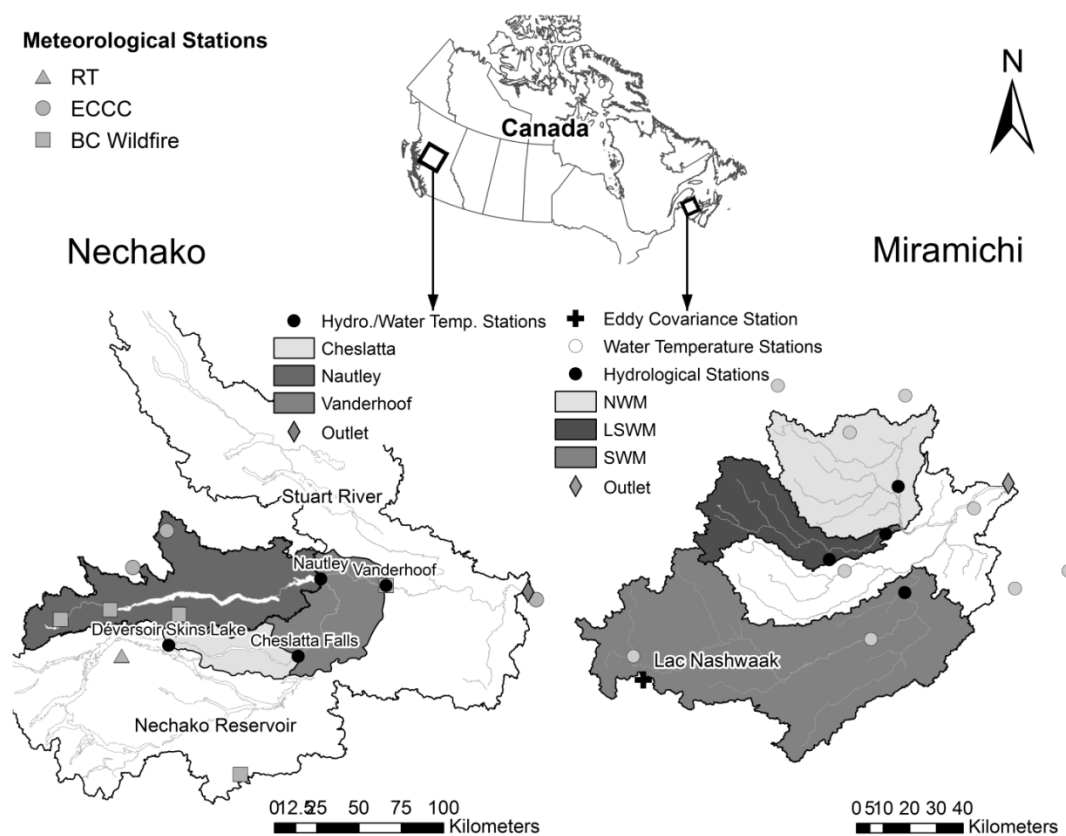
Figure 5.23: Maps of the Nechako and the Miramichi watersheds. On the map for Miramichi, NWM stands for Northwest Miramichi, LSWM for Little Southwest Miramichi and NWM for Northwest Miramichi. Catamaran Brook is too small to be represented on the figure.

146

Wind speed, atmospheric pressure and relative humidity measurement recorded at Ootsa Lake, Burns Lake and Prince George by Environment and Climate Change Canada (*ECCC*) were used as model inputs. Precipitation and air temperature measurements from Rio Tinto (*RT*) and British Columbia Wildfire (*BC Wildfire*) meteorological stations were also used. All wind measurements were recorded at a 10 m standard height. However, the tested wind functions were designed to use wind measurements taken at different heights. Consequently, measurements taken at 10 m were converted to the appropriate height for each method using a power law wind profile (Hsu, Meindl, & Gilhousen, 1994).

5.3.3.2   Miramichi

The Miramichi watershed has a drainage area of 13 000 km^2 and has a natural hydrological regime. Data from four subwatersheds of the Miramichi were used to validate discharge and water temperature simulations. The three main subwatersheds (SWM, LSWM and NWM) merge together downstream of the hydrological stations. They can be considered as independent watersheds. However, Catamaran Brook is a tributary of the LSWM. Water temperature data on the Miramichi watershed were extracted from the rivTemp database (http://rivtemp.ca) for the Southwest Miramichi (SWM; Figure 5.23) at Wades Lodges, the Little Southwest Miramichi (LSWM; Figure 5.23) at Oxbow, Northwest Miramichi (NWM; Figure 5.23) at Call Pool and at Catamaran Brook (CAT). Discharge data were retrieved from the Water Survey of Canada database on the Southwest branch at Blackville (5 050 km^2), on the Little Southwest branch at Lyttleton (1340 km^2), on the Northwest branch at Trout Brook (948 km^2) and on Catamaran Brook at Repap Road Bridge (28.7 km^2). As performed on the Nechako watershed, the model was calibrated to best replicate discharge in the summer period (day 152 to 273) at one site, namely the Southwest Miramichi, but results for all hydrometric stations are presented.

Benyahya et al. (2010) assessed the difference between meteorological observations recorded at a remote meteorological station and observations recorded above the river on the Miramichi watershed (New Brunswick). They found that on the Little Southwest

Miramichi River (≈ 80 m width), wind speed measured above the river during the summer was 32.2% of the wind speed recorded at the remote meteorological station, on average. Air temperature, relative humidity and solar radiation were somewhat higher (respectively 103%, 106% and 101%) above the River compared to the meteorological station. Consequently, these corrections were applied to the meteorological observations used in this study.

5.3.3.3 *Evaporation/Evapotranspiration validation data*

Brown et al. (2014) installed two eddy covariance systems in northern British Columbia between 2007 and 2010 at two sites respectively located at 100 km (Crooked River) and 160 km (Kennedy Siding) north of Prince George. They recorded the average daily evapotranspiration, which ranged between 1.36 mm (2010) and 1.54 mm (2008) at Crooked River and between 1.12 mm (2007) and 1.21 mm (2009) at Kennedy Siding during the growing season. For the same period, maximum daily evapotranspiration was respectively 3 mm day^{-1} and 2.5 mm day^{-1}. Annual totals ranged between 280 mm (2007; 2009) and 297 mm (2008), and 226 mm (2007) and 237 mm (2008).

In eastern Canada, Malloy and Price (2014) measured mean daily evapotranspiration of 2.6 mm (2008) and 3.3 mm (2009) in the Bic region (Quebec) during the months of June and July. These values were derived from estimations using Priestley-Taylor (1972) method with an α value adjusted from five lysimeters. Xing et al. (2008) measured a mean daily evapotranspiration of 1.45 mm and a maximum evapotranspiration of 2.5 mm in the Fredericton region (New Brunswick) from May to October (2004-2007).

Eddy covariance data were also retrieved from the FluxNet database (http://fluxnet.ornl.gov). Latent heat fluxes from Nashwaak Lake station (2003-2005; .5.23) were used to calculate evapotranspiration. These evapotranspiration values were used for comparison on the Miramichi watershed.

Brown *et al.* (2014) calculated Priestley-Taylor α coefficients (Equation 5.31) of 0.51 and 0.53 using micrometeorological tower data from two sites located close the Nechako watershed (100 km). For the Miramichi watershed, α coefficients were

calculated based on the evapotranspiration values derived from the eddy covariance data.

A weighing lysimeter was also installed at about 400 m southeast of the Ootsa Lake/Skins Lake meteorological station (Environment and Climate Change Canada station # 1085836) during summer 2015. The lysimeter was made of a 60 cm soil column constrained in a 12" radius PVC pipe sealed at the bottom. The soil column was placed on a platform scale (PL-100 - UMS) connected to a data logger (CR1000). The platform scale has a 14 g precision which translates into 0.20 mm of water. Measurements were recorded every 15 minutes between June 4th and October 1[rst] 2015. Negative differences in weight would indicate evapotranspiration while a positive difference would indicate rainfall. The lysimeter was installed approximately 350 m from the Ootsa Lake meteorological station. Figure 5.24 presents data recorded using the weighting lysimeter installed on the Nechako watershed between June 4th and October 1st 2015. A maximum daily evapotranspiration of 3.23 mm was measured with a mean value of 1.33 mm. The total daily precipitation was plotted over the lysimeter data to validate that positive weight variations accurately represent the variation in water content associated with rainfall.
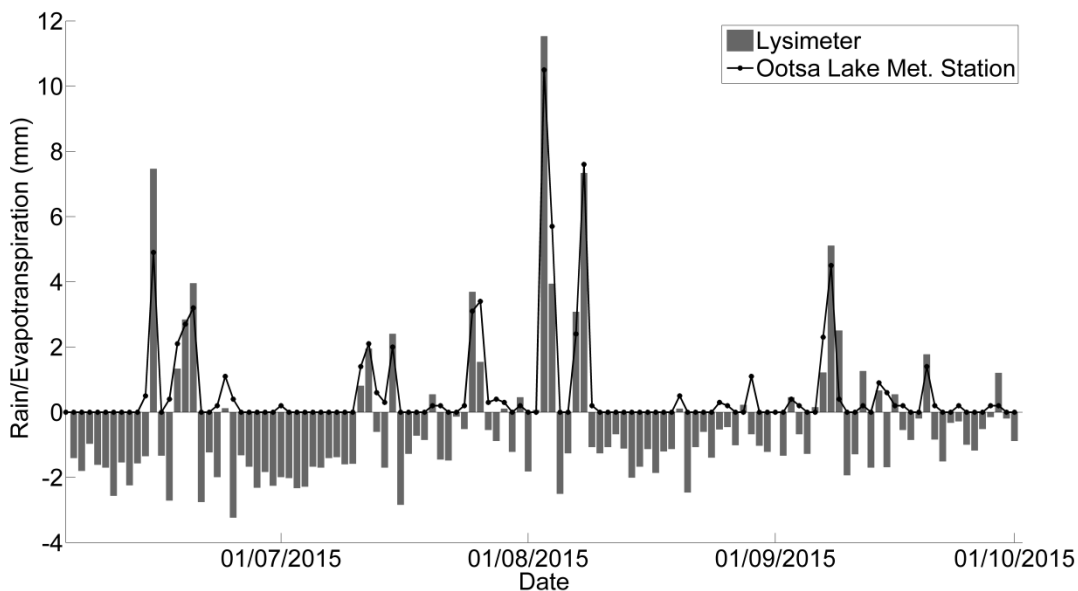
Figure 5.24: Evapotranspiration and rain measurements from the weighting lysimeter and precipitation measured at the Ootsa Lake meteorological station.

5.3.3.4   Model calibration and parameter's uncertainty

Both the hydrological and the thermal modules were recalibrated when either the evapotranspiration or the evaporation method was changed using a split sample method. For the two watersheds used in the present study, the calibration period is 2001 to 2006 and the validation period is 2007 to 2010. The hydrological component has 28 parameters and the thermal component has 12 parameters. All parameters were optimized using the covariance matrix adaptation evolution strategy (CMA-ES; Hansen and Ostermeier, 1996) with 1500 iterations. Two different objective functions were used: one for optimizing the hydrological component of the model and one for optimizing the thermal module.

For the hydrological component, the objective function was the maximisation of the Kling-Gupta Efficiency coefficient (KGE) computed for simulated discharge compared to observations. The KGE is a metric proposed by Gupta et al. (2009) that accounts simultaneously for accurate simulation of the mean discharge, the associated variance and the correlation between simulated and observed discharge. The KGE also puts less emphasis on high discharge values compared to the widely used Nash-Sutcliffe Coefficient (NSE; Nash and Sutcliffe, 1970).

Because of the strong seasonality in water temperature time series, performance metrics such as the KGE or the NSE always tend to be high for modelled water temperature. Hence, they do not have a high discrimination power and are not as informative for this variable as they are deemed to be for discharge. For this reason, the minimisation of the root mean squared error (RMSE) between simulated and observed temperature was used for optimizing the parameters of the thermal module. Akaike information criterion was also computed, as implemented by Ahmadi-Nedushan et al. (2007), for evapotranspiration on the Miramichi watershed for years with available data. The AIC takes the goodness of fit and the complexity of the model, through the number of parameters, into account.

The parameters were optimized for each specific evapotranspiration and evaporation methods tested. To compare the impact of the parameters and the impact of the method

on the resulting simulations, a permutation of all 11 sets of parameters and 11 methods (the original method implemented in CEQUEAU and the 10 additional methods) was performed. Performance variation of a given method according to the set of parameters used as well as the performance variation of a given set of parameters according to the method was assessed.

Using the meteorological data, the *XAA* and *XIT* parameters are estimated respectively as 0.76 and 15.7 on the Nechako watershed and 0.94 and 27.56 on the Miramichi watershed, with equations 5.25 and 5.26.

5.3.4   Results

5.3.4.1   *Evapotranspiration*

Evapotranspiration measured at Nashwaak Lake using eddy covariance method was plotted against evapotranspiration estimated at the same location (selected CEQUEAU grid cell; Figure 5.25) by the evapotranspiration methods described in section 5.3.2.2. Corresponding performance metrics are listed in Table 5.10. In terms of correlation, indicated by Pearson's correlation coefficient, Kimberly-Penman (r = 0.70), Priestley-Taylor (r = 0.72), Penman-Monteith (r = 0.71) and Morton (r = 0.73) clearly dominate. All other methods returned r < 0.2 with an absolute low of 0.13 by Thornthwaite combined with Guenther et al. wind function. The Penman-Monteith retuned highly biased evapotranspiration values (relative bias = 0.46). Priestly-Taylor and Morton returned the lowest biases, with a relative bias of respectively 0.06 and 0.01. According to both metrics, Priestley-Taylor and Morton are the best performing methods to estimate evapotranspiration. However, when the number of meteorological inputs is taken into account through the AIC, Priestly-Taylor is considered to be a better method. On average, Morton better replicates total annual evapotranspiration (Table 5.10; Mean annual bias = 0.89 mm) followed by Kimberly-Penman (Mean annual bias = -7.81 mm). Penman-Monteith has the largest annual bias (Mean annual bias = 207.15 mm).

Table 5.12: Performance metrics of evapotranspiration methods compared to eddy covariance measurements at Nashwaak Lake (Miramichi watershed)

	RMSE (mm)	Absolute relative bias	r	AIC	Mean annual bias (mm)
Thornthwaite	1.51	0.25	0.19	341	98.81
Kimberly-P.	1.11	0.12	0.70	87	-7.81
Priest.-Taylor (alpha = 0.82)	<u>0.98</u>	0.06	0.72	<u>3</u>	-37.74
McGuinness	1.58	0.29	0.18	370	108.97
Penman-Mont.	1.73	0.46	0.71	356	207.15
Morton (alpha = 0.43)	1.01	<u>0.01</u>	<u>0.73</u>	15	<u>0.89</u>
Benner	1.51	0.25	0.19	341	98.81
Webb and Zhang	1.46	0.21	0.17	325	77.16
Maheu et al.	1.51	0.25	0.19	341	98.81
Guenther et al.	1.33	0.04	0.13	252	-45.65
Jobson	1.51	0.25	0.19	341	98.81
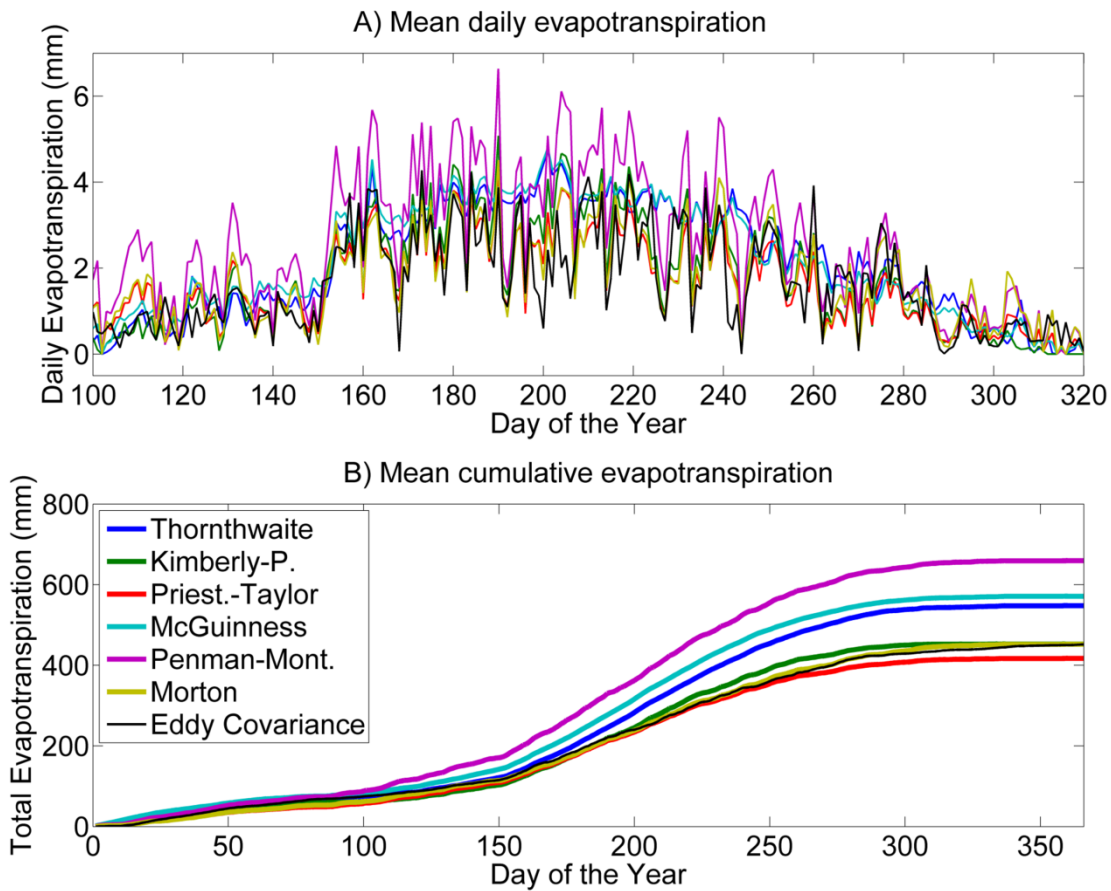
Figure 5.25: A) Mean daily evapotranspiration measured at Nashwaak Lake (2003-2005; Eddy Covariance) and corresponding estimations and B) Cumulative evaporation and corresponding estimation.

Results for daily evapotranspiration estimated using the 11 methods or combination of methods described in section 5.3.2.2 are presented in Figure 5.26. Grey areas are derived from mean and maximum values found in the literature. The minimum values are not displayed because they were not mentioned in the cited literature but are expected to be close to zero mm. The middle horizontal line of the boxes represents the annual mean, while the boundaries of the central box represent the 25th and 75th percentiles, the dashed vertical lines are the maximum and minimum values that are not considered as outliers, and the triangles represent outliers. A Kruskal-Wallis test (Kruskal and Wallis, 1952) was performed to verify if the distributions of ETP values calculated by the different methods have significantly different median. The alternative

hypothesis is that at least one of the ETP methods yields median values that are significantly different than the others. This test was used instead of the parametric ANOVA because all simulated evapotranspiration series did not meet the assumption of normality. This was verified first, using the Kolmogorov-Smirnov normality test (Massey, 1951). A Tukey-Kramer (Tukey, 1949) test was performed *a posteriori* to find which methods were not significantly different. Letters (A-H) were added to Figure 5.26 to display the methods that belong to the same groups.
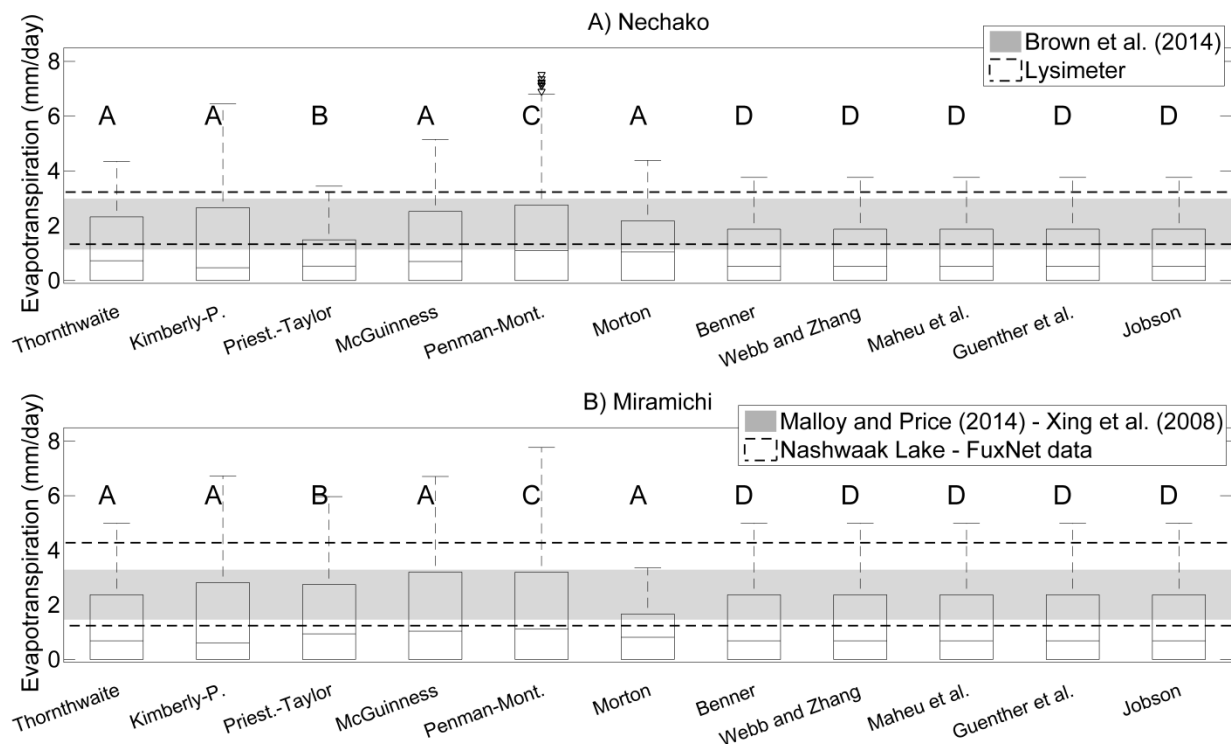
Figure 5.26: Box plots of mean daily evapotranspiration on A) the Nechako watershed and B) the Miramichi watershed during the summer (June-September; 2001-2010). Methods with matching letters (A-D) do not have significantly different median values.

According to our results, the maximum daily evapotranspiration ranges between 3.4 mm/day (Priestley-Taylor) and 7.5 mm/day (Penman-Monteith) on the Nechako and between 3.4 mm/day (Morton) and 7.8 mm/day (Penman-Monteith) on the Miramichi. No significant difference is observed when a mass transfer method is used for open water evaporation when computing overall evapotranspiration on the Miramichi

154

watershed (group A; Figure 5.26-B) compared to the Thornthwaite equation, as well as the Kimberly-Penman equation. Morton's equation returned values significantly different from all other methods. On the Nechako, all mass transfer methods belong to the same group (group D; Figure 5.26 - A) but are significantly different from results yielded by the Thornthwaite equation (group A; Figure 5.26 - A). The Kimberly-Penman, McGuinness and Morton methods belong to the same group (group A). When compared to data published by Brown *et al.* (2014) and the data recorded with the lysimeter (mean and maximum values), all the methods tested on the Nechako watershed overestimate evapotranspiration (Figure 5.26). However, the Priestley-Taylor equation provides results that are less overestimated than all the other equations compared in this study. On both watersheds, the Kimberly-Penman and the Penman-Monteith equations yielded the highest and the more variable evapotranspiration values during the summer. It should be noted that those equations are the only ones among our selection that directly include wind speed and air vapour pressure in their formulation. Wind speed, known to be more spatially variable than other variables such as air temperature and relative humidity (Luo et al., 2008), is a potential source of error in the implementation of these methods.

When compared to evapotranspiration data from the literature and to lysimeter measurements, the most appropriate method on the Nechako watershed is Priestley-Taylor ($\alpha = 0.5$), followed by Thornthwaite's equation coupled with a mass transfer equation (regardless of which wind function is used). On the Miramichi, the best performing method is Morton (as shown using the Nashwaak Lake eddy covariance data). When the interannual ranges of estimated values obtained from Morton and Thornthwaite are plotted on the same graph, the lower values simulated by the Morton equation on the Miramichi watershed become obvious (Figure 5.27 - B). The same pattern is visible on the Nechako for Priestley-Taylor when compared to Thornthwaite's method Figure 5.27 – A).
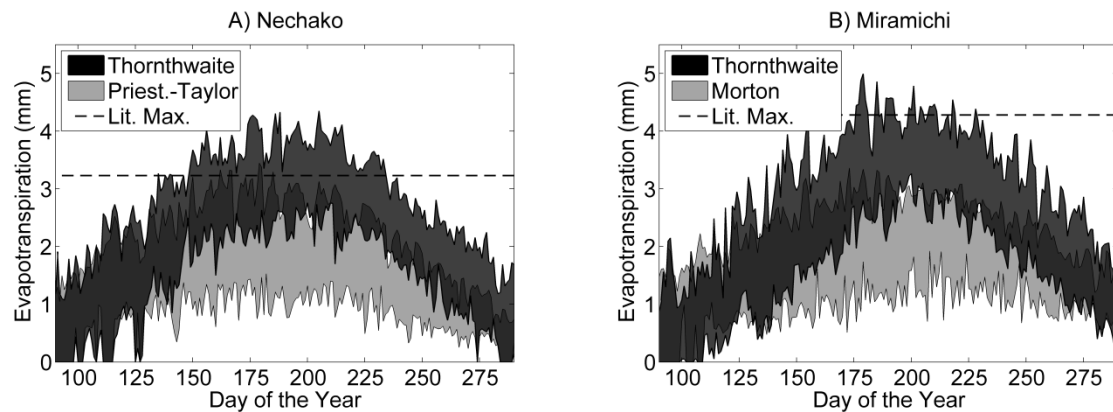
Figure 5.27: Interannual range of evapotranspiration simulated using Priestley-Taylor equation and Morton. equation on A) the Nechako watershed and B) the Miramichi watershed. Lit. Max. is the maximum evapotranspiration retrieved from the literature.

5.3.4.2 *Evaporation*

Box plots were also produced for open water evaporation estimations (Figure 5.28). The grey area represents the mean and maximum values retrieved from the literature. The maximum daily evaporation ranges between 3.4 mm (Priestley-Taylor; Guenther et al.) and 9.8 mm (Benner) on the Nechako watershed and between 1.96 mm (Guenther et al.) and 8.5 mm (Benner) on the Miramichi watershed. All mass transfer equations returned days with no evaporation on both watersheds.
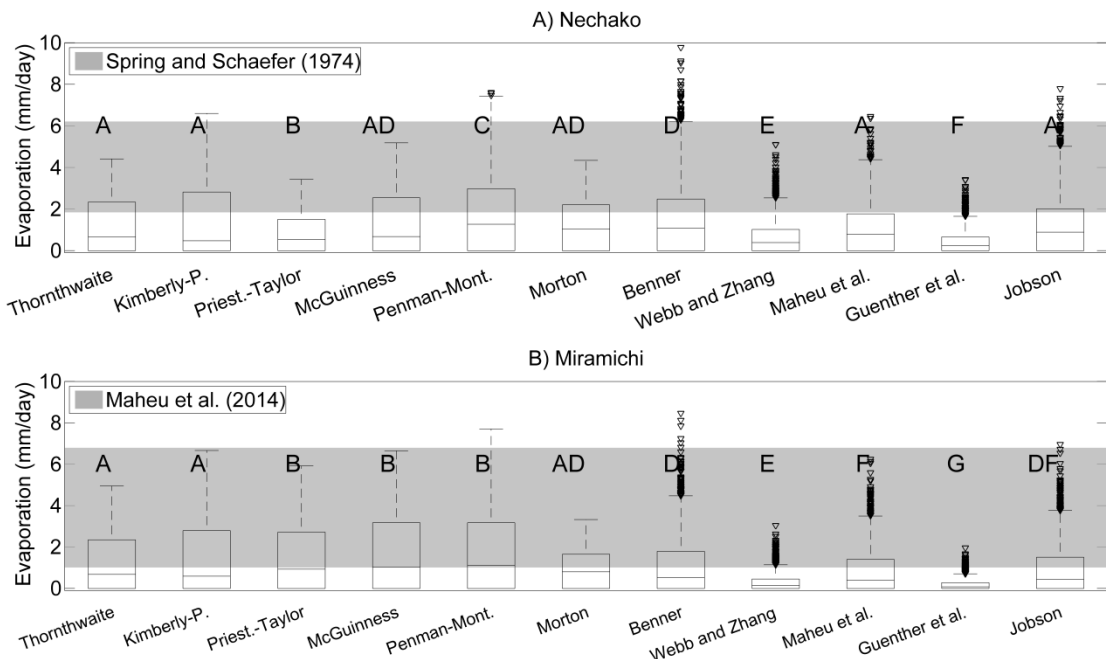
Figure 5.28: Box plots of mean daily river evaporation on A) the Nechako watershed and B) the Miramichi watershed during the summer (June-September). Methods with matching letters (A-G) do not have significantly different median.

More variability among the methods is visible for evaporation (Figure 5.28) compared to evapotranspiration (Figure 5.26). On the Nechako watershed, the methods of Thornthwaite, Kimberly-Penman, McGuinness, Morton, Maheu et al. and Jobson belong to the same group (A). McGuinness, Morton and Benner are also not significantly different (D). More diversity among the methods is visible on the Miramichi watershed. Thornthwaite, Kimberly-Penman and Morton are not significantly different (group A). Priestley-Taylor, McGuinness and Penman-Monteith belongs to the same group (B), Morton, Benner and Jobson form another group (D) and Maheu et al. and Jobson form the last group (F). The other methods are all significantly different from each other.

Evaporation estimations computed with Penman-Monteith's and Benner's equations on both watersheds appear overestimated while the Priestley-Taylor, Webb and Zhang and Guenther et al. equations return large underestimations when compared to data found in the literature (Spring and Schafer, 1974). More overestimation is observed on the

157

Nechako watershed, especially for the Benner wind function, which returned maximum evaporation of 9.8 mm/day. In comparison, the maximum recorded by Spring and Schafer (1974) was only 6.22 mm/day.

When compared to maximum daily evaporation found in the literature, the equations proposed by Maheu et al. and by Kimberly-Penman appear to be the most appropriate. However, when the ranges of values returned by those methods are plotted on the same graph (Figure 5.29), it can be seen that the Kimberly-Penman equation generally estimates higher values than the Maheu et al. equation. On the other hand, the latter is more variable. This leads to large differences in total summer (June to September) evaporation estimations, with mean totals of 391 mm (Kimberly-P.) and 235 mm (Maheu et al.) on the Miramichi watershed and 428 mm (Kimberly-P.) and 260 mm (Maheu et al.) on the Nechako watershed.
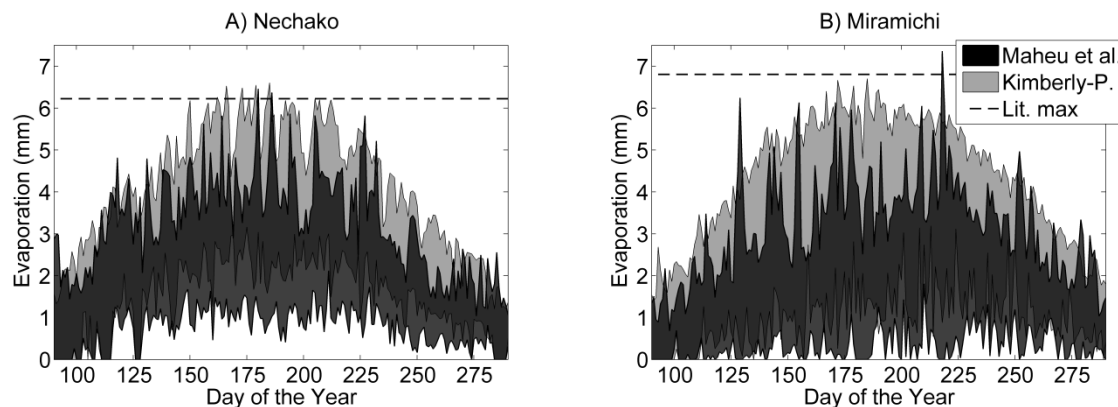
Figure 5.29: Interannual range of evaporation simulated by Kimberly-Penman and Maheu et al. on the A) Nechako and the B) Miramichi watersheds. Lit. Max. is the maximum evaporation retrieved from literature.

The contributions of land evapotranspiration and river evaporation are plotted together in stacked bar plots on Figure 5.30. Regardless of the method used to estimate both processes, the contribution of river evaporation never exceeds 5.9% (Benner on the Nechako watershed) and can be as low as 0.6% (Guenther et al. on the Miramichi). This indicates that river evaporation has little effect on the discharge compared to

evapotranspiration. Therefore, in the context of this study, the method for estimating land evapotranspiration most likely drives the estimation of the total evapotranspiration.
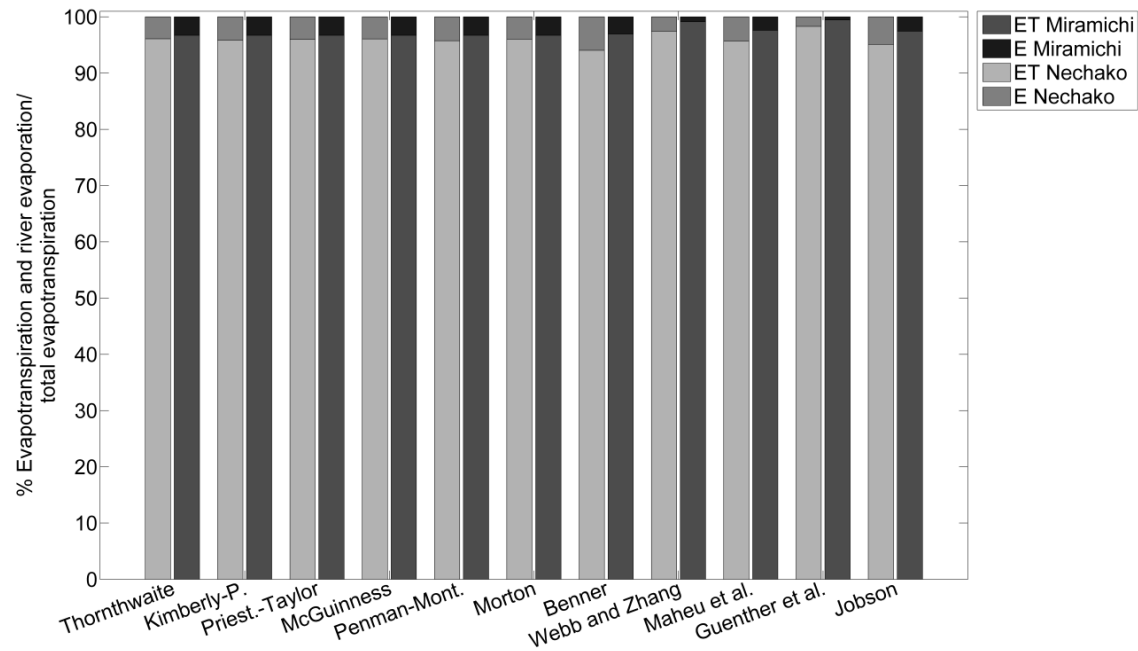
Figure 5.30: Relative contribution of land evapotranspiration (ET) and river evaporation (E) on the Nechako and Miramichi watersheds.

5.3.4.3 Model calibration

On the Nechako watershed, the KGE ranges between 0.75 and 0.91 in calibration (2001-2006) and between 0.80 and 0.87 in validation (2007-2010; Table 5.11). For the Thornthwaite, Priestley-Taylor and all mass transfer equations, the relative bias is lower during the validation period than during the calibration period. On the Miramichi watershed, the KGE ranges between 0.68 and 0.86 in calibration and between 0.64 and 0.80 in validation (Table 5.11). All relative biases decrease in validation, except for the Penman-Monteith, Maheu et al. and Jobson methods. This decrease can be partly explained by the presence of meteorological stations in the calibration dataset that were not in the validation dataset (Nepisiguit Falls [2001-2006], Doaktown [2001-2009]). This affects the precipitation field and consequently the discharge simulations.

Table 5.13: Performance indices obtained in calibration and validation

Method	Nechako at Vanderhoof Calibration KGE	Nechako at Vanderhoof Calibration Rel. Bias	Nechako at Vanderhoof Validation KGE	Nechako at Vanderhoof Validation Rel. Bias	Southwest Miramichi Calibration KGE	Southwest Miramichi Calibration Rel. Bias	Southwest Miramichi Validation KGE	Southwest Miramichi Validation Rel. Bias
Thornthwaite	0.87	0.12	0.86	0.01	0.81	0.06	0.74	0.04
Kimberly-Penman	0.89	0.03	0.82	0.15	0.78	0.09	0.67	0.17
Priestley-Taylor	0.77	0.22	0.84	0.08	0.77	0.08	0.70	0.15
McGuinness and Bordne	0.91	0.06	0.87	0.06	0.71	0.15	0.69	0.01
Penman-Monteith	0.88	0.06	0.80	0.20	0.87	0.04	0.78	0.06
Morton	0.92	0.18	0.81	0.07	0.74	0.19	0.77	0.04
Benner	0.78	0.21	0.83	0.08	0.83	0.06	0.74	0.04
Webb and Zhang	0.75	0.24	0.82	0.09	0.81	0.13	0.79	0.01
Maheu et al.	0.77	0.22	0.83	0.08	0.76	0.04	0.64	0.13
Guenther et al.	0.75	0.25	0.81	0.10	0.77	0.12	0.74	0.00
Jobson	0.78	0.22	0.83	0.08	0.86	0.04	0.80	0.06

With regards to the water temperature simulations on the Nechako watershed, RMSE values ranging between 0.99°C (Morton) and 1.32°C (Webb and Zhang) are obtained using the calibration dataset and RMSE ranging between 1.31°C (Maheu et al.) and 1.51°C (Webb and Zhang) using the validation dataset (Table 5.12). On the Miramichi, RMSE ranges from 0.98°C (Penman-Monteith) to 1.25°C (McGuinness and Bordne) when calibration dataset is used and from 1.52°C (Thornthwaite) to 1.82°C (Maheu et al.) in validation. Larger differences between results obtained in calibration and validation are observed on the Miramichi watershed (mean difference in RMSE Δ= 0.56°C) compared to the Nechako watershed (mean $\Delta = 0.31$°C).

Table 5.14: Root mean squared error (RMSE; °C) calculated for the calibration and validation periods of the thermal model.

	Nechako at Vanderhoof		Southwest Miramichi	
	Calibration (°C)	**Validation (°C)**	**Calibration (°C)**	**Validation (°C)**
Thornthwaite	1.05	1.49	1.17	1.52
Kimberly-Penman	1.06	1.46	1.21	1.56
Priestley-Taylor	1.18	1.40	1.02	1.69
McGuinness and Bordne	1.04	1.47	1.25	1.60
Penman-Monteith	1.00	1.45	0.98	1.77
Morton	0.99	1.47	1.08	1.58
Benner	1.26	1.48	1.09	1.69
Webb and Zhang	1.32	1.51	1.13	1.68
Maheu et al.	1.15	1.31	1.06	1.82
Guenther et al.	1.30	1.47	1.14	1.72
Jobson	1.22	1.48	1.15	1.76

5.3.4.4   Discharge

Discharge simulations are shown in Figure 5.31 (Nechako) and Figure 5.32 (Miramichi). In Figure 5.31 – B, it can be seen that the selected evapotranspiration method has little effect on the simulated discharge at Cheslatta Falls. On average, the difference between the lowest and highest simulated discharge for the same day is 6.8 m^3/s, or 4.9% of the observed discharge at that site. The same value is 28.1 m^3/s (55.3 % of observed discharge) at the Nautley station and 51.5 m^3/s (25.3% of observed discharge) at Vanderhoof. The uncertainty associated with the choice of the evapotranspiration method induces an uncertainty on the discharge simulations.
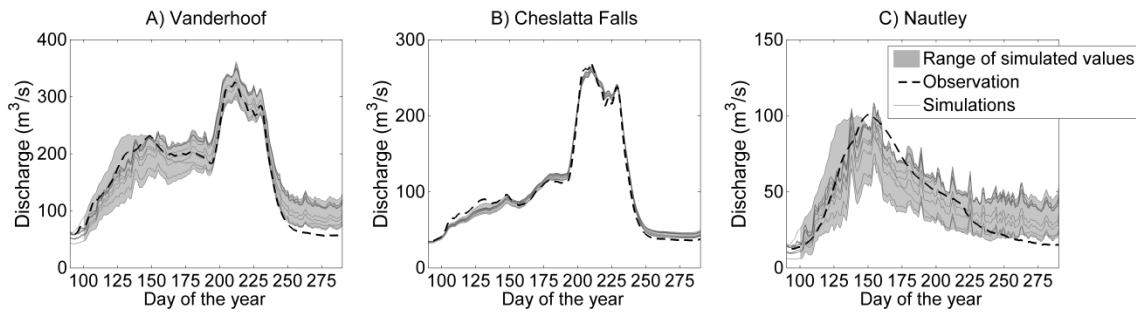
Figure 5.31: Discharge simulations on the Nechako watershed at A) Vanderhoof, B) Cheslatta Falls and C) at the outlet of the Nautley River.

The KGE values and relative biases calculated for all methods are presented in Table 5.13. At Cheslatta Falls, all methods to estimate evapotranspiration perform similarly well, with a KGE > 0.92. At Vanderhoof, Morton's method performs best (KGE = 0.95; rel. bias = 0.08), closely followed by the McGuinness and Bordne method (KGE = 0.92; rel. bias = 0.07). On the Nautley watershed, Morton's equation offers the best results (KGE = 0.75; rel. bias = 0.05) followed by McGuinness and Thornthwaite (KGE = 0.74; rel. bias = 0.12). NSE values were calculated but are not shown because they follow the same trends as the KGE.
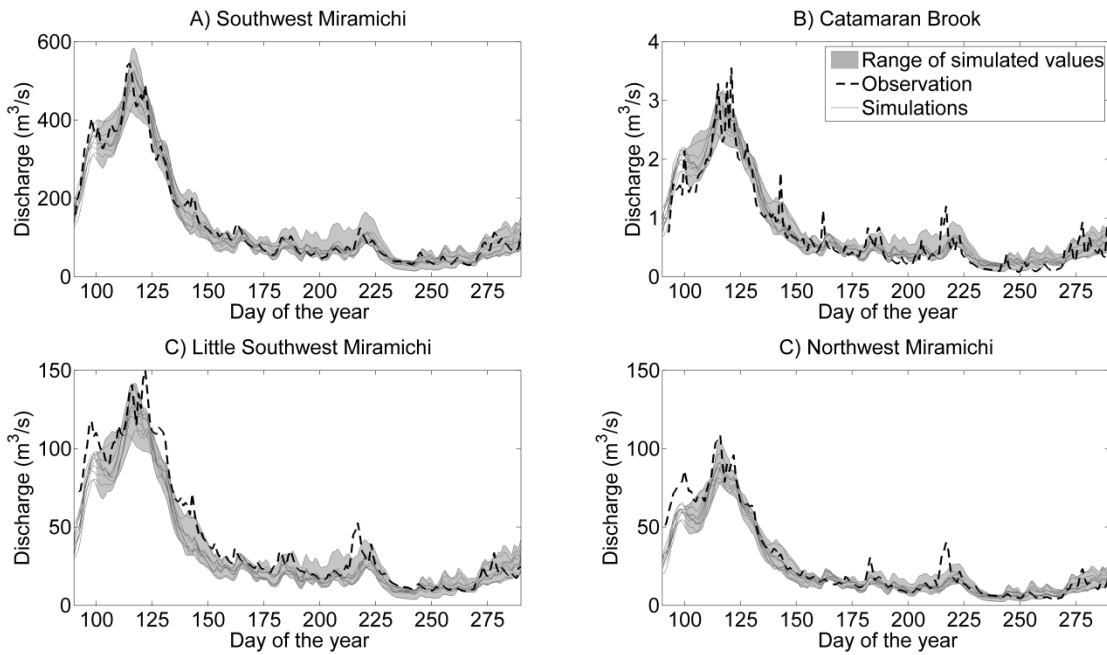
Figure 5.32: Simulated and observed discharge on the A) Southwest Miramichi, B) Catamaran Brook, C) Little Southwest Miramichi and D) Northwest Miramichi.

The hydrographs shown on Figure 5.32 represent the discharge simulated on the Miramichi watershed at four hydrometric stations. Although the model was calibrated to best replicate discharge on the Southwest branch, it adequately reproduces discharge at all four stations. Underestimation of the spring flood is visible on the Little Southwest Miramichi and some summer peaks are not well reproduced at the three uncalibrated stations. The falling limb of the spring flood simulation is shifted early, toward the winter for all evapotranspiration estimation methods. The average difference, derived from interannual means between the highest and lowest simulated discharge is 47.0 m^3/s (81.9% of observed discharge) on the Southwest branch, 11.9 m^3/s (66.5% of observed discharge) on the Little Southwest branch, 0.27 m^3/s (110% of observed discharge) on Catamaran Brook and 7.96 m^3/s (82.2% of observed discharge) on the Northwest branch. According to the KGE, the best performing methods at all four stations are Maheu et al. (KGE = [0.66-0.84]; rel. bias = [0.01-0.11]) and Jobson (KGE = [0.66-0.84]; rel. bias = [0.02-0.11]) closely followed by Penman-Monteith (KGE = [0.65-0.83]; rel.

bias = [0.01-0.10]). The poorest results are returned by the McGuinness and Bordne method (KGE = [0.52-0.71]; rel. bias = [0.01-0.23]).

Table 5.15: KGE and relative bias calculated between observed and simulated discharge for all evapotranspiration estimation methods

KGE

Method	Nechako			Miramichi			
	V	C	N	SW	LSW	CAT	NW
Thornthwaite	0.90	0.94	0.74	0.79	0.59	0.74	0.66
Kimberley-Penman	0.89	<u>0.95</u>	0.51	0.74	0.55	0.65	0.60
Priestley-Taylor	0.81	0.93	0.63	0.80	0.60	0.71	0.66
McGuinness and Bordne	0.92	<u>0.95</u>	0.70	0.71	0.52	0.67	0.63
Penman-Monteith	0.87	<u>0.95</u>	0.48	0.83	0.65	0.73	0.70
Morton	<u>0.96</u>	<u>0.95</u>	<u>0.75</u>	0.80	0.60	<u>0.77</u>	<u>0.73</u>
Benner	0.81	0.93	0.67	0.79	0.59	0.73	0.66
Webb and Zhang	0.79	0.92	0.63	0.80	0.60	0.73	0.69
Maheu et al.	0.81	0.93	0.66	<u>0.84</u>	<u>0.67</u>	0.76	0.71
Guenther et al.	0.78	0.92	0.61	0.76	0.55	0.71	0.65
Jobson	0.81	0.93	0.66	<u>0.84</u>	<u>0.67</u>	0.76	0.71

Relative Bias

Method	Nechako			Miramichi			
	V	C	N	SW	LSW	CAT	NW
Thornthwaite	0.12	0.05	0.12	0.02	0.16	0.05	0.04
Kimberley-Penman	<u>0.02</u>	0.02	0.17	0.06	0.18	0.03	<u>0.01</u>
Priestley-Taylor	0.27	0.08	0.43	<u>0.01</u>	0.14	0.07	0.05
McGuinness and Bordne	0.07	0.04	<u>0.03</u>	0.10	0.23	<u>0.01</u>	0.03
Penman-Monteith	0.08	<u>0.01</u>	0.28	<u>0.01</u>	<u>0.10</u>	0.10	0.07
Morton	0.08	0.04	0.05	0.10	0.24	<u>0.01</u>	0.04
Benner	0.23	0.07	0.36	0.02	0.17	0.05	0.04
Webb and Zhang	0.26	0.08	0.41	0.07	0.20	0.02	<u>0.01</u>
Maheu et al.	0.24	0.07	0.38	<u>0.01</u>	0.11	0.09	0.07
Guenther et al.	0.27	0.08	0.42	0.08	0.21	<u>0.01</u>	<u>0.01</u>
Jobson	0.24	0.07	0.37	0.02	0.11	0.09	0.07

At the Vanderhoof station on the Nechako watershed, all simulated water temperatures stay close to the observations, with some overestimation at the beginning of the summer period (Figure 5.33). The absolute divergence between the methods ranges from 0.53°C (early August) to 1.34°C (early June). The opposite is visible at the Cheslatta falls station where water temperature is underestimated between June and September, with absolute differences ranging from 0.12°C (late July) to 1.22°C (mid-July). On the Nautley subwatershed, water temperature is strongly overestimated by all methods at the beginning of the summer period and underestimated at the end of the summer. Better performances are visible from the end of June through the end of August. Differences between daily values of simulated and observed temperatures, ranged between 0.56°C (late September) and 1.41°C (mid-July).
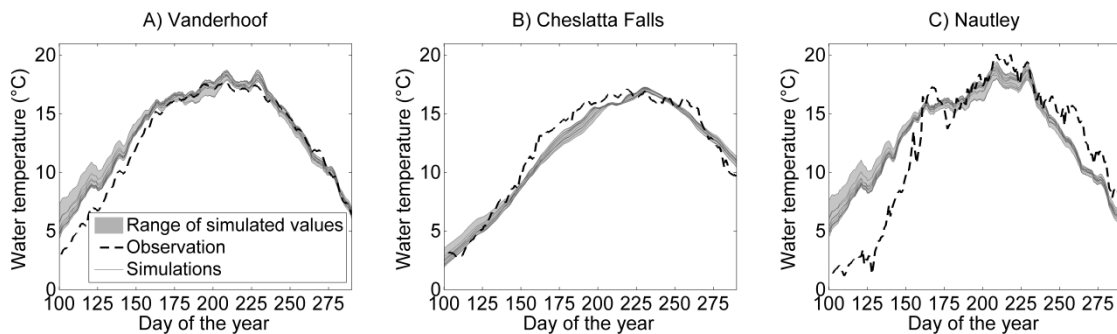
Figure 5.33: Water temperature simulations on the Nechako at A) Vanderhoof, B) Cheslatta Falls and C) at the outlet of the Nautley River.

The lowest RMSE (RMSE = 1.28°C; Table 5.14) at Vanderhoof is obtained when the wind function proposed by Maheu et al. is used. It represents the second best performance at Cheslatta Falls (RMSE = 1.71°C) and the best performance at the Nautley station (RMSE = 2.01°C).

On the Miramichi watershed, a good representation of the seasonal cycle of water temperature is observed on the Southwest branch during the summer (Figure 5.34). On Catamaran Brook and on the Northwest branch, summer temperature is overestimated

166

(mean bias = 1.14°C) by all evaporation estimation methods while it is underestimated (mean bias = -0.93°C) on the Little Southwest branch at the beginning of the summer. The differences in water temperatures returned by the different methods go from 0.47°C (early September) to 1.33°C (late June) on the Southwest branch. This absolute difference goes from 0.48°C (mid-September) to 1.63°C (early August) on the Little Southwest branch. On the Catamaran brook, a wider range of values is observed and the differences go from 0.75°C (mid-July) to 3.5°C (early June). Lastly, on the Northwest branch, the bias on water temperature simulations ranges from 0.63°C (mid-June) to 2.26°C (late August). The best performances are obtained when using the methods of Kimberly-Penman (Southwest branch; RMSE = 1.30°C), Benner (Catamaran Brook; RMSE = 2.36°C and Northwest branch; RMSE = 2.11°C) and Priestley-Taylor (Little-Southwest; RMSE = 1.70°C), as shown in Table 5.14.

Table 5.16: Root mean squared error (RMSE) calculated between observed and simulated water temperatures for all methods (best scores are underlined)

Water Temperature (RMSE ; °C)

	Nechako			Miramichi			
	V	C	N	SW	LSW	CAT	NW
Thornthwaite	1.34	2.18	2.38	1.35	1.97	3.08	1.89
Kimberley-Penman	1.32	1.97	2.19	<u>1.30</u>	1.88	3.16	2.13
Priestley-Taylor	1.34	1.87	2.02	1.39	<u>1.76</u>	2.56	1.89
McGuinness and Bordne	1.33	2.25	2.24	1.43	1.91	3.29	<u>1.75</u>
Penman-Monteith	1.30	2.08	2.19	1.43	1.81	2.79	1.81
Benner	1.42	1.82	2.22	1.42	1.96	<u>2.36</u>	2.09
Morton	<u>1.18</u>	1.87	<u>1.99</u>	1.41	1.86	2.95	1.98
Webb and Zhang	1.46	<u>1.68</u>	2.27	1.42	1.95	3.26	2.33
Maheu et al.	1.28	1.71	2.01	1.46	2.04	3.58	2.85
Guenther et al.	1.43	1.77	2.17	1.45	1.99	3.64	2.43
Jobson	1.41	2.00	2.08	1.45	2.02	3.40	2.83
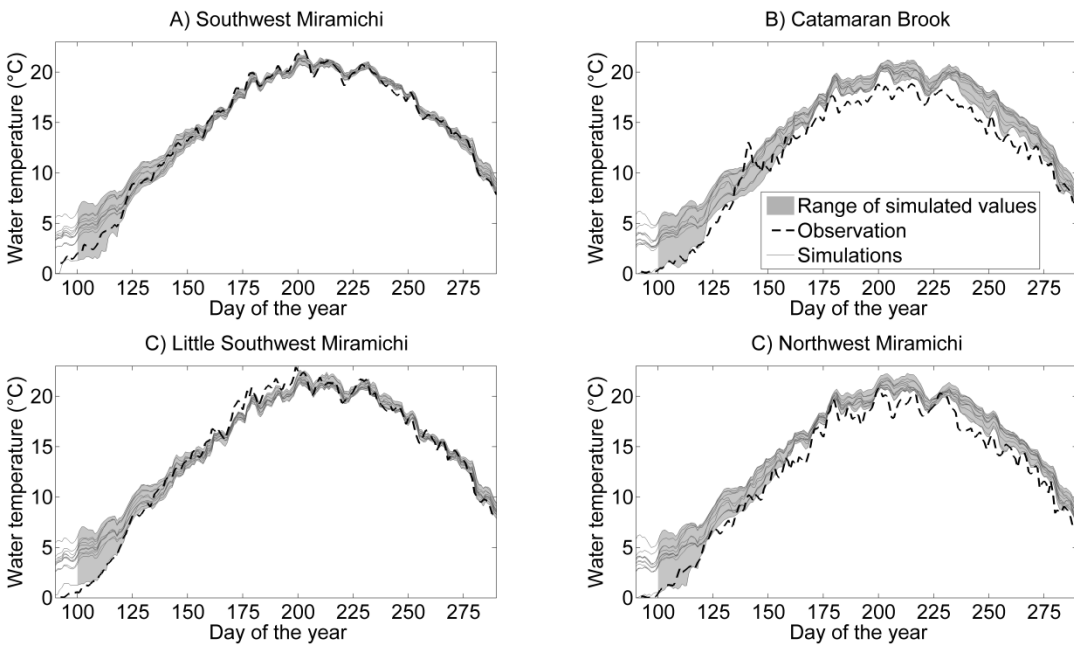
Figure 5.34: Water temperature simulations on the A) Southwest Miramichi, B) Catamaran Brook, C) Little Southwest Miramichi and D) Northwest Miramichi.

Heat lost by evaporation on the Miramichi and the Nechako watersheds was also plotted as a percentage of total heat loss in water courses (Figure 5.35). Similar contributions are returned on both watersheds for the same method. It can be observed that when an evapotranspiration estimation method is used to estimate river evaporation, four out of five models return percentages above 50% on both watersheds. This percentage diminishes below 25% for the methods of Webb and Zhang, and of Guenther et al. The other methods return contributions between 45% and 30%.

On the Miramichi watershed, Maheu et al. (2014) reported percentages of heat lost by evaporation of 42% on the Little Southwest branch and of 34% on Catamaran Brook. This suggests an overestimation of evapotranspiration from all methods apart from Morton's on the Miramichi watershed. It also points towards an important underestimation returned by the methods of Webb and Zhang and of Guenther et al.

According to these results, the estimation methods of Morton, Benner, Maheu et al. and Jobson return the most realistic percentages.
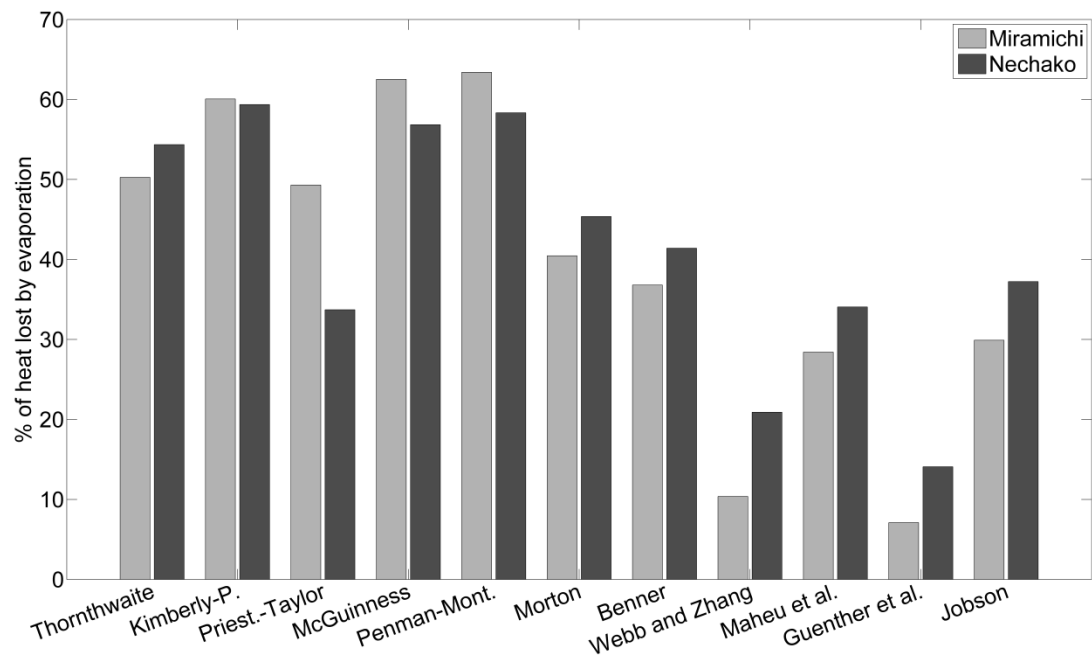
Figure 5.35: Portion of total heat lost by evaporation on the Nechako and Miramichi watersheds.

Lastly, Figure 5.36 presents the performance variations of discharge (A) and water temperature (B) simulations when the different methods are used (x-axis) and when the different sets of parameters are used (y-axis). The difference between the original performance metric when a given method is used with its optimized set of parameters, and its performance when the set of parameters of the best performing method is used is plotted on the x-axis. On the y-axis, the difference between the original performance metric and the performance of the best performing method when all sets of parameters are applied is represented. With regards to the KGE (RMSE), a value located above (below) the horizontal zero line indicates that performances improve when an alternative set of parameters is used. On the x-axis, a value located on the right (left) side of the zero vertical line indicates an improvement of the KGE (RMSE) when an alternative method is used. Best performing sets of parameters and methods were selected based on results presented in Table 5.13 (discharge) and Table 5.14 (temperature).
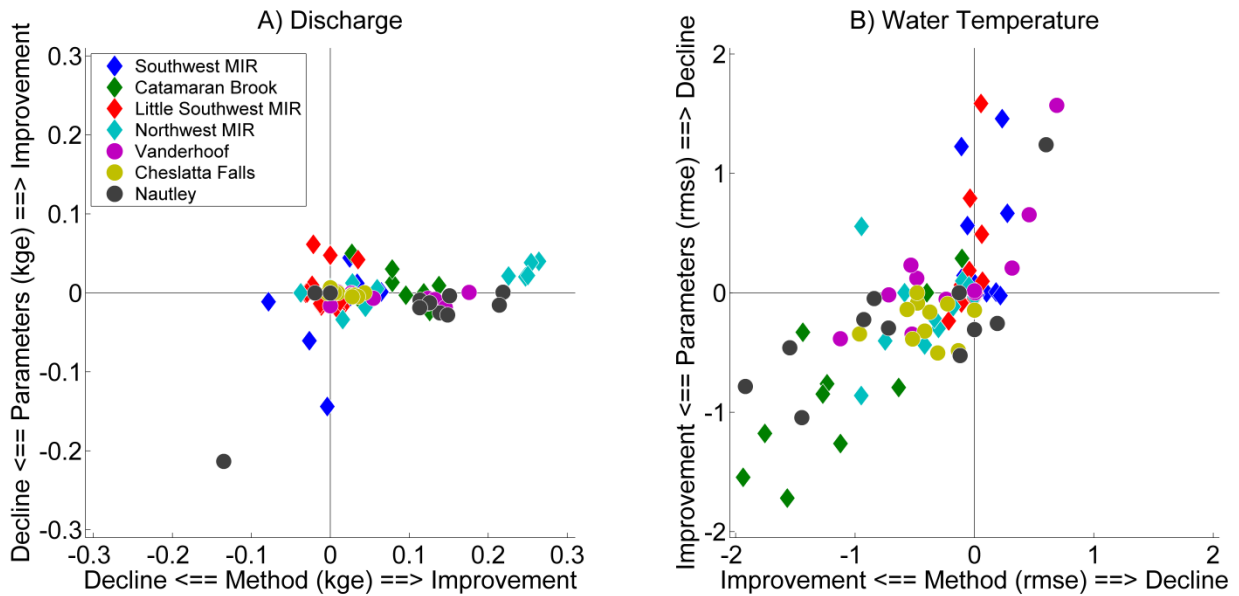
Figure 5.36: Scatter plots of the differences between the original performance metric and the performance metric when best method is used (x-axis) and the differences between the original performance metric and the performance metric when best set of parameters is used (y-axis) for A) discharge and B) water temperature on both watersheds.

Results show that most performance variations in discharge for all Miramichi stations are induced by selected evapotranspiration method (Figure 5.36 – A, diamonds). The Southwest Miramichi (Figure 5.36 – A, blue diamonds) is more sensible to parameter selection compared to all other stations. On the Nechako, all methods at all three sites are marginally impacted by parameters selection (Figure 5.36 – A, circles), while the selection of evapotranspiration method influences discharge simulation performances. More scatter can be observed for water temperature, indicating an influence of both the choice of method and the parameters. On the Miramichi watershed, simulation at both the Southwest and the Little Southwest stations are majorly impacted by the parameters (Figure 5.36 – A, red and blue diamonds). However, simulation performances on Catamaran Brook, and to a lesser extent on the Northwest Miramichi, are influenced by

170

both parameters and evaporation method selection (Figure 5.36 – B, green and cyan diamonds). On the Nechako, simulation performances at Vanderhoof are mostly impacted by parameters selection (Figure 5.36 – B, purple circles) while method selection dominates for Cheslatta Falls and Nautley stations (Figure 5.36 – B, grey and yellow circles).

5.3.5 Discussion and conclusion

In discharge and water temperature modelling, the choices related to model formulations are key elements to a proper representation of the physical processes and in turn impact model performance. Evapotranspiration and open water evaporation equations are often interchanged and used without prior validation. In the absence of field measurements, which is often the case in hydrological studies, it is difficult to validate which method better represents these variables across a watershed. The results presented in this study offer insights on the consequences associated with modelling choices pertaining to evaporative losses.

5.3.5.1   *Evapotranspiration and discharge*

The estimation of evapotranspiration directly influences discharge simulations. They are discussed together here. In terms of evapotranspiration, the Priestley-Taylor and the Morton methods offer the most realistic estimations on both watersheds when compared to literature and observed data. All the other methods overestimate evapotranspiration on both watersheds. The methods that overestimate evapotranspiration the most in this study (Kimberly-Penman and Penman-Monteith) both include wind speed, relative humidity and solar radiation as inputs (Equation 5.32 and Equation 5.34). Data for those two variables can be difficult to acquire, especially if a good spatial resolution is required. The methods of Kimberly-Penman and Penman-Monteith are also the most data intensive formulations, with respectively five and six input variables. Since the methods are used for large areas (watersheds), meteorological inputs are subject to important uncertainties associated with data interpolation and with the heterogeneity of the area (land use, topography, etc.). More

complex methods, such as Penman-Monteith, often considered as a reference, can become less reliable when used on large heterogeneous watersheds.

In terms of discharge, the best performing method at all three validation stations on the Nechako watershed is the Morton method (KGE at Vanderhoof = 0.96; Cheslatta Falls = 0.95; Nautley = 0.75) which estimates realistic evapotranspiration values (Figure 5.26 - A). However, the method is data intensive as it requires six input variables. On the Miramichi watershed, the Maheu et al. and Jobson equations perform best in terms of simulated discharge (in addition to the Thornthwaite method) at the Southwest and Little Southwest branches stations, while Morton's equation offers the best performances at the Catamaran Brook and Northwest stations. The Priestley-Taylor and Morton equations better represent evapotranspiration. Nevertheless, no method clearly dominates the others in terms of estimating discharge in this study. A set of methods requiring a small number of input variables (McGuinness and Bordne, Thornthwaite with or without mass transfer, and Priestley-Taylor) returned better discharge simulations compared to more complex methods (e.g. Penman-Monteith) while being easier to implement because of their less extensive data requirements.

5.3.5.2 *Evaporation and water temperature*

The influence of open water evaporation on water temperature is observed through latent heat loss. In terms of evaporation, the method of Maheu et al. followed by the method of Kimberly-Penman offer the most realistic estimations on the Nechako watershed, and Kimberly-Penman method, followed by Maheu et al. and McGuinness, offer more realistic estimations on the Miramichi watershed. In terms of water temperature simulations for the Nechako watershed, the method of Morton is the best performing method, followed by Maheu et al. For the Miramichi watershed, the method of Kimberly-Penman performs best, followed by the methods of Priestley-Taylor and Thornthwaite. There is thus an apparent adequacy between the ability of these methods to properly estimate evaporation and the performance of the water temperature simulation. This adequacy cannot be extended to evapotranspiration estimation and discharge modelling because the best performing methods were not the same for both

processes. These findings support the hypothesis stated in the introduction of this paper, namely that evapotranspiration and evaporation processes should be estimated separately using distinct equations in discharge and water temperature modelling.

In the present study, the use of a mass transfer equation to estimate open water evaporation does not automatically improve its estimation compared to the use of a method initially designed to estimate evapotranspiration. An important disparity is observed among the evaporation estimates returned by the mass transfer method with different wind functions. This disparity was observed on the same watershed with different wind functions as well as for the same wind function on different watersheds. For instance, the Webb and Zhang equation, widely used in water temperature modelling (e.g. Leach and Moore, 2010), underestimates evaporation on both watersheds used in our study. The mass transfer equation is only influenced by two inputs (wind speed and vapour pressure deficit), by the α_ψ parameter (free convection) and by the β parameter (forced convection). When looking at the distribution of vapour pressure deficit (Figure 5.37 – A), it can be seen that higher values are estimated on the Miramichi watershed compared to the Nechako watershed. This suggests a greater sensibility of the Miramichi watershed to α_ψ values, returning low evaporation values if α_ψ is small. This is coherent with the α_ψ values obtained with Webb and Zhang equation ($\alpha_\psi = 0.12$ mm/kPa/day) and with Guenther et al. equation ($\alpha_\psi = 0$ mm/kPa/day). In contrast, Maheu et al. equation and Jobson equation lead to greater α_ψ values, respectively 3.09 and 3.01 mm/kPa/day. With regards to wind speed (Figure 5.37 – B), a larger range of values and a higher frequency of higher wind velocities are observed on the Nechako watershed. Since β multiplies wind speed, it has a greater influence on the Nechako watershed compared to Miramichi. This suggests that the parameters of the wind function of a mass transfer equation should be carefully evaluated *in situ* before using it to estimate river evaporative fluxes.
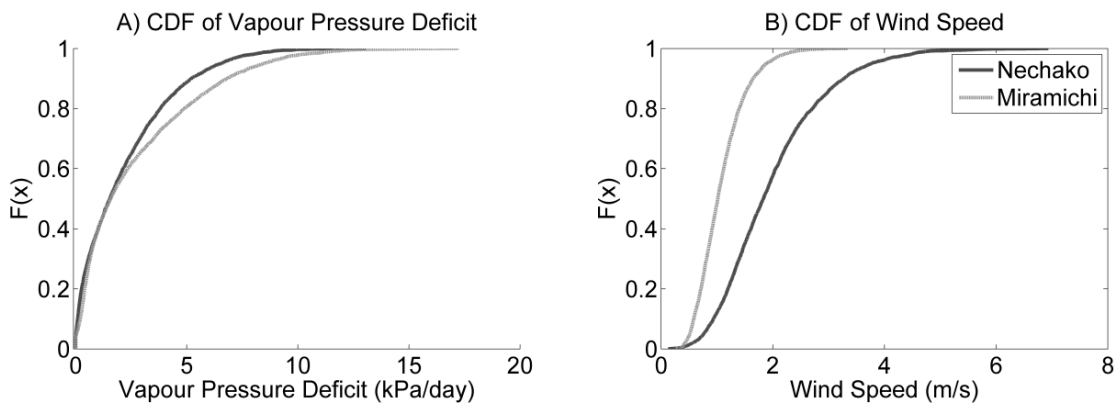
Figure 5.37: Cumulative density function (CDF) of A) vapour pressure deficit and B) wind speed on the Nechako and the Miramichi watersheds (mean value on each watershed).

5.3.5.3 *Final selection of method*

According to the results obtained in the present study, certain considerations should be well weighed when selecting evapotranspiration and evaporation methods for discharge and water temperature modelling. In this case, the best method to estimate evapotranspiration does not necessarily results in the best discharge simulation. This inconsistency highlights a dilemma associated with conceptual models in general. Should the adequacy of discharge (or water temperature) simulations take precedence over the good representation of the processes represented by the model? In the context of the implementation of conceptual models, the question is somewhat moot, as the level of conceptualization determines the extent to which processes can be adequately represented. This dilemma can be resolved by increasing model complexity, which is not always possible or desirable because of the operational context and data availability. However, understanding the limits associated with a more conceptual representation of physical processes and quantifying the related uncertainty are of the utmost importance.

The validity of the adjusted parameters should also be considered when evaluating evapotranspiration estimation methods based on subsequent simulation results. Clark *et al.* (2015) showed the equivalent and sometimes stronger influence of model parameters compared to processes representation on the modelling uncertainty. In this

174

study, the impact of parameters was found more important in thermal simulations than in hydrological simulations. In both cases, the influence of the parameters selection was more important at the calibration stations compared to other validation sites on the watershed.

Many hydrological studies go beyond a good reproduction of observed discharge at a specific site and require a realistic representation of the hydrology of a watershed. Climate projection studies over large watersheds (e.g. Morrison et al. 2002) are good examples of such applications. Thompson *et al.* (2014) showed that evapotranspiration estimation induces uncertainty in future discharge projections using climate change scenarios. In such a context, an evaporative loss estimation method should be selected for its ability to adequately represent the evaporative response to changing atmospheric conditions. Here, results suggest that river evaporation marginally contributes to total water loss through evaporative processes. Efforts should thus first be concentrated on evapotranspiration in studies interested in discharge simulations.

In conclusion, the present study concentrates on various evapotranspiration and open water evaporation estimation methods that were evaluated in a discharge-water temperature modelling cascade. The comparison of five evapotranspiration equations and five mass transfer equations revealed an important uncertainty on both discharge and water temperature carried by the modelling of these processes. Yet, no method clearly outperforms the others for all validation stations. Finally, our results suggest that the method used to estimate evapotranspiration and open water evaporation, especially in a water temperature modelling context, should be established separately and not solely based on the subsequent simulation results. A careful attention should also be given to parameters selection as their uncertainty can dominate over processes uncertainty. Ensemble simulations through multimodule methods would allow the representation of these uncertainty sources into a modelling process (e.g. Clark et al., 2015).

5.3.6 Acknowledgements

6   RÉFÉRENCES BIBLIOGRAPHIQUES

Ahmadi-Nedushan, B., St.-Hilaire, A., Ouarda, T. B. M. J., Bilodeau, L., Robichaud, É., Thiémonge, N., & Bobée, B. (2007). Predicting river water temperatures using stochastic models: Case study of the Moisie River (Québec, Canada). *Hydrological Processes*, *21*(1), 21–34. https://doi.org/10.1002/hyp.6353

Ahrens, C. D. (2015). *Essentials of meteorology : an invitation to the atmosphere* (7th ed.). Stamford, CT Cengage Learning.

Allen, R. G., Walter, I. A., Elliot, R. L., Howell, T. A., Itenfisu, D., Jensen, M. E., & Snyder, R. (2005). *The ASCE standardized reference evapotranspiration equation*. Reston, VA.

Amatya, D. M. M., Skaggs, R. W. W., & Gregory, J. D. (1995). Comparison of Methods for Estimating Ref-Et. *Journal of Irrigation and Drainage Engineering*, *121*(6), 427–435. https://doi.org/10.1061/(ASCE)0733-9437(1995)121:6(427)

Andersson, L. (1992). Improvements of Runoff Models - What Way to Go? *Nordic Hydrology*, *23*(5), 315–315. https://doi.org/10.2166/nh.1992.022

Aronica, G., Hankin, B., & Beven, K. (1998). Uncertainty and equi nality in calibrating distributed roughness coef cients in a ood propagation model with limited data. *Advances in Water Resources*, *22*(4), 349–365.

Bal, G., Rivot, E., Baglinière, J.-L., White, J., & Prévost, E. (2014). A Hierarchical Bayesian Model to Quantify Uncertainty of Stream Water Temperature Forecasts. *PLoS ONE*, *9*(12), e115659. https://doi.org/10.1371/journal.pone.0115659

Barr, A. G., Kite, G. W., Granger, R., & Smith, C. (1997). Evaluating three evapotranspiration methods in the SLURP macroscale hydrological model. *Hydrological Processes*, *11*(13), 1685–1705. https://doi.org/10.1002/(SICI)1099-1085(19971030)11:13<1685::AID-HYP599>3.0.CO;2-T

Bartholomew, A., & Bohnsack, J. A. (2005). A review of catch-and-release angling mortality with implications for no-take reserves. *Reviews in Fish Biology and*

Fisheries. https://doi.org/10.1007/s11160-005-2175-1

Bartholow, J. M. (2003). Modeling uncerainty: Quicksand for water temperature modeling. In *Proceedings of American Institute of Hydrology conference on Hydrologic Extremes: Challenges for Science and Management* (pp. 221–232). Portland, Or.

Benedetti, R. (2010). Scoring Rules for Forecast Verification. *Monthly Weather Review*, *138*(1), 203–211. https://doi.org/10.1175/2009MWR2945.1

Benner, D. A. (1999). *Evaporative Heat Loss of the Upper Middle Fork of the John Day River, Northeastern Oregon*. Oregon State University.

Benyahya, L., Caissie, D., El-Jabi, N., & Satish, M. G. (2010). Comparison of microclimate vs. remote meteorological data and results applied to a water temperature model (Miramichi River, Canada). *Journal of Hydrology*, *380*(3–4), 247–259. https://doi.org/10.1016/j.jhydrol.2009.10.039

Benyahya, L., Caissie, D., St-Hilaire, A., Ouarda, T. B. M. ., & Bobée, B. (2007). A Review of Statistical Water Temperature Models. *Canadian Water Resources Journal*, *32*(3), 179–192. https://doi.org/10.4296/cwrj3203179

Beven, K., & Freer, J. (2001). Equifinality, data assimilation, and uncertainty estimation in mechanistic modelling of complex environmental systems using the GLUE methodology. *Journal of Hydrology*, *249*(1–4), 11–29. https://doi.org/10.1016/S0022-1694(01)00421-8

Beven, K. J. (1993). Prophecy, reality and uncertainty in distributed hydrological modelling., *16*. https://doi.org/10.1016/0309-1708(93)90028-E

Blaney, H. F., & Criddle, W. D. (1950). *Determining water requirements in irrigated areas from climatological and irrigation data. Technical Paper no. 96*. US Department of Agriculture, Soil Conservation Service. Washington, DC.

Boucher, M. A., Anctil, F., Perreault, L., & Tremblay, D. (2011). A comparison between ensemble and deterministic hydrological forecasts in an operational context. *Advances in Geosciences*, *29*, 85–94. https://doi.org/10.5194/adgeo-29-85-2011

Boucher, M. A., Tremblay, D., Delorme, L., Perreault, L., & Anctil, F. (2012). Hydro-economic assessment of hydrological forecasting systems. *Journal of Hydrology*, *416–417*, 133–144. https://doi.org/10.1016/j.jhydrol.2011.11.042

Boudreau, K. (2005). *Nechako Watershed Council Report: Assessment of potential flow regimes for the Nechako watershed*. Vancouver.

Breau, C. (2012). *The use of fish physiology to set water temperature threshold to closure the recreational fishery of Atlantic salmon (Salmo salar) during warm water events*. Moncton.

Breau, C., & Caissie, D. (2013). *Adaptive management strategies to protect salmon (Salmo salar) under environmentally stressful conditions*. Ottawa.

Brier, G. W. (1950). Verification of forecasts expressed in terms of probability. *Monthly Weather Review*, *78*(1), 1–3. https://doi.org/10.1126/science.27.693.594

Bröcker, J., & Smith, L. A. (2007). Increasing the Reliability of Reliability Diagrams. *Weather and Forecasting*, *22*(3), 651–661. https://doi.org/10.1175/WAF993.1

Brown, M. G., Black, T. A., Nesic, Z., Foord, V. N., Spittlehouse, D. L., Fredeen, A. L., Meyer, G. (2014). Evapotranspiration and canopy characteristics of two lodgepole pine stands following mountain pine beetle attack. *Hydrological Processes*, *28*(8), 3326–3340. https://doi.org/10.1002/hyp.9870

Caissie, D. (2006). The thermal regime of rivers: A review. *Freshwater Biology*, *51*(8), 1389–1406. https://doi.org/10.1111/j.1365-2427.2006.01597.x

Caissie, D., & Breau, C. (2013). *Water temperature characteristics within the Miramichi and Restigouche rivers*. Moncton.

Caissie, D., Satish, M. G., & El-Jabi, N. (2005). Predicting river water temperatures using the equilibrium temperature concept with application on Miramichi River catchments (New Brunswick, Canada). *Hydrological Processes*, *19*(11), 2137–2159. https://doi.org/10.1002/hyp.5684

Caissie, D., Satish, M. G., & El-Jabi, N. (2007). Predicting water temperatures using a deterministic model: Application on Miramichi River catchments (New Brunswick,

Canada). *Journal of Hydrology*, *336*(3–4), 303–315. https://doi.org/10.1016/j.jhydrol.2007.01.008

Caissie, D., Thistle, M. E., & Benyahya, L. (2016). River temperature forecasting: case study for Little Southwest Miramichi River (New Brunswick, Canada). *Hydrological Sciences Journal*, *62*(5). https://doi.org/http://dx.doi.org/10.1080/02626667.2016.1261144

Casati, B., Wilson, L. J., Stephenson, D. B., Nurmi, P., Ghelli, A, Pocernich, M., Mason, S. (2008). Forecast verification : current status and future directions. *Meteorological Applications*, *18*(1), 3–18. https://doi.org/10.1002/met

Chen, H., Yang, D., Hong, Y., Gourley, J. J., & Zhang, Y. (2013). Hydrological data assimilation with the Ensemble Square-Root-Filter: Use of streamflow observations to update model states for real-time flash flood forecasting. *Advances in Water Resources*, *59*, 209–220. https://doi.org/10.1016/j.advwatres.2013.06.010

Chen, J., Brissette, F. P., Poulin, A., & Leconte, R. (2011). Overall uncertainty study of the hydrological impacts of climate change for a Canadian watershed. *Water Resources Research*, *47*(12). https://doi.org/10.1029/2011WR010602

Chikita, K. A., Kaminaga, R., Kudo, I., Wada, T., & Kim, Y. (2010). Parameters determining water temperature of a proglacial stream: The Phelan Creek and the Gulkana Glacier, Alaska. *River Research and Applications*, *26*(8), 995–1004. https://doi.org/10.1002/rra.1311

Clark, M. P., Nijssen, B., Lundquist, J. D., Kavetski, D., Rupp, D. E., Woods, R. A, Marks, D. G. (2015). A unified approach for process-based hydrologic modeling: 2. Model implementation and case studies, 1–28. https://doi.org/10.1002/2015WR017198.A

Clark, M. P., Rupp, D. E., Woods, R. A., Zheng, X., Ibbitt, R. P., Slater, A. G., Uddstrom, M. J. (2008). Hydrological data assimilation with the ensemble Kalman filter: Use of streamflow observations to update states in a distributed hydrological model. *Advances in Water Resources*, *31*(10), 1309–1324. https://doi.org/10.1016/j.advwatres.2008.06.005

Clark, M. P., Wilby, R. L., Gutmann, E. D., Vano, J. A., Gangopadhyay, S., Wood, A. W., Brekke, L. D. (2016). Characterizing Uncertainty of the Hydrologic Impacts of Climate Change. *Current Climate Change Reports*, *2*(2), 55–64. https://doi.org/10.1007/s40641-016-0034-x

Cloke, H. L., & Pappenberger, F. (2009). Ensemble flood forecasting: A review. *Journal of Hydrology*, *375*(3–4), 613–626. https://doi.org/10.1016/j.jhydrol.2009.06.005

Cole, J. C., Maloney, K. O., Schmid, M., & McKenna, J. E. (2014). Developing and testing temperature models for regulated systems: A case study on the Upper Delaware River. *Journal of Hydrology*, *519*, 588–598. https://doi.org/10.1016/j.jhydrol.2014.07.058

Crisp, D. T. (1987). Thermal "resetting" of streams by reservoir releases with special reference to effects on salmonid fishes. In J. F. Craig & J. B. Kemper (Eds.), *Regulated Streams: Advances in Ecology* (pp. 163–182). Plenum Press.

Cristea, N. C., Kampf, S. K., & Burges, S. J. (2013). Revised Coefficients for Priestley-Taylor and Makkink-Hansen Equations for Estimating Daily Reference Evapotranspiration. *Journal of Hydrologic Engineering*, *18*(10), 1289–1300. https://doi.org/10.1061/(ASCE)HE.1943-5584.0000679

Daneshkar Arasteh, P., & Tajrishy, M. (2008). Calibrating Priestley- Taylor model to estimate open water evaporation under regional advec- tion using volume balance method—Case study: Chahnimeh Reservoir, Iran. *Journal of Applied Sciences*, *8*, 4097–4104.

Danner, E. M., Melton, F. S., Pike, A., Hashimoto, H., Michaelis, A., Rajagopalan, B., Nemani, R. R. (2012). River temperature forecasting: A coupled-modeling framework for management of river habitat. *IEEE Journal of Selected Topics in Applied Earth Observations and Remote Sensing*, *5*(6), 1752–1760. https://doi.org/10.1109/JSTARS.2012.2229968

Deas, M. L., & Lowney, C. L. (2000). Water Temperature Modeling Review - Central Valley. *Report Sponsored by the Bay Delta Modelling Forum*, (September), 74.

deBruin, H. A. R., & Keijman, J. Q. (1979). The Priestley-Taylor Evaporation Model

Applied to a Large, Shallow Lake in the Netherlands. *Journal of Applied Meteorology*. https://doi.org/10.1175/1520-0450(1979)018<0898:TPTEMA>2.0.CO;2

Dempson, J. B., Furey, G., & Bloom, M. (2002). Effects of catch and release angling on Atlantic salmon, Salmo salar L., of the Conne River, Newfoundland. *Fisheries Management and Ecology*, *9*(3), 139–147. https://doi.org/10.1046/j.1365-2400.2002.00288.x

Department of Fisheries and Oceans Canada [DFO]/Ministère pêches et océans Canada [MPO]. (2012). *Temperature threshold to define management strategies for Atlantic salmon (Salmo salar) fisheries under environmentally stressful conditions*. Moncton.

Doucet, A., Godsill, S., & Andrieu, C. (2000). On sequential Monte Carlo sampling methods for Bayesian filtering. *Statistics and Computing*, *10*(3), 197–208. https://doi.org/10.1023/A:1008935410038

Douglas, D. H., & Peucker, T. K. (2011). Algorithms for the Reduction of the Number of Points Required to Represent a Digitized Line or its Caricature. In *Classics in Cartography: Reflections on Influential Articles from Cartographica* (pp. 15–28). https://doi.org/10.1002/9780470669488.ch2

Duan, Q., Ajami, N. K., Gao, X., & Sorooshian, S. (2007). Multi-model ensemble hydrologic prediction using Bayesian model averaging. *Advances in Water Resources*, *30*(5), 1371–1386. https://doi.org/10.1016/j.advwatres.2006.11.014

Ducharne, A. (2008). Importance of stream temperature to climate change impact on water quality. *Hydrology and Earth System Sciences*, *12*(3), 797–810. https://doi.org/10.5194/hess-12-797-2008

Dugdale, S. J., St-Hilaire, A., & Curry, R. A. (2017). Automating physiography and flow routing inputs to the CEQUEAU hydrological model: sensitivity testing on the St. John River Watershed. *Journal of Hydroinformatics*. https://doi.org/10.2166/hydro.2017.051

Ebert, E., Wilson, L., Weigel, A., Mittermaier, M., Nurmi, P., Gill, P., Watkins, A. (2013).

Progress and challenges in forecast verification. *Meteorological Applications*, *20*(2), 130–139. https://doi.org/10.1002/met.1392

Envirocon Ltd. (1984). *Documentation of the Nechako unsteady state water temperature model*. Vancouver.

Evans, E. C., Mcgregor, Ã. G. R., & Petts, G. E. (1998). River energy budgets with special reference to river bed processes, *595*(April 1997).

Fan, Y. R., Huang, G. H., Baetz, B. W., Li, Y. P., Huang, K., Chen, X., & Gao, M. (2017). Development of integrated approaches for hydrological data assimilation through combination of ensemble Kalman filter and particle filter methods, *550*, 412–426. https://doi.org/10.1016/j.jhydrol.2017.05.010

Fleming, S. W., Bourdin, D. R., Campbell, D., Stull, R. B., & Gardner, T. (2015). Development and Operational Testing of a Super-Ensemble Artificial Intelligence Flood-Forecast Model for a Pacific Northwest River. *JAWRA Journal of the American Water Resources Association*, *51*(2), 502–512. https://doi.org/10.1111/jawr.12259

Massey, F. J. (1951). Kolmogorov-Smirnov Test for Goodness of Fit. *Test*, *46*(253), 68–78. https://doi.org/10.1080/01621459.1951.10500769

Franz, K. J., Hartmann, H. C., Sorooshian, S., & Bales, R. (2003). Verification of National Weather Service Ensemble Streamflow Predictions for Water Supply Forecasting in the Colorado River Basin. *Journal of Hydrometeorology*. https://doi.org/10.1175/1525-7541(2003)004<1105:VONWSE>2.0.CO;2

Fry, F. E. J. (1967). Responses of vertebrate poikilotherms to temperature. In *Thermobiology* (pp. 375–409).

Fry, F. E. J. (1971). The effect of environmental factors on the physiology of fish. *Fish Physiology*, *6*, 1–98. https://doi.org/10.1016/S1546-5098(08)60146-6

Fulford, J. M., & Sturm, T. W. (1984). Evaporation from Flowing Channels. *Journal of Energy Engineering*, *110*(1), 1–9.

Gagnon, N., Beauregard, S., Muncaster, R., Abrahamowicz, M., Lahlou, R., & Lin, H.

(2014). *Improvements to the Global Ensemble Prediction System (GEPS) from version 3.1.0 to version 4.0.0.* Dorval.

Gneiting, T., & Raftery, A. E. (2007). Strictly Proper Scoring Rules, Prediction, and Estimation. *Journal of the American Statistical Association*, *102*(477), 359–378. https://doi.org/10.1198/016214506000001437

Gneiting, T., Raftery, A. E., Westveld, A. H., & Goldman, T. (2005). Calibrated Probabilistic Forecasting Using Ensemble Model Output Statistics and Minimum CRPS Estimation. *Monthly Weather Review*, *133*(5), 1098–1118. https://doi.org/10.1175/MWR2904.1

Goodrich, R. D. (1931). Rapid calculation of reservoir discharge. *Civil Engineering*, *1*, 417–418.

Granger, R. J. (1989). A complementary relationship approach for evaporation from nonsaturated surfaces. *Journal of Hydrology*, *111*(1–4), 31–38. https://doi.org/10.1016/0022-1694(89)90250-3

Gu, R., Montgomery, S., & Austin, T. Al. (1998). Quantifying the effects of stream discharge on summer river temperature. *Hydrological Sciences*, *43*(6), 885–904. https://doi.org/10.1080/02626669809492185

Gudmundsson, L., Bremnes, J. B., Haugen, J. E., & Engen-Skaugen, T. (2012). Technical Note: Downscaling RCM precipitation to the station scale using statistical transformations – A comparison of methods. *Hydrology and Earth System Sciences*, *16*(9), 3383–3390. https://doi.org/10.5194/hess-16-3383-2012

Guenther, S. M., Moore, R. D., & Gomi, T. (2012). Riparian microclimate and evaporation from a coastal headwater stream, and their response to partial-retention forest harvesting. *Agricultural and Forest Meteorology*, *164*, 1–9. https://doi.org/10.1016/j.agrformet.2012.05.003

Guitjens, J. C. (1982). Models of alfalfa yield and evapotranspiration. *American Society of Civil Engineers*, *108 (IR3)*, 212–222.

Gupta, H. V., Kling, H., Yilmaz, K. K., & Martinez, G. F. (2009). Decomposition of the mean squared error and NSE performance criteria: Implications for improving

hydrological modelling. *Journal of Hydrology*, *377*(1–2), 80–91. https://doi.org/10.1016/j.jhydrol.2009.08.003

Hague, M. J., & Patterson, D. A. (2014). Evaluation of Statistical River Temperature Forecast Models for Fisheries Management. *North American Journal of Fisheries Management*, *34*(1), 132–146. https://doi.org/10.1080/02755947.2013.847879

Hamill, T. M. (1997). Reliability Diagrams for Multicategory Probabilistic Forecasts. *Weather and Forecasting*, *12*(4), 736–741. https://doi.org/10.1175/1520-0434(1997)012<0736:RDFMPF>2.0.CO;2

Hamill, T. M., & Colucci, S. J. (1997). Verification of Eta–RSM Short-Range Ensemble Forecasts. *Monthly Weather Review*, *125*(6), 1312–1327. https://doi.org/10.1175/1520-0493(1997)125<1312:VOERSR>2.0.CO;2

Hannah, D. M., Malcolm, I. A., Soulsby, C., & Youngson, A. F. (2004). Heat exchanges and temperatures within a salmon spawning stream in the Cairngorms, Scotland: Seasonal and sub-seasonal dynamics. *River Research and Applications*, *20*(6), 635–652. https://doi.org/10.1002/rra.771

Hannah, D. M., Malcolm, I. A., Soulsby, C., & Youngson, A. F. (2008). A comparison of forest and moorland stream microclimate, heat exchanges and thermal dynamics. *Hydrological Processes*, *22*(7), 919–940. https://doi.org/10.1002/hyp.7003

Hansen, N., & Ostermeier, A. (1996). Adapting Arbitrary Normal Mutation Distributions in Evolution Strategies: The Covariance Matrix Adaptation. *Evolutionary Computation, 1996., Proceedings of IEEE International Conference on*, 312–317. https://doi.org/10.1109/ICEC.1996.542381

Harbeck, G. E. (1962). A practical field technique for measuring reservoir evaporation utilizing mass-transfer theory. *United States Geological Survey Professional Paper*, *272–E*, 101–105.

Hersbach, H. (2000). Decomposition of the Continuous Ranked Probability Score for Ensemble Prediction Systems. *Weather and Forecasting*, *15*(5), 559–570. https://doi.org/10.1175/1520-0434(2000)015<0559:DOTCRP>2.0.CO;2

Hopson, T. H., & Webster, P. J. (2010). A 1–10-Day Ensemble Forecasting Scheme for

the Major River Basins of Bangladesh : Forecasting Severe Floods of 2003 – 07 *. *Journal of Hydrometeorology*, *11*, 618–641. https://doi.org/10.1175/2009JHM1006.1

Hsu, S. A., Meindl, E. A., & Gilhousen, D. B. (1994). Determining the power-law wind-profile exponent under near-neutral stability conditions at sea. *American Meteorological Society*. https://doi.org/10.1175/1520-0450(1994)033<0757:DTPLWP>2.0.CO;2

Huang, B., Langpap, C., & Adams, R. M. (2011). Using instream water temperature forecasts for fisheries management: An application in the pacific northwest. *Journal of the American Water Resources Association*, *47*(4), 861–876. https://doi.org/10.1111/j.1752-1688.2011.00562.x

Huang, B., Langpap, C., & Adams, R. M. (2012). The value of in-stream water temperature forecasts for fisheries management. *Contemporary Economic Policy*, *30*(2), 247–261. https://doi.org/10.1111/j.1465-7287.2011.00261.x

Isabelle, P., & Giroux, B. (2014). *Simplification de l'estimation des taux d'évapotranspiration sur les tourbières boréales par la quasi-neutralité de l'atmosphère.* Institut National de la recherche scientifique.

Jackson, F. L., Fryer, R. J., Hannah, D. M., & Malcolm, I. A. (2017). Can river temperature models be transferred between catchments? *Hydrology and Earth System Sciences Discussions*, (February), 1–28. https://doi.org/10.5194/hess-2017-43

Jensen, M. E., Burman, R. D., & Allen, R. G. (1990). *Evapotranspiration and irrigation water requirements. ASCE Manuals and Reports on Engineering Practice No. 70* (Vol. 1).

Jensen, M. E., & Haise, H. R. . (1963). Estimating evapotranspiration from solar radiation. *American Society of Civil Engineers*, *89 (LR4)*, 15–41.

Jobson, H. E. (1980). Thermal modeling of flow in the San Diego Aqueduct, California, and its relation to evaporation, Issues 1122-1126 (Google eBook). *U.S. Geological Survey*, 24. Retrieved from

http://books.google.com/books?hl=en&lr=&id=H6c_AAAAIAAJ&pgis=1

Kamarianakis, Y., Velasco, S., Cristóbal, E., & Toro, M. (2016). Journal of Hydrology : Regional Studies Water temperature forecasting for Spanish rivers by means of nonlinear mixed models. *Biochemical Pharmacology*, *5*, 226–243. https://doi.org/10.1016/j.ejrh.2016.01.003

Kang, T. H., Kim, Y. O., & Hong, I. P. (2010). Comparison of pre- and post-processors for ensemble streamflow prediction. *Atmospheric Science Letters*, *11*(2), 153–159. https://doi.org/10.1002/asl.276

Katerji, N., & Rana, G. (2011). Crop Reference Evapotranspiration: A Discussion of the Concept, Analysis of the Process and Validation. *Water Resources Management*, *25*(6), 1581–1600. https://doi.org/10.1007/s11269-010-9762-1

Kavetski, D., Kuczera, G., & Franks, S. W. (2006). Bayesian analysis of input uncertainty in hydrological modeling: 2. Application. *Water Resources Research*, *42*(3). https://doi.org/10.1029/2005WR004376

Kelleher, C., McGlynn, B., & Wagener, T. (2016). Characterizing and reducing equifinality by constraining a distributed catchment model with regional signatures, local observations, and process understanding. *Hydrology and Earth System Sciences Discussions*, (December), 1–46. https://doi.org/10.5194/hess-2016-642

Khakbaz, B., Imam, B., Hsu, K. & Sorooshian, S. (2012). From lumped to distributed via semi-distributed: Calibration strategies for semi-distributed hydrologic models. Journal of Hydrologie. 418–419, 61–77. doi:10.1016/j.jhydrol.2009.02.021

Kim, S., Seo, D. J., Riazi, H., & Shin, C. (2014). Improving water quality forecasting via data assimilation - Application of maximum likelihood ensemble filter to HSPF. *Journal of Hydrology*, *519*(PD), 2797–2809. https://doi.org/10.1016/j.jhydrol.2014.09

Kirchner, J. W. (2006). Getting the right answers for the right reasons: Linking measurements, analyses, and models to advance the science of hydrology. *Water Resources Research*, *42*(3), 1–5. https://doi.org/10.1029/2005WR004362

Komma, J., Bloschl, G., & Reszler, C. (2008). Soil moisture updating by Ensemble Kalman Filtering in real-time flood forecasting, 228–242. https://doi.org/10.1016/j.jhydrol.2008.05.020

Kruskal, W. H., & Wallis, W. A. (1952). Use of ranks in one-criterion variance analysis. *Journal of the American Statistical Association*, *47*(260), 583–621. https://doi.org/10.1080/01621459.1952.10483441

Krzysztofowicz, R. (2001). The case for probabilistic forecasting in hydrology. Journal of Hydrology, *249*, 2–9. https://doi.org/10.1016/S0022-1694(01)00420-6

Kustas, W. P., Stannard, D. I., & Allwine, K. J. (1996). Variability in surface energy flux partitioning during Washita '92: Resulting effects on Penman-Monteith and Priestley-Taylor parameters. *Agricultural and Forest Meteorology*, *82*(1–4), 171–193. https://doi.org/10.1016/0168-1923(96)02334-9

Kwak, J., St-Hilaire, A., Chebana, F. (2017). A comparative study for water temperature modelling in a small basin, the Fourchue River, Quebec, Canada. Hydrological Sciences Journal. 62, 64–75. doi:10.1080/02626667.2016.1174334

Laio, F., & Tamea, S. (2007). Verification tools for probabilistic forecasts of continuous hydrological variables. *Hydrology and Earth System Sciences*, *3*(4), 2145–2173. https://doi.org/10.5194/hessd-3-2145-2006

Larabi, S., St-Hilaire, A., Chebana, F., Latraverse, M. (2018). Using Functional Data Analysis to Calibrate and Evaluate Hydrological Model Performance. Journal of Hydrologic Engineering. 23, 04018026. doi:10.1061/(ASCE)HE.1943-5584.0001669

Leach, J. A., & Moore, R. D. (2010). Above-stream microclimate and stream surface energy exchanges in a wildfire-disturbed riparian zone. *Hydrological Processes*, *24*(17), 2369–2381. https://doi.org/10.1002/hyp.7639

Leisenring, M., & Moradkhani, H. (2011). Snow water equivalent prediction using Bayesian data assimilation methods. *Stochastic Environmental Research and Risk Assessment*, *25*(2), 253–270. https://doi.org/10.1007/s00477-010-0445-5

Li, H., Luo, L., Wood, E. F., & Schaake, J. (2009). The role of initial conditions and

forcing uncertainties in seasonal hydrologic forecasting. *Journal of Geophysical Research Atmospheres*, *114*(4). https://doi.org/10.1029/2008JD010969

Linacre, E. T. (1977). A simple formula for estimating evaporation rates in various climate, using temperature data alone. *Agricultural Meteorology*, *18*, 409–424.

Liu, Y., & Gupta, H. V. (2007). Uncertainty in hydrologic modeling: Toward an integrated data assimilation framework. *Water Resources Research*. https://doi.org/10.1029/2006WR005756

Liu, Y., Weerts, A. H., Clark, M., Hendricks Franssen, H. J., Kumar, S., Moradkhani, H., Restrepo, P. (2012). Advancing data assimilation in operational hydrologic forecasting: Progresses, challenges, and emerging opportunities. *Hydrology and Earth System Sciences*, *16*(10), 3863–3887. https://doi.org/10.5194/hess-16-3863-2012

Lohani, A. K., Goel, N. K., & Bhatia, K. K. S. (2014). Improving real time flood forecasting using fuzzy inference system. *Journal of Hydrology*, *509*, 25–41. https://doi.org/10.1016/j.jhydrol.2013.11.021

Lorenz, E. N. (1963). Deterministic Nonperiodic Flow. *Journal of the Atmospheric Sciences*. https://doi.org/10.1175/1520-0469(1963)020<0130:DNF>2.0.CO;2

Luo, W., Taylor, M. C., & Parker, S. R. (2008). A comparison of spatial interpolation methods to estimate continuous wind speed surfaces using irregularly distributed data from England and Wales. *International Journal of Climatology*, *28*(7), 947–959. https://doi.org/10.1002/joc

Lynch, P. (2003). Richardson Extrapolation: the power of the 2-gon. *Mathematics Today*, *39*(5), 159–160. Retrieved from http://mathsci.ucd.ie/~plynch/Publications/2gon.pdf

Macdonald, J. S., Morrison, J., & Patterson, D. A. (2012). The Efficacy of Reservoir Flow Regulation for Cooling Migration Temperature for Sockeye Salmon in the Nechako River Watershed of British Columbia. *North American Journal of Fisheries Management*, *32*(3), 415–427. https://doi.org/10.1080/02755947.2012.675946

Magnusson, J., Jonas, T., & Kirchner, J. W. (2012). Temperature dynamics of a

proglacial stream: Identifying dominant energy balance components and inferring spatially integrated hydraulic geometry. *Water Resources Research*, *48*(6). https://doi.org/10.1029/2011WR011378

Maheu, A., Caissie, D., St-Hilaire, A., & El-Jabi, N. (2014). River evaporation and corresponding heat fluxes in forested catchments. *Hydrological Processes*, *28*(23), 5725–5738. https://doi.org/10.1002/hyp.10071

Maheu, A., Poff, N. L., & St-Hilaire, A. (2016). A Classification of Stream Water Temperature Regimes in the Conterminous USA. *River Research and Applications*, *32*(5), 896–906. https://doi.org/10.1002/rra.2906

Malloy, S., & Price, J. S. (2014). Fen restoration on a bog harvested down to sedge peat: A hydrological assessment. *Ecological Engineering*, *64*, 151–160. https://doi.org/10.1016/j.ecoleng.2013.12.015

Mamono, A. (2010). *Mise À Jour des Variables d'État du Modèle Hydrologique Hydrotel en Fonction des Débits Mesurés.* Mémoire. Montréal (Québec, Canada), Université du Québec à Montréal, Maîtrise en sciences de la Terre.

Martins, E. G., Hinch, S. G., Patterson, D. A., Hague, M. J., Cooke, S. J., Miller, K. M., Farrell, A. P. (2012). High river temperature reduces survival of sockeye salmon (*Oncorhynchus nerka*) approaching spawning grounds and exacerbates female mortality. *Canadian Journal of Fisheries and Aquatic Sciences*, *69*(2), 330–342. https://doi.org/10.1139/F2011-154

Matheson, J. E., & Winkler, R. L. (1976). Scoring Rules for Continuous Probability Distributions. *Management Science*, *22*(10), 1087–1096. https://doi.org/10.1287/mnsc.22.10.1087

Matte, S., Boucher, M. A., Boucher, V., & Fortier Filion, T. C. (2017). Moving beyond the cost-loss ratio: Economic assessment of streamflow forecasts for a risk-Averse decision maker. *Hydrology and Earth System Sciences*, *21*(6), 2967–2986. https://doi.org/10.5194/hess-21-2967-2017

McCullough, D. (2010). Are coldwater fish populations of the United States actually being protected by temperature standards? *Freshwater Reviews*, *3*(2), 147–199.

https://doi.org/10.1608/FRJ-3.2.4

McCullough, D. A., Spalding, S., Sturdevant, D., & Hicks, M. (2001). Summary of Technical Literature Examining the Physiological Effects of Temperature on Salmonids. *US Environmental Protection Agency*, (May), 1–119.

McGuinness, J. L., & Bordne, E. F. (1972). A comparison of lysimeter-derived potential evapotranspiration with computed values. *Arsusda*, *Technical*(1452), 80. Retrieved from http://books.google.se/books?id=oqYoAAAAYAAJ

McMahon, T. A., Peel, M. C., Lowe, L., Srikanthan, R., & McVicar, T. R. (2013). Estimating actual, potential, reference crop and pan evaporation using standard meteorological data: A pragmatic synthesis. *Hydrology and Earth System Sciences*, *17*(4), 1331–1363. https://doi.org/10.5194/hess-17-1331-2013

McMillan, H., Jackson, B., Clark, M., Kavetski, D., & Woods, R. (2011). Rainfall uncertainty in hydrological modelling: An evaluation of multiplicative error models. *Journal of Hydrology*, *400*(1–2), 83–94. https://doi.org/10.1016/j.jhydrol.2011.01.026

Mestekemper, T., Windmann, M., & Kauermann, G. (2010). Functional hourly forecasting of water temperature. *International Journal of Forecasting*, *26*(4), 684–699. https://doi.org/10.1016/j.ijforecast.2009.10.010

Mohan, S. (1991). Intercomparison of evapotranspiration estimates. *Hydrological Sciences Journal*, *36*(5), 447–460. https://doi.org/10.1080/02626669109492530

Mohseni, O., Stefan, H. G., & Erickson, T. R. (1998). A nonlinear regression model for weekly stream temperatures. *Water Resources Research*, *34*(10), 2685. https://doi.org/10.1029/98WR01877

Molteni, F., Buizza, R., Palmer, T. N., & Petroliagis, T. (1996). The ECMWF Ensemble Prediction System: Methodology and validation. *Quarterly Journal of the Royal Meteorological Society*, *122*(529), 73–119. https://doi.org/10.1002/qj.49712252905

Montanari, A., & Di Baldassarre, G. (2013). Data errors and hydrological modelling: The role of model structure to propagate observation uncertainty. *Advances in Water Resources*, *51*, 498–504. https://doi.org/10.1016/j.advwatres.2012.09.007

Monteith, J. L. (1965). Evaporation and environment. *Symposia of the Society for Experimental Biology*, *19*, 205–234. https://doi.org/10.1613/jair.301

Moradkhani, H., Dechant, C. M., & Sorooshian, S. (2012). Evolution of ensemble data assimilation for uncertainty quantification using the particle filter-Markov chain Monte Carlo method. *Water Resources Research*, *48*(12). https://doi.org/10.1029/2012WR012144

Moradkhani, H., Hsu, K.-L., Gupta, H., & Sorooshian, S. (2005). Uncertainty assessment of hydrologic model states and parameters: Sequential data assimilation using the particle filter. *Water Resources Research*, *41*(5). https://doi.org/10.1029/2004WR003604

Morin, G., & Couillard, D. (1990). Predicting river temperatures with a hydrological model. In *Encyclopedia of Fluid Mechanics* (pp. 171–209). Hudson, Texas: Gulf Publishing Compagny.

Morin, G., & Paquet, P. (1995). *Le modèle de simulation de quantité et de qualité CEQUEAU, guide de l'utilisateur. Research Report No. 435*. Quebec City.

Morrison, J., & Foreman, M. G. . (2005). Forecasting Fraser River flows and temperatures during upstream salmon migration. *Journal of Environmental Engineering and Science*, *4*(2), 101–111. https://doi.org/10.1139/s04-046

Morton, F. I. (1983). Operational estimates of areal evapotranspiration and their significance to the science and practice of hydrology. *Journal of Hydrology*, *66*(1–4), 1–76. https://doi.org/10.1016/0022-1694(83)90177-4

Nash, J. E., & Sutcliffe, J. V. (1970). River flow forecasting through conceptual models part I - A discussion of principles. *Journal of Hydrology*, *10*(3), 282–290. https://doi.org/10.1016/0022-1694(70)90255-6

Nechako Fisheries Conservation Program technical data review 1988-2002. (2005). Retrieved from http://www.nfcp.org/Tech_Data_Review/NFCP-Summary.pdf

Nester, T., Komma, J., & Blöschl, G. (2016). Real time flood forecasting in the Upper Danube basin. *Journal of Hydrology and Hydromechanics*, *64*(4), 404–414. https://doi.org/10.1515/johh-2016-0033

Neumann, D. W., Zagona, E. A., & Rajagopalan, B. (2006). A decision support system to manage summer stream temperatures. *Journal of the American Water Resources Association*, *42*, 1275–1284.

Noh, S. J., Tachikawa, Y., Shiiba, M., & Kim, S. (2011). Applying sequential Monte Carlo methods into a distributed hydrologic model : lagged particle filtering approach with regularization, (2001), 3237–3251. https://doi.org/10.5194/hess-15-3237-2011

Olden, J. D., & Naiman, R. J. (2010). Incorporating thermal regimes into environmental flows assessments: Modifying dam operations to restore freshwater ecosystem integrity. *Freshwater Biology*, *55*(1), 86–107. https://doi.org/10.1111/j.1365-2427.2009.02179.x

Orrell, D., Smith, L., Barkmeijer, J., & Palmer, T. N. (2001). Model error in weather forecasting. *Nonlinear Processes in Geophysics*, *8*(6), 357–371. https://doi.org/10.5194/npg-8-357-2001

Oudin, L., Michel, C., & Anctil, F. (2005). Which potential evapotranspiration input for a lumped rainfall-runoff model? *Journal of Hydrology*, *303*(1–4), 275–289. https://doi.org/10.1016/j.jhydrol.2004.08.025

Ouellet-Proulx, S., St-Hilaire, A., & Boucher, M.-A. (2017). Water Temperature Ensemble Forecasts: Implementation Using the CEQUEAU Model on Two Contrasted River Systems. *Water*, *9*(7), 457. https://doi.org/10.3390/w9070457

Ouellet, V., Pierron, F., Mingelbier, M., Fournier, M., Marlène, F., & Couture, P. (2013). Thermal Stress Effects on Gene Expression and Phagocytosis in the Common Carp (Cyprinus Carpio): a Better Understanding of the Summer 2001 St. Lawrence River Fish Kill. *The Open Fish Science Journal*, *6*, 99–106. https://doi.org/10.2174/1874401X01306010099.

Papadakis, N., Memin, E., Cuzol, A., & Gengembre, N. (2010). Data assimilation with the weighted ensemble Kalman filter. *Tellus, Series A: Dynamic Meteorology and Oceanography*, *62*(5), 673–697. https://doi.org/10.1111/j.1600-0870.2010.00461.x

Park, Y. Y., Buizza, R., & Leutbecher, M. (2008). TIGGE: Preliminary results on

comparing and combining ensembles. *Quarterly Journal of the Royal Meteorological Society*, *134*(637), 2029–2050. https://doi.org/10.1002/qj.334

Parmele, L. H. (1972). Errors in output of hydrologic models due to errors in input potential evapotranspiration. *Water Resources Research*, *3*(2), 348–359.

Pathiraja, S., Marshall, L., Sharma, A., & Moradkhani, H. (2016). Advances in Water Resources Detecting non-stationary hydrologic model parameters in a paired catchment system using data assimilation. *Advances in Water Resources*, *94*, 103–119. https://doi.org/10.1016/j.advwatres.2016.04.021

Penman, H. L. (1948). Natural Evporation from Open Water, Bare Soil and Grass. *The Royal Society*, *193*(1032), 120–145. https://doi.org/10.1098/rspa.1948.0037

Pike, A., Danner, E., Boughton, D., Melton, F., Nemani, R., Rajagopalan, B., & Lindley, S. (2013). Forecasting river temperatures in real time using a stochastic dynamics approach. *Water Resources Research*, *49*(9), 5168–5182. https://doi.org/10.1002/wrcr.20389

Plaza, D. A., Keyser, R. De, Lannoy, G. J. M. De, Giustarini, L., Matgen, P., & Pauwels, V. R. N. (2012). The importance of parameter resampling for soil moisture data assimilation into hydrologic models using the particle filter, 375–390. https://doi.org/10.5194/hess-16-375-2012

Poff, N. L., & Hart, D. D. (2002). How Dams Vary and Why It Matters for the Emerging Science of Dam Removal: An ecological classification of dams is needed to characterize how the tremendous. *BioScience*, *52*, 659. https://doi.org/10.1641/0006-3568(2002)052[0659:HDVAWI]2.0.CO;2

Poole, G. C., & Berman, C. H. (2001). An ecological perspective on in-stream temperature: Natural heat dynamics and mechanisms of human-caused thermal degradation. *Environmental Management*. https://doi.org/10.1007/s002670010188

Priestley, C. H. B., & Taylor, R. J. (1972). On the Assessment of Surface Heat Flux and Evaporation Using Large-Scale Parameters. *Monthly Weather Review*, *100*(2), 81–92. https://doi.org/10.1175/1520-0493(1972)100<0081:OTAOSH>2.3.CO;2

Raftery, A. E., Gneiting, T., Balabdaoui, F., & Polakowski, M. (2005). Using Bayesian

Model Averaging to Calibrate Forecast Ensembles. *Monthly Weather Review*, *133*(5), 1155–1174. https://doi.org/10.1175/MWR2906.1

Reichle, R. H. (2008). Data assimilation methods in the Earth sciences. *Advances in Water Resources*, *31*(11), 1411–1418. https://doi.org/10.1016/j.advwatres.2008.01.001

Renner, M., Werner, M. G. F., Rademacher, S., & Sprokkereef, E. (2009). Verification of ensemble flow forecasts for the River Rhine. *Journal of Hydrology*, *376*(3–4), 463–475. https://doi.org/10.1016/j.jhydrol.2009.07.059

Richardson, D. S. (2000). Skill and relative economic value of the ECMWF ensemble prediction system. *Quarterly Journal of the Royal Meteorological Society*, *126*(563), 649–667. https://doi.org/10.1002/qj.49712656313

Rodriguez-Rincon, J. P., Pedrozo-Acuna, A., & Brena-Naranjo, J. A. (2015). Propagation of hydro-meteorological uncertainty in a model cascade framework to inundation prediction. *Hydrology and Earth System Sciences*, *19*(7), 2981–2998. https://doi.org/10.5194/hess-19-2981-2015

Rosenberry, D. O., Winter, T. C., Buso, D. C., & Likens, G. E. (2007). Comparison of 15 evaporation methods applied to a small mountain lake in the northeastern USA. *Journal of Hydrology*, *340*(3–4), 149–166. https://doi.org/10.1016/j.jhydrol.2007.03.018

Roulin, E. (2007). Skill and relative economic value of medium-range hydrological ensemble predictions. *Hydrology and Earth System Sciences*, *11*(2), 725–737. https://doi.org/10.5194/hess-11-725-2007

Roulin, E., & Vannitsem, S. (2015). Post-processing of medium-range probabilistic hydrological forecasting: Impact of forcing, initial conditions and model errors. *Hydrological Processes*, *29*(6), 1434–1449. https://doi.org/10.1002/hyp.10259

Sahoo, G. B., Schladow, S. G., & Reuter, J. E. (2009). Forecasting stream water temperature using regression analysis , artificial neural network , and chaotic non-linear dynamic models. *Journal of Hydrology*, *378*(3–4), 325–342. https://doi.org/10.1016/j.jhydrol.2009.09.037

Sakov, P., & Oke, P. R. (2008). A deterministic formulation of the ensemble Kalman filter: An alternative to ensemble square root filters. *Tellus, Series A: Dynamic Meteorology and Oceanography*, *60 A*(2), 361–371. https://doi.org/10.1111/j.1600-0870.2007.00299.x

Salamon, P., & Feyen, L. (2009). Assessing parameter, precipitation, and predictive uncertainty in a distributed hydrological model using sequential data assimilation with the particle filter. *Journal of Hydrology*, *376*(3–4), 428–442. https://doi.org/10.1016/j.jhydrol.2009.07.051

Salamon, P., & Feyen, L. (2010). Disentangling uncertainties in distributed hydrological modeling using multiplicative error models and sequential data assimilation. *Water Resources Research*, *46*(12). https://doi.org/10.1029/2009WR009022

Savenije, H. H. G. (2004). The importance of interception and why we should delete the term evapotranspiration from our vocabulary. *Hydrological Processes*, *18*(8), 1507–1511. https://doi.org/10.1002/hyp.5563

Savenije, H. H. G. (2009). The art of hydrology. *Hydrology and Earth System Sciences*, 157–161.

Schaake, J. C., Hamill, T. M., Buizza, R., & Clark, M. (2007). HEPEX: The hydrological ensemble prediction experiment. *Bulletin of the American Meteorological Society*, *88*(10), 1541–1547. https://doi.org/10.1175/BAMS-88-10-1541

Seiller, G., Anctil, F., & Perrin, C. (2012). Multimodel evaluation of twenty lumped hydrological models under contrasted climate conditions. *Hydrology and Earth System Sciences*, *16*(4), 1171–1189. https://doi.org/10.5194/hess-16-1171-2012

Seo, D.-J., Koren, V., & Cajina, N. (2003). Real-Time Variational Assimilation of Hydrologic and Hydrometeorological Data into Operational Hydrologic Forecasting. *Journal of Hydrometeorology*, *4*(3), 627–641. https://doi.org/10.1175/1525-7541(2003)004<0627:RVAOHA>2.0.CO;2

Seo, D. J., Cajina, L., Corby, R., & Howieson, T. (2009). Automatic state updating for operational streamflow forecasting via variational data assimilation. *Journal of Hydrology, 367*(3–4), 255–275. https://doi.org/10.1016/j.jhydrol.2009.01.019

Shen, Z., & Tang, Y. (2014). Amodified ensemble Kalman particle filter for non-Gaussian systems with nonlinearmeasurement functions. *Journal of Advances in Modeling Earth Systems*, *7*, 50–66. https://doi.org/10.1002/2014MS000373.

Singh, V. P., & Xu, C.-Y. (1997). Evaluation and Generalization of 13 Mass-Transfer Equations for Determining Free Water Evaporation. *Hydrological Processes*, *11*(January 1996), 311–323. https://doi.org/10.1002/(SICI)1099-1085(19970315)11:3<311::AID-HYP446>3.3.CO;2-P

Sinokrot, B. A., & Stefan, H. G. (1993). Stream temperature dynamics: measurements and modeling. *Water Resources Research*. https://doi.org/10.1029/93WR00540

Spittlehouse, D. L. (1989). Estimating evapotranspiration from land surfaces in British Columbia. In *Estimation of Areal Evapotranspiration* (pp. 245–253). IAHS Publication.

Spring, K., & Schaefer, D. G. (1974). *Mass transfer evaporation estimates for Babine Lake, British Columbia*. Downsview, ON.

St-Hilaire, A., Boucher, M.-A., Chebana, F., Ouellet-Proulx, S., Zhou, Q.-X., Larabi, S., & Dugdale, S. (2015). Breathing a new life to an older model: the CEQUEAU tool for flow and water temperature simulations and forecasting. In *Canadian Society of Civil Engineering Conference Paper: L'eau pour le développement durable : adaptation aux changements du climat et de l'environnement*. Montreal.

St-Hilaire, A., Morin, G., El-Jabi, N., & Caissie, D. (2000). Water temperature modelling in a small forested stream: implication of forest canopy and soil temperature. *Canadian Journal of Civil Engineering*, *27*(6), 1095–1108. https://doi.org/10.1139/l00-021

Stanski, H., Wilson, L., & Burrows, W. (1989). *Survey of common verification methods in meteorology*. *Vasa*. Retrieved from http://medcontent.metapress.com/index/A65RM03P4874243N.pdf%5Cnhttp://www.eumetcal.org/resources/ukmeteocal/verificationSAV/www/english/msg/library/SWB_Chapter1.pdf

Steel, E. A., Tillotson, A., Larsen, D. A., Fullerton, A. H., Denton, K. P., & Beckman, B.

R. (2012). Beyond the mean: The role of variability in predicting ecological effects of stream temperature on salmon. *Ecosphere*, *3*(11), 104. https://doi.org/10.1890/ES12-00255.1

Stephens, E., & Cloke, H. (2014). Improving flood forecasts for better flood preparedness in the UK (and beyond). *Geographical Journal*, *180*(4), 310–316. https://doi.org/10.1111/geoj.12103

Sullivan, K., Martin, D. J., Cardwell, R. D., Toll, J. E., & Steven, D. (2000). *An analysis of the effects of temperature on salmonids of the Pacific Northwest with implications for selecting temperature criteria*.

Sumner, D. M., & Jacobs, J. M. (2005). Utility of Penman-Monteith, Priestley-Taylor, reference evapotranspiration, and pan evaporation methods to estimate pasture evapotranspiration. *Journal of Hydrology*, *308*(1–4), 81–104. https://doi.org/10.1016/j.jhydrol.2004.10.023

Tait, A., & Liley, B. (2009). Interpolation of daily solar radiation for New Zealand using a satellite data-derived cloud cover surface. *Weather and Climate*, *29*, 70–88.

Talagrand, O., Vautard, R., & Strauss, B. (1997). Evaluation of Probabilistic Prediction Systems. In *Workshop on Predictability* (p. 1:25). ECMWF.

Tetens, O. (1930). Uber einige meteorologische. *Begriffe, Zeitschrift Fur Geophysik*, (6), 297–309.

Thiboult, A., Anctil, F., & Boucher, M. A. (2016). Accounting for three sources of uncertainty in ensemble hydrological forecasting. *Hydrology and Earth System Sciences*, *20*(5), 1809–1825. https://doi.org/10.5194/hess-20-1809-2016

Thielen, J., Bartholmes, J., Ramos, M.-H., & de Roo, A. (2009). The European Flood Alert System – Part 1: Concept and development. *Hydrology and Earth System Sciences*, *13*(2), 125–140. https://doi.org/10.5194/hess-13-125-2009

Thirel, G., Martin, E., Mahfouf, J. F., Massart, S., Ricci, S., Regimbeau, F., & Habets, F. (2010). A past discharge assimilation system for ensemble streamflow forecasts over France - Part 2: Impact on the ensemble streamflow forecasts. *Hydrology and Earth System Sciences*, *14*(8), 1639–1653. https://doi.org/10.5194/hess-14-1639-

2010

Thompson, J. R., Green, A. J., & Kingston, D. G. (2014). Potential evapotranspiration-related uncertainty in climate change impacts on river flow: An assessment for the Mekong River basin. *Journal of Hydrology*, *510*, 259–279. https://doi.org/10.1016/j.jhydrol.2013.12.010

Thornthwaite, C. W. (1948). An Approach toward a Rational Classification of Climate. *Geographical Review*, *38*(1), 55. https://doi.org/10.2307/210739

Toffolon, M., & Piccolroaz, S. (2015). A hybrid model for river water temperature as a function of air temperature and discharge. *Environmental Research Letters*, *10*(11), 114011. https://doi.org/10.1088/1748-9326/10/11/114011

Toth, Z., & Kalnay, E. (1993). Ensemble Forecasting at NMC: The Generation of Perturbations. *Bulletin of the American Meteorological Society.* 74(12), 2317–2330. https://doi.org/10.1175/1520-0477(1993)074<2317:EFANTG>2.0.CO;2

Troccoli, A., & Morcrette, J. J. (2014). Skill of direct solar radiation predicted by the ECMWF global atmospheric model over Australia. *Journal of Applied Meteorology and Climatology*, *53*(11), 2571–2588. https://doi.org/10.1175/JAMC-D-14-0074.1

Tsuyuki, T., & Miyoshi, T. (2007). Recent Progress of Data Assimilation Methods in Meteorology. *Journal of the Meteorological Society of Japan*, *85B*, 331–361. https://doi.org/10.2151/jmsj.85B.331

Tukey, J. W. (1949). Comparing individual means in the analysis of variance. *Biometrics*, *5*(2), 99–114. https://doi.org/10.2307/3001913

van Leeuwen, P. J. (2009). Particle Filtering in Geophysical Systems. *Monthly Weather Review*, *137*(12), 4089–4114. https://doi.org/10.1175/2009MWR2835.1

Van Vliet, M. T. H., Franssen, W. H. P., Yearsley, J. R., Ludwig, F., Haddeland, I., Lettenmaier, D. P., & Kabat, P. (2013). Global river discharge and water temperature under climate change. *Global Environmental Change*, *23*(2), 450–464. https://doi.org/10.1016/j.gloenvcha.2012.11.002

Velázquez, J. A., Anctil, F., Ramos, M. H., & Perrin, C. (2011). Can a multi-model

approach improve hydrological ensemble forecasting? A study on 29 French catchments using 16 hydrological model structures. *Advances in Geosciences*, *29*, 33–42. https://doi.org/10.5194/adgeo-29-33-2011

Verkade, J. S., Brown, J. D., Reggiani, P., & Weerts, A. H. (2013). Post-processing ECMWF precipitation and temperature ensemble reforecasts for operational hydrologic forecasting at various spatial scales. *Journal of Hydrology*, *501*, 73–91. https://doi.org/10.1016/j.jhydrol.2013.07.039

Viney, N. R., Bormann, H., Breuer, L., Bronstert, A., Croke, B. F. W., Frede, H., Willems, P. (2009). Assessing the impact of land use change on hydrology by ensemble modelling (LUCHEM) II: Ensemble combinations and predictions. *Advances in Water Resources*, *32*(2), 147–158. https://doi.org/10.1016/j.advwatres.2008.05.006

Vrugt, J. A., ter Braak, C. J. F., Diks, C. G. H., & Schoups, G. (2013). Hydrologic data assimilation using particle Markov chain Monte Carlo simulation: Theory, concepts and applications. *Advances in Water Resources*, *51*, 457–478. https://doi.org/10.1016/j.advwatres.2012.04.002

Walker, W. E., Harremoës, P., Rotmans, J., van der Sluijs, J. P., van Asselt, M. B. A., Janssen, P., & Krayer von Krauss, M. P. (2003). Defining Uncertainty: A Conceptual Basis for Uncertainty Management in Model-Based Decision Support. *Integrated Assessment*, *4*(1), 5–17. https://doi.org/10.1076/iaij.4.1.5.16466

Ward, J. (1982). Ecological aspects of stream regulation: responses in downstream lotic reaches. *Water Pollution and Management Reviews*, (2), 1–26.

Ward, J. V., & Stanford, J. A. (1982). Thermal responses in the evolutionary ecology of aquatic insects. *Annual Review of Entomology*, *27*(1), 97–117. https://doi.org/10.1146/annurev.en.27.010182.000525

Webb, B. W., Hannah, D. M., Moore, R. D., Brown, L. E., & Nobilis, F. (2008). Recent advances in stream and river temperature research, *918*(February), 902–918. https://doi.org/10.1002/hyp

Webb, B. W., & Zhang, Y. (1997). Spatial and seasonal variability in the components of

the river heat budget. *Hydrological Processes*, *11*(1), 79–101. https://doi.org/10.1002/(SICI)1099-1085(199701)11:1<79::AID-HYP404>3.0.CO;2-N

Weerts, A. H., & El Serafy, G. Y. H. (2006). Particle filtering and ensemble Kalman filtering for state updating with hydrological conceptual rainfall-runoff models. *Water Resources Research*, *42*(9), 1–17. https://doi.org/10.1029/2005WR004093

Weijs, S. V., Schoups, G., & Van De Giesen, N. (2010). Why hydrological predictions should be evaluated using information theory. *Hydrology and Earth System Sciences*, *14*(12), 2545–2558. https://doi.org/10.5194/hess-14-2545-2010

Wilks, D. S. (2010). Sampling distributions of the Brier Score and Brier skill score under serial dependence. *Quarterly Journal of the Royal Meteorological Society*, *136*(653), 2109–2118. https://doi.org/10.1002/qj.709

Wilks, D. S. (2011). *Forecast Verification. International Geophysics* (Vol. 100). https://doi.org/10.1016/B978-0-12-385022-5.00008-7

Wilson, L. J., Burrows, W. R., & Lanzinger, A. (1999). A Strategy for Verification of Weather Element Forecasts from an Ensemble Prediction System. *Monthly Weather Review*, *127*(6), 956–970. https://doi.org/10.1175/1520-0493(1999)127<0956:ASFVOW>2.0.CO;2

Winter, T. C., Rosenberry, D. O., & Sturrock, A. M. (1995). Evaluation of 11 Equations for Determining Evaporation for a Small Lake in the North Central United States. *Water Resources Research*, *31*(4), 983–993. https://doi.org/10.1029/94WR02537

Wright, J. L. (1982). New Evapotranspiration Crop Coefficients. *Proceedings of the American Society of Civil Engineers, Journal of the Irrigation and Drainage Division*, *108*(IR2), 57–74.

Xia, Y., Winterhalter, M., & Fabian, P. (2000). Interpolation of daily global solar radiation with thin plate smoothing splines. *Theoretical and Applied Climatology*, *66*(1–2), 109–115. https://doi.org/10.1007/s007040070036

Xing, Z., Chow, L., Meng, F. R., Rees, H. W., Stevens, L., & Monteith, J. (2008). Validating evapotranspiraiton equations using bowen ratio in New Brunswick,

Maritime, Canada. *Sensors*, *8*(1), 412–428. https://doi.org/10.3390/s8010412

Xu, C. Y., & Singh, V. P. (2000). Evaluation and generalization of radiation-based methods for calculating evaporation. *Hydrological Processes*, *14*(2), 339–349. https://doi.org/10.1002/(SICI)1099-1085(20000215)14:2<339::AID-HYP928>3.0.CO;2-O

Ye, M., Meyer, P. D., & Neuman, S. P. (2008). On model selection criteria in multimodel analysis. *Water Resources Research*, *44*(3), 1–12. https://doi.org/10.1029/2008WR006803

Yearsley, J. R. (2009). A semi-Lagrangian water temperature model for advection-dominated river systems. *Water Resources Research*, *45*(12), 1–19. https://doi.org/10.1029/2008WR007629

Yilmaz, M. T., DelSole, T., & Houser, P. R. (2012). Reducing Water Imbalance in Land Data Assimilation: Ensemble Filtering without Perturbed Observations. *Journal of Hydrometeorology*, *13*(1), 413–420. https://doi.org/10.1175/JHM-D-11-010.1

Yuan, W., Xu, B., Chen, Z., Xia, J., Xu, W., Chen, Y., Fu, Y. (2014). Validation of China-wide interpolated daily climate variables from 1960 to 2011. *Theoretical and Applied Climatology*, *119*(3–4), 689–700. https://doi.org/10.1007/s00704-014-1140-0